

Investigation of Organic Materials for Lithium Batteries

A thesis presented for the award of the degree of

Doctor of Philosophy

from

University of Technology Sydney

By Jinqiang Zhang, B. Sc., M. Sc.

July, 2017

Certificate of original authorship

I certify that the work in this thesis has not previously been submitted for a degree nor has it been submitted as part of requirements for a degree except as fully acknowledged within the text.

I also certify that the thesis has been written by me. Any help that I have received in my research work and the preparation of the thesis itself has been acknowledged. In addition, I certify that all information sources and literature used are indicated in the thesis.

Production Note:
Signature removed prior to publication.

Jinqiang Zhang

July 2017

Acknowledgements

It has been four years since I was enrolled as a PhD student in 2013. It is not a particularly long time, but I have received numerous help from many members from our institute to support me finishing my PhD study. Firstly, I would like to express my sincere gratitude to my supervisor, Prof Guoxiu Wang, who has patiently guided, supported and encouraged me during my four-year study. I cannot thank you enough for all the advice that lead to the improvement of my research and all the concern of my life. I also would like to thank my co-supervisors, Associate Professor Alison Ung and Associate Professor Andrew McDonagh for their kindness and selfless suggestions. They helped build up my knowledge, my skills, and my research. I am truly lucky and grateful to have you as my teachers, my supervisors, and my mentors.

I wish to thank all my colleagues in the research team of Centre for Clean Energy Technology, Dr Hao Liu, Dr Xiaodan Huang, Dr Bing Sun, Dr Dawei Su, Dr Kefei Li, Dr Anjon Kumar Mondal, Dr Shuangqiang Chen, Dr Yufei Zhao, Dr Xiuqiang Xie, Dr Sinho Choi, Dr Jianjun Song, Jing Xu, Katja Kretschmer, Linfeng Zheng, Xin Guo, Weizhai Bao, Tuhin Subhra Sahu, Anastasia Tkacheva, and all the new members for the help both in my research and life during my PhD period. Special thanks would be addressed to Dr Yueping (Jane) Yao, for the administrative assistance and lab management as well as the great support for our life. It is a great pleasure to work with all of you and I wish you all the best luck.

I wish to thank Dr Ronald Shimmon, Alexander Angeloski, Dr Linda Xiao, and all the staff members from Faculty of Science for the training and their kind support. And I am

also grateful for the administration help from the staff who have helped so much to support my study in the university.

Financial support provided by the Commonwealth of Australia through the Automotive Australia 2020 Cooperative Research Centre (Excellerate Australia) and the Australian Research Council (ARC) through the ARC Discovery Project (DP160104340) is gratefully acknowledged.

Finally, I would love to thank my family for their help and support. I wish to thank my parents and my brother for their endless love and support. They believe in me even in the toughest time when I did not believe in myself anymore. And there is always a time that I so despaired that I wished so much to quit. It is my beloved wife, Dr Yufei Zhao, who is standing beside me always, supporting me, and selflessly helping me. It is she who persuades me to continue my research, it is she who makes it certain that she will be with me all the time, and it is she who brings me light when there is only darkness inside my heart. I cannot ever express my gratitude and my love for her because she makes me the person that I always dreamt of being. Thank you and I love you, with all my heart.

Abstract

The performances of lithium-based batteries can be significantly influenced by the electrolyte and cathode materials. In this PhD project, functional organic materials were synthesised and applied as electrolyte and cathode components for lithium-ion (Li-ion) and lithium-oxygen (Li-O₂) batteries to improve overall performances. Theoretically, organic materials can be tailored with functional groups to fit various purposes, making them suitable for battery applications. Post-synthesis techniques such as field emission scanning electron microscopy, X-ray diffraction, and Fourier transform infrared spectroscopy were used to characterise the physical properties. Electrochemical analyses including galvanostatic discharge-charge method, cyclic voltammetry, linear sweep voltammetry, and impedance spectroscopy were conducted to determine the electrochemical performance of the materials.

Porous polymer membranes based on poly(vinylidene fluoride-co-hexafluoropropylene) (PVDF-HFP) are prepared using the breath-figure method. The as-prepared PVDF-HFP porous membrane showed a highly ordered honeycomb-like structure. The highly porous structure could absorb large quantities of liquid electrolyte, resulting in a high ionic conductivity. Moreover, the non-combustible PVDF-HFP membrane could significantly enhance safety properties of Li-ion batteries compared to the one using a conventional Celgard separator. The combination of the PVDF-HFP membrane with liquid electrolyte resulted in a higher capacity and prolonged cycle life.

Further investigation on coating poly(methyl methacrylate) (PMMA) on PVDF-HFP porous membranes to achieve hierarchical structures with sandwich-like morphology was

carried and studied. By the combination of porous PVDF-HFP and PMMA with higher affinity towards liquid electrolyte, the ionic conductivity was further improved. As a result, the electrochemical performance of Li-ion battery was significantly enhanced.

A bi-functional organic catalyst poly(2,2,6,6-tetramethylpiperidinyloxy-4-yl methacrylate) (PTMA) was synthesized by a two-step method. The unique properties of PTMA during n-doping and p-doping could facilitate the discharge and charge processes, respectively. It was discovered that the discharge capacity increased and the charge over-potential was reduced. The mechanism investigation showed that it was the functional N-O radical interacting with oxygen and Li_2O_2 to catalyse the battery reactions. As a result, the cycling life of the Li- O_2 battery was significantly prolonged.

Further investigation of employing co-polymers as binder in the cathode for Li- O_2 batteries was carried out. The binder was synthesized by co-polymerizing methyl methacrylate (MMA) and 2,2,6,6-tetramethylpiperidinyloxy-4-yl methacrylate (TMA) monomers. The ratio between both monomers was also studied. The results indicated that the direct contact of co-polymer binder and liquid electrolyte would transfer it into a gel polymer electrolyte membrane which enabled the catalytic N-O radical group to function as restricted redox mediator. The electrochemical performance of Li- O_2 batteries can be further enhanced by employing PTMA.

An investigation of the mechanism when tetrathiafulvalene (TTF) was used in Li- O_2 batteries in the presence of LiCl was studied. It is revealed that the addition of LiCl in the electrolyte completely changed the functional mechanism of TTF in Li- O_2 batteries. Instead of functioning as a solution-based redox mediator, the combination of TTF and LiCl

resulted in a deposition of an organic conductor on the surface of Li_2O_2 , providing additional ways for electron transference. As a result, the cycling efficiency was improved, and with the use of porous graphene as cathode material the cycle life was prolonged.

Publication list

1. **Zhang, J.**; Sun, B.; Zhao, Y.; Kretschmer, K.; Wang, G., Modified tetrathiafulvalene as an organic conductor for improving performances of Li-O₂ batteries, *Angewandte Chemie International Edition* **2017**. Accepted, in press. DOI: 10.1002/ange.201703784, and DOI: 10.1002/anie.201703784.
2. **Zhang, J.**; Sun, B.; McDonagh, AM.; Zhao, Y.; Kretschmer, K.; Guo, X.; Wang, G., A multi-functional gel co-polymer bridging liquid electrolyte and solid cathode nanoparticles: An efficient route to Li-O₂ batteries with improved performance, *Energy Storage Materials* **2017**, 7, 1-7. Selected as one of the cover images.
3. **Zhang, J.**; Sun, B.; Xie, X.; Zhao, Y.; Wang, G., A bifunctional organic redox catalyst for rechargeable lithium-oxygen batteries with enhanced performances, *Advanced Science* **2016**, 3, 1500285.
4. **Zhang, J.**; Sun, B.; Xie, X.; Kretschmer, K.; Wang, G., Enhancement of stability for lithium oxygen batteries by employing electrolytes gelled by poly (vinylidene fluoride-co-hexafluoropropylene) and tetraethylene glycol dimethyl ether, *Electrochimica Acta* **2015**, 183, 56-62.
5. **Zhang, J.**; Chen, S.; Xie, X.; Kretschmer, K.; Huang, X.; Sun, B.; Wang, G., Porous poly (vinylidene fluoride-co-hexafluoropropylene) polymer membrane with sandwich-like architecture for highly safe lithium ion batteries, *Journal of Membrane Science* **2014**, 472, 133-140.

6. **Zhang, J.**; Sun, B.; Huang, X.; Chen, S.; Wang, G., Honeycomb-like porous gel polymer electrolyte membrane for lithium ion batteries with enhanced safety, *Scientific reports* **2014**, 4, 6007.
7. **Zhang, J.**; Sun, B.; Ahn, H.-J.; Wang, C.; Wang, G., Conducting polymer-doped polyprrole as an effective cathode catalyst for Li-O₂ batteries, *Materials Research Bulletin* **2013**, 48, 4979-4983.
8. Zhao, Y., **Zhang, J.**, Li, K., Ao, Z., Wang, C., Liu, H., Sun, K., Wang, G., Electrospun cobalt embedded porous nitrogen doped carbon nanofibers as an efficient catalyst for water splitting, *Journal of Materials Chemistry A* **2016**, 4, 12818-12824.
9. Wang, Y., Kretschmer, K., **Zhang, J.**, Mondal, A.K., Guo, X., Wang, G., Organic sodium terephthalate@graphene hybrid anode materials for sodium-ion batteries, *RSC Advances* **2016**, 6, 57098-57102.
10. Kretschmer, K., Sun, B., **Zhang, J.**, Xie, X., Liu, H., Wang, G., 3D Interconnected Carbon Fiber Network - Enabled Ultralong Life Na₃V₂(PO₄)₃@ Carbon Paper Cathode for Sodium-Ion Batteries, *Small* **2016**.
11. Guo, X., Sun, B., **Zhang, J.**, Liu, H., Wang, G., Ruthenium decorated hierarchically ordered macro-mesoporous carbon for lithium oxygen batteries, *Journal of Materials Chemistry A*, **2016**, 4, 9774-9780.

12. Zhao, Y., Xie, X., **Zhang, J.**, Liu, H., Ahn, H.J., Sun, K., Wang, G., MoS₂ nanosheets supported on 3D graphene aerogel as a highly efficient catalyst for hydrogen evolution, *Chemistry–A European Journal* **2015**, 21, 15908-15913.
13. Xie, X., Su, D., **Zhang, J.**, Chen, S., Mondal, A.K., Wang, G., A comparative investigation on the effects of nitrogen-doping into graphene on enhancing the electrochemical performance of SnO₂/graphene for sodium-ion batteries, *Nanoscale* **2015**, 7, 3164-3172.
14. Xie, X., Kretschmer, K., **Zhang, J.**, Sun, B., Su, D., Wang, G., Sn@ CNT nanopillars grown perpendicularly on carbon paper: a novel free-standing anode for sodium ion batteries, *Nano Energy* **2015**, 13, 208-217.
15. Xie, X., Ao, Z., Su, D., **Zhang, J.**, Wang, G., MoS₂/Graphene Composite Anodes with Enhanced Performance for Sodium - Ion Batteries: The Role of the Two - Dimensional Heterointerface, *Advanced Functional Materials* **2015**, 25, 1393-1403.
16. Su, D., **Zhang, J.**, Dou, S., Wang, G., Polypyrrole hollow nanospheres: stable cathode materials for sodium-ion batteries, *Chemical Communications* **2015**, 51, 16092-16095.
17. Xie, X., Su, D., Sun, B., **Zhang, J.**, Wang, C., Wang, G., Synthesis of Single - Crystalline Spinel LiMn₂O₄ Nanorods for Lithium - Ion Batteries with High Rate Capability and Long Cycle Life, *Chemistry - A European Journal* **2014**, 20, 17125-17131.

18. Xie, X., Su, D., Chen, S., **Zhang, J.**, Dou, S., Wang, G., SnS₂ Nanoplatelet@ Graphene Nanocomposites as High - Capacity Anode Materials for Sodium - Ion Batteries, *Chemistry - An Asian Journal* **2014**, 9, 1611-1617.
19. Sun, B., Huang, X., Chen, S., Zhao, Y., **Zhang, J.**, Munroe, P., Wang, G., Hierarchical macroporous/mesoporous NiCo₂O₄ nanosheets as cathode catalysts for rechargeable Li-O₂ batteries, *Journal of Materials Chemistry A* **2014**, 2, 12053-12059.
20. Sun, B., Huang, X., Chen, S., **Zhang, J.**, Wang, G., An optimized LiNO₃/DMSO electrolyte for high-performance rechargeable Li-O₂ batteries, *RSC Advances* **2014**, 4, 11115-11120.
21. Mondal, A.K., Su, D., Chen, S., **Zhang, J.**, Ung, A., Wang, G., Microwave-assisted synthesis of spherical β-Ni (OH)₂ superstructures for electrochemical capacitors with excellent cycling stability, *Chemical Physics Letters* **2014**, 610, 115-120.
22. Chen, S., Huang, X., Liu, H., Sun, B., Yeoh, W., Li, K., **Zhang, J.**, Wang, G., 3D Hyperbranched Hollow Carbon Nanorod Architectures for High - Performance Lithium - Sulfur Batteries, *Advanced Energy Materials* **2014**, 4.

Table of Contents

Certificate of original authorship.....	i
Acknowledgements.....	ii
Abstract.....	iv
Publication list.....	vii
Table of Contents.....	xi
List of Figures.....	xvii
List of Tables.....	xxx
Introduction.....	xxxii
Chapter 1 Literature reviews.....	1
1.1 Overview.....	1
1.2 Lithium ion (Li-ion) batteries.....	4
1.2.1 History of Li-ion batteries.....	4
1.2.2 Basic concepts and designs for Li-ion batteries.....	5
1.2.3 Overall criteria for commercial Li-ion battery systems.....	12
1.2.4 Organic Electrolyte for Li-ion batteries.....	13
1.2.4.1 Ion transport.....	15
1.2.5 Organic porous polymer membrane.....	31
1.3 Lithium oxygen (Li-O ₂) batteries.....	34
1.3.1 Anode.....	37

1.3.2 Organic electrolyte	42
1.3.3 Cathode.....	48
1.4 Summary	52
Chapter 2 Experimental	53
2.1 Overview	53
2.2 Materials and chemicals.....	54
2.3 Material preparations	55
2.3.1 Breath-figure method	56
2.3.2 General organic synthesis.....	57
2.4 Material characterization	58
2.4.1 X-ray diffraction analysis (XRD)	58
2.4.2 Raman spectroscopy.....	60
2.4.3 Thermogravimetric analysis (TGA).....	61
2.4.4 Scanning electron microscopy (SEM).....	63
2.4.5 Fourier transform infrared (FTIR) spectroscopy	64
2.4.6 Ultraviolet-visible (UV-vis) spectroscopy	64
2.4.7 Nuclear magnetic resonance (NMR) spectroscopy.....	65
2.5 Electrode preparation and battery assembly	67
2.5.1 Lithium ion (Li-ion) battery	67
2.5.2 Lithium oxygen (Li-O ₂) battery	68

2.6 Electrochemical measurements	70
2.6.1 Cyclic voltammetry (CV)	70
2.6.2 Electrochemical impedance spectroscopy (ESI).....	71
2.6.3 Linear Sweep Voltammetry (LSV)	72
2.6.4 Galvanostatic discharge-charge	73
Chapter 3 Honeycomb-like porous gel polymer electrolyte membrane for lithium ion batteries with enhanced safety.....	75
3.1 Introduction	75
3.2 Experimental details	77
3.2.1 Preparation of PVDF-HFP polymer electrolyte membranes	77
3.2.2 Characterization of PVDF-HFP membranes	77
3.2.3 Electrochemical characterization of PVDF-HFP electrolyte membrane	78
3.3 Results and Discussions	79
3.3.1 Optimisation	79
3.3.2 Morphology	82
3.3.3 Physical Characterization	86
3.3.4 Electrochemical characterizations.....	90
3.3.5 Battery performances	94
3.4 Summary	98

Chapter 4 Porous poly(vinylidene fluoride-co-hexafluoropylene) polymer membrane with sandwich-like architecture for highly safe lithium ion batteries	100
4.1 Introduction	100
4.2 Experimental details	102
4.2.1 Preparation of PVDF-HFP porous polymer membranes.....	102
4.2.2 Preparation of PMMA/PVDF-HFP porous polymer membranes.....	103
4.2.3 Preparation of gel polymer electrolyte membranes	103
4.2.4 Characterizations of the as-prepared porous polymer membranes.....	103
4.2.5 Electrochemical characterization of polymer electrolyte membranes	104
4.3 Results and discussions.....	105
4.3.1 Morphology	105
4.3.2 Physical characterizations	109
4.3.3 Electrochemical characterizations.....	117
4.3.4 Battery performances	120
4.4 Summary	122
Chapter 5 A Bi-functional Organic Redox Catalyst for Rechargeable Lithium-Oxygen Batteries with Enhanced Performances.....	123
5.1 Introduction.....	123
5.2 Experimental details	124
5.2.1 Synthesis of PTMA.....	124

5.2.2 Characterization	126
5.2.3 Electrochemical characterization	126
5.3 Results and discussions.....	128
5.3.1 Physical characterizations	128
5.3.2 Electrochemical characterizations.....	131
5.3.3 Battery performances	134
5.3.4 Mechanisms	140
5.3.5 Catalytic behavior	144
5.4 Summary	145
Chapter 6 A Multi-Functional Gel Co-Polymer Bridging Liquid Electrolyte and Solid Cathode Nanoparticles: An Efficient Route to Li-O ₂ Batteries with Improved Performance	146
6.1 Introduction.....	146
6.2 Experimental	148
6.2.1 Synthesis of P(TMA-MMA) co-polymers	148
6.2.2 Characterization	150
6.2.3 Electrochemical characterization	150
6.3 Results and discussions.....	151
6.3.1 Physical characterizations	151
6.3.2 Electrochemical performances.....	155

6.3.3 ¹ HNMR tests.....	157
6.3.4 Battery performances	159
6.3.5 Mechanisms	162
6.4 Summary	177
Chapter 7 Transform tetrathiafulvalene as an organic conductor for improving performances of Li-O ₂ batteries	178
7.1 Introduction.....	178
7.2 Experimental details	179
7.2.1 Electrolyte preparation	179
7.2.2 Carbon black electrode preparation	179
7.2.3 Porous graphene electrode preparation	180
7.2.4 Characterizations.....	180
7.2.5 Electrochemical characterizations.....	181
7.3 Results and discussions.....	182
7.3.1 Electrochemical characterizations.....	182
7.4 Summary	199
Chapter 8 Conclusions	200
8.1 General conclusions.....	200
8.2 Outlook	202
References	204

List of Figures

Figure 1-1 The timeline of battery evolution.	2
Figure 1-2 The gravimetric energy density of commonly used rechargeable batteries.	3
Figure 1-3 Schematic illustration of the rocking chair mechanism during discharge and charge.	5
Figure 1-4 The potential ranges vs. Li^+/Li and specific capacities of electrode materials for Li-ion batteries.	7
Figure 1-5 Comparison of self-diffusivities for Li^+ , counter-anions, and solvent molecules and their dependences on salt concentration. The asterisk at 0 M represents D_{GBL} of neat GBL.	17
Figure 1-6 Schematic illustrations of the primary solvation sheath of Li^+ in 0.1 M LiBF_4 solution in EC-DMC (1-1) with different coordination numbers based on MD simulation of LiBF_4 in EC/DMC.	19
Figure 1-7 Viscosity versus cosolvent content plots for sulfolane–binary solutions: sulfolane + dimethylcarbonate.	21
Figure 1-8 Cycling performance of $\text{Li}/\text{LiNi}_{0.5}\text{Mn}_{1.5}\text{O}_4$ cells with standard (STD) and DMMP containing electrolyte.	23
Figure 1-9 Common ionic liquids ion families utilized in lithium-ion batteries.	25
Figure 1-10 Improved cycling performances of lithium-ion cells at elevated temperatures 75°C for NCA and 60°C for LFP.	27
Figure 1-11 Schematic mechanism of Li^+ movement through PEO based polymer electrolyte.	29

Figure 1-12 (a) Surface and (b) cross-section morphologies of the prepared porous polymer membrane.....	34
Figure 1-13 Specific energy densities of various rechargeable batteries.	35
Figure 1-14 Schematic illustration of the discharge and charge processes of Li-O ₂ batteries.	36
Figure 1-15 The characterizations of anodic lithium during discharge-charge cycling.	38
Figure 1-16 Voltage profiles of Li-O ₂ battery with 1 M LiNO ₃ in DMA at 0.1 mA cm ⁻² at room temperature.....	41
Figure 1-17 Schematic mechanism of decomposition of PC electrolyte in Li-O ₂ batteries.	44
Figure 1-18 a) First charge/discharge profiles of carbon paper/Li cells with and without 0.05 M TEMPO at a current rate of 0.025 mA cm ⁻² . b) The cycling stabilities and efficiencies of the cell with 0.05 M of TEMPO at a current rate of 0.025 mA cm ⁻² . c,d) Nyquist plots of the impedances of the Li/Li symmetric cell with bare Li and with TEMPO (c), and with the CPL-coated Li and with TEMPO (d). e) Digital pictures of bare Li and CPL-coated Li electrodes after prolonged storage test (scale bar, 5 mm).	47
Figure 1-19 Schematics of reactions on discharge (left) and the effect of DBBQ on the potential determining step (right).	51
Figure 2-1 Schematic illustration for material preparation, characterization and application.	53
Figure 2-2 Conventional BF methods. (a) Dynamic and (b) static BF processed.	57
Figure 2-3 Schematic drawing of Bragg's law.	59
Figure 2-4 Photo of the XRD instrument of Bruker D8 Discover.....	60
Figure 2-5 Photo of the Raman instrument	61

Figure 2-6 The photo of the TGA instrument	62
Figure 2-7 The photo of SEM of Supra 55 VP.....	63
Figure 2-8 Photo of the thermo FTIR instrument	64
Figure 2-9 Photo of the UV instrument of Cary 60	65
Figure 2-10 Photo of the NMR instrument	66
Figure 2-11 Photo of the glovebox used to assemble the batteries.....	67
Figure 2-12 Schematic illustration of the construction of a Li-ion battery	68
Figure 2-13 Schematic illustration of the construction of a Li-O ₂ battery.....	69
Figure 2-14 Photo of the CH instrument Electrochemical workstation.....	71
Figure 2-15 A typical impedance Nyquist curve of a battery system.....	72
Figure 2-16 Photo of the Neware battery testing system	74
Figure 3-1 SEM images of porous membranes prepared with different concentrations of PVDF-HFP: (a) 1 wt%, (b) 2 wt%, (c) 5 wt%, and 10 wt%. The scale bar is 1 μm for all images.	80
Figure 3-2 SEM images of porous membrane prepared in different humidities of (a) 65 %, (b) 76 %, (c) 86 %, and (d) 98 %. The scale bar is (a) 2 μm, (b) 2 μm, (c) 2 μm, and (d) 1 μm.	81
Figure 3-3 FESEM images of (a, b) the front side, (c, d) the back side, and (e, f) the cross-section of the PVDF-HFP honeycomb-like porous polymer membrane	83
Figure 3-4 FESEM image of (a) the front side and (b) the back side of the PVDF-HFP honeycomb-like porous membrane.....	84
Figure 3-5 Schematic illustration: (a) The preparation process of the PVDF-HFP porous polymer membrane. (b) The 3D architecture of PVDF-HFP polymer membrane. And (c)	

the porous gel polymer electrolyte with the combination of two membranes as one integrated separator (two back sides are exposed to the outside).....	85
Figure 3-6 FTIR spectrum of the PVDF-HFP membrane.....	87
Figure 3-7 Thermogravimetry (TG, solid line) and differential scanning calorimetry (DSC, dot line) curves of PVDF-HFP porous polymer membrane in air. The temperature rising rate is 10 °C min ⁻¹	88
Figure 3-8 The thermal shrinking test of the PVDF-HFP porous membrane (a) before and (b) after heating to 150 °C for 30 min, and the combustion test of the membrane (c) before and (d) after set on fire.....	89
Figure 3-9 Thermogravimetry (TG) and differential scanning calorimetry (DSC) curves of the PVDF-HFP polymer electrolyte membrane in N ₂ . The temperature rising rate is 2 °C min ⁻¹	90
Figure 3-10 The Arrhenius plots of the ionic conductivity vs. temperature. The inset is the a.c. impedance spectra.....	91
Figure 3-11 The linear sweep voltammogram of the PVDF-HFP polymer electrolyte membrane and Celgard 2400 separator. The scanning rate is 0.1 mV s ⁻¹	93
Figure 3-12 The cyclic voltammetry curve of lithium ion cells with the PVDF-HFP polymer electrolyte membranes. The scanning rate is 0.1 mV s ⁻¹ . The potential range is set between 2.0 to 4.2 V.....	94
Figure 3-13 Electrochemical performances of lithium ion cells with LiFePO ₄ as cathode materials: (a) Charge-discharge curves using PVDF-HFP polymer electrolyte membranes, (b) Charge-discharge curves using Celgard 2400 separators saturated with liquid electrolyte, (c) Cycling performances. The cut-off voltages are 2 V and 4.2 V. The current density is	

0.2 C. (d) Rate behaviour. The current densities of discharge and charge are 0.2 C, 0.5 C, 1 C, and 2 C respectively.	96
Figure 3-14 The cycling performance of the lithium ion cells with the PVDF-HFP polymer electrolyte membrane. The current density is 1 C.	97
Figure 3-15 The charge-discharge curves of the lithium ion cells with the PVDF-HFP polymer electrolyte membranes at different current densities.	98
Figure 4-1 FESEM images of (a) the front side, (b) the back side, and (c) the cross-section of the PVDF-HFP porous polymer membrane, and (d) the outside surface, (e, f) the cross-section of the PMMA/PVDF-HFP porous polymer membrane.	107
Figure 4-2 FTIR spectra of the PVDF-HFP and PMMA/PVDF-HFP membranes	110
Figure 4-3 Thermogravimetry (TG) and differential scanning calorimetry (DSC) curves of the PVDF-HFP and PMMA/PVDF-HFP porous polymer membranes in air. The temperature rising rate is 10 °C min ⁻¹	112
Figure 4-4 The thermal shrinking test of (left) the Celgard 2400 separator, (middle) the PVDF-HFP porous polymer membrane, and (right) the PMMA/PVDF-HFP porous polymer membrane (a) before and (b) after heating to 150 °C for 30 min, and the combustion test of (left) the Celgard 2400 separator, (middle) the PVDF-HFP porous polymer membrane, and (right) the PMMA/PVDF-HFP porous polymer membrane (c) before and (d) after set on fire	114
Figure 4-5 Thermogravimetry (TG) and differential scanning calorimetry (DSC) curves of the PVDF-HFP and PMMA/PVDF-HFP polymer electrolyte membrane in N ₂ . The temperature rising rate is 2 °C min ⁻¹	117

Figure 4-6 The Arrhenius plots of the ionic conductivity vs. temperature. The inset is the a.c. impedance spectra	118
Figure 4-7 The linear sweep voltammogram of the electrolyte membranes and Celgard 2400 separator. The scanning rate is 0.1 V mV s ⁻¹	120
Figure 4-8 Electrochemical performances of lithium ion cells with LiFePO ₄ as cathode material. (a) The cycling performances of the polymer electrolyte membranes and Celgard 2400 separator. The cut-off voltages are 2 V and 4.2 V. The current density is 0.2 C. (b) The rate behaviour. The current densities of discharge and charge are 0.2 C, 0.5 C, 1 C, and 2 C, respectively	121
Figure 5-1 (a) The illustration of the PTMA synthesis process and (b) digital photo of the as-prepared PTMA, reactant MTMP, and intermediate PMTMP.	125
Figure 5-2 FT-IR spectra of the as-prepared MTMP and PTMA.....	128
Figure 5-3 (a) Illustration of the processes to form the PTMA / carbon black electrode material. Insets show SEM images of the materials (b) before and (c) after dissolving in NMP. (d) The digital photos of PTMA dissolving into NMP.....	129
Figure 5-4 EDX mapping of the PTMA electrode	130
Figure 5-5 (a) Digital photos of PTMA before and after soaked in DEGDME solvent. (b) FTIR spectra of the DEGDME solvent before and after PTMA soaked for two hours.	131
Figure 5-6 (a) The cyclic voltammetry curves of the sealed cells in an argon atmosphere with PTMA and bare CB electrodes. Scanning rate is 0.1 mV s ⁻¹ and potential range is 2.0 to 4.5 V. The inset is the redox reactions of PTMA during p-doping and n-doping. (b) The CV curves of PTMA electrodes both in argon and oxygen atmosphere. Scanning rate is 0.1	

mV s ⁻¹ and potential range is 2.0 to 4.5 V. The inset is the enlarged curves from 2.5 V to 3.3 V.....	133
Figure 5-7 (a) Discharge/charge profiles of Li-O ₂ batteries with PTMA electrode and bare CB electrode at a discharge depth of 1000 mAh g ⁻¹ and a current density of 200 mA g ⁻¹ . (b) Cycling profile of both Li-O ₂ batteries. And discharge/charge profile during cycling of Li-O ₂ batteries with (c) PTMA electrode, and (d) bare CB electrode. The cut-off voltage was set to be 2.3 V/4.8 V. The current density and capacities were calculated by the weight of the active materials in the electrodes (PTMA+CB and CB).	134
Figure 5-8 (a) Fully discharge/charge profile of Li-O ₂ batteries with PTMA and bare CB electrodes. The current density is 200 mAh g ⁻¹ . The cut-off voltage is set at 2.3 V/4.5 V. (b) The full discharge/charge profile of the cell with PTMA electrode in Argon atmosphere. The current density is 200 mAh g ⁻¹ . The cut-off voltage is set as 2.3 V-4.5V.....	135
Figure 5-9 Rate capabilities of Li-O ₂ batteries with PTMA (a), and bare CB (b) with current density from 50 to 1000 mA g ⁻¹	137
Figure 5-10 The rate capability of Li-O ₂ batteries with PTMA electrodes with current densities from 100 to 500 mA g ⁻¹ . The cut-off voltage is set at 2.3 V/4.5 V.....	138
Figure 5-11 The SEM images of PTMA electrode (a) before discharge, (b) after first discharge, and (c) after first charge. (d) XRD pattern of the electrode after discharge.	139
Figure 5-12 The FTIR spectrum of the PTMA electrode after discharge.	140
Figure 5-13 Aqueous ORR and OER with PTMA electrocatalyst. Operating in an O ₂ -saturated 1 M KOH aqueous solution, the results are electrochemically measured LSVs of (a) PTMA and (b) CB towards ORR at different rotation rates indicated; (c) ORR and (d) OER catalytic activity of PTMA and CB at a rotation rate of 1600 rpm.	141

Figure 5-14 Schematic illustration of mechanism of PTMA during discharge and charge processes. To simplify the illustration, the structure of PTMA is replaced by its nitride oxide moiety as it is the main functional group.	143
Figure 5-15 Liner sweep voltammetry of electrode with and without commercial Li_2O_2 . The scanning rate is 0.1 mV s^{-1} . The range is set from open circuit voltage to 4.4 V.....	145
Figure 6-1 Schematic synthesis process of the co-polymers.....	149
Figure 6-2 (a) Digital photos, (b) FTIR spectra, and (c) Raman spectra of the as-prepared P_{11} , P_{12} , P_{13} , and P_{14} co-polymers.	152
Figure 6-3 (a) Schematic illustration of the electrode fabrication process, and SEM images of the electrodes with (b) P_{11} , (c) P_{12} , (d) P_{13} , and (e) P_{14} co-polymer binders. The insets are higher magnification SEM images of the electrodes.	154
Figure 6-4 EDX mapping results of the electrode. A P_{13} co-polymer electrode was chosen to represent the co-polymers.	155
Figure 6-5 (a) Impedance spectra of test batteries with different binders in Argon atmosphere. (b) The discharge-charge profiles and (c) cyclabilities of the Li- O_2 batteries with P_{11} , P_{12} , P_{13} , P_{14} co-polymers, and PTFE binder. The current density was 200 mA g^{-1} . The cut-off voltages were 2.3 V /4.6 V.....	156
Figure 6-6 The digital image of P_{13} co-polymer (a) before and (b) after soaking with electrolyte for one day. P_{13} co-polymer has been used as a representative for the P(TMA-MMA) co-polymers. It is evident that the powder-like P_{13} co-polymer changed to a transparent gel-like morphology after soaking in liquid electrolyte, confirming its capability to form a gel polymer membrane.....	157

Figure 6-7 (a) Schematic illustration of the preparation for NMR testing. The ¹HNMR results of the solution extracted from (b) the P₁₃ electrode, and (c) the PTFE electrode. ...158

Figure 6-8 Discharge-charge profiles of the Li-O₂ batteries with P₁₁, P₁₂, P₁₃ co-polymers and PTFE binder. The current density was 500 mA g⁻¹.....160

Figure 6-9 SEM images of (a) the pristine electrode, (b) the electrode after discharge, and (c) the electrode after charge. A P₁₃ co-polymer was used as a representative, and the current density was 200 mA g⁻¹. (d) XRD patterns of the electrode after discharge. Compared with the pristine electrode (a), toroidal-shaped structures were observed after discharge (b) and vanished after charge (c). The discharge products have been confirmed to be Li₂O₂ by XRD measurement (d). These results further indicate the stability and compatibility of P₁₃ in Li-O₂ batteries.161

Figure 6-10 FTIR spectra of the cathode with P₁₃ before cycle and after 5 cycles. The characteristic peaks of the co-polymer remain unchanged after 5 cycles, indicating the exceptional stability of the co-polymer in the attack of Li₂O₂.162

Figure 6-11 Schematic mechanisms of the co-polymers facilitating Li-O₂ battery reactions during discharge and charge.....164

Figure 6-12 The LSV curves of the Li-O₂ batteries with (a) CB electrodes and (b) CB+Li₂O₂ electrodes. The scan rate is 0.1 mV s⁻¹.....166

Figure 6-13 (a) The discharge-charge profiles and (b) cyclabilities of Li-O₂ batteries with P₁₃ and PTMA-PMMA. The current density was 200 mA g⁻¹, and the cut-off voltages were 2.3 V/4.6 V. (c) Graphical illustration of the Li₂O₂ formation mechanism on P₁₃ and PTMA+PMMA electrodes during discharge.167

Figure 6-14 (a) Orientation of the sample during ATR-FTIR experiments. (b) ATR-FTIR spectra of the electrodes surfaces. A band assigned to the N-O group of the TMA unit in P ₁₃ at 1332 cm ⁻¹ is indicated by *.....	168
Figure 6-15 Discharge profiles of Li-O ₂ batteries with P ₁₃ and PTMA+PMMA electrodes. The current density was 200 mA g ⁻¹ , and the cut-off voltage was 2.3 V.....	169
Figure 6-16 Discharge-charge profiles of Li-O ₂ batteries with (a) P ₁₃ and (c) PTMA+PMMA electrodes. The current density was 200 mA g ⁻¹ and cut-off potentials were 2.3 V/4.3 V. The dQ/dV vs voltage profiles of (b) P ₁₃ and (d) PTMA+PMMA electrodes based on (a, c) profiles.	170
Figure 6-17 Rate performance of the Li-O ₂ batteries with P ₁₃ co-polymer as catalyst/binder. The discharge and charge current densities of each cell were kept the same.	171
Figure 6-18 Discharge-charge profiles of Li-O ₂ batteries with (a) P ₁₃ and (b) PTFE all discharged at 100 mA g ⁻¹ , charged at 100, 200, and 500 mA g ⁻¹ , respectively. Discharge-charge profiles of Li-O ₂ batteries with (c) P ₁₃ and (d) PTFE discharged at 100, 200, and 500 mA g ⁻¹ , respectively, all charged at 100 mA g ⁻¹	172
Figure 6-19 Discharge-charge profiles of Li-O ₂ batteries with (a, c) P ₁₃ and (b, d) PTFE all discharged at (a, b) 200 mA g ⁻¹ or (c, d) 500 mA g ⁻¹ , charged at 100, 200, and 500 mA g ⁻¹ , respectively.....	173
Figure 6-20 The SEM images of discharged electrodes at current densities of (a) 100 mA g ⁻¹ , (c) 200 mA g ⁻¹ , and (e) 500 mA g ⁻¹ . (b, d, f) Illustration of the proposed mechanism for forming different morphologies of Li ₂ O ₂	174
Figure 6-21 FTIR spectra of the electrolyte before and after 1 cycle when using P ₁₃ co-polymer catalyst/binder.....	175

Figure 6-22 The discharge-charge profiles of Li-O ₂ batteries with different percentages of P ₁₃ co-polymer in the cathode. The current density was 200 mA g ⁻¹	176
Figure 7-1 (a) CV curves of the cells with different electrolytes in argon atmosphere. The scan rate is 0.5 mV s ⁻¹ . The galvanostatic discharge and charge profiles with current densities of (b) 200 mA g ⁻¹ and (c) 500 mA g ⁻¹ , and (d) the cycling performances of Li-O ₂ batteries in oxygen atmosphere. The current density is 200 mA g ⁻¹ , and the cut-off voltages are 2.0 V/4.6 V. The positive electrodes are prepared with carbon black.	182
Figure 7-2 CV curves of the two-electrode (Li-O ₂) cells with different electrolytes in oxygen atmosphere. The scan rate is 0.5 mV s ⁻¹ . The cell is constructed by assembling a swagelok-type cell using a lithium metal as the anode, and a carbon black electrode as the cathode.	184
Figure 7-3 XRD patterns of the electrodes after (a) discharge and (b) charge.....	185
Figure 7-4 FTIR post-characterization of the electrode before and after first cycle. The electrolyte contains 30 mM TTF and 30 mM LiCl. (a) All the electrodes are carefully rinsed several times with electrolyte solvents DEGDME until there is no colour detected in the upper liquid. The electrodes are then dried in vacuum before test. (b) FTIR result of the electrodes.....	186
Figure 7-5 SEM images of carbon black electrodes (a) before cycling, (b) after discharge, (c) after charge, and (d) after second discharge to 3.0 V. The electrolyte is 30 mM TTF+30 mM LiCl. The highlighted thread-like structure is the deposited TTF ⁺ Cl _x ⁻ . The cycle depth is 1000 mAh g ⁻¹ based on the electrode mass.	186
Figure 7-6 The second cycle discharge-charge profiles of the batteries with different electrolytes. The current density is 200 mA g ⁻¹	187

Figure 7-7 The discharge-charge profiles of the Li-O ₂ batteries with different electrolyte cycling at larger fixed capacities of 3000 mAh g ⁻¹ . The electrolytes used are (a) 30 mM TTF and (b) 30 mM TTF+30 mM LiCl in DEGDME electrolyte. The current density is 200 mA g ⁻¹ . Compared to the large reversible capacities, the capacity of TTF redox is insignificant.....	188
Figure 7-8 Digital photos of the separators after 5 cycles in the Li-O ₂ batteries (discharge state). The electrolytes are (a) pure electrolyte, (b) 30 mM TTF, (c) 30 mM TTF+30 mM LiCl.....	189
Figure 7-9 FTIR spectra of the electrodes after the first charge. The peaks referring to the formation of TTF are visible on the charged TTF+LiCl electrode indicating the deposit of TTF-species.....	190
Figure 7-10 EDX results of the electrode after first cycle (a) discharge and (b) charge. The electrolyte is 30 mM TTF+30 mM LiCl+ 0.5 M LiTFSI in DEGDME.....	190
Figure 7-11 UV spectra of the electrolytes after the first (a) discharge and (b) charge. (c) The digital photos of a two-electrode device with TTF electrolyte and TTF+LiCl electrolyte. The scan rate is 1 mV s ⁻¹ . (d) Schematic illustration of the mechanism of TTF ⁺ Cl _x ⁻ facilitating the decomposition of Li ₂ O ₂	192
Figure 7-12 Visual experiment of TTF ⁺ Cl _x ⁻ when a GC electrode is used. The scanning rate is 50 mV s ⁻¹	193
Figure 7-13 The SEM image of the electrode after charge. The thread-like structure is the as-deposit TTF ⁺ Cl _x ⁻ , which is different from the morphology of glass fibre (shown in the inset image).....	194

Figure 7-14 (c, e) Digital photos and (d, f) SEM images of the lithium anode after five cycles. (a, b) are the pristine lithium anode. (c, d) are the lithium anode in 30 mM TTF electrolyte, and (e, f) are the lithium anode in 30 mM TTF+30 mM LiCl electrolyte. The fibre-like structures in (b, d) originate from the glass fibre separators.....	195
Figure 7-15 The discharge and charge profiles of Li-O ₂ batteries containing electrolytes with different concentrations of (a) TTF and (b) LiCl in oxygen atmosphere. The cycling performance of a Li-O ₂ battery with 50 mM TTF and 0.1 M LiCl in oxygen atmosphere with (c) a carbon black electrode and (d) a porous graphene electrode. The current densities are 200 mA g ⁻¹ . The cut-off voltages are 2.3 V/4.6 V.	196
Figure 7-16 LSV result of the cells with different electrolytes and electrodes. The electrolytes are 30 mM LiCl in DEGDME (referring as LiCl) and pure DEGDME (referring as Blank), and the electrodes used are carbon black electrode and carbon black+Li ₂ O ₂ electrode.	197
Figure 7-17 The discharge-charge profiles of the Li-O ₂ batteries with 30 mM LiCl in DEGDME electrolyte at different fixed capacities in oxygen atmosphere. One cell is directly charged in argon atmosphere and another cell is used without the addition of LiCl, as comparisons. The current densities are 200 mA g ⁻¹	197
Figure 7-18 Schematic illustration of the material loss during discharge and charge processes with (a) carbon black electrode and (b) porous graphene electrode.	198
Figure 7-19 SEM images of PGE.	198
Figure 7-20 The cycling performance of the battery with 50 mM TTF electrolyte using a PGE electrode. The current density is 200 mA g ⁻¹	199

List of Tables

Table 1-1 The electrolytes used for Li-ion batteries.	8
Table 2-1 Materials and chemicals used in the research project.	54

Introduction

The use of fossil-based fuels in today's society as a source of energy supply has caused severe environmental pollution and global warming, while the limited supplies of fossil fuel have forced mankind to search for alternative sources. Green energy devices have demonstrated their capability to store and provide energy similar to coals and oils without the emission of pollution gas in the atmosphere. As one of the promising candidates in green energy devices, batteries have been investigated for centuries, and nowadays they have been employed in various applications to support daily lives and industries.

The lithium-ion (Li-ion) battery is one of the most popular green energy storage devices and it has dominated the battery market for the last few decades. However, the use of flammable electrolytes in the battery system could potentially cause safety issues, including leakage, fire, and even explosion. Additionally, based on the unique rocking-chair mechanism, the energy density of Li-ion batteries is acceptable for most small applications, such as cellphones and laptops. But due to its theoretical energy limitation, the conventional Li-ion battery could not meet all the requirements for large-scale applications such as electric vehicles. Among all the other promising new battery systems, the lithium-oxygen (Li-O₂) battery has been intensively studied owing to its extremely high theoretical energy density. Nevertheless, the sluggish kinetics of the battery reactions and rigid reaction environment make it difficult for actual industrial applications. The development of novel materials that either enhance the stability of the overall system or improve electrochemical performance is preferable. Organic materials have much potential as, theoretically, they can be tailored to fit most applications. Many approaches have been

made to develop efficient and powerful organic materials to enhance the properties of existing organic components in the batteries, including electrolytes, binders, and separators.

The main purpose of this thesis is to improve the electrochemical performances of Li-ion and Li-O₂ batteries by synthesizing and tailoring organic materials in the battery system. The outline of each chapter is listed below,

- ❖ Chapter 1 contains introductions of Li-ion batteries and Li-O₂ batteries. Recent progress in anode, cathode, electrolyte, and separators for both battery systems are reviewed. The organic components in these systems have been specifically investigated in this chapter as well.
- ❖ Chapter 2 provides the methodology of research applied in this thesis. The material preparation methods, physical characterization methods, the electrode preparation methods and electrochemical testing methods are all illustrated. The preparation methods were the breath-figure method for porous polymer membranes and general organic synthesis for other catalysts. Field emission scanning electron microscopy was used for investigating morphology and X-ray diffraction was employed to determine the crystal structures. Galvanostatic discharge and charge and a series of electrochemical characterizations, such as cyclic voltammetry, linear sweep voltammetry, and impedance spectroscopy were performed to evaluate the properties of as-prepared materials.
- ❖ Chapter 3 and 4 show the investigation of porous polymer membrane used in Li-ion batteries. In Chapter 3, a porous polymer membrane with highly ordered honeycomb-like structure based on poly(vinylidene fluoride-co-hexafluoropropylene) (PVDF-HFP) was prepared through the breath-figure method.

In Chapter 4, a poly(methyl methacrylate) (PMMA) combined with PVDF-HFP porous membrane forming a sandwich structure was prepared and investigated.

- ❖ Chapter 5 and 6 report the organic synthesis of materials based on the 2,2,6,6-tetramethylpiperidinyloxy (TEMPO) functional group for Li-O₂ batteries. In Chapter 5, poly(2,2,6,6-tetramethylpiperidinyloxy-4-yl methacrylate) (PTMA) was synthesized as bi-functional catalyst for Li-O₂ batteries. The mechanism is also investigated. In Chapter 6, a binder synthesized based on the co-polymerization of MMA and TMA monomers was investigated. The ratio between the moieties was investigated and mechanisms were revealed.
- ❖ Chapter 7 gives an investigation of tetrathiafulvalene (TTF), a redox mediator, in Li-O₂ batteries, by altering the functional mechanism of TTF. The influences of salt concentration and to the electrodes have been studied.
- ❖ Chapter 8 concludes this thesis, and provides a brief summary of the previous work on organic materials for lithium batteries and an outlook for future research.

Chapter 1 Literature reviews

1.1 Overview

The concept of employing energy storage devices has been created for thousands of years. In the last few decades this concept has drawn increasingly intense attractions, owing to the fact that the depletion of fossil fuel-based energy sources such as coal and oil, is becoming severe. Fossil fuels have been used for centuries as one of the most reliable energy resources due to the large quantity of potential energy released during consumption. However, due to limited sources of fossil-originated coal and oil, and the pollution caused by CO₂ and other waste gas emission, more sustainable and environmentally friendly energy storage and convention systems are urgently needed. Electrochemical devices including supercapacitors, fuel cells, and batteries are employed to solve the problems raised by using fossil-based fuels. Battery systems are considered one of the perfect candidates for next-generation energy storage devices. The first recorded battery was reported in 1800 by Alessandro Volta, which is known as the Voltaic Pile. The battery contained a stack of alternating zinc and copper discs are separated by a cloth soaked with brine. Since then, many forms of batteries based on different new chemistries have been introduced and developed, shown in the timeline in Figure 1-1.

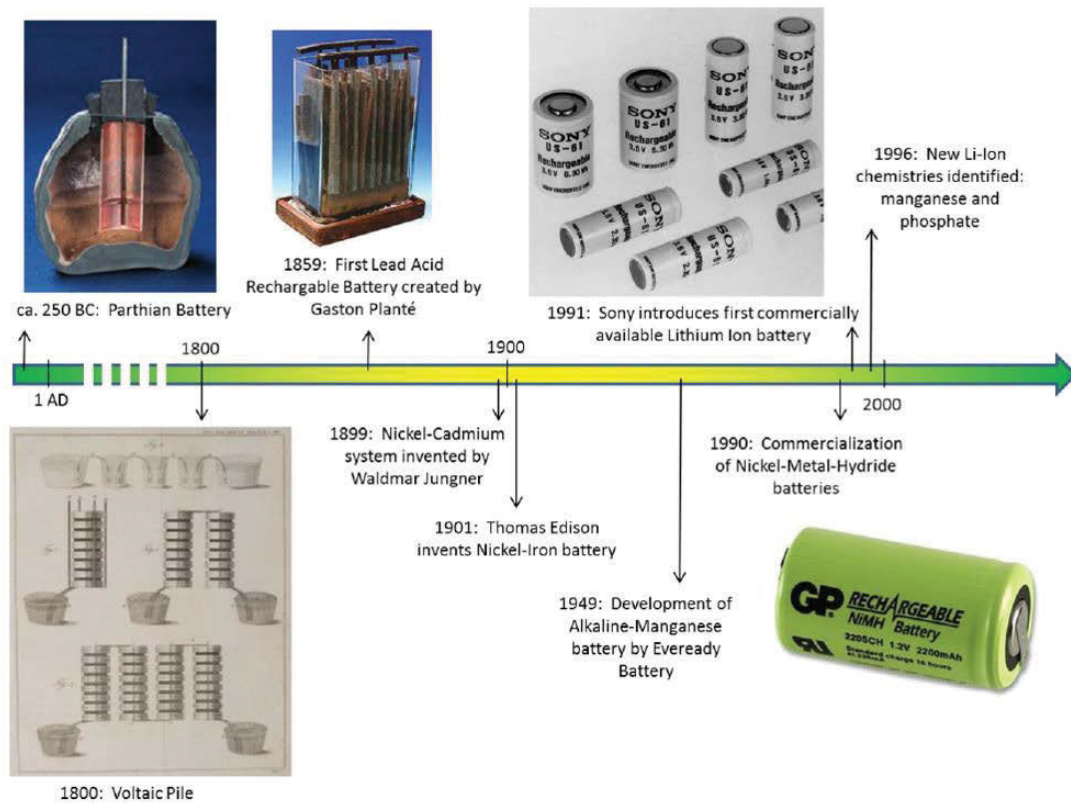


Figure 1-1 The timeline of battery evolution.^[1]

Lithium ion (Li-ion) batteries have proven themselves to be one of the most advanced energy storage devices for portable electronics such as laptops and cellphones, in the past few decades due to their relatively high energy and power densities.^[2-4] Recently, Li-ion battery has been developed as the power devices for electric vehicles and hybrid electric vehicles, in the aim of reducing air pollution and global warming.^[5] However, the current generation of Li-ion batteries does not fully meet the requirements in today's society. Therefore, great efforts should be devoted to increasing the electrochemical performances of the existing Li-ion batteries. Or as an alternative route, batteries based on new chemistries should be developed to fulfill the energy requirements.^[3] Figure 1-2 shows the theoretical and practical energy density of different batteries. As shown, the energy density

of current commercial Li-ion batteries is around 200 Wh kg⁻¹, which is significantly higher than of conventional lead-acid and Ni-Cd batteries. However, further improvement is still required to replace gasoline for vehicles. Lithium air batteries or lithium oxygen (Li-O₂) batteries, on the other hand, provide a theoretical energy density of 11680 Wh kg⁻¹ (based on lithium metal only). Even a practical energy density of 1700 Wh kg⁻¹ is still favorable for large electric devices. Therefore, to power up future electric devices including electric vehicles, a highly efficient battery system, such as new lithium ion and lithium oxygen batteries is urgently needed.

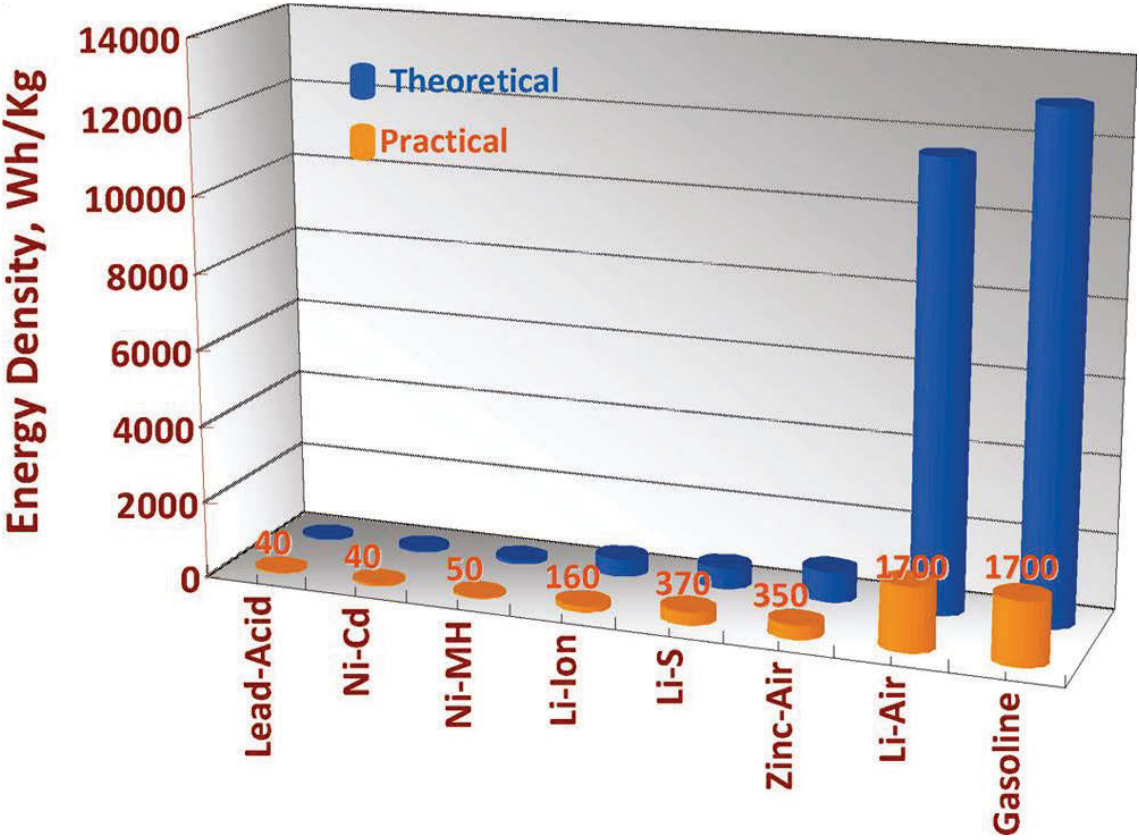


Figure 1-2 The gravimetric energy density of commonly used rechargeable batteries.^[6]

1.2 Lithium ion (Li-ion) batteries

1.2.1 History of Li-ion batteries

The introduction of rechargeable Li-ion batteries occurred in the early 1990s, when a major breakthrough was made in battery evolution. Since then, Li-ion batteries have been dominating the power supply market for portable devices for the past two decades. However, despite the increasingly demand for high power sources, the development of Li-ion batteries is still far from satisfactory. Gamble et al. discovered the ion intercalation chemistry in layered dichalcogenides by a large range of electron donating molecules in the 1970s.^[7] Among all the dichalcogenides, titanium disulfide (TiS_2) was considered the most promising electrode candidate.^[8-10] By coordinating with Li^+ , its structure forms a single phase Li_xTiS_2 ($0 \leq x \leq 1$) covering the entire composition range.^[11, 12] However, despite its relatively high conductivity, low over-potential and high cost of the TiS_2 make it difficult for commercialization.^[13] Alternatively, layered metal oxides have been intensive studied since they possess similar lithium intercalation behavior. Vanadium pentoxides (V_2O_5), among these, have been mostly investigated. However, it has been demonstrated not to be suitable for Li-ion batteries due to its complex phase transition during lithium intercalations.^[14-16] Goodenough discovered LiCoO_2 as suitable electrode material for Li-ion batteries due to its resembling layer structure of dichalcogenides. The intercalation and extraction of Li^+ are found highly reversible, which makes it promising for long term cycling in Li-ion batteries.^[17, 18] Meanwhile, Yazami et al. reported the reversible lithium intercalation into graphite to form LiC_6 .^[19] This reaction can eliminate the growth of lithium dendrite, improving safety issues caused by short-circuiting. Thus, combining

LiCoO₂ as the cathode material and graphite as the anode material, the Li-ion battery system was finally commercialized by SONY after more than 20 years of development.^[20]

1.2.2 Basic concepts and designs for Li-ion batteries

A rechargeable Li-ion battery is designed based on reversible lithium intercalation and extraction reactions. A typical Li-ion battery consists of an anode (negative electrode), a cathode (positive electrode), and a porous membrane soaked in a liquid electrolyte. Generally, a lithium metal oxide with a layered structure is used as the cathode and graphite is employed as the anode. The liquid electrolyte is a solution of a lithium salt in organic solvents. To maintain the mechanical integrity of the Li-ion battery, a separator is usually needed to separate the anode and cathode while providing sufficient ionic conductivity. A schematic illustration of the battery configuration is shown in Figure 1-3. The discharge-charge mechanism of a Li-ion battery is based on a “rocking chair” process, where Li⁺ is extracted from the anode, passes through the electrolyte, and intercalates into the cathode during discharge, and reverses during charge. The electrons pass through the external wires to close the circuit.

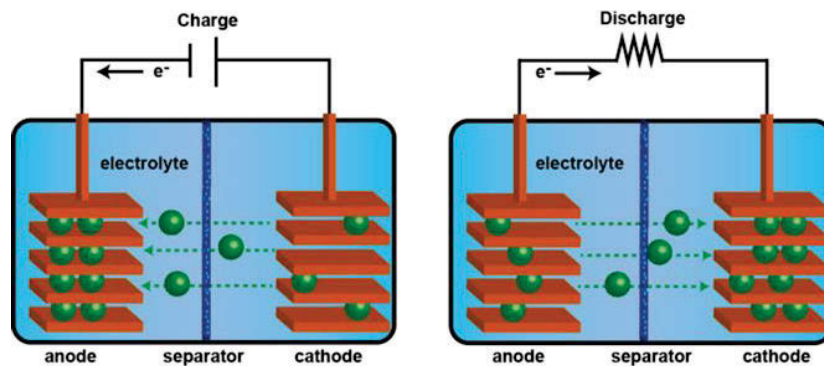
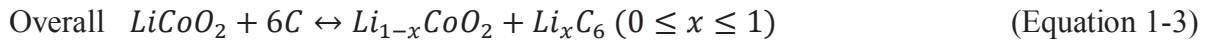
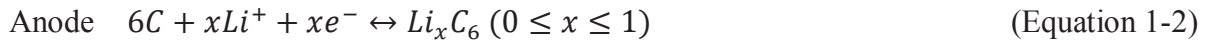
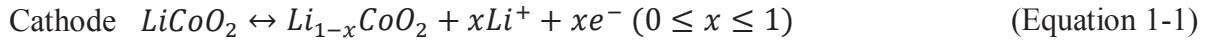


Figure 1-3 Schematic illustration of the rocking chair mechanism during discharge and charge.^[21]

The electrochemical reactions of the Li-ion battery when the LiCoO₂/graphite configuration is used:^[22]



1.2.2.1 Electrode

Electrodes are fabricated by pasting complex materials to the corresponding current collectors (copper foil for the anode and aluminum foil for the cathode). Generally, the electrode materials consist of active materials, conducting additives, and binders. The active materials are the materials (eg. LiCoO₂ for cathode and graphite for anode) that undergo reversible intercalation reactions during discharge and charge. Conductive additives are conductive materials (eg. carbon black) added to enhance the overall conductivity since some of the active materials provide poor electronic conductivity. The binders are a group of polymers with a long molecular chain structure that enables them to hold the electrode materials on the current collectors.

1.2.2.2 Active materials

The active materials are the materials that are involved in the battery reactions within the battery during discharge and charge. Generally, a material with a relative potential higher than 2 V vs. Li⁺/Li is defined as a cathode, while a material with a relative potential lower than 2 V vs. Li⁺/Li is defined as an anode.^[23] The potential ranges and specific capacities of different electrode materials are listed in Figure 1-4.

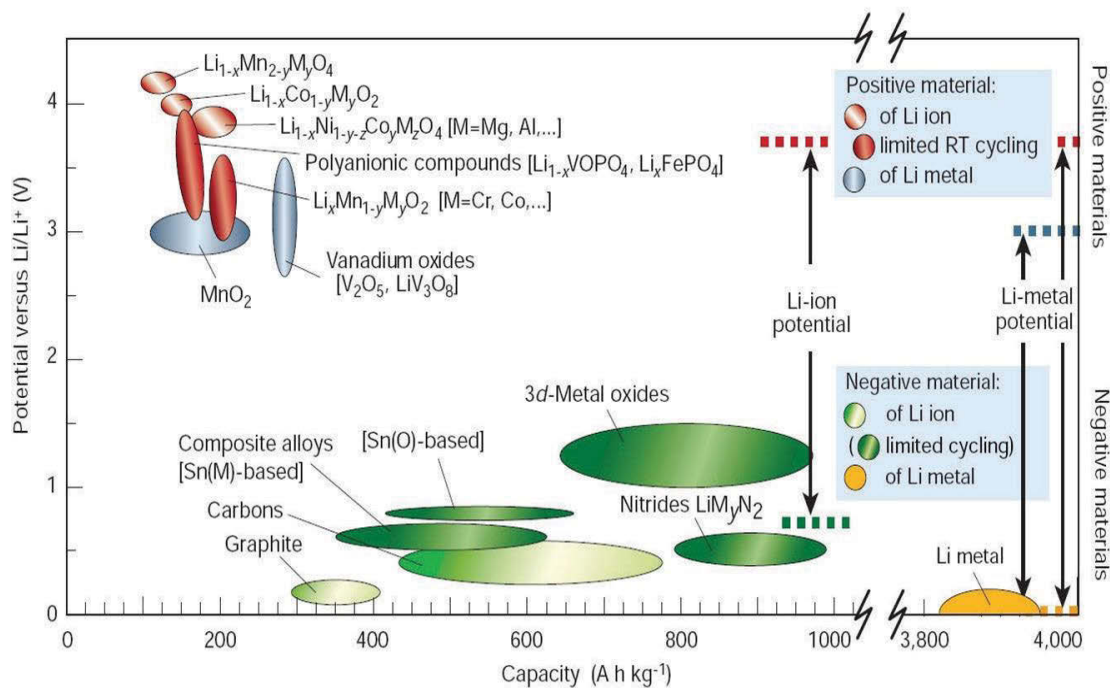


Figure 1-4 The potential ranges vs. Li^+/Li and specific capacities of electrode materials for Li-ion batteries.^[24]

1.2.2.3 Electrolyte

The electrolytes are ionic conductors which provide sole ionic conductivity to connect both cathode and anode in Li-ion batteries. The electrolytes for Li-ion batteries generally consist of two components, lithium salts and solvents. The lithium salts dissolved in the solvents are the main lithium source for the intercalation and extraction in the electrodes while the solvents provide a pathway for Li^+ diffusion. Commonly used electrolytes in Li-ion batteries are mainly non-aqueous electrolytes, including organic liquid electrolytes, ionic liquid electrolytes, inorganic liquid electrolytes, solid polymer electrolytes, inorganic solid electrolytes, and hybrid electrolytes.^[25-47] A list of reported electrolytes with different compositions is shown in Table 1-1.

Table 1-1 The electrolytes used for Li-ion batteries.^[48]

Electrolytes	Examples of classical electrolytes	Ionic conductivity ($10^{-3} \text{ s cm}^{-1}$) at room temperature	Electrochemical window (V) vs. Li^+/Li		Remarks
			Reduction	Oxidation	
Organic liquid	1M LiPF_6 in EC:DEC (1:1)	7	1.3	4.5	Flammable
	1M LiPF_6 in EC:DMC (1:1)	10	1.3	>5.0	
Ionic liquids	1 M LiTFSI in EMI-TFSI	2.0	1	5.3	Non-flammable
	1M LiBF_4 in EMI- BF_4	8.0	0.9	5.3	
Polymer	$\text{LiTFSI-P(EO/MEEGE)}$	0.1	<0.0	4.7	Flammable
	$\text{LiClO}_4\text{-PEO}_8 + 10 \text{ wt } \% \text{ TiO}_2$	0.02	<0.0	5.0	
Inorganic solid	$\text{Li}_{4-x}\text{Ge}_{1-x}\text{P}_x\text{S}_4$ ($x = 0.75$)	2.2	<0.0	>5.0	Non-flammable
	$0.05\text{Li}_4\text{SiO}_4 + 0.57\text{Li}_2\text{S} + 0.38\text{SiS}_2$	1.0	<0.0	>8.0	
Inorganic liquid	$\text{LiAlCl}_4 + \text{SO}_2$	70	-	4.4	Non-flammable
Liquid organic + polymer	$0.04\text{LiPF}_6 + 0.2\text{EC} + 0.62\text{DMC} + 0.14\text{PAN}$	4.2	-	4.4	Flammable
	$\text{LiClO}_4 + \text{EC} + \text{PC} + \text{PVdF}$	3.0	-	5.0	
Ionic liquid + polymer	1M $\text{LiTFSI} + \text{P}_{13}\text{TFSI} + \text{PVdF-HFP}$	0.18	<0.0	5.8	Less flammable
Ionic liquid + polymer + liquid	56 wt% $\text{LiTFSI-Py}_{24}\text{TFSI} +$	0.81	1.5	4.2	Less flammable
	30 wt% $\text{PVdF-HFP} +$				
Polymer + inorganic solid	14 wt% EC/PC	0.03	<0.0	>4.5	Non-flammable
	2 vol% $\text{LiClO}_4\text{-TEC-19} +$				
	98 vol% $95 (0.6\text{Li}_2\text{S} + 0.4\text{Li}_2\text{S}) + 5\text{Li}_4\text{SiO}_4$				

Based on the references, the electrolytes should fulfill a series of requirements before being employed in Li-ion batteries:^[48, 49]

1. High Li^+ conductivity (usually $> 10^{-4} \text{ S cm}^{-1}$) and low electric conductivity (preferable $< 10^{-10} \text{ S cm}^{-1}$) over the entire temperature range of battery operation.
2. High thermodynamic stability window ($\geq 4 \text{ V}$)
3. Capable to retain the electrode/electrolyte interfaces during discharge and charge when the electrode particles are changing their volume.
4. A transference number $\sigma_{\text{Li}^+}/\sigma_{\text{total}} \approx 1$, where σ_{total} includes conductivities by other ions in the electrolytes as well as σ_{Li^+} and σ_{e^-} .
5. Good chemical stability at temperatures and voltages over the entire battery operation ranges.
6. Good chemical stability towards electrode materials, including the capability to rapidly form a passivating solid/electrolyte interface (SEI).
7. Good safety properties such as non-flammability and non-explosiveness.
8. Low toxicity and cost.

Theoretically, it is preferable to have all the properties listed above. However, it is a great challenge to meet all these requirements. Therefore, so far most of the reports are mainly focusing on several critical properties that could enhance the overall electrochemical performances.

1.2.2.4 Separator

The separators are a group of porous membranes (mostly polymer membranes) that serve as physical barrier to separate the anode and cathode while providing sufficient

mechanical support for the liquid electrolyte within. Basically, the separators have to be permeable to ions and inert in the battery environment. So far, the most commonly used porous membranes in Li-ion batteries are polyolefins, including polyethylene (PE), polypropylene (PP), and laminates of PE and PP. These porous membranes can provide excellent chemical stability, mechanical properties, and low cost.^[50]

1.2.2.5 Electrochemical terms

1. Cell potential: The theoretical potential of the cell depends on the active materials used in the cell. It can be calculated from free-energy data or the standard electrode potentials which can be found in Figure 1-4. The open circuit voltage is the potential difference between the cathode and anode and is usually close to the theoretical voltage.

2. Discharge-charge: When the cell is connected to an external load, electrons flow from the anode through the external circuit to the cathode. Meanwhile, the electric circuit is closed in the electrolyte by the flow of anions and cations to the anode and cathode respectively. This process is defined as discharge process. During the charge process, the current flow is reversed.

3. Specific capacity: The amount of electric charge the cell can store per unit mass. The theoretical specific capacity (Ah g^{-1}) is calculated by the electrode reactions according to the Faraday equation:

$$Q_s = n \times F/M \quad \text{(Equation 1-4)}$$

Where Q_s is the specific capacity (Ah g^{-1}), n is the number of electrons transferred during battery reactions, F is the Faraday constant ($96485.33 \text{ C mol}^{-1}$), and M is the molecular weight of the active material (g mol^{-1}).

The discharge-charge specific capacity during galvanostatic discharge-charge can be calculated by the equation below:

$$Q = I \times t/m \quad (\text{Equation 1-5})$$

Where Q is the discharge-charge specific capacity (Ah g^{-1}), I is the current (A), t is the time (s), and m is the mass of the active material (g).

4. Specific energy: It is defined as the energy per unit mass. The specific energy (SE, Wh kg^{-1}) is calculated by the equation shown below:

$$SE = (E \times Q)/1000 \quad (\text{Equation 1-6})$$

5. Energy density: It is defined as the amount of energy stored. The energy density (ED, Wh L^{-1}) can be calculated by the equation below:

$$ED = (E \times Q \times m)/(1000 \times V) \quad (\text{Equation 1-7})$$

6. Specific power: It is defined as the capability of the battery to deliver power per unit mass. The specific power (SP, Wh kg^{-1}) can be calculated from the following equation:

$$SP = SE/t \quad (\text{Equation 1-8})$$

7. Power density: It is a term used for the capability of the battery to deliver power per unit volume. It can be calculated by the equation shown below,

$$PD = ED/t \quad (\text{Equation 1-9})$$

8. Coulombic efficiency: The coulombic efficiency (η) of a battery is the ratio of the charge capacity (Q_c) to the discharge capacity (Q_d). The coulombic efficiency can be calculated through the equation shown below:

$$\eta = Q_c/Q_d \times 100\% \quad (\text{Equation 1-10})$$

9. Irreversible capacity: The irreversible capacity (Q_I) is defined as the capacity loss during each cycle

$$\text{For cathode materials: } Q_I = n^{th}Q_d - n^{th}Q_c \quad (\text{Equation 1-11})$$

$$\text{For anode materials: } Q_I = n^{th}Q_c - n^{th}Q_d \quad (\text{Equation 1-12})$$

10. C-rate: C-rate is introduced to indicate the discharge-charge current of a battery, which can be calculated as follows:

$$I = C \times Q_s \quad (\text{Equation 1-13})$$

Where I is the current (A), Q_s is the theoretical specific capacity of the active material (Ah g^{-1}). A battery discharge-charge at 1 C rate represents 1 hour charge and discharge of the battery to its cut-off voltage.

1.2.3 Overall criteria for commercial Li-ion battery systems

A commercial Li-ion battery system requires the following criteria:^[23, 51]

1. The reactants employed in the battery must be able to provide a sufficient current and voltage for normal battery operation. The normal energy density for a Li-ion battery is between 100 and 150 Wh L⁻¹.

2. The battery operation temperature should be in the range of 0-40 °C and the storage temperature of a battery should be in the range of -20 to 85 °C.

3. The materials should be chemically and mechanically stable in the battery operation environment during cycling to avoid any unwanted side-reaction between the materials used or irreversible phase change.

4. A general commercial battery must be able to discharge and charge completely over 300 cycles with a capacity loss of less than 20 %. The cycle life requirement increases to 2000 cycles if it is applied to automotive applications.

5. The cost of a general commercial Li-ion battery should not be over-expensive for the consumers.

6. All commercial batteries must be safe in the normal operating environment. Additionally, they should neither release any hazardous materials, nor present any hazard under mild abuse conditions.

1.2.4 Organic Electrolytes for Li-ion batteries

The electrolyte component is often considered critical as it separates the electrodes and serves as a lithium ion transport medium. In this way, the electrolyte is usually known as a separator between electrodes in lithium-ion batteries. The separator is constituted by a porous polymer membrane matrix soaked by the liquid electrolyte solution consisting of

lithium salts and solvents. The liquid solvents are required to meet a series of conditions which is not easy to accomplish. The ideal solvents for the use as electrolyte should possess several characteristics such as high dielectric constant for dissolving high salt concentrations, low viscosity for improving ion transportation, inert towards all cell components, and liquid state in a wide temperature range. Therefore the most used solvents belong to organic esters and ethers, such as ethylene carbonate (EC), propylene carbonate (PC), dimethyl carbonate (DMC), diethyl carbonate (DEC), and ethyl methyl carbonate (EMC). It is also possible to directly incorporate lithium salts into the polymer matrix, known as solid polymer electrolyte.

Comparing to active dynamics of the electrode research, the development of electrolyte in the lithium ion batteries did not proceed rapidly in the last few decades. Possible reasons for this statement should be attributed to the following factors.^[52]

1. Electrolyte components are more sensitive towards the operating potential window; therefore, the choices of electrolyte candidates are limited. As long as carbonate-based electrolytes can fulfil the requirements of the given electrode materials, a change of electrolyte is not mandatory.

2. More research aiming at designing and using electrolyte additives has been intensively studied to obtain more fundamental knowledge of solid electrolyte interphases (SEI) formed on the electrode surfaces. Therefore the skeleton of electrolyte is not mandatory required as long the artificial sacrificial components contribute to the overall electrolyte.

3. Considering an actual application in the battery industry, cost efficiency limits the battery industry to replace the existing electrolyte unless it is not suitable for the further battery systems.

Although little has changed in the composition of electrolytes for Li-ion batteries during the past decades, major advances have been made in order to understand the electrolyte bulk properties, such as the existence and movement for Li^+ in bulk electrolyte, the interphases formed at both electrode surfaces, and Li^+ transportation across these interphases.

1.2.4.1 Ion transport

Ionic conductivity of the electrolyte is a key property as it quantifies the mobility of ions for the electrochemical reactions, which determines the power output of the cell. The ionic conductivity of the commonly used non-aqueous electrolyte for Li-ion batteries is usually provided by dissolving suitable lithium salts in organic solvents, specifically carbonate ester solvents. So far, there has not been a single solvent available that possesses high dielectric permittivity and low viscosity, while still meeting the requirements of interfacial stability on both electrodes. Therefore as a compromise, mixed solvents are used to enhance the overall viscosity and dielectric permittivity at the same time. EC has been used as solvent with high dielectric permittivity, which functions as an indispensable ingredient in electrolytes of most Li-ion batteries, and various acyclic carbonates or carboxylic esters, such as DMC, DEC, and EMC, are used to increase the bulk properties. The ionic conductivity of the state-of-art non-aqueous electrolytes can reach the level of 5-10 mS cm^{-1} at ambient temperature, and support the routine cell operations in the temperature range of -30 to 60 °C.

To better understand the transportation of Li^+ , Ding et al. tried to reveal the factors that affect the ionic conductivity in mixed solvent systems, including cation and anion species and their interactions, solvents with different dielectric permittivity, viscosities, and glass transition temperatures.^[53, 54] They found that the cation solvated with solvent molecules plays a dominant role in determining its mobility, while anion influences their properties by forming ion pairs with cations. These results explain why lithium salts have lower conductivity than their tetraalkyl ammonium counterparts in the same non-aqueous solvents. Aihara et al. also used a pulse-gradient spin-echo NMR technique to monitor the diffusivity of Li^+ , six different anions including PF_6^- , tetrafluoroborate (BF_4^-), triflate (CF_3SO_3^-), bis(trifluoromethanesulfonyl)imide (TFSI), bis(pentafluoroethanesulfonyl)imide (BETI), and bis(oxalato)borate (BOB), and a single solvent γ -butyrolactone (GBL).^[55] They conclude that Li^+ moves the slowest, while GBL moves the fastest, as shown in Figure 1-5. They claim that the speed of Li^+ is limited by its association with the solvent molecules, and the speed of anions is somehow unchanged because they remain almost unsolvated.

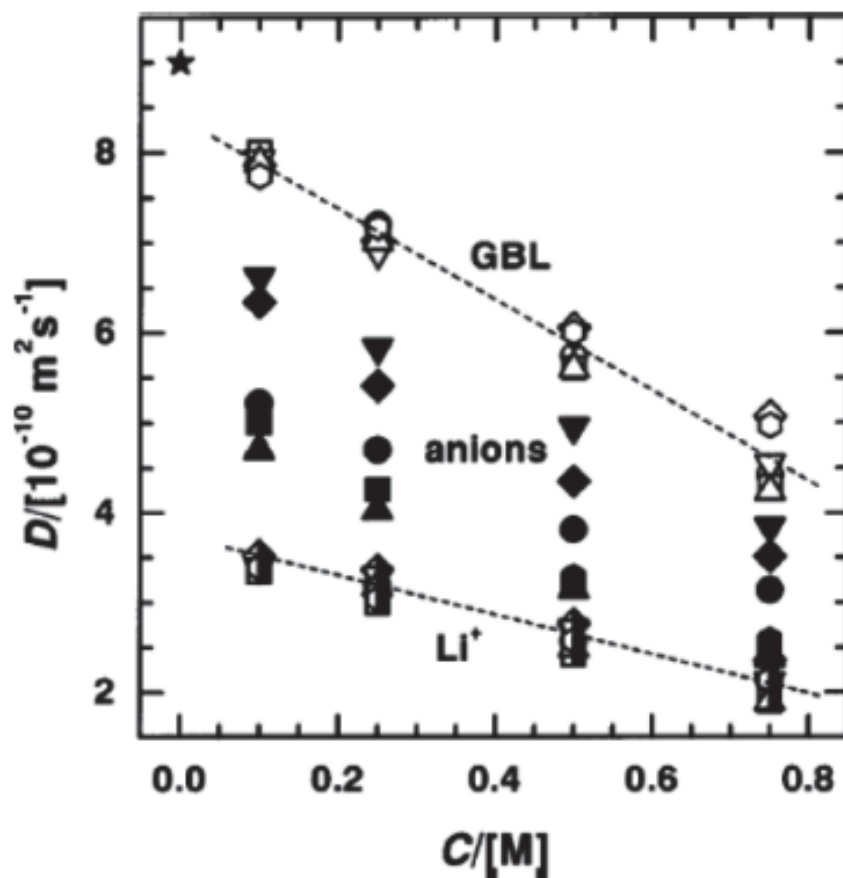


Figure 1-5 Comparison of self-diffusivities for Li^+ , counter-anions, and solvent molecules and their dependences on salt concentration. The asterisk at 0 M represents the D_{GBL} of neat GBL.^[55]

The solvents used in Li-ion batteries also play important roles in ionic conductivity. In order to achieve optimal properties of electrolyte, mixed solvent system are often employed. However, choosing the right combination becomes intensively difficult due to the variety of solvents that can be used. To generate a complete conductivity contour map, the combination of temperature, solvent components, salt species, and concentration must be fully investigated.^[56, 57]

Ion transference number is also an important factor besides the ionic conductivity, especially in polymer-based electrolyte systems. The ion transference number is used to quantify the fraction of ionic conductivity which is useful to the battery reactions. However, the measurement of the ion transference number is difficult to establish because it is different from the well-defined measurement of ionic conductivity. Zugmann et al. have concluded that four methods have been mainly employed to determine the ion transference numbers and the variations are consequences of different assumptions and constraints applied to establish these individual methods.^[58]

1.2.4.2 Li⁺ solvation

There are two most commonly used interaction systems of lithium salts and non-aqueous electrolyte solvents, namely conventional solutions and highly concentrated solutions. The conventional solutions include lithium salt whose concentration is around 1.0 M while the highly concentrated solutions have lithium salts of comparable molarities with the solvent molecules. Different from the conventional solutions, the highly concentrated electrolytes are considered as something between the neat ionic liquids and the conventional electrolyte solutions.

1.2.4.3 Li⁺-solvent interaction

The lithium salt dissolved in non-aqueous solvents ionizes into cation and anion, and the interaction of cation and solvent molecule is more significant than that of anion and solvent molecule.^[59] As Li⁺ is the second smallest cation, it is expected that its binding capability to nucleophilic sites on solvent molecules is significantly stronger than other metal cations. Further investigation shows that in most carbonate-based electrolytes, Li⁺

binds to the carbonyl oxygen of carbonates, as shown in Figure 1-6. And the coordination number of Li^+ in the electrolyte is around 4-6, based on the salt concentration, dissociation vs. ion-pairing, and dielectric constant of the solvents.^[59]

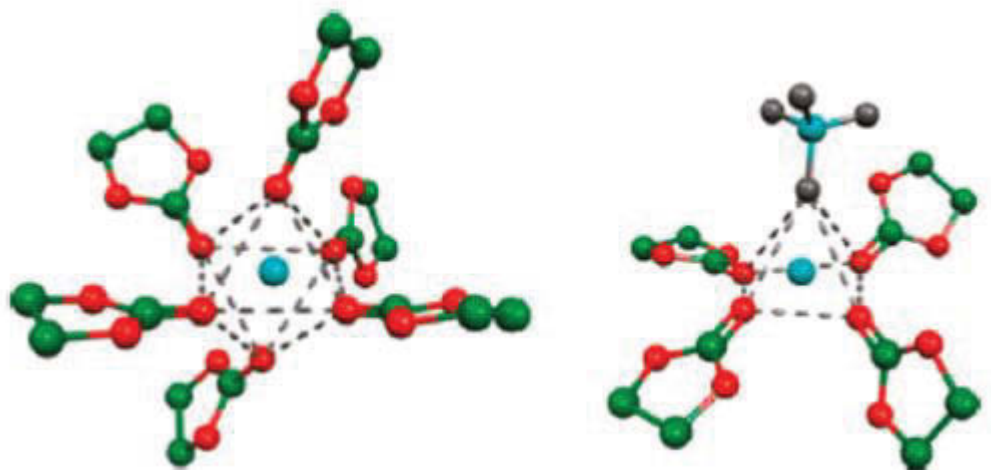


Figure 1-6 Schematic illustrations of the primary solvation sheath of Li^+ in 0.1 M LiBF_4 solution in EC-DMC (1-1) with different coordination numbers based on MD simulation of LiBF_4 in EC/DMC.^[60]

1.2.4.4 Solvents

Solvents are used to dissolve lithium salt while providing a safe environment for battery reactions. Therefore in order to be used in Li-ion batteries, they have to be polar enough to dissociate the lithium salts and electrochemically stable in the normal operation potential range (usually 0-5.0 V vs. Li). In commercial Li-ion batteries, aprotic organic solvents such as organic esters are often selected due to their high resistance towards battery components. However, to achieve better electrochemical performances and safer operating environments, efforts are still being made to replace these existent candidates.^[52]

1. Carbonates: Organic carbonate esters are the most common electrolyte solvents used in commercial Li-ion batteries. However, despite their significant resistance towards the oxidation reactions at the cathode side, they usually have little stability for the anode materials when operated at low potentials, especially for graphitic anodes. The result is the formation of a SEI layer to prevent further reactions. Further improvements were made by altering the molecular structures of the carbonates. Vetter et al. studied various acyclic carbonates with different degrees of chain branching and found that high degree usually results in higher reversible capability and longer cycle life when a graphitic anode is used, although lower ionic conductivity is shown due to the high viscosity.^[61, 62] Cyclic carbonates have also been investigated because of their relatively high resistance towards the graphitic anode.^[62] So far, the mixture of EC, DMC, and DEC has been demonstrated as the most favourable choice for Li-ion batteries with exceptional electrochemical performances.

2. Sulfones and sulfoxides: Different from carbonates, alkyl sulfones were not compatible with graphitic anode due to their inability to form protection interfaces. Their ionic conductivities were relatively low, as well as their wettability towards other battery components, despite their superiorly high dielectric permittivity, low flammability, and high stability towards most cathode materials.^[63-66] Abouimrane et al. reported that the electrochemical stability of sulfones at high voltage makes them suitable for most high voltage cathodes, such as LiMn_2O_4 , $\text{LiNi}_{0.5}\text{Mn}_{1.5}\text{O}_4$.^[67] Mixtures of sulfones and carbonates were reported by Angell et al. shown in Figure 1-7 where the viscosity could be significantly reduced, and the battery functioned well at temperatures higher than 55 °C, while the ionic conductivity dropped quickly at lower temperatures.^[68]

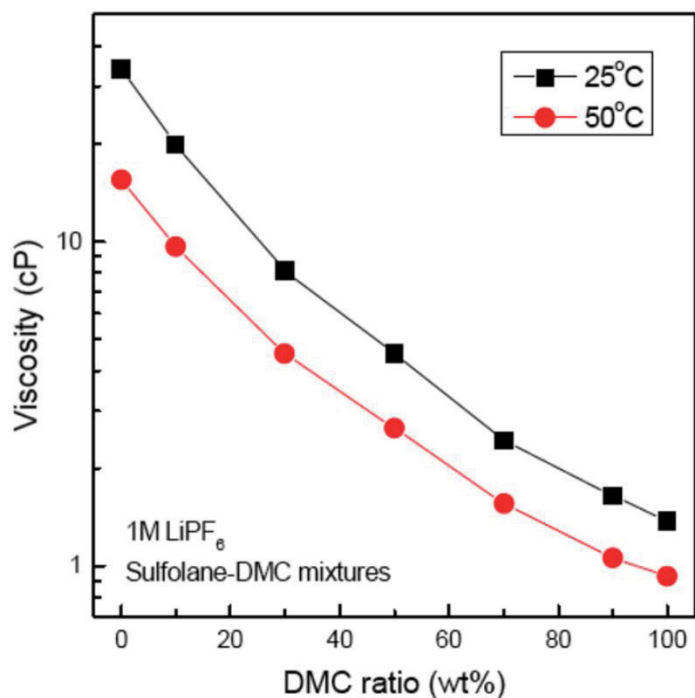


Figure 1-7 Viscosity versus cosolvent content plots for sulfolane–binary solutions: sulfolane + dimethylcarbonate.^[68]

Sulfoxides showed intrinsically less stability than the sulfones due to their insufficient oxidation state (4 vs. 6).^[52] Dimethyl sulfoxide (DMSO) is the most commonly used sulfoxide in the application of Li-ion batteries. Sirenko et al. discovered that the combination of DMSO and lithium perchlorate (LiClO_4) could provide extremely high ionic conductivity despite the fact that DMSO could induce additional oxidation side-reaction when LiMnO_2 and V_2O_5 electrodes were used.^[69] Additionally, DMSO molecules were known for their capability to co-intercalate with Li^+ into graphite to form stable ternary compounds.^[70] This result would surely disqualify DMSO as an electrolyte solvent for some applications.

3. Nitriles: Nitriles have been investigated as solvents for Li-ion batteries due to their high ionic conductivities.^[71-76] Acetonitrile, as one of the representatives, has been widely used, only second to carbonate esters. Apparently, the low viscosity and decent dielectric permittivity ensure a high ionic conductivity and compatibility with most electrode materials. However, the relatively low electrochemical stability window often limits its actual applications.

Besides acetonitrile, a great number of nitriles have been explored as electrolyte solvents. Alkoxy-substituted nitriles were the most reported solvents in this aspect. It has been demonstrated that the use of these nitriles leads not to the formation of SEI layers unless VC or FEC is added. Therefore they are not suitable for graphite anodes solely.

4. Ethers: Ether-based electrolytes have been widely used in various applications. Surprisingly, seldom reports have been recognized when organic ethers were used as solvents for Li-ion batteries. It is probably due to the instability of most ethers at round 4 V.^[77] Fluorinated ethers, however, have been demonstrated to facilitate LiCoO₂ cathodes with no obvious performance decay.^[78] Naoi et al. reported that different degrees of fluorination contributed differently to the overall properties, such as fire-retardance, and rate capabilities.^[79, 80] Additionally, some ether species could actually be beneficial for anodic stabilities.

5. Phosphorus and silicon: Different from the organic solvents mentioned above, phosphorus and silicon-based solvents are known for their fire retardance. Phosphorus-based solvents are often used as non-flammable co-solvents to improve the safety of Li-ion batteries. Lucht et al. discovered that dimethyl methylphosphonate, one of the phosphorus

families, could not only prevent fire and explosion, but also function as a high voltage additive.^[81-84] Additionally, capacity retention was also reported improving.^[83] Further characterization techniques indicated that the presence of phosphorus solvents resulted in the inhibition of electrolyte oxidative decomposition at the cathode side. However, similar to sulfones and nitriles, phosphorus were not able to form stable protective SEI layers on graphite electrode unless VC or FEC were added (Figure 1-8).^[83]

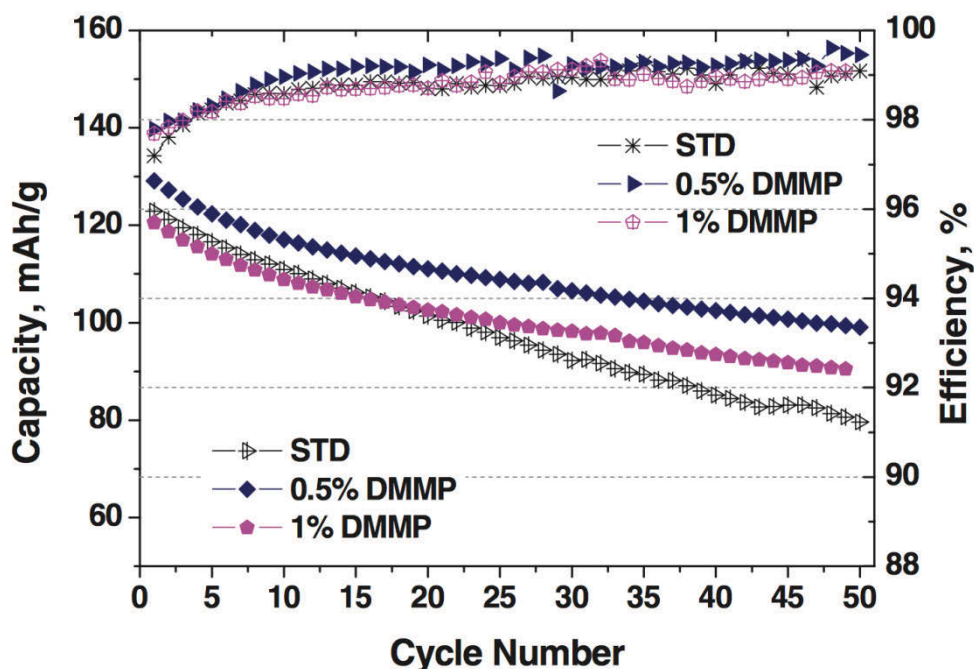
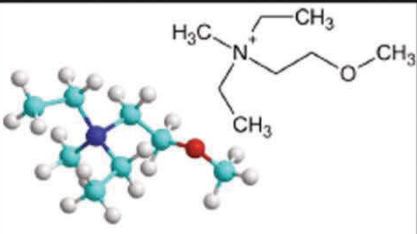
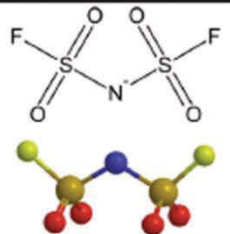
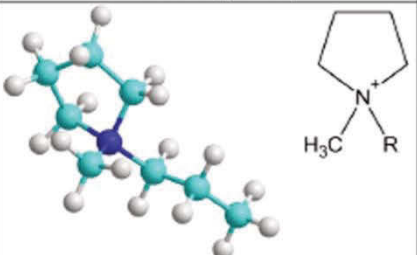
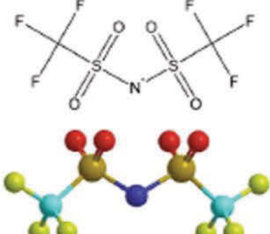
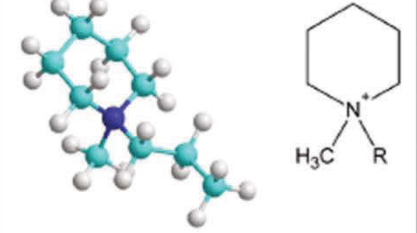
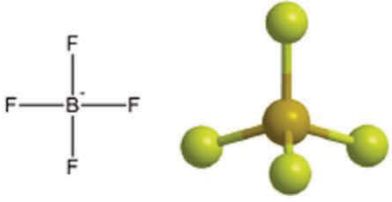
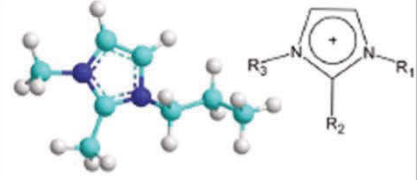
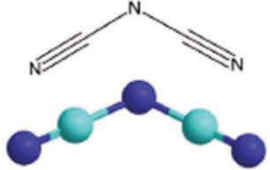


Figure 1-8 Cycling performance of Li/LiNi_{0.5}Mn_{1.5}O₄ cells with standard (STD) and DMMP containing electrolyte.^[83]

The application of silicon-based solvents is limited by their low solvation towards lithium salts. Therefore, the intrinsic ionic conductivity is relatively low when employed. A series of oligosiloxanes and silanes with functional moieties were synthesized by Amine

and Zhang et al. to reach acceptable ionic conductivities.^[85-88] They also discovered that LiBOB was preferred over the commonly used LiTFSI and LiPF₆ in the silicon system.

6. Ionic liquids: Ionic liquids are a group of solvents that consist of cations and anions in molten states.^[59] There are no “solvent molecules” present in the system. The first report of a simple triethylammonium nitrate as a pure ionic liquid was published more than a century ago.^[89] In Li-ion batteries, the commonly used ionic liquids are non-lithium room temperature ionic liquids, which remain the liquid state at room temperature.^[90] The most popular cations are quaternary ammoniums, including imidazolium, pyridinium, pyrrolidinium, and other ammonium-based cations (Figure 1-9).^[91-96] They usually consist of heterocyclic structures while conjugation is not intrinsically necessary. Lithium salt is often added at sufficient concentration as the Li⁺-conductive source. Different from the regular lithium electrolyte with molecular solvents, the Li⁺ conductivity is just a small fraction of the overall conductivity.^[52] Meanwhile, the use of anions as the counterpart of large cations also influences the overall electrochemical properties of the corresponding ionic liquid.

Cations	Anions
 <p><i>N,N</i>-diethyl-<i>N</i>-methyl-<i>N</i>-(2-methoxyethyl) ammonium, [DEME]⁺</p>	 <p>Bis(fluorosulfonyl)imide, [FSI]⁻</p>
 <p><i>N</i>-methyl-<i>N</i>-alkyl pyrrolidinium, [C_nmpyr]⁺</p>	 <p>Bis(trifluoromethanesulfonyl)amide, [NTf₂]⁻</p>
 <p><i>N</i>-methyl-<i>N</i>-alkyl piperidinium, [C_nmpip]⁺</p>	 <p>Tetrafluoroborate, [BF₄]⁻</p>
 <p>1,2-dialkyl methylimidazolium, C_nC_nmim⁺</p>	 <p>Dicyanamide, [dca]⁻</p>

* R groups – typically ethyl, propyl, butyl.

this compound (along with many other nitrogen centered anions) is described as an "amide" in the inorganic literature, but incorrectly as an "imide" in the materials and electrochemical literature. FSI should also be described as an amide (ie FSA) but that is so uncommon in this field that we have retained FSI in this article.

Figure 1-9 Common ionic liquids ion families utilized in lithium-ion batteries.^[97]

The application of ionic liquids in Li-ion batteries is first hindered by its incapability to form a stable SEI layer. However, with the development of ionic liquids with different structures, the use of ionic liquids, especially pyrrolidinium-based ones, is enabled in the Li-ion batteries.^[98, 99] Ionic liquids are mainly employed because of their non-flammability and

stability, both thermal and electrochemical.^[96] Much effort has been made in order to create ionic liquids with low viscosity and high ionic conductivity.

1.2.4.5 Lithium salts

The lithium salts used in Li-ion batteries are the main source in the electrolyte to provide Li^+ for battery reactions. The combination of appropriate lithium salts and solvents results in solvation of Li^+ , thus ensures the Li^+ ionic conduction between anodes and cathodes. LiPF_6 is one of the most used lithium salts in the majority of Li-ion batteries, due to its capability of providing sufficient ionic conductivity.^[100] Nevertheless, the use of LiPF_6 in Li-ion batteries sometimes induces additional issues owing to its instability towards high temperature as well as rigid chemical reactions.^[52] To overcome these issues, new types of lithium salts have been developed.

Borate-based lithium salts, especially LiBF_4 , are known to be the second famous salts used in Li-ion batteries. However, the relatively low solubility of LiBF_4 in carbonate electrolytes limits its expanded applications. Similar issues are spotted when LiBOB is used. Although it suffers from low solubility as well as low anodic stability, its compatibility with LiFePO_4 and most polymers has won its place in some battery applications (Figure 1-10).^[101, 102]

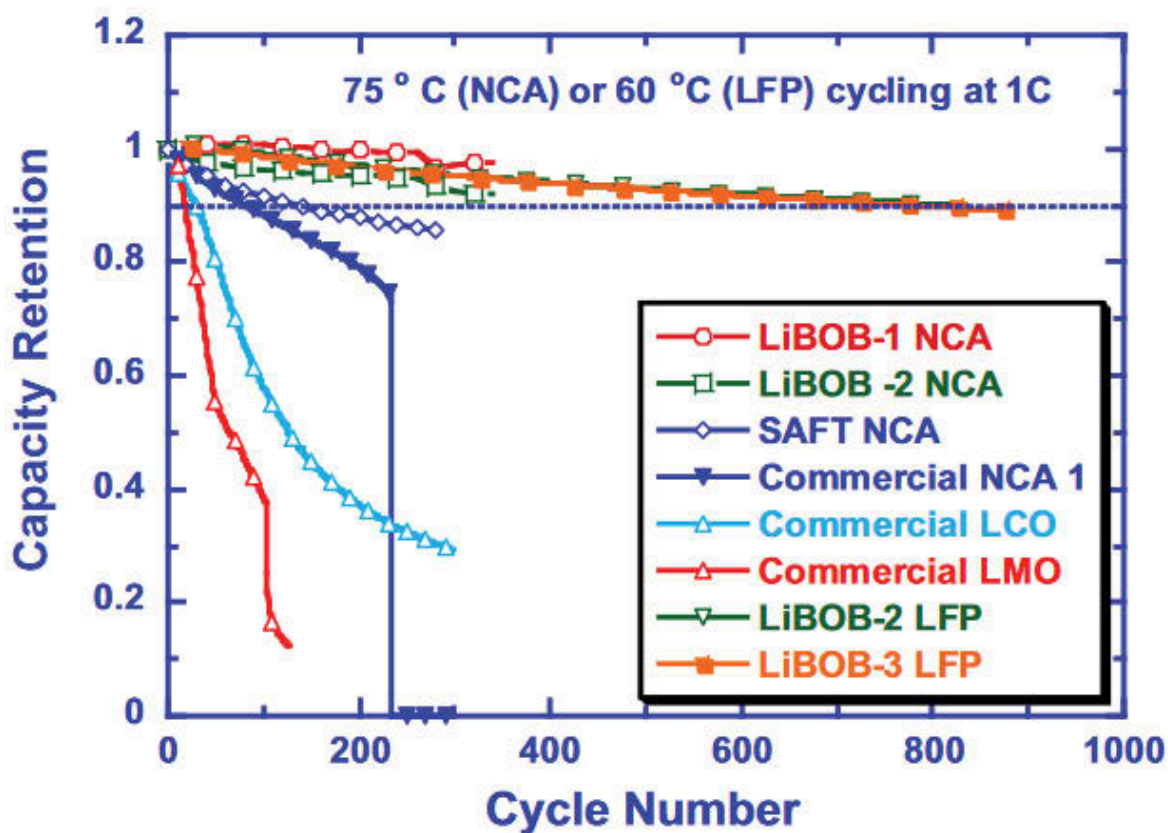


Figure 1-10 Improved cycling performances of lithium-ion cells at elevated temperatures 75°C for NCA and 60 °C for LFP.^[101]

Imides are also proven to be suitable for Li-ion batteries owing to their high solubility and acceptable ionic conductivity. Their advantage lies with the fact that the electron-withdrawing capability of the N-substituents to reduce the Lewis basicity leading to more an easy dissociation of the Li^+ in the electrolyte. LiTFSI, as one of representatives, has been widely used in Li-ion batteries. By the replacement of fluorinated alkyl by F, LiTFSI has shown higher ionic conductivity and higher solubility as well as the thermal stability.^[103] However, the application of LiTFSI is limited due to its decomposition into LiF or trace HF despite its capability to form a stable SEI layer on the graphitic anode. As a result, LiTFSI is only suitable for cathode chemistries such as LiFePO_4 .

1.2.4.7 Polymer electrolytes

Most of the organic solvents used in Li-ion batteries are often flammable, which would induce safety issues when applied in commercial Li-ion batteries. Additionally, the use of liquid electrolyte was always accompanied by the employment of separators, which may somehow influence the electrochemical performances. Meanwhile, the use of liquid-based electrolyte also induces the risk of electrolyte leakage, resulting in energy loss and safety problems. The concept of polymer electrolytes has been brought up as possible alternative to overcome these issues. Polymer electrolytes are divided into two categories, based on the addition of liquid components. Those based on polymers serving as both solvents to dissolve lithium salts and at the same time mechanical support are known as solid polymer electrolytes, while those based on polymer gels in which the polymer matrix is encaged in liquid solutions are categorized as gel polymer electrolytes.^[104-107] The purpose of polymer electrolytes in Li-ion batteries is to separate anode and cathode while connecting them with ionic conductivity. Compared with liquid electrolytes, polymer electrolytes display much better mechanical, thermal, and electrochemical stability.

1. Solid polymer electrolytes: The first discovery that polymer polyethylene oxide was capable of dissolving inorganic lithium salts and providing certain ionic conductivity was reported in 1973.^[108] Since then, solid polymer electrolytes based on oligoether (-CH₂-CH₂-O)_n polymeric linkage have been widely investigated. So far, polyether-based solid polymer electrolyte is still the most investigated structure. Compared with liquid electrolytes, the use of solid polymer electrolytes can offer exceptional processability and flexibility with can support various geometric shapes of Li-ion batteries. The chemical stability of solid polymer electrolytes can ensure a safe environment for battery reactions,

while the mechanical stability would eliminate the additional use of separators. However, the relatively low ionic conductivity as well as the interfacial contacts between electrode and electrolyte limits further applications, which requires further investigation and improvements.

Ionic conductivity of solid polymer electrolytes can be roughly determined by the effective number of mobile ions, elementary electric charge, and ion mobility.^[109] Combining with lithium salts with high degrees of dissociation would provide an acceptable number of free ions which ensures high ionic conductivity. However, in a typical Li-ion battery, the usable mobile ion which contributes to the battery reaction is Li^+ . Therefore, the Li^+ transference number is critical for Li-ion batteries.^[110, 111] The movement of Li^+ in solid polymer electrolyte is closely associated with local segmental motion of the matrix polymer chains. The interactions between Li^+ and electron-withdrawing atoms such as oxygen and fluorine from the polymer chains are the main driving forces for Li^+ motion (shown in Figure 1-11). Typically in poly(ethylene oxide) (PEO)-based solid polymer electrolytes, the optimal ratio of Li^+ to ether oxygen is 1 to 5. Li^+ moves from PEO chain to chain through complexation between each other.^[110]

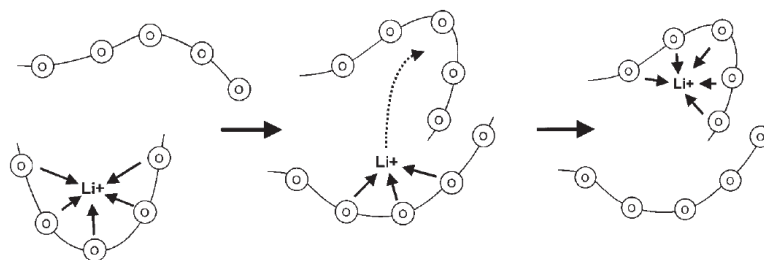


Figure 1-11 Schematic mechanism of Li^+ movement through PEO based polymer electrolyte.^[109]

The movement of polymer chains or so-called segmental motion is often characterized by its glass transition temperature which is responsible for the mechanical properties as well. Most of the commonly used polymer matrices in solid polymer electrolytes have relatively low glass transition temperatures, though their lack of chemical and mechanical stability limits further applications.^[111-113] The attachment of side-chains is one of the solutions to enhance the properties.^[114, 115]

So far, numerous polymer matrices have been investigated for solid polymer electrolytes since the first discovery of the PEO-based one in 1973. Polyacrylonitrile (PAN), poly(methylmethacrylate) (PMMA), and poly(vinylidene fluoride) (PVDF) are studied for their unique properties in solid polymer electrolytes. However, the ionic conductivities of these pure candidates are still far from satisfactory. Besides operating the Li-ion batteries at relatively high temperatures, which can significantly enhance the ionic conductivity of solid polymer electrolytes, ceramic fillers such as Al_2O_3 , SiO_2 , MgO , LiAl_2O_3 , and TiO_2 are added to effectively improve the overall performances.^[116, 117] The hypothesis is that the addition of ceramic fillers can significantly improve the interfacial properties based on acid-base type interactions.^[118]

2. Gel polymer electrolytes: Although the use of solid polymer electrolytes can partially overcome some of the issues induced by the employment of liquid electrolytes, the drawbacks limit the performances of Li-ion batteries. Gel polymer electrolytes share similar properties with solid polymer electrolytes, while the existence of liquid plasticizer encaged in polymer matrices enhances the ionic conductivity. Different from solid polymer electrolytes, Li-ion batteries based on gel polymer electrolytes have been commercialized in the battery industry. The use of gel polymer electrolytes has significantly enhanced the

overall stability of batteries. Meanwhile, the elastic gel structure can provide high tolerance towards volume change, which is especially useful for conversion-based electrode materials.

The choices of polymer matrices in gel polymer electrolytes are similar to solid polymer electrolytes. PEO, as one of the more favourable polymers in solid polymer electrolytes, has been widely studied. The addition of liquid plasticizer in the system can significantly reduce the crystalline content of PEO, and the segmental movement of polymer chain increases, leading to an increased ionic conductivity. Generally, the plasticizers are organic solvents such as polyethers, with low molecular weight.^[119-121] The function of polymers in gel polymer electrolytes is to provide dimensional stability, different from solid polymer electrolytes where polymers function additionally as solvents. Therefore, the interactions between Li^+ and electron-withdrawing atoms are no longer necessary, leading to a broader choices of polymer matrices, such as PAN, PMMA, PVDF, poly(vinyl chloride) (PVC), polypropylene (PP), and polyethylene (PE). Poly(vinylidene fluoride-hexafluoropropylene) (PVDF-HFP) has drawn intensive attention in Li-ion batteries due to its unique properties originating from its co-polymer nature.^[122-133] The amorphous phase of the HFP moiety can encage large quantities of liquid solvents while the crystalline phase of the VDF moiety provides mechanical support.

1.2.5 Organic porous polymer membrane

The porous polymer matrix is also considered as important part of the electrolyte. To be used in lithium-ion batteries, such a polymer matrix should meet certain requirements, such as low ionic strength, mechanical and dimensional stability, physical strength to allow easy handling, resist thermal and chemical degradation by electrolyte impurities and chemical reagents, easily wetted by liquid electrolytes and show uniform thickness.^[134] In

conventional separators, the liquid electrolyte is absorbed inside the porous matrix and is responsible for ionic transportation.

The concept of porous polymer electrolytes originates from the porous separator used in lithium-ion batteries. However, different from the conventional porous separators where only the liquid phase was responsible for ion transportation, a porous polymer electrolyte usually provides three phases: solid polymer matrix, absorbed liquid electrolyte, and gel phase formed by polymer swelling liquid electrolyte. The three-phase structure of porous polymer electrolytes can not only guarantee relatively high lithium ion conductivity and good mechanical property, but can also provide good capability to retain the liquid electrolyte, which further eliminates the risk of electrolyte leakage.^[107, 109, 133, 135-141] Therefore, the porous polymer electrolyte has a very promising application in future lithium-ion battery development.

The choices for polymer matrices are versatile. For example, PEO, PAN, PMMA, PVDF, and PVDF-HFP have been intensively studied.^[142-147] Sometimes, in order to increase the mechanical property, inorganic fillers such as inert oxide ceramics (Al_2O_3 , SiO_2), molecular sieves (zeolites), ferroelectric materials (BaTiO_3) and carbonaceous fillers are incorporated into the polymer hosts.^[125, 148-153] Some have been demonstrated to increase the ionic conductivity at the same time.

Among all the polymers, PVDF has been the most widely studied. PVDF is a semi-crystalline polymer with amorphous chains embedded between the crystalline structures. In this way, the PVDF polymer as battery separator was proven to have good capacity to enhance the lithium transport number. Generally, the ionic conductivity of PVDF porous

polymer electrolytes is associated with the liquid electrolyte uptake, which is closely related to the porosity and pore size. The liquid solution is poured through the membrane, penetrates into the polymer, and swells the polymer network.^[154] Several papers have been published in light of tailoring the porosity of PVDF membranes in order to achieve enhanced electrochemical performance.^[155, 156] Experimental results indicate that in order to obtain good performance, the porosity of the membrane should be around 80 % and the pore diameter should be smaller than 1 μm . The affinity of the PVDF polymer towards liquid electrolytes is also very important. Saunier et al. studied the effect of liquid organic solvents in PVDF membranes and demonstrated it largely influenced the mechanical strength and battery safety.^[157]

The introduction of amorphous chains into the PVDF molecular structure further reduces the crystallinity of PVDF.^[158] PVDF-HFP has attracted particular interests because of its semi-crystallinity originating from the co-polymerization of amorphous hexafluoropropylene (HFP) that can trap liquid electrolytes, and crystal VDF that provides mechanical support.^[118] Therefore, PVDF-HFP can offer not only high ionic conductivity, but also good mechanical properties. It is also a significant advantage that it can be easily tailored in different geometries, including very thin cells.

The first lithium-ion battery using a PVDF-HFP polymer host for the electrolyte was reported by Tarascon et al. in 1996.^[159] Since then, this polymer has been intensively studied. PVDF-HFP has been used directly as single polymer host. Pu et al. reported a simple phase inversion method to prepare a PVDF-HFP microporous membrane in 2006 while Li et al. showed a phase separation process to prepare a similar structure, as shown in Figure 1-12.^[130] Xiao et al. also investigated the effect of different pore forming agents

towards the PVDF-HFP porous polymer electrolytes and Kim et al. tailored the pore morphologies by inducing different ratios of HFP towards PVDF.^[131] Polymer blends are also a strategy for enhancing the ionic conductivity and mechanical properties. PVDF-HFP has been used as blend polymer to prepare high performance lithium-ion batteries such as PVDF-HFP/PAN, PVDF-HFP/PE, and PVDF-HFP/PEO.^[160-162] It is proven that the best combination of polymer blends is when one polymer shows good affinity towards the liquid electrolyte while the other provides good mechanical properties.

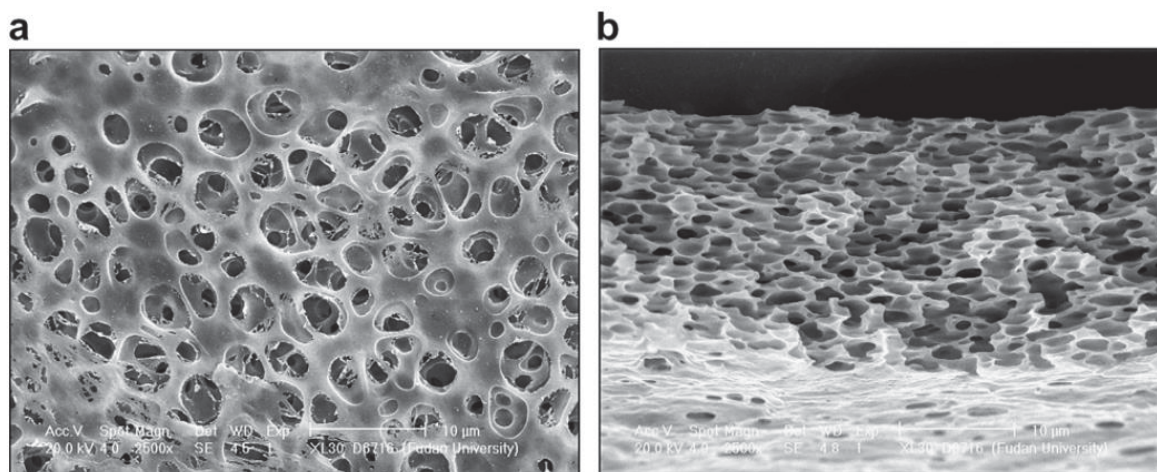


Figure 1-12 (a) Surface and (b) cross-section morphologies of the prepared porous polymer membrane.^[130]

1.3 Lithium oxygen (Li-O₂) batteries

Li-ion batteries have been dominating the battery market for decades. They are commonly applied in various portable devices, such as cellphones and laptops. However, the energy density and power density of current Li-ion batteries cannot fulfill the increasing requirements of energy consumption for large applications, such as electric vehicles. The limitation mainly originates from their inherent low theoretical energy density. Battery

systems based on new battery chemistry are urgently needed. Lithium air batteries, also known as lithium oxygen (Li-O₂) batteries, have been intensively studied due to their extremely high theoretical energy density, compared with other battery systems (Figure 1-13).^[6, 163-166]

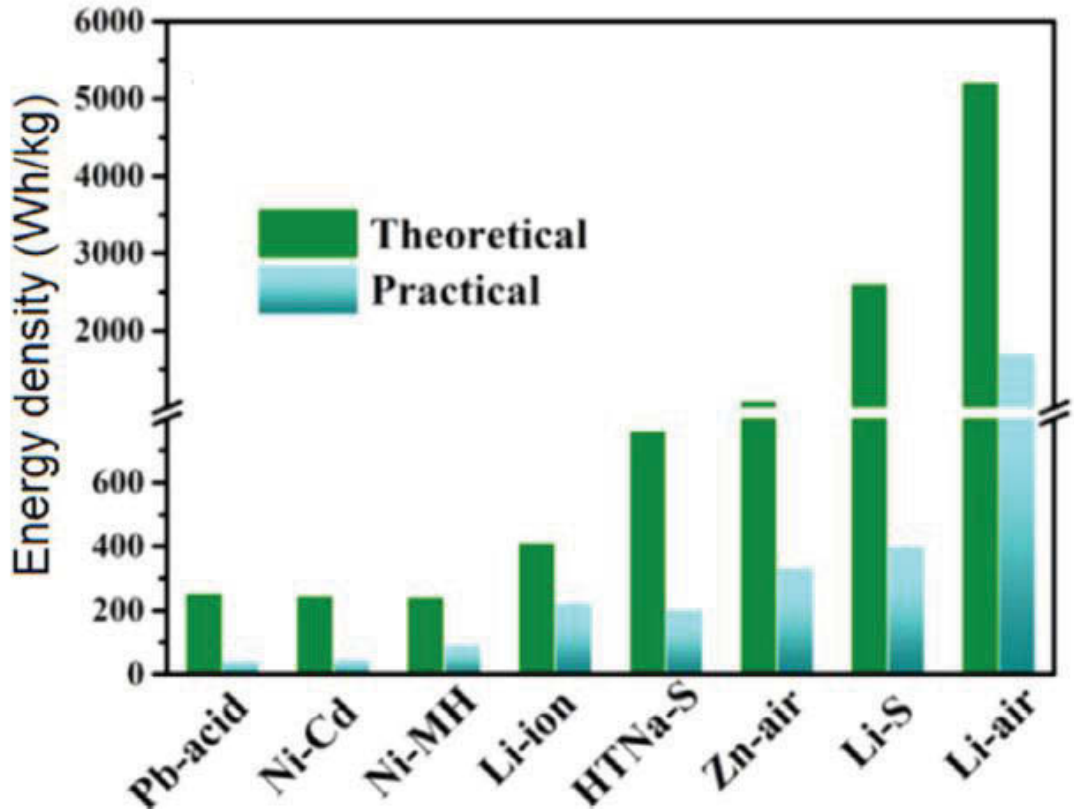


Figure 1-13 Specific energy densities of various rechargeable batteries.^[167]

One advantage of Li-O₂ batteries is that cathode reactant oxygen does not need to be stored inside the battery architecture. The fact that oxygen can be replenished at any time from the ambient air makes it possible to reduce the weight of batteries. Basically, a Li-O₂ battery is the combination of a lithium battery and a fuel cell, which relies on a lithium ion system and an oxygen system at the same time. Therefore, a typical Li-O₂ battery consists of a lithium foil, which replenishes Li⁺ to the electrolyte, electrolyte that provides Li⁺

pathways between the anode and cathode, and a porous cathode to allow the flow of oxygen into the system. During the discharge process, oxygen is consumed together with Li^+ from the electrolyte on the cathode to form discharge products while the reaction reverses during the charge process. The process is illustrated by Figure 1-14.

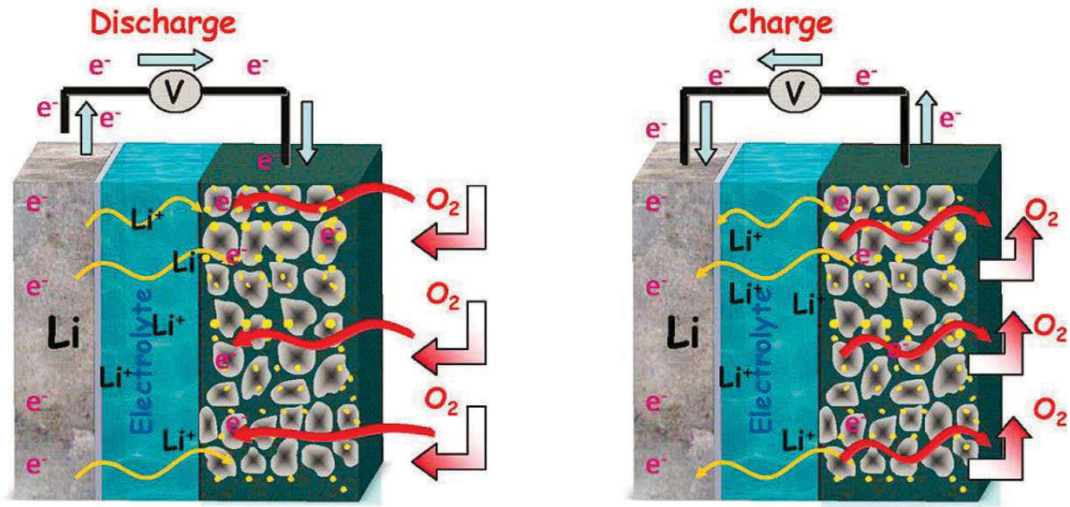


Figure 1-14 Schematic illustration of the discharge and charge processes of Li-O₂ batteries.^[6]

The Li-O₂ batteries have attracted immense research attention; however, main issues still exist which limit the actual realization at the industrial level.

- Low practical capacity due to insufficient porosity of the cathodes in the aprotic batteries to accommodate the insoluble discharge products.
- Poor cycling performance due to unwanted side-reactions originating from the decomposition of battery components.

- Reaction of the lithium metal anode with electrolyte solvents, especially in aqueous system.
- Large over-potentials during discharge and charge processes.
- Contaminates such as CO₂ and H₂O which cause serious side-reactions.

A comprehensive knowledge in Li-O₂ battery should be necessarily developed to solve the above issues.

1.3.1 Anode

Lithium metal is usually used as the anode for Li-O₂ batteries. The main purpose of the lithium anode is to replenish Li⁺ during the battery reactions. The typical anode reaction is shown below:



During the discharge process, the lithium anode is oxidized into Li⁺ and the reaction reverses during the charge process.

Although the direct use of lithium, a light-weight metal, provides extremely high energy density, the vulnerability of lithium metal still limits the electrochemical performance of Li-O₂ batteries. The dendrite growth on lithium metal and its relatively high reactivity towards most contaminants, such as CO₂ and H₂O, often cause detrimental termination of the battery operation. Tan et al. exhibited that the corrosion of the lithium anode was the main factor that deteriorated the overall battery performance with suitable cathode catalysts.^[168] Shui et al. investigated further the use of lithium anode after each cycle.^[169] They found out that the lithium metal only partially recovered after the charging cycle. The

continuous accumulation of side-products, such as LiOH, on the surface will allow the electrolyte contact with the active lithium metal surface, enabling the ceaseless consumption of lithium metal (Figure 1-15).

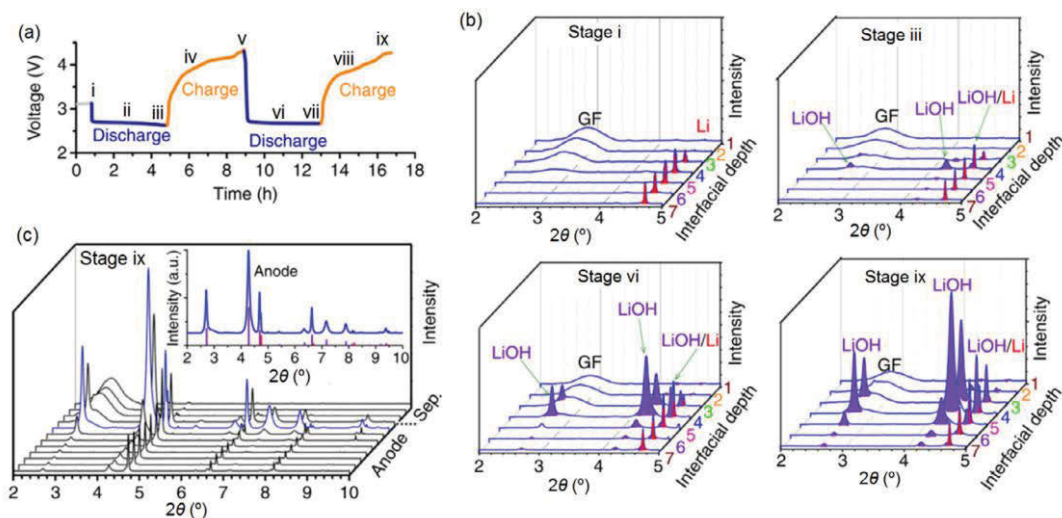


Figure 1-15 The characterization of anodic lithium during discharge-charge cycling.^[169]

To address this issue, several strategies have been proposed, including using an alternative stable anode, adding additives to obtain stable SEI films, and adding a protective layer between the anode and electrolyte.

1.3.1.1 Alternative anode

The direct use of lithium metal as anode for Li-O₂ batteries would always be accompanied by safety issues related to the relatively high reactivity of lithium metal towards the electrolyte components and dissolved O₂. The dendrite growth on the lithium anode, which can cause short-circuits, is also another pathway to the deterioration of the battery performance.^[170-172] Moreover, contaminants such as CO₂ and H₂O could also induce side-reactions when in direct contact with the lithium anode, when operating the Li-

O₂ battery in the ambient air. The replacement of lithium metal with alternative materials is one of the promising ways to achieve better performances.

1. LiFeO₄: The first report of using LiFePO₄ as the replacement of the lithium metal anode for a Li-O₂ battery is by Bruce et al. in 2012.^[173] The stability of LiFePO₄ resolves the issue caused by the reaction between lithium metal and dimethyl sulfoxide (DMSO). As investigated in the research, LiFePO₄ is used as anode as well as the reference electrode, which stabilizes at 3.45 V vs. Li. The anode reaction of LiFePO₄ involves a two-phase reaction of Li_{1-x}FePO₄ and FePO₄.^[174] The relatively stable LiFePO₄ can significantly reduce the side-reaction of electrolyte decomposition on the anode side, which ensures a better electrochemical performance and enables deeper understanding of the battery mechanisms. Similar results were obtained by McCloskey et al. confirming that LiFePO₄ is suitable as anode for quantifying O₂ using differential electrochemical mass spectrometry (DEMS) in acetonitrile (CH₃CN) electrolyte.^[175]

2. Graphite: Technically, most Li⁺ intercalation materials are eligible to be used to replace the lithium metal anode, based on the result when LiFePO₄ is used as the anode.^[176] Chun et al. applied graphite as the anode which showed improved cyclability and reversibility in Li-O₂ batteries.^[177] However, these materials are not quite so suitable to fully replace the metallic lithium, since the high energy density of Li-O₂ is dramatically reduced.

3. Lithium-alloying compounds: Li_xSi has been demonstrated to be a potential anode candidate in Li-O₂ batteries. The relatively low anodic potential (0.3 V vs. Li) enables the battery to discharge at 2.7 V.^[178] Similar result are obtained when Li_xSn (0.5 V vs. Li) is

used.^[179] However, a voltage decay of these materials can be observed after a few cycles. Therefore, a breakthrough is still urgently needed in this aspect.

1.3.1.2 Additive

The decay of the lithium metal anode is usually caused by the direct contact between the relatively reactive lithium metal and the electrolyte components (and contaminants within). Therefore, building an artificial SEI layer on the lithium anode can prevent the direct contact, thus reducing the side-reactions while still maintain acceptable Li^+ conductivity to ensure normal operation of a Li-O_2 battery. Lithium nitrate (LiNO_3) has been demonstrated to be responsible for forming stable SEI layers in lithium sulfur (Li-S) batteries with enhanced electrochemical performances.^[180-182] Furthermore, it has been first reported by Walker et al. that the inclusion of LiNO_3 in the *N,N*-dimethylacetamide (DMA) solvent can significantly eliminate the side-reaction between lithium metal and DMA by forming a stable SEI layer through the combination of amide and nitrate anion.^[183] The electrochemical performance profile is shown in Figure 1-16. Further investigation on the synergistic effect of O_2 and LiNO_3 has also been reported by Giordani et al.^[184] Inspired by this concept, the combination of LiNO_3 and DMSO has been used in Li-O_2 batteries to stabilize the anode and prolong battery cycle life.^[185] Vinylene carbonate and other fluorinated amides have also been investigated as additives to form stable SEI layers.^[186-188]

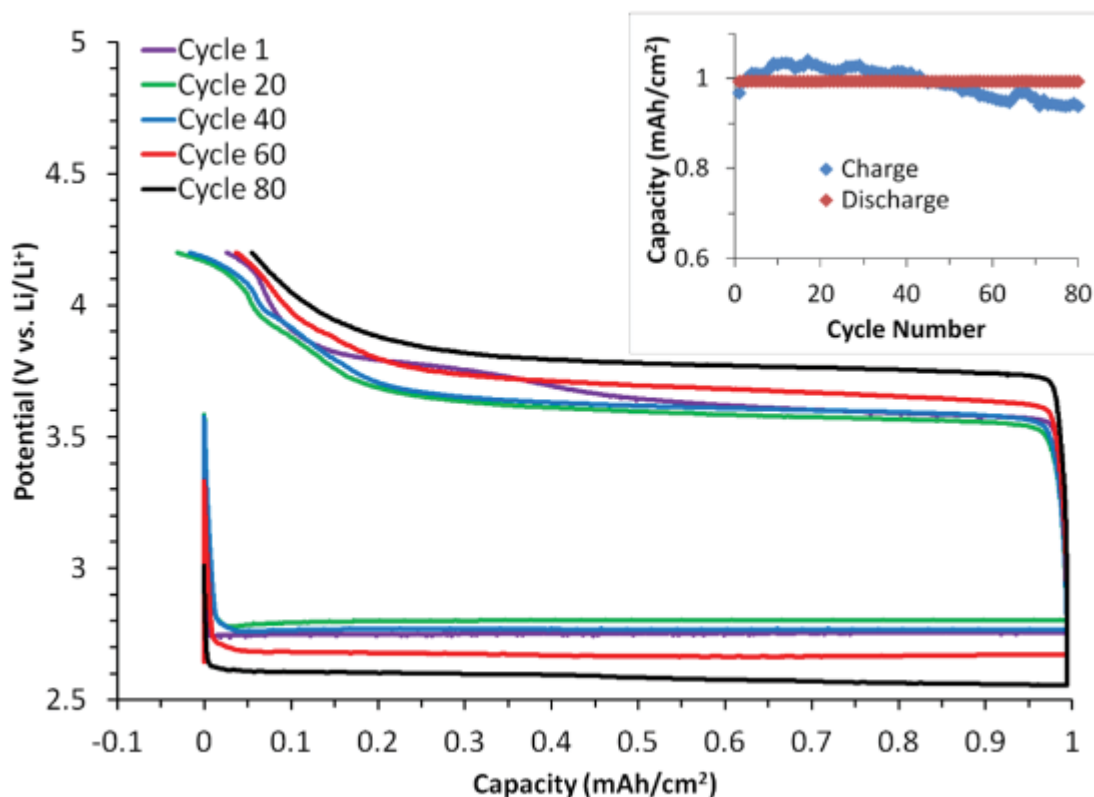


Figure 1-16 Voltage profiles of Li-O₂ battery with 1 M LiNO₃ in DMA at 0.1 mA cm⁻² at room temperature.^[183]

1.3.1.3 Protection layer

Although several additives have been investigated to form stable SEI layers on lithium metal anodes, additives can still somehow influence the battery performances negatively. Therefore, creating artificial protection layers between the lithium anode and electrolyte is an alternative method to reduce side-reactions and protect the lithium metal.^[189, 190] Polymer separators have been considered as one of the suitable candidates for protecting the lithium anode.^[191] The direct coating of a PVDF blend with Al₂O₃ on the lithium anode was reported to lower the contact resistance and enhance the stability.^[192] The result shows

that with the existence of a protection layer, the dendrite growth can be significantly suppressed.

The use of redox mediators, a solution-based catalyst, in Li-O₂ batteries also induces additional issues to the lithium metal anode (more detail in the following chapter 1.3.2.3). The oxidation phase of redox mediators can significantly corrupt the lithium anode and terminate the battery. Building an artificial protection layer between the lithium metal anode and electrolyte can result in higher efficiency and better cycling performance.^[193-195]

1.3.2 Organic electrolyte

The electrolyte in a Li-O₂ battery is essential because it provides sufficient Li⁺ transport, separates the anode and cathode, and provides a safe environment for battery reactions. In terms of electrochemical reversibility, cycle life, and rate capability, the electrolyte is considered as the key element that strongly influences the electrochemical performances. An ideal electrolyte suitable for a Li-O₂ battery should possess several criteria, beyond Li-ion batteries, such as high O₂ solubility and mobility, high chemical resistance towards discharge products and reaction intermediates, and good compatibility with most commonly used anodes and cathodes.^[6] In terms of developing suitable electrolyte candidates for Li-O₂ batteries, numerous research has been conducted regarding their viscosity, ionic conductivity, polarity, and chemical/electrochemical stability.

An electrolyte used in a Li-O₂ battery generally consists of three components: solvent, lithium salt, and additives.

1.3.2.1 Solvent

The solvent in a Li-O₂ battery is used to dissolve lithium salt and provides an environment for continuous battery reactions. Different from a Li-ion battery, the Li-O₂ battery is operated in an open system, where electrolyte volatility is also considered. Rigid battery reactions involving O₂ also require better stability of the electrolyte solvent in a Li-O₂ battery than a Li-ion battery. The commonly used solvents in Li-O₂ batteries are carbonates, ethers, sulfones, and others.

1. Carbonates: carbonate-based solvents have been widely used in Li-ion batteries due to their high solubility of lithium salts, good compatibility with the anode and cathode materials, and low prices.^[196] Naturally, carbonates have also been applied in Li-O₂ batteries in the beginning stage of research. Similar to their performances in Li-ion batteries, the carbonates displayed acceptable ionic conductivities which in terms to maintain the battery reactions smoothly. However, the cycle lives of these Li-O₂ batteries are often limited to a few cycles. Freunberger et al. gave a comprehensive explanation that the carbonate solvents are instable towards the rigid O₂-involved battery reactions.^[197] During the initial discharge process, superoxide radicals (O₂^{•-}) would attack the carbonate molecules due to their strong nucleophilicity, and break the molecules into several semi-carbonate intermediates. The possible mechanisms of carbonate decomposition are shown as Figure 1-17 below. Large quantities of side-products including Li₂CO₃ requires extra energy to decompose which results in large charge over-potentials and short cycle life. Similar results were reported by McCloskey et al.^[198]

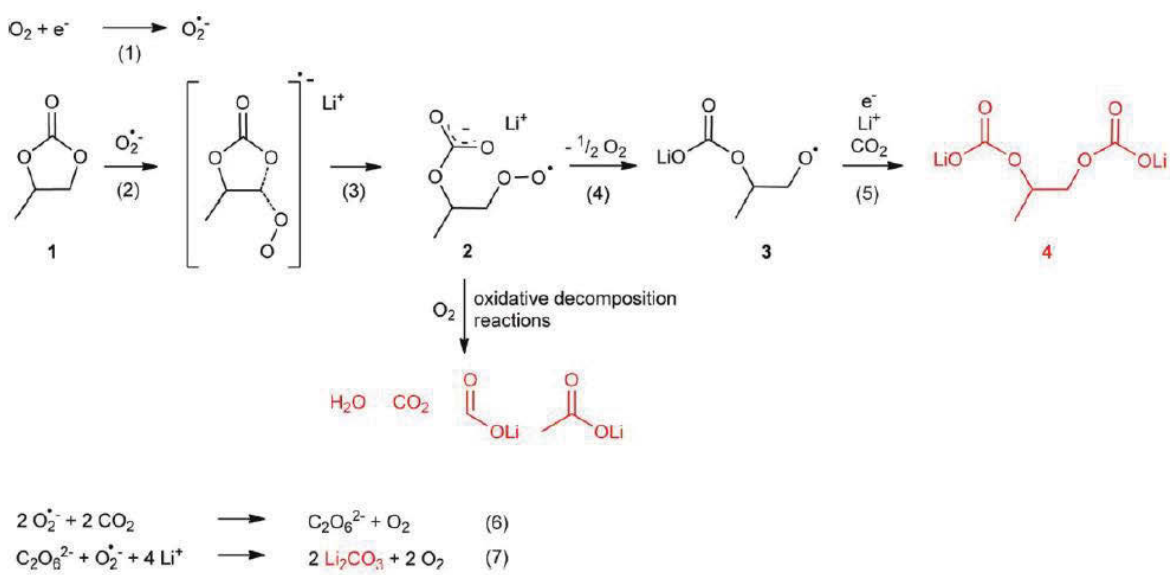


Figure 1-17 Schematic mechanism of the decomposition of PC electrolyte in Li-O₂ batteries.^[197]

2. Ethers: Comparing to carbonate solvents, ether-based solvents have shown significantly enhanced stability. Zhang et al. reported the use of triglyme with a graphene cathode to achieve an extremely high discharge capacity.^[199] Since then, most reported results demonstrated that the formation of Li₂O₂ is somehow favourable as the main discharge product.^[200-203]

However, ether-based solvents have been demonstrated not to be ideal candidates for Li-O₂ batteries as most linear ethers, such as triglyme and tetraglyme had the potential to react with the intermediates irreversibly during the discharge process. Freunberger et al. reported the decomposition of ether molecules by superoxide radicals on the basis of FTIR.^[204] Similar results are discovered by Ryan et al. on the instability of ether molecules.^[205]

3. Sulfonate: Sulfoxides have been demonstrated to be applied in Li-O₂ batteries. Dimethyl sulfoxide (DMSO) has been widely used due to its relatively high stability towards the rigid reactions and fast O₂ distribution. The formation of Li₂O₂ is often favourable in DMSO-based electrolytes, which has been demonstrated by the use of cyclic voltammetry techniques.^[206, 207] Furthermore, by combining DMSO and a porous gold electrode, the performance of the Li-O₂ battery could reach 100 cycles with only 5% capacity fading.^[208] However, based on the results McCloskey et al. reported, DMSO still suffered from serious decomposition issues in the rigid Li-O₂ battery reaction atmosphere.^[175]

4. Other Solvents: Various electrolyte solvents have been proposed and studied. Nitriles and lactam have been reported to be used in Li-O₂ batteries.^[183, 209, 210] However, it seems that none of these candidates proven to be the perfect solvent based on a series of computational and experimental approaches. Ionic liquids, as stable melted salts, have been applied as alternatives of these candidates. Piperidinium, pyrrolidinium, and phosphonium based ionic liquids have been investigated.^[201, 211-213] Furthermore, blended electrolytes have also been studied. By combining different solvents, the overall properties can be further improved. For instance, a blended electrolyte of room temperature ionic liquid and carbonate was reported by Kim et al.^[214] The superior electrochemical stability of the ionic liquid has significantly enhanced the resistance of the electrolyte against nucleophilic attack from the superoxide radicals, while the existence of the carbonate with low viscosity and polarity has been beneficial for Li⁺ and O₂ transports.

1.3.2.2 Lithium salt

The use of lithium salts in the electrolyte is to provide sufficient Li^+ to support smooth battery reactions during discharge and charge processes. Different from solvents, the lithium salts applied in Li-O₂ batteries have no significant influence on the electrochemical performances.^[52] Numerous studies show that most lithium salts are suitable for Li-O₂ batteries due to their relatively high stability in the rigid environment. LiPF_6 , however, shows an unstable nature with rapid decomposition to LiF in the Li-O₂ atmosphere.^[215] The most commonly used lithium salts are LiClO_4 , LiTFSI, LiTf, LiBr, and LiNO_3 , among which LiClO_4 is considered to be the most stable candidate.^[216]

1.3.2.3 Redox mediator

Redox mediators are a series of solution-based catalysts that are mobile in the electrolytes. Diffusible redox mediators can easily gain access to the surface of the discharge product (Li_2O_2), thus efficiently reduces the energy barrier and charge overpotentials.^[174] This process is particularly beneficial for decomposing solid discharge products that are detached or isolated from the electrode. Generally, the redox mediators possess unique redox properties at certain voltages, and react with the discharge product Li_2O_2 in their oxidation form. Based on this principle, a series of redox mediators have been designed and studied. So far, several types of redox mediators including tetrathiafulvalene (TTF), tetramethylpiperidinyloxy (TEMPO), phthalocyanine (FePc), heme, LiNO_3 , LiI, and LiBr have been demonstrated to exhibit significantly reduced overpotentials.^[217-222]

Although the use of solution-based catalysts could significantly improve the round-trip efficiency and achieve low over-potentials, the diffusive capabilities of these redox mediators could carry additional issues.^[223] The direct contact between the redox mediator in its oxidation state and the lithium metal anode would induce side-reactions, which affects the overall cycle life. In order to solve these issues, protection layers have been proposed to be used accompanied by the mobile catalysts (Figure 1-18).^[194, 224]

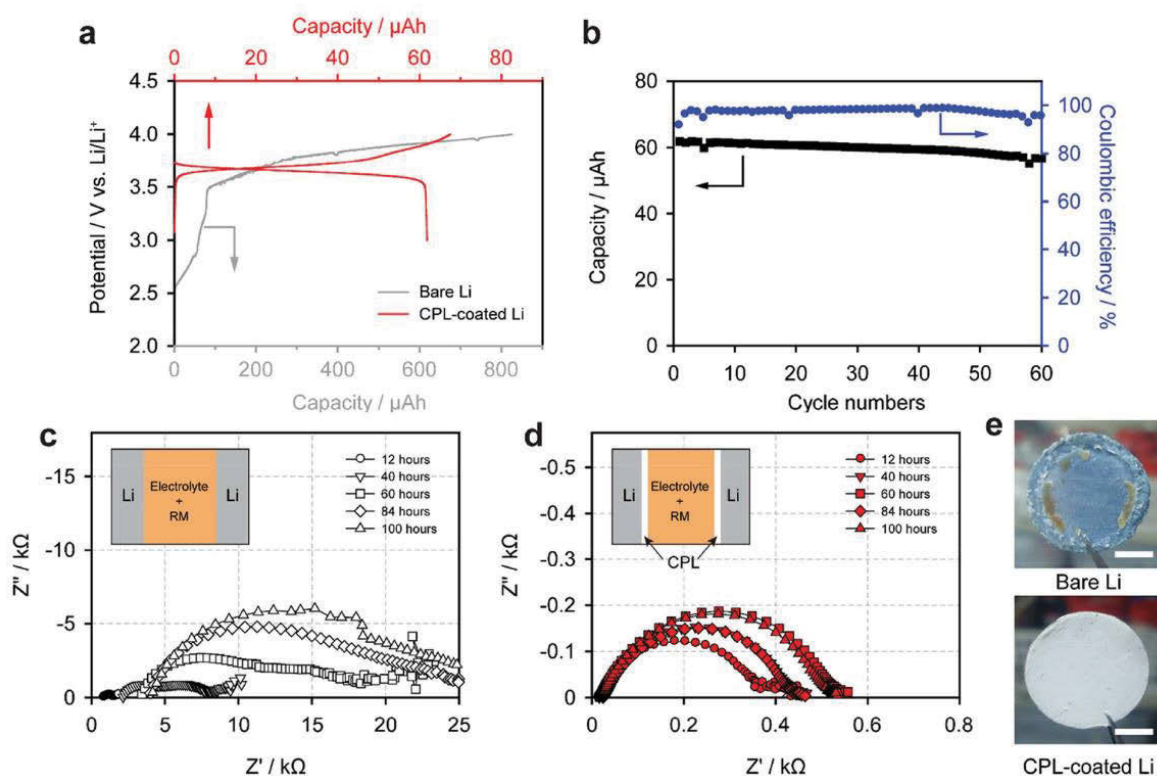


Figure 1-18 a) First charge/discharge profiles of carbon paper/Li cells with and without 0.05 M TEMPO at a current rate of 0.025 mA cm^{-2} . b) The cycling stabilities and efficiencies of the cell with 0.05 M of TEMPO at a current rate of 0.025 mA cm^{-2} . c,d) Nyquist plots of the impedances of the Li/Li symmetric cell with bare Li and with TEMPO

(c), and with the CPL-coated Li and with TEMPO (d). e) Digital pictures of bare Li and CPL-coated Li electrodes after prolonged storage test (scale bar, 5 mm).^[194]

1.3.2.4 Organic polymer electrolyte

The concept of polymer electrolytes has been investigated in previous section 1.2.4.7. The first application of polymer electrolytes in Li-O₂ batteries is reported by Zhang et al in 1997.^[225] Since then, numerous applications have been reported, including natural rubber, PVDF-HFP, PMMA, and PEO-based polymer electrolytes, either as solvents (solid polymer electrolytes), or as polymer matrices gelling with organic solvents (gel polymer electrolytes).^[226-230] Some of these have shown enhanced electrochemical performances and stabilities. However, compared to the candidates in Li-ion batteries, the use of gel polymer electrolytes does not match the liquid ones in Li-O₂ batteries. Therefore, polymer electrolytes are mainly employed solely as protection layers or combined as composites for Li-O₂ batteries.

1.3.3 Cathode

The cathode is one of the most critical components in Li-O₂ batteries, as the oxygen reduction and oxygen evolution reactions occur on the surface of the cathode. A cathode consists of a conductive matrix (usually conductive carbon) for electron transference, a catalyst for lowering the reaction barrier, and a binder maintaining mechanical integrity of the overall cathode.

1.3.3.1 Conductive matrix

Conductive materials are often added to enhance the electron flow to support smooth battery reactions. The commonly used conductive matrix is based on carbon materials, due

to their intrinsic high conductivity and light weight. Additionally, conductive carbon materials have various forms which could easily be suitable for all kinds of battery applications. Based on the operation mechanism of Li-O₂ batteries, the discharge product, ideally Li₂O₂, is insoluble in most aprotic organic electrolytes. Therefore, properties such as porosity, surface area, and morphology are highly critical for overall battery performance.^[231, 232] So far, various carbon materials including carbon black particles, carbon nanotubes, carbon nanofibers, mesoporous carbon, graphene nanosheets, and porous graphene have been investigated.^[233-241] N-doped carbon prepared from N-rich polymers is also a commonly applied conductive matrix.^[242]

However, the direct use of carbon matrices in Li-O₂ batteries induces additional issues. The relatively high reactivity of carbon makes it vulnerable towards the rigid battery reaction environment, leading to the formation of side-products Li₂CO₃.^[243, 244] The existence of Li₂CO₃ results in large charge over-potential and low round-trip efficiency. Carbon-free conductive substrates have been studied for the replacement of carbon in order to solve this issue. Some transition metal oxides could provide acceptable conductivity to support electron flow. Cui et al. reported a carbon free electrode based on Co₃O₄ which achieved enhanced cycling performance.^[245] Porous gold has been proposed by Peng et al. which achieved more than 300 cycles with only 5% drop of its initial capacity.^[208] Organic materials are also applied in this aspect. A tubular polypyrrole was used to replace carbon materials due to its relatively high stability and conductivity.^[246] The Li-O₂ battery achieved excellent electrochemical performance. Alternatively, surface coating of carbon with stable organic materials is also an efficient method for improving overall stability.^[247]

1.3.3.2 Organic binder

The use of binders in Li-O₂ batteries is to create an integrated cathode with no mass loss during battery reactions. To physically bind all the materials, the binders are usually linear polymers with high degrees of polymerization. Reports on using PVDF, PVDF-HFP, PMMA, and co-polymers have been revealed. Interestingly, a combination of polypyrrole and carbon was applied in a Li-O₂ battery due to its relatively high conductivity to combine cathode materials.^[248]

However, different from Li-ion batteries, Li-O₂ batteries offer an extremely rigid environment where most commonly used materials in Li-ion batteries could not survive. Therefore, most binders used in Li-O₂ batteries suffer severely from decomposition.^[249] Nazar et al. reported comprehensively about the decomposition of PVDF binder during battery reactions, and blamed it for the decay of battery performance.^[250] Vankova et al. suggested the replacement of PVDF with F-free carboxymethyl cellulose (CMC) to suppress side-reactions.^[251] Additionally, numerous binder-free materials have been proposed.

1.3.3.3 Catalyst

Due to the sluggish kinetics of battery reactions, Li-O₂ batteries often suffer from large over-potentials which lead to large side-reactions and short cycle life. Catalysts are employed in order to achieve good performances. Commonly used catalysts for Li-O₂ batteries are carbon, precious metals, transition metal oxides, and organic materials.

Carbon materials have been widely used as conductive matrices to fabricate cathodes. Meanwhile, many reports indicate that carbon materials, especially graphene-based ones,

can also offer acceptable catalytic activities towards ORRs and OERs.^[199, 252, 253] However, the direct use of carbon can induce additional side-reactions. Precious metals and their oxides have demonstrated their catalytic capabilities in aqueous OERs and ORRs, and many have been applied in Li-O₂ batteries.^[254-256] However, Pt, as one of the best catalysts in aqueous system, has been proved not suitable for Li-O₂ batteries due to its capability to decompose electrolyte solvents. Ru or its oxides, on the other hand, is the most popular for reducing over-potentials in Li-O₂ batteries.^[257-263] However, the scarcity and high price are the main limitations for the real application of precious metals. Cheap transition metal oxides show similar activities compared to precious metals and their abundant sources make them favourable candidates for industry applications.^[264-268] Organic materials, such as redox mediators, have been used for reducing charge over-potentials. Recently, a new concept has been brought up by Bruce et al. that an organic material (Figure 1-19) could significantly enhance the discharge process by interacting with oxygen and Li⁺.^[269]

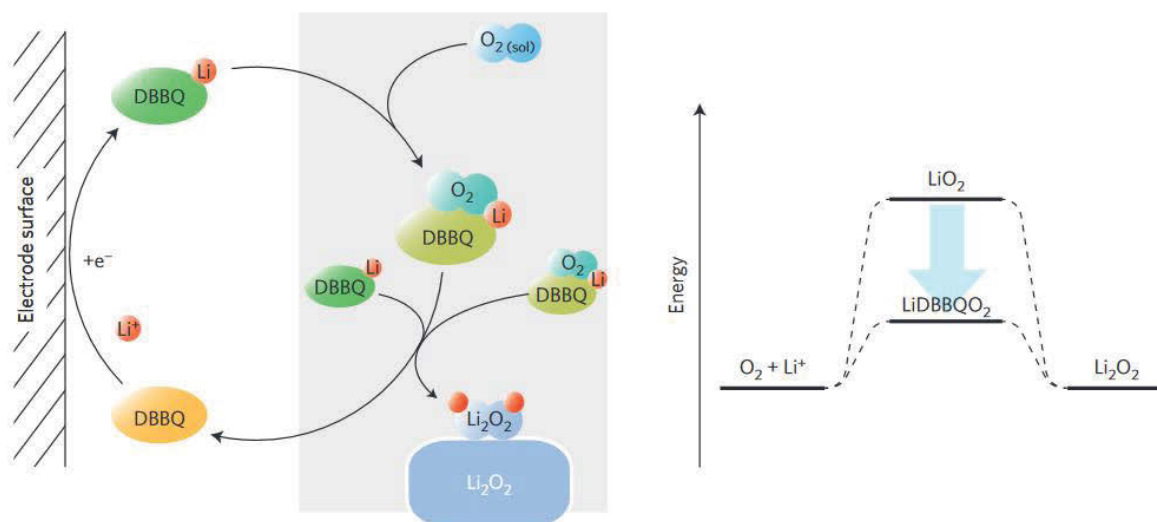


Figure 1-19 Schematics of reactions on discharge (left) and the effect of DBBQ on the potential determining step (right).^[269]

Although the use of catalysts results in high capacity and low over-potential, there are still researchers believing the employment of catalysts in Li-O₂ batteries is unnecessary or even detrimental because it would lead to the decomposition of the electrolyte.

1.4 Summary

Great efforts have been made to achieve acceptable performances for lithium batteries. The organic components in Li-ion and Li-O₂ batteries have shown significant potential to improve the overall battery performances. By utilizing different function organic materials, batteries can be enhanced at every prospect according to the needs. For this project, porous polymer membranes based on PVDF-HFP and PMMA have been chosen as electrolytes in Li-ion batteries in Chapter 3 and 4. Additionally, organic catalysts and binders for Li-O₂ batteries based on 2, 2, 6, 6-tetramethylpiperidinyloxy (TEMPO) moiety have been investigated in Chapter 5 and 6, respectively. The mechanism of redox mediator tetrathiafulvalene (TTF) was also studied and altered by adding LiCl in the electrolyte system for Li-O₂ batteries, and the results are shown in Chapter 7.

Chapter 2 Experimental

2.1 Overview

The overall research route of this project mainly involves three procedures, as shown in Figure 2-1. Firstly, the materials are prepared through different methods, typically breath-figure method for preparing porous membranes as porous gel polymer electrolyte, and organic synthesis for preparation of N-O radical containing organic materials. Characterizations are performed after the preparation step. Generally, scanning electron microscopy (SEM) is used to observe the morphology of the as-prepared materials, Fourier transform infrared (FTIR) spectroscopy, Raman spectroscopy, and Nuclear magnetic resonance (NMR) spectroscopy are employed for molecular examinations, ultraviolet-visible spectroscopy (UV-vis) for property characterization, X-ray diffraction (XRD) and thermogravimetric analysis (TGA) for additional experiments. After the characterization, electrochemical impedance spectroscopy (EIS), cyclic voltammetry (CV), and galvanostatic discharge-charge techniques are used to determine the electrochemical performances in Li-ion or Li-O₂ batteries. Postmortem characterization may be used to analyze mechanism of the battery reactions.

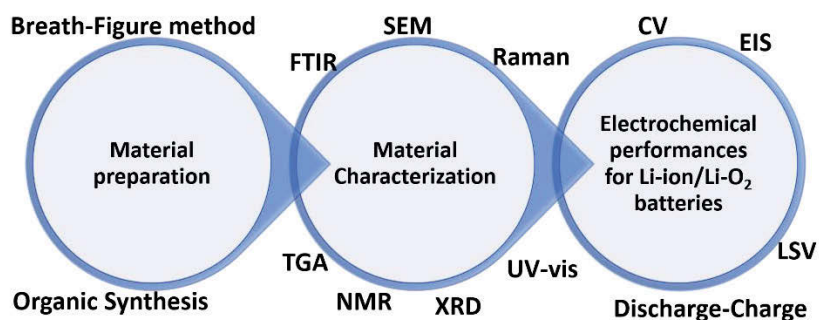


Figure 2-1 Schematic illustration for material preparation, characterization and application.

2.2 Materials and chemicals

A list of the names of materials and chemicals used in the project along with their formula, purity and supplier, is shown below in Table 2-1.

Table 2-1 Materials and chemicals used in the research project.

Materials and chemicals	Formula	Purity	Supplier
Carbon black	C	99%	Lexel
Poly(vinylidene difluoride) (PVdF)	$(\text{CH}_2\text{CF}_2)_n$	-	Sigma-Aldrich
Poly(vinylidene fluoride-co-hexafluoropropylene) PVDF-HFP	$(\text{CH}_2\text{CF}_2)_n-(\text{CF}_2\text{CF}(\text{CF}_3))_m$	-	Sigma-Adrich
N-Methyl-2-pyrrolidinone (NMP, anhydrous)	$\text{C}_5\text{H}_9\text{NO}$	99.5%	Sigma-Adrich
Isopropyl alcohol	$\text{C}_3\text{H}_8\text{O}$	99%	Chem-Supply
Poly(methyl methacrylate)	$(\text{CH}_2\text{C}(\text{CH}_3)(\text{CO}_2\text{CH}_3))_n$	-	Sigma-Aldrich
Diethylene glycol dimethyl ether, anhydrous	$(\text{CH}_3\text{OCH}_2\text{CH}_2)_2\text{O}$	99.5%	Sigma-Aldrich
Bis(trifluoromethane)sulfonimide	$\text{CF}_3\text{SO}_2\text{NLiSO}_2\text{CF}_3$	99.95%	Sigma-Aldrich

lithium salt

Acetone	CH_3COCH_3	99.9%	Chem-Supply
Lithium hexafluorophosphate	LiPF_6	99.99%	Sigma-Aldrich
Ethylene carbonate, anhydrous	$\text{C}_3\text{H}_4\text{O}_3$	99%	Sigma-Aldrich
Dimethyl carbonate, anhydrous	$(\text{CH}_3\text{O})_2\text{CO}$	99%	Sigma-Aldrich
Dichloromethane	CH_2Cl_2	99%	Chem-Supply
2,2,6,6-tetramethyl-4-piperidy methacrylate	$\text{C}_{13}\text{H}_{23}\text{NO}_2$	99%	TCI
2,2'-Azobis(2- methylpropionitrile)	$(\text{CH}_3)_2\text{C}(\text{CN})\text{N}=\text{NC}(\text{CH}_3)_2\text{CN}$	99%	Sigma-Aldrich
Sodium tungstate dihydrate	$\text{Na}_2\text{WO}_4 \cdot 2\text{H}_2\text{O}$	99%	Sigma-Aldrich
Methanol	CH_3OH	100%	Chem-Supply
Hydrogen peroxide	H_2O_2	30%	Chem-Supply

2.3 Material preparations

In this project, two different approaches are mainly used to prepare organic materials for Li-ion or Li-O₂ batteries: breath-figure method and general organic synthesis method.

2.3.1 Breath-figure method

The use of the breath-figure (BF) method in materials science is an example where scientists learn from nature. BF refers to the fog that forms when water vapor contacts a cold surface. It is a commonly observed phenomenon in daily life, and for a long time, it was considered just a natural phenomenon without practical applications in materials science. In 1994, Francois et al. reported the preparation of polymeric porous films with honeycomb structures by exposing a drop of polystyrene-*b*-polyparaphenylene (PS-*b*-PPP) solution in carbon disulfide (CS₂) to a flow of moist air. In the past two decades, this simple process has been widely utilized as a versatile soft-template method for the fabrication of honeycomb-patterned films with controlled pore sizes and different potential functions and applications.

In a conventional BF process, a drop of polymer (or other substance) solution is cast onto a solid substrate and allowed to evaporate in a humid environment. After the solvent and the condensed water droplets evaporate completely, a porous film forms on the substrate. The process can be divided into dynamic and static BF processes according to how the humid environment is established. In a dynamic BF process, the moisture is supplied by a gas flow blown over the substrate (Figure 2-2a). And in a static BF process, the evaporation of solvent is completed spontaneously without the aid of gas flow (Figure 2-2b).

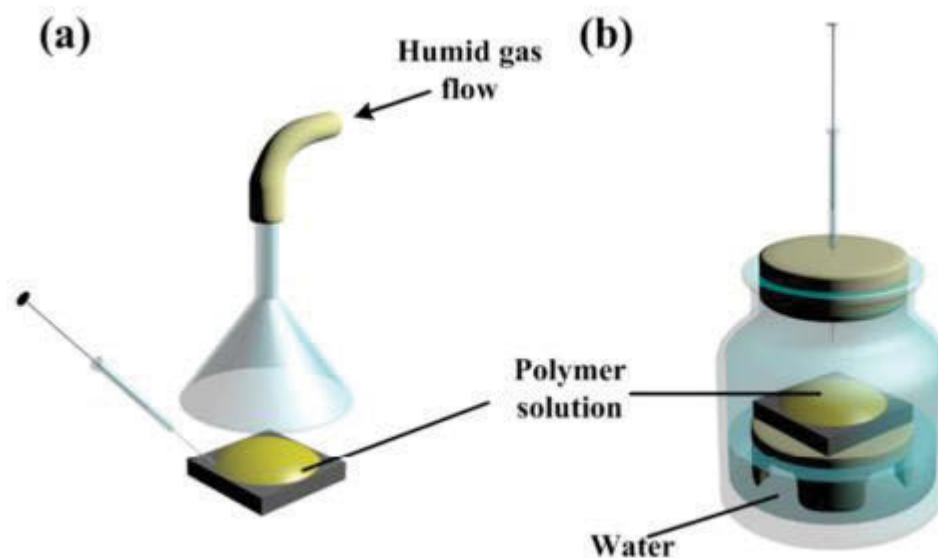


Figure 2-2 Conventional BF methods. (a) Dynamic and (b) static BF processed.

In this project, the dynamic BF process is mainly used to synthesize the porous membrane with honeycomb-like structure as separator in Li-ion batteries.

2.3.2 General organic synthesis

Organic synthesis is a special branch of chemical synthesis and is concerned with the construction of organic compounds via organic reactions. Organic molecules often contain a higher level of complexity than purely inorganic compounds, so that the synthesis of organic compounds has developed into one of the most important branches of organic chemistry. The organic synthesis route in this project mainly involves the preparation of polymers known as free-radical polymerization, and oxidation reaction initialized by H_2O_2 .

Free-radical polymerization is a method of polymerization by which a polymer forms by the successive addition of free-radical building blocks. Free radicals can be formed by several different mechanisms, usually involving separate initiator molecules. Following its

generation, the initiating free radical adds (nonradical) monomer units, thereby growing the polymer chain. In this project, free-radical polymerization is used to prepare functionalized polymers as binders and catalysts for Li-O₂ batteries.

Oxidation reaction initialized by H₂O₂ is a reaction where H₂O₂ is used as oxidant. This method is used in this project to prepare organic compounds with nitride oxide radical groups for Li-O₂ batteries.

2.4 Material characterization

2.4.1 X-ray diffraction analysis (XRD)

X-ray diffraction (XRD) is a non-destructive analytical characterization method which reveals detailed information about chemical composition, crystal phase, and structure of certain materials. An X-ray diffractometer generates an X-ray beam hitting a sample as a function of incident and scattered angle, polarization, and wavelength or energy. A certain sample has a particular atom arrangement within the unit cell which leads to particular relative intensities of the recorded diffraction peaks upon X-ray hitting. Therefore, the unit cell size and geometry may be resolved from the angular positions of the X-ray diffraction results. The resultant diffraction lines with obvious peaks together are called an XRD pattern which can provide information on crystal structure, chemical composition, and physical properties of certain materials. Each crystal has a unique XRD pattern according to Bragg's law,

$$n\lambda = 2d\sin\theta \quad \text{(Equation 2-1)}$$

Where n stands for integer, λ is the wavelength of the incident X-ray beam, d is the distance between atomic layers in a crystal and θ stands for the incident angle. The theory of Bragg's law is shown in Figure 2-3.

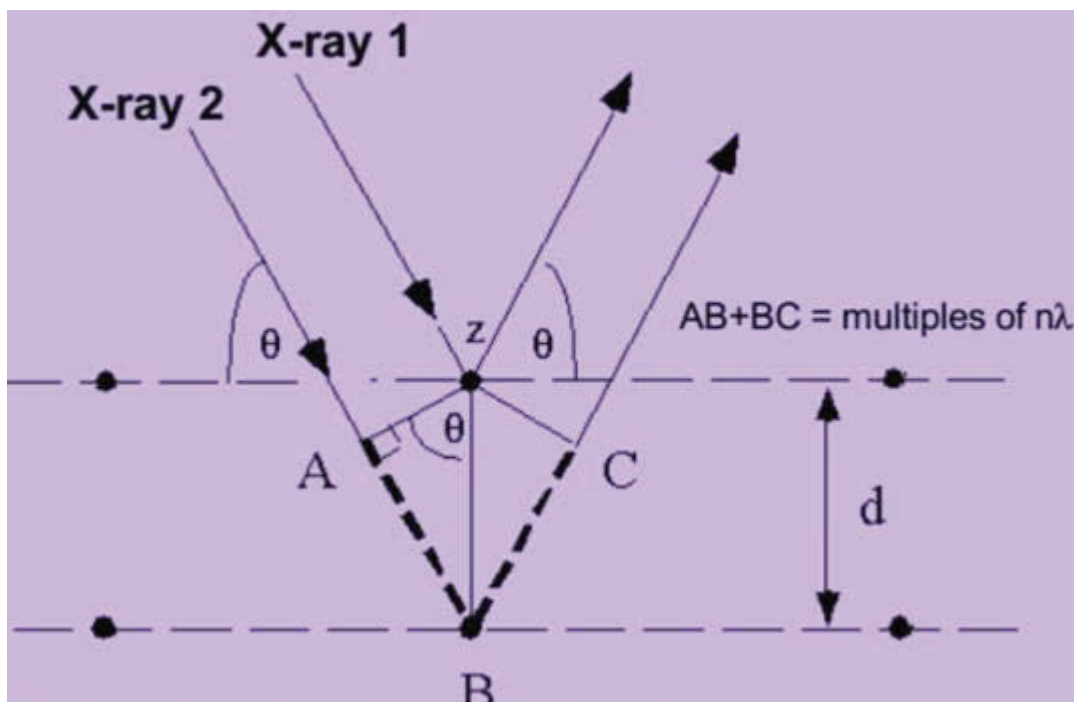


Figure 2-3 Schematic drawing of Bragg's law.

The basic use of XRD in this research project was to determine the composition and phase of discharge products in Li-O₂ batteries. The XRD instrument used in this research project was Bruker D8 Discover (Figure 2-4) with a monochromatized Cu K α radiation ($\lambda=0.15406$ nm) at a scan rate of 1° min^{-1} and step size of 0.02° .

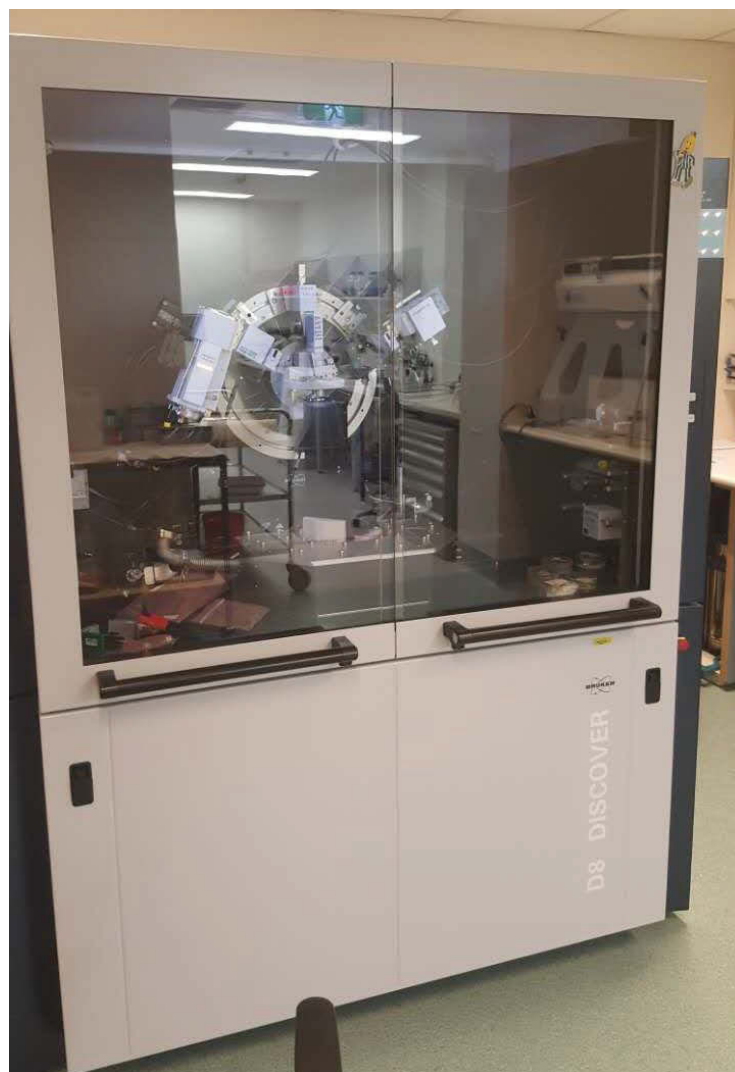


Figure 2-4 Photo of the XRD instrument of Bruker D8 Discover

2.4.2 Raman spectroscopy

Raman spectroscopy, named after C. V. Raman, is a non-destructive and fast-detecting spectroscopic technique, relying on a laser in a range of visible, near infrared, and near ultraviolet to observe vibrational, rotational and other low-frequency modes. The specific vibrational information obtained in Raman spectroscopy is specific to the molecules' chemical bonds and symmetry, which provide sufficient information to identify a specific molecular structure. In this thesis, Raman spectroscopy is mainly used to identify the

organic composite of the as-obtained materials. The Renishaw inVia Raman spectrometer system used for this project is equipped with a Leica DMLB microscope (Wetzlar, Germany) and a 17 mW at 633 nm Renishaw helium neon laser in Figure 2-5.



Figure 2-5 Photo of the Raman instrument

2.4.3 Thermogravimetric analysis (TGA)

Thermogravimetric analysis (TGA) is a type of measurement generally used to determine the weight changes of a certain sample during the changing of temperature in a controlled atmosphere. Such analysis can detect the weight of a sample as temperature elevates accurately. The results are often concluded in a figure with a continuous line to identify weight loss processes which are related to the chemical reactions occurring at certain temperatures.

In this project, the TGA was used to determine the weight ratio of liquid electrolyte retained in as-prepared gel polymer electrolyte. The TGA instrument used in this project was Simultaneous TG-DTA (SDT 2960, Figure 2-6) with a platinum plate as the sample holder. The temperature was set to increase to certain degrees in air atmosphere with a speed of 5-10 °C/min.



Figure 2-6 The photo of the TGA instrument

2.4.4 Scanning electron microscopy (SEM)

The scanning electron microscope (SEM) is a characterization technique that can visualize a sample by scanning it in a raster scan pattern with the high-energy electron beam. After each scan, the sample produced signals that contain information about the sample's surface topography, composition, and electrical conductivity were made up by electrons interacting with the sample atoms. Generally, SEM is used for preliminary analysis of certain materials.

The basic use of SEM in this research project was to observe the morphology of porous membranes and surface of electrodes during cycling. The SEM instrument used in this project was Zeiss Supra 55VP field emission SEM (FE-SEM) with an accelerating voltage of 5-20 kV and 10-30 mm aperture (Figure 2-7). The images were taken by an in-lens secondary detector. A thin layer of carbon deposited on the surface of the materials if the conductivity was too low.

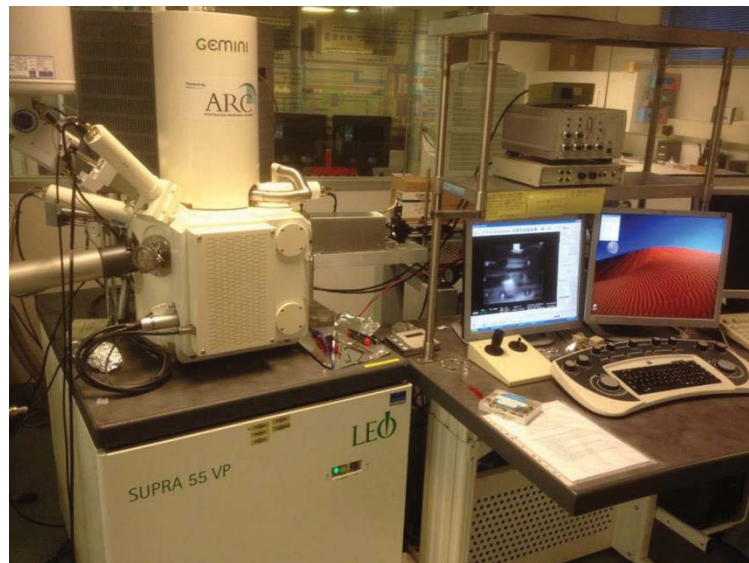


Figure 2-7 The photo of SEM of Supra 55 VP

2.4.5 Fourier transform infrared (FTIR) spectroscopy

Fourier transform infrared spectroscopy (FT-IR) is used for obtaining infrared spectra of absorption, emission, photoconductivity or Raman scattering of a solid, liquid or gas. A FTIR spectrometer simultaneously collects spectral data in a wide spectral range. This confers a significant advantage over a dispersive spectrometer which measures intensity over a narrow range of wavelengths at a time.

The basic use of FTIR in this research project was to analyse the structure of polymer materials and products that were produced during cycling. The FTIR instrument used in this project was Thermo Scientific FT-IR spectrometer using 4 cm^{-1} resolution and 64 scans at room temperature (Figure 2-8).



Figure 2-8 Photo of the Thermo Scientific FTIR instrument

2.4.6 Ultraviolet-visible (UV-vis) spectroscopy

Ultraviolet-visible spectroscopy, using electromagnetic radiation in the range of ultraviolet to visible and adjacent light, is a technique that utilizes absorption or reflectance

spectroscopy. Molecules in specimens containing π -electrons or non-bonding electrons excite the electrons to higher anti-bonding molecular orbitals after absorbing the energy from the ultraviolet or visible lights.

In this project, the UV-vis instrument is mainly used to determine the chemical composition of organic redox mediator during cycling. The UV-vis absorption spectra, using the Beer-Lambert Law, in this thesis are measured by a Cary 60 UV-vis spectrophotometer (Figure 2-9).

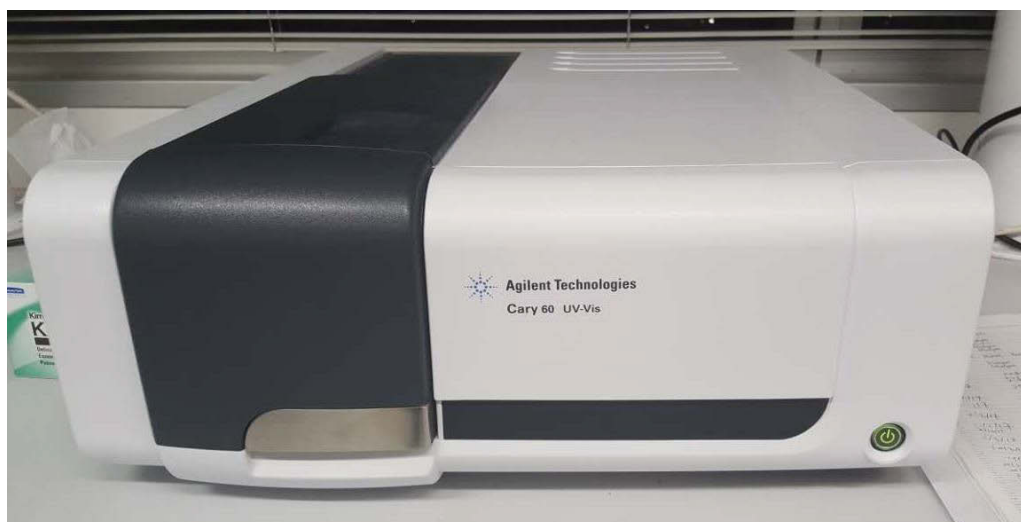


Figure 2-9 Photo of the UV instrument of Cary 60

2.4.7 Nuclear magnetic resonance (NMR) spectroscopy

Nuclear magnetic resonance spectroscopy, known as NMR spectroscopy, is a research technique that exploits the magnetic properties of certain atomic nuclei. This type of spectroscopy determines the physical and chemical properties of atoms or the molecules in which they are contained. It relies on the phenomenon of nuclear magnetic resonance and can provide detailed information about the structure, dynamics, reaction state, and chemical

environment of molecules. The intramolecular magnetic field around an atom in a molecule changes the resonance frequency, thus giving access to details of the electronic structure of a molecule and its individual functional groups.

The NMR spectroscopy technique used in this project is mainly for the identification of certain organic compounds. The instrument used is Agilent 500MHz NMR (Figure 2-10).



Figure 2-10 Photo of the NMR instrument

2.5 Electrode preparation and battery assembly

2.5.1 Lithium ion (Li-ion) battery

The working electrodes for Li-ion batteries are prepared by first mixing PVDF (10%), carbon black (10%), and LiFePO_4 (80%) together in 1-Methyl-2-pyrrolidinone (NMP). The mixture is stirred with an adjustable high-speed electric agitator, forming a black slurry. The mixture was then coated onto aluminium foil using a doctor blade, dried at 80 °C for 12 h under vacuum, and punched into disks. All cells were assembled in an argon-filled glove box with water and oxygen content lower than 0.1 ppm (Figure 2-11).



Figure 2-11 Photo of the glovebox used to assemble the batteries

A CR2032 type coin cell is used. The liquid electrolyte used in Li-ion batteries is 1 M LiPF_6 dissolved in a 1:1 (volume ratio) mixture of ethylene carbonate and diethyl carbonate. A schematic illustration of the components of Li-ion batteries is shown in Figure 2-12.

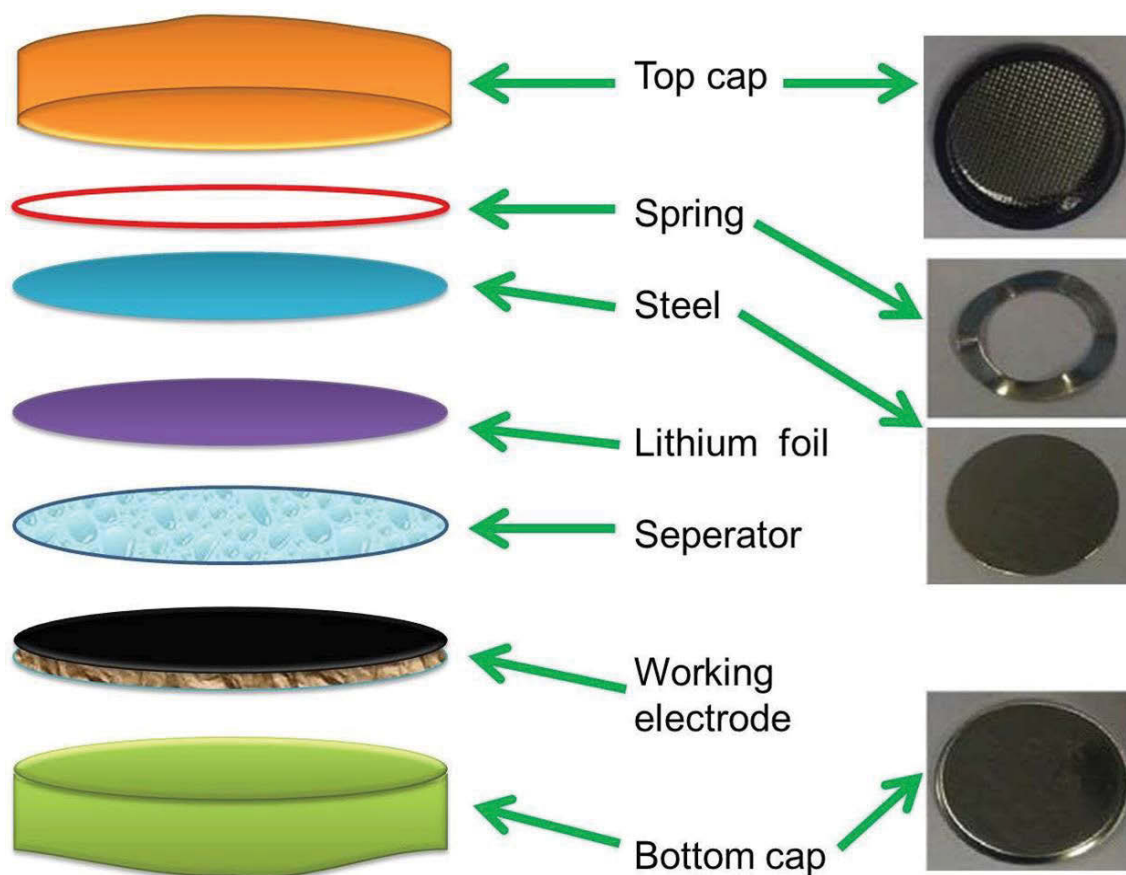


Figure 2-12 Schematic illustration of the construction of a Li-ion battery

2.5.2 Lithium oxygen (Li-O₂) battery

The catalyst mesh was prepared by mixing the as-prepared materials, conducting matrices, and binders together in certain a ratio in isopropanol under continuous stirring. The mixture was then pressed onto the stainless-steel mesh or a nickel mesh to form the air cathode. The cathode film was punched into discs with a diameter of 14 mm and dried at 80°C in a vacuum oven for 12 h and then kept in the glove box. The typical loading of the air electrode is about 1 mg cm⁻². A Swagelok type cell with an air hole (0.785 cm²) on the cathode side was used to investigate the electrochemical performance. The cell was assembled in an Ar filled glove box (Mbraun) with water and oxygen level less than 0.1

ppm. The as-prepared air cathode was used as the working electrode and a lithium foil was used as the counter and reference electrode. The electrodes were separated by a glass microfiber filter (Whatman). The formula of electrolytes depend on the experiments operated. The cell was gas-tight except for the air side window that exposed the porous cathode film to the oxygen atmosphere. The brief diagram of the structure of the Li-O₂ battery is shown in Figure 2-13. All experiments were tested in 1 atm dry oxygen atmosphere to avoid any negative effects of humidity and CO₂.

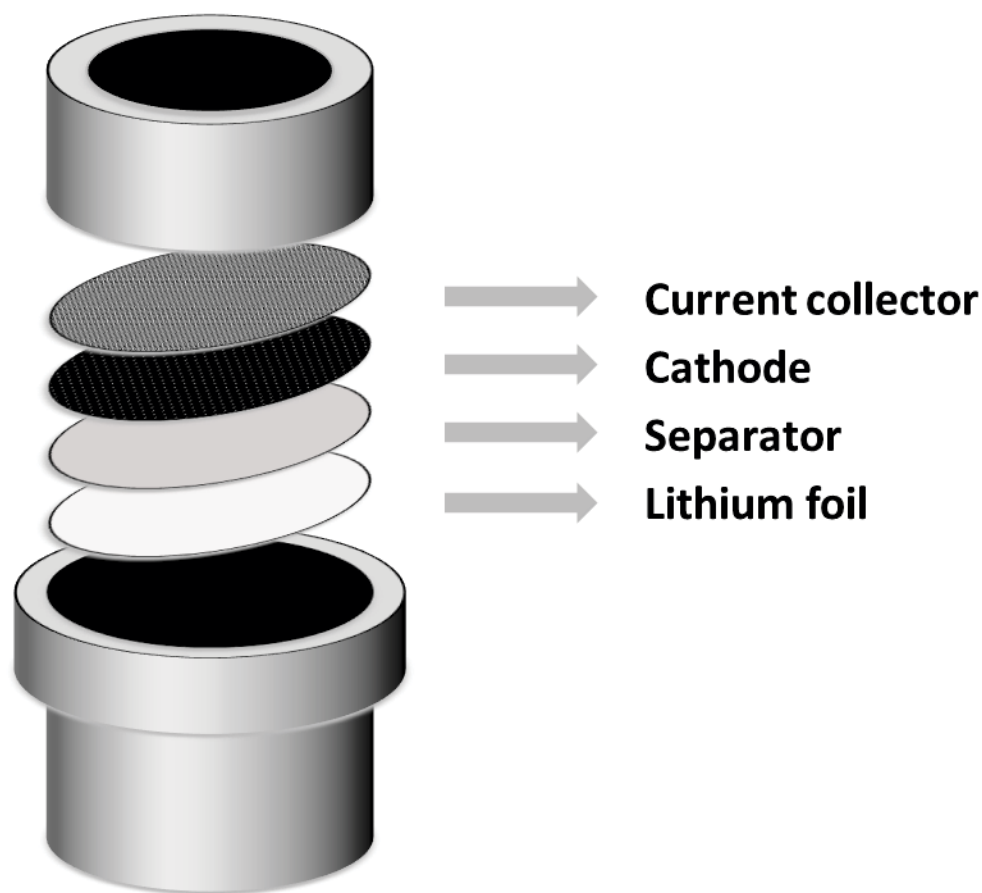


Figure 2-13 Schematic illustration of the construction of a Li-O₂ battery

2.6 Electrochemical measurements

The electrochemical measurements of Li-ion and Li-O₂ batteries with different electrolytes and cathode materials are evaluated by using three different approaches of measurements: cyclic voltammetry, electrochemical impedance spectroscopy, and galvanostatic discharge-charge techniques.

2.6.1 Cyclic voltammetry (CV)

Cyclic voltammetry or CV is a type of potentiodynamic electrochemical measurement which has been widely used in electrochemical characterization of materials in Li-ion and Li-O₂ batteries. It records the relationship of current and voltage when the potential of the working electrode is ramped linearly over time. This ramping is known as scan rate ($V s^{-1}$). CV can be conducted in two-electrode and three-electrode systems. In a typical three-electrode system, the potential is applied between a reference electrode and a working electrode and the current is measured between a working electrode and a counter electrode while in a typical two-electrode system, the potential and current are both measured between a working electrode and counter electrode.

In this project, the CV measurements were mainly performed by two-electrode systems, where a lithium anode was used as both reference and counter electrode. During the scanning, an analyte can be reduced or oxidized and re-oxidized or re-reduced on the return scan, which is known as a sign of highly reversible redox couples. The peaks on the CV results indicate the oxidation and reduction potentials. The CV measurements in this project were mainly conducted via a CHI 660C or CHI 660D electrochemical workstation (CH Instrument, Cordova, TN, Figure 2-14).



Figure 2-14 Photo of the CH instrument Electrochemical workstation

2.6.2 Electrochemical impedance spectroscopy (ESI)

Electrochemical impedance spectroscopy (EIS) has also been known as Alternating current (AC) Impedance. EIS is often used to characterize the dynamics of an electrochemical process in terms of an electrochemical cell's response to an applied potential at different frequencies. By observing the current response, the resistance within different frequencies can be examined. The resistance can be read from a typical Nyquist curve. Figure 2-15 shows the typical impedance Nyquist curve of a battery system consisting of a compressed semicircle in a medium frequency region which represents the charge-transfer resistance (R_{ct}) and an inclined line in the low frequency range which represents the Warburg impedance attributed to a diffusion-controlled process. The high frequency intercept at the real axis corresponds to the electrolyte bulk resistance and electronic resistance of the current collector.

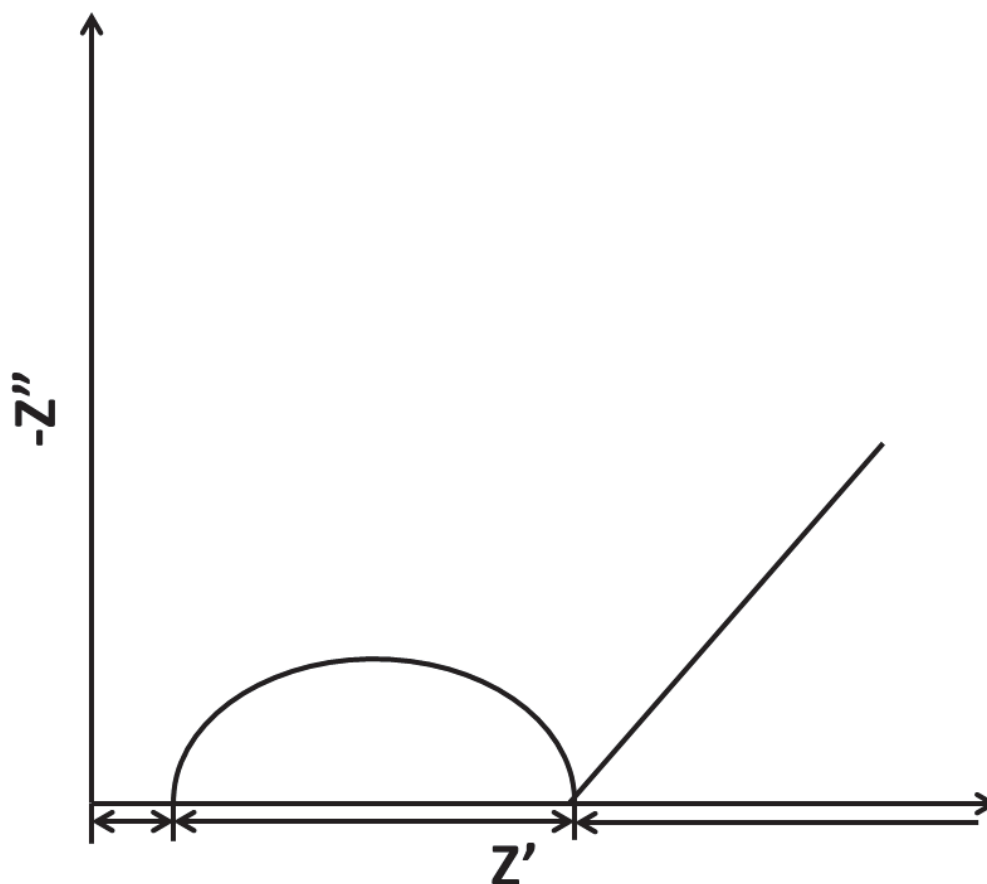


Figure 2-15 A typical impedance Nyquist curve of a battery system

EIS data were mainly collected using a CHI 660C or CHI660D electrochemical workstation (CH Instrument, Cordova, TN) in this project. The frequency range was set between 100 kHz and 0.01 Hz at controlled temperatures when the amplitude of the AC signal applied was set to 5 mV.

2.6.3 Linear Sweep Voltammetry (LSV)

Linear sweep voltammetry (LSV) is also a commonly used potentiodynamic electrochemical measurement where the current at a working electrode is measured while

the potential between the working electrode and a reference electrode is swept linearly in time. The whole scanning process is carried on through constant scanning rate (V/s). During the scanning, materials on the working electrode will undertake redox reactions. Oxidation or reduction of species is registered as a peak or trough the current signal at the potential at which the species begins to be oxidized or reduced. The scanning process can be operated only once or repeatedly. The basic mechanism is similar to CV measurement.

The LSV measurements in this project were mainly conducted via a CHI 660 C or CHI 660 D electrochemical workstation (CH Instrument, Cordova, TN).

2.6.4 Galvanostatic discharge-charge

Galvanostatic charge and discharge is used as electrochemical tests in which a constant current density is used to determine the electrochemical performances such as specific capacity and cycling performances. The capacities during charge or discharge can be calculated through the following equation,

$$Q = I \times t \quad \text{(Equation 2-2)}$$

I represents the current density, t is the charge or discharge time and Q stands for the capacity during charge or discharge process. In a three-electrode system, the galvanostatic charge and discharge performance is tested through a chronoamperometry technique on an electrochemistry workstation with an aqueous electrolyte in open circumstances. For a two-electrode system, a sealed or open battery cell is used for the testing. Usually, the galvanostatic charge and discharge tests can exhibit electrochemical information such as capacities, charge/discharge profiles, Columbic efficiency, and cycle properties.

In this project, the galvanostatic charge and discharge measurements were conducted on a computer-controlled Neware battery testing system or a Land Battery testing system, shown in Figure 2-16.



Figure 2-16 Photo of the Neware battery testing system

Chapter 3 Honeycomb-like porous gel polymer electrolyte membrane for lithium ion batteries with enhanced safety

3.1 Introduction

Currently, lithium ion batteries are the dominant power sources for portable electronic devices owing to their high energy density and efficiency. It is also well recognised that lithium batteries are the preferred system for electric vehicles and large-scale energy storage. Despite all efforts to improve the performances of lithium ion batteries, safety concerns remain a formidable challenge, due to the use of flammable liquid organic electrolyte and polymer separator.^[270, 271] Internal short-circuit and the combustion of the organic electrolyte could cause fire and explosion, which is a major obstacle for large-scale applications of lithium ion batteries.

Solid-state electrolytes can overcome the safety problem of lithium ion batteries because they do not contain flammable liquid chemicals.^[116, 272-274] However, solid-state electrolytes based on inorganic Li^+ conductors usually have low ionic conductivity. On the other hand, gel polymer electrolytes, which are prepared by gelling liquid electrolytes with polymer matrices, have advantages over both liquid electrolyte and ceramic (glass) electrolytes. Porous gel polymer electrolytes (PGPEs) combine electrolyte and separator as an integrated membrane.^[50, 107, 109, 133, 135, 136, 141] Compared with liquid electrolytes, polymer electrolytes can effectively prevent electrolyte leakage and reduce the firing hazard, which leads to the high safety of batteries. Meanwhile, porous polymer electrolytes can provide high ionic conductivity, good processability, a wide electrochemical operating window, and good thermal stability.^[137-140] Especially, several efforts have been made to accomplish

polymer electrolyte with enhanced thermal stability towards high temperature.^[275, 276] The porous structures in polymer membranes are also important because they are responsible for the uptake of liquid electrolytes. Though, membranes with too large pores can induce an internal short circuit, causing the failure of batteries. In order to solve this problem, several approaches have been carried out to reduce the pore size, such as embedding inorganic nanoparticles and coating with other polymer matrices.^[125, 148-150, 152]

The choices for polymer matrices are versatile. For example, poly(ethylene oxide) (PEO), polyacrylonitrile (PAN), poly(methyl methacrylate) (PMMA), poly(vinylidene fluoride) (PVDF), and poly(vinylidene fluoride-co-hexafluoropropylene) (PVDF-HFP) have been intensively studied.^[142-144, 146, 147, 153, 277] Among these polymers, PVDF-HFP has attracted particular interest because its semi-crystallinity, originating from the copolymerization of amorphous HFP, can trap liquid electrolytes, and crystal VDF can provide mechanical support.^[118] Therefore, PVDF-HFP can offer not only high ionic conductivity, but also good mechanical properties. In this paper, PVDF-HFP membranes with honeycomb-like regular porous structures were prepared by a breath-figure method. The as-prepared PVDF-HFP membranes have a unique porous architecture with highly ordered multi-sized pores. When applied as the separator in lithium ion batteries, PVDF-HFP gel polymer electrolyte membranes exhibited a high ionic conductivity at ambient temperature, an outstanding stability, and fire-proof capability. The as-developed porous gel polymer membranes are attractive for lithium ion batteries with enhanced safety.

3.2 Experimental details

3.2.1 Preparation of PVDF-HFP polymer electrolyte membranes

PVDF-HFP based porous membranes were prepared by a breath-figure method.^[278, 279] In the first step, PVDF-HFP (Sigma-Aldrich, Mw= 455,000) was dissolved in acetone solvent by mechanical stirring to obtain a homogeneous 10% PVDF-HFP/acetone solution. Then the solution was casted onto a flat glass substrate and allowed to dry under a controlled humidity of 86%. After fully drying, the obtained membrane was peeled off from the substrate and dried again in a vacuum oven at 60 °C for 12 h. The polymer electrolyte membranes were prepared by immersing the porous membrane overnight into 1M LiPF₆ in 1:1 ethylene carbonate (EC): dimethyl carbonate (DMC) liquid electrolyte. The excess liquid residue on the membrane surface was carefully wiped off with a tissue.

3.2.2 Characterization of PVDF-HFP membranes

A field emission scanning electron microscope (FESEM, Zeiss Supra 55 VP) was used to investigate the morphology of the as-prepared PVDF-HFP porous membrane. Thermal stability of the polymer membrane was measured by Thermogravimetric analysis using a Mettler Toledo TGA/DSC instrument. Infrared spectroscopy was conducted on a Nicolet Magna 6700 FT-IR spectrometer. All spectra were obtained using 4 cm⁻¹ resolution and 64 scans at room temperature.

The porosity of the polymer membrane was measured using *n*-butanol. The membrane was immersed in *n*-butanol for 2 h. The porosity of the polymer membranes was calculated based on the Equation 3-1.

$$p = \frac{(m_a - m_p) / \rho_a}{(m_a - m_p) / \rho_a + m_p / \rho_p} \quad (\text{Equation 3-1})$$

where p is the porosity, m_a and m_p are the mass of the membrane after and before the absorption of *n*-butanol, respectively, while ρ_a and ρ_p are the density of *n*-butanol and the polymer matrix, respectively.

The amount of liquid electrolyte uptake is calculated using the Equation 3-2.

$$\eta = \frac{W_t - W_o}{W_o} \times 100\% \quad (\text{Equation 3-2})$$

where η is the uptake of liquid electrolyte, and W_o and W_t are the weights of the membranes before and after absorption of liquid electrolyte respectively.

3.2.3 Electrochemical characterization of PVDF-HFP electrolyte membrane

Linear sweep voltammetry measurements were conducted to determine the stability of the PVDF-HFP polymer membrane. The polymer membrane was sandwiched between a lithium anode and stainless steel (SS) electrode. The electrochemical impedances at different temperatures were measured by sandwiching polymer electrolyte membranes between two stainless steel electrodes. The ionic conductivity was calculated using the Equation 3-3.

$$\sigma = d / (R_b \times S) \quad (\text{Equation 3-3})$$

where σ is the ionic conductivity, d is the thickness of the PGPE, R_b is the bulk resistance, and S is the area of the electrodes. All these electrochemical characterizations were conducted using a CH Instrument 660D electrochemical workstation.

The electrochemical performances of Li-ion batteries with PVDF-HFP polymer membrane was conducted by assembling CR2032 coin cells with lithium metal as the counter and reference electrode. LiFePO_4 prepared by conventional solid state reaction was used as the working electrode active material. The working electrode was prepared by first mixing PVDF (10%), carbon black (10%), and LiFePO_4 (80%) together in 1-Methyl-2-pyrrolidinone (NMP, Sigma-Aldrich). The mixture was then coated onto aluminium foil, dried at 80 °C for 12 h under vacuum, and punched into disks. All cells were assembled in an argon-filled glove box with water and oxygen content lower than 0.1 ppm.

3.3 Results and Discussions

The PVDF-HFP porous polymer membranes can be prepared by breath-figure method. According to literature related to this area, the concentration of PVDF-HFP in the solution and the atmosphere humidity are considered very crucial conditions to determine the morphology. In order to identify the most suitable morphology for lithium ion batteries, a series of experiments was conducted.

3.3.1 Optimisation

The most suitable concentration of PVDF-HFP in acetone solution was determined by operating parallel experiments with acetone solution of 1 wt%, 2 wt%, 5 wt%, and 10 wt%. The experiment was carried out under 80 % humidity. The results are shown in Figure 3-1.

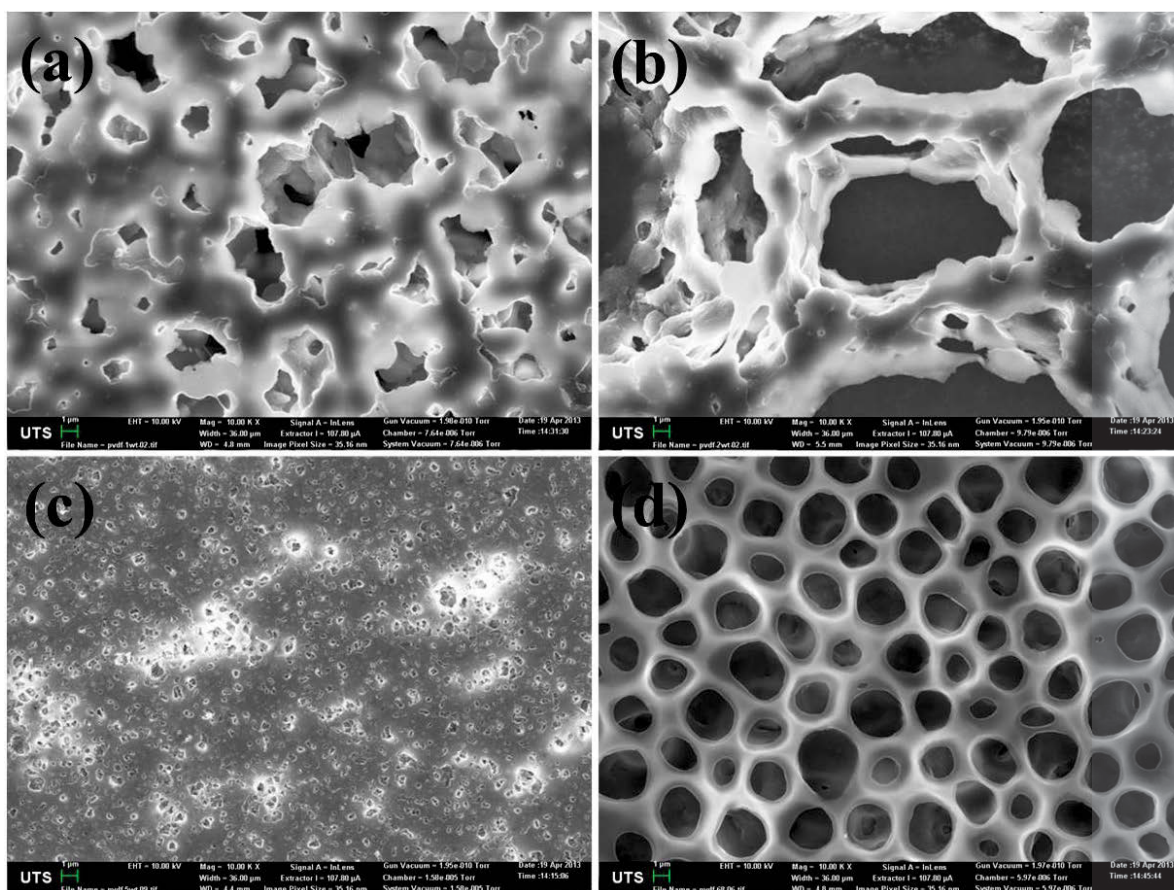


Figure 3-1 SEM images of porous membranes prepared with different concentrations of PVDF-HFP: (a) 1 wt%, (b) 2 wt%, (c) 5 wt%, and 10 wt%. The scale bar is 1 μm for all images.

When increasing the concentration of PVDF-HFP, the porous structure becomes more regular. When the concentration reaches 10 wt%, the surface morphology appears to be the best. Further increasing the concentration will lead to difficulties dissolving PVDF-HFP and forming a thin film. The results clearly indicate the best ratio for preparing a porous polymer membrane with regular pores and high porosity is 10 wt% of PVDF-HFP in acetone solution.

The humidity was controlled by pumping suitable water vapour into the drying atmosphere. The humidity was controlled from 65 % to 98 % with 10 wt% concentration of PVDF-HFP. The SEM images are shown in Figure 3-2.

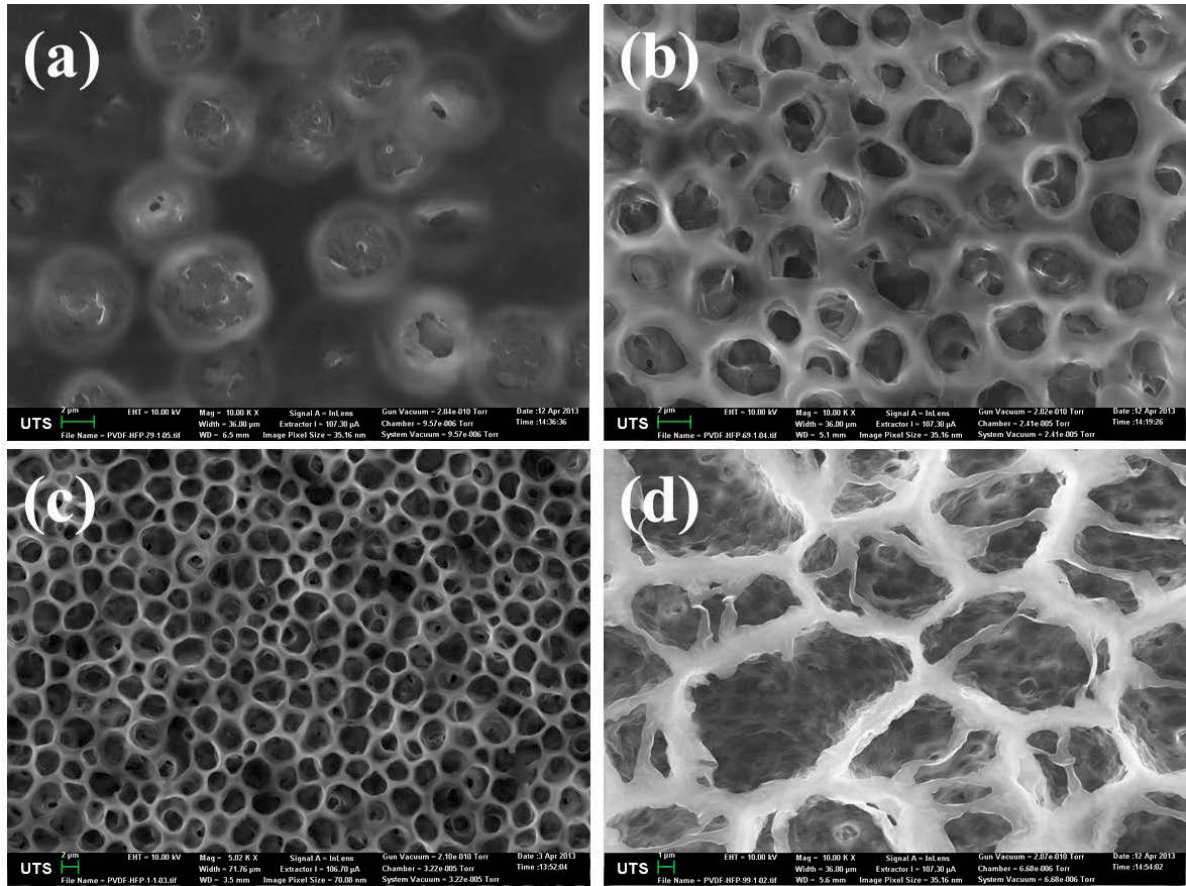


Figure 3-2 SEM images of porous membrane prepared in different humidities of (a) 65 %, (b) 76 %, (c) 86 %, and (d) 98 %. The scale bar is (a) 2 μm , (b) 2 μm , (c) 2 μm , and (d) 1 μm .

The results indicate the humidity has crucial influence on the morphology. It seems that by controlling the humidity, the size and regularity of the water droplet template can be easily tailored. By comparing the SEM images, it is safe to conclude that the porous

polymer membrane possesses the highest porosity and regularity when the atmosphere humidity reaches 86 %. Further increase will deteriorate the regular structure.

3.3.2 Morphology

Figure 3-3 shows FESEM images of porous PVDF-HFP gel polymer membranes. The membrane peeled from the glass substrate has two different sides. For convenience, the side in direct contact with humid air is defined as the front side, and the other side in direct contact with the glass substrate is called the back side. In Figure 3-3(a), an ordered honeycomb-like structure can be observed on the front side of the membrane. The diameters of the regular pores are in the range of 2 to 3 μm . The high magnification SEM image shown in Figure 3-3(b) indicates that there are also smaller pores inside the regular pores on the front surface of the membrane. This unique hierarchical porous structure could provide high porosity for further absorption of electrolyte. However, on the back side of the membrane, much less density of pores can be observed (as shown in Figure 3-3(c) and 3-3(d)). The diameters of the pores are smaller than 1 μm . Although the size and amount of the pores have decreased, these pores still interconnect inside the membrane (as shown in Figure 3-3(d)), which can provide a path way for fast ion transportation. Figure 3-3(e) and 3-3(f) show the FESEM images of the cross-section of the membrane. The thickness of the PVDF-HFP membrane is around 8 to 10 μm , which is thinner than the separators obtained by other techniques. It is very interesting to find that the porosity, diameters and regularity of pores decrease from the front side to the back side of the membrane. The three-dimension structure of the front side is shown in Figure 3-3(e) and the structure of the back side is shown in Figure 3-3(f). These results are consistent with the observation shown in

Figure 3-3(a) ~ (d) and Figure 3-4. The low porosity on the back side can prevent the risk of short circuit when applied in lithium ion batteries.

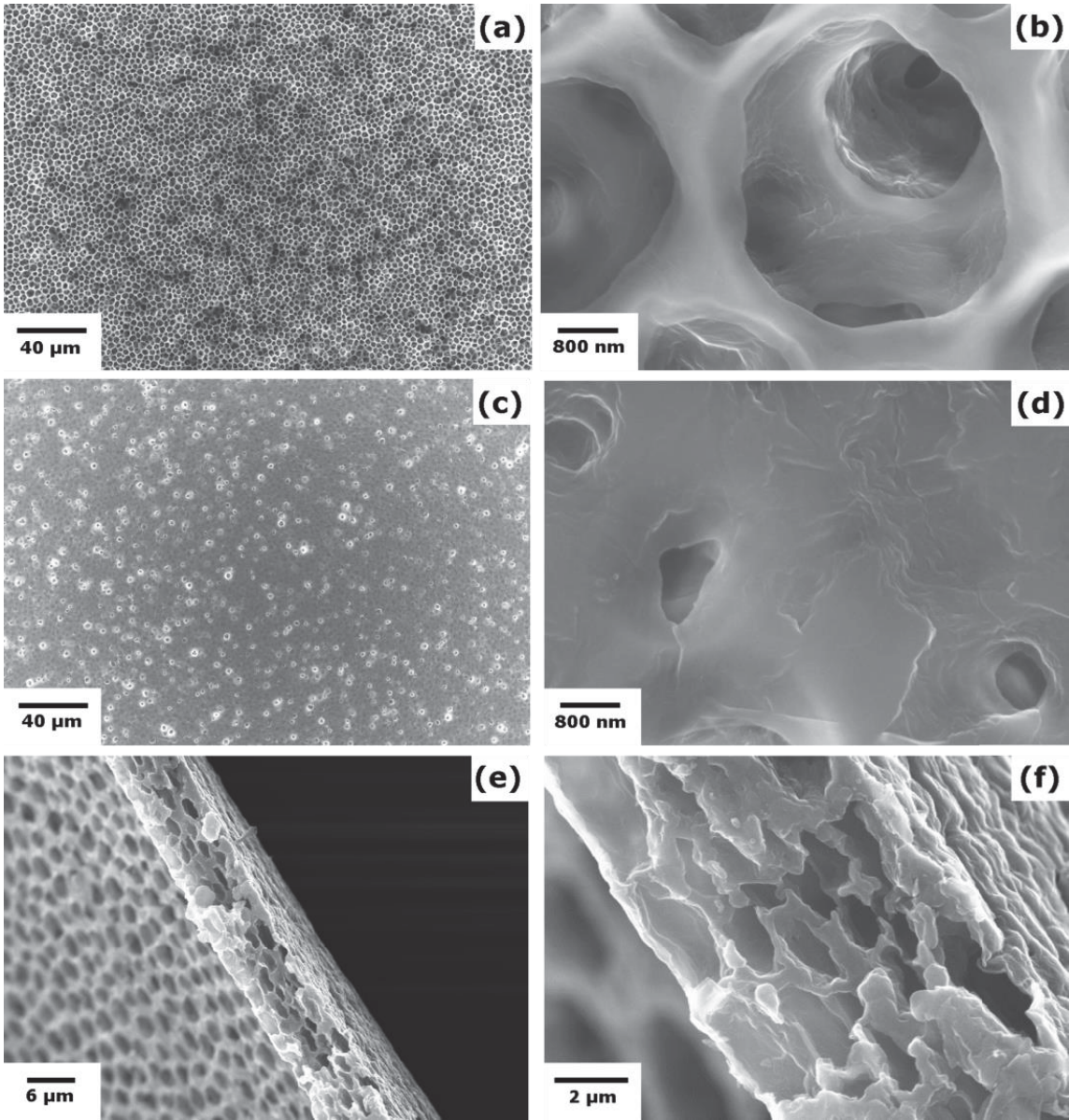


Figure 3-3 FESEM images of (a, b) the front side, (c, d) the back side, and (e, f) the cross-section of the PVDF-HFP honeycomb-like porous polymer membrane

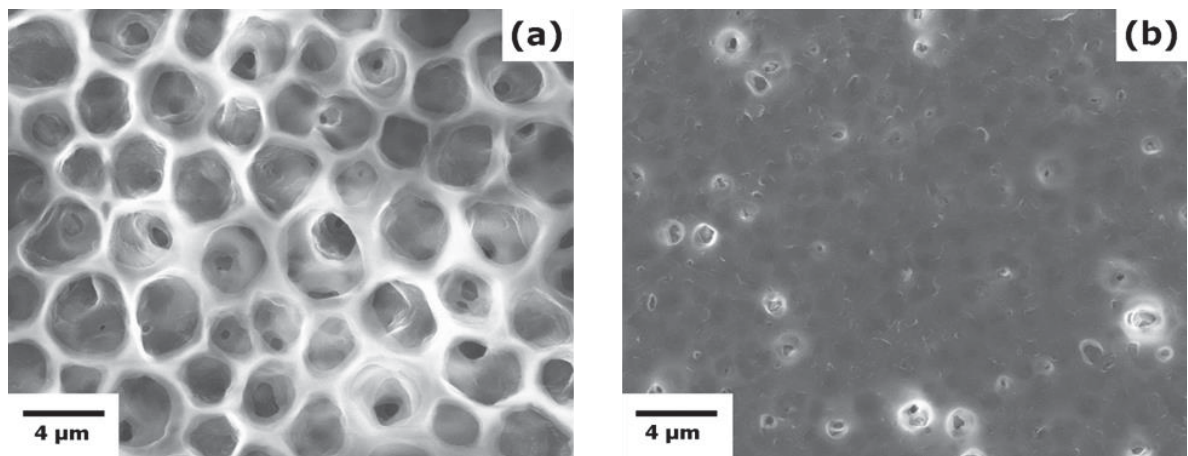


Figure 3-4 FESEM image of (a) the front side and (b) the back side of the PVDF-HFP honeycomb-like porous membrane

The formation of this unique porous structure could originate from the breath-figure preparation method.^[280-283] The preparation process is illustrated in Figure 3-5(a). When PVDF-HFP/acetone solution is naturally evaporated in an atmosphere with high humidity, water droplets will deposit onto the surface of the solution because of the decrease of the local temperature, owing to the endothermic nature of the evaporating process. PVDF-HFP molecules will gather and create a polymer shield around the water droplets. The water droplets will then further re-assemble and pack into a regular hexagonal pattern owing to the capillary force on the solution surface, which leads to the formation of the honeycomb-like architecture. After the formation of the first layer, the water droplets in the second layer are not facile to assemble into a regular porous structure because of the geometry blocking effect from the first layer and the decrease of humidity. This induces lower regularity, smaller size of pores and lower porosity. On the bottom of the membrane, the humidity is very low and the morphology is also influenced by the flat surface of the glass substrate, which results in a flat morphology with lower porosity and smaller pore size than

that on the front side of the membrane. Figure 3-5(b) shows the schematic structure of the obtained PVDF-HFP porous membrane, which is consistent with the SEM images shown in Figure 3-3.

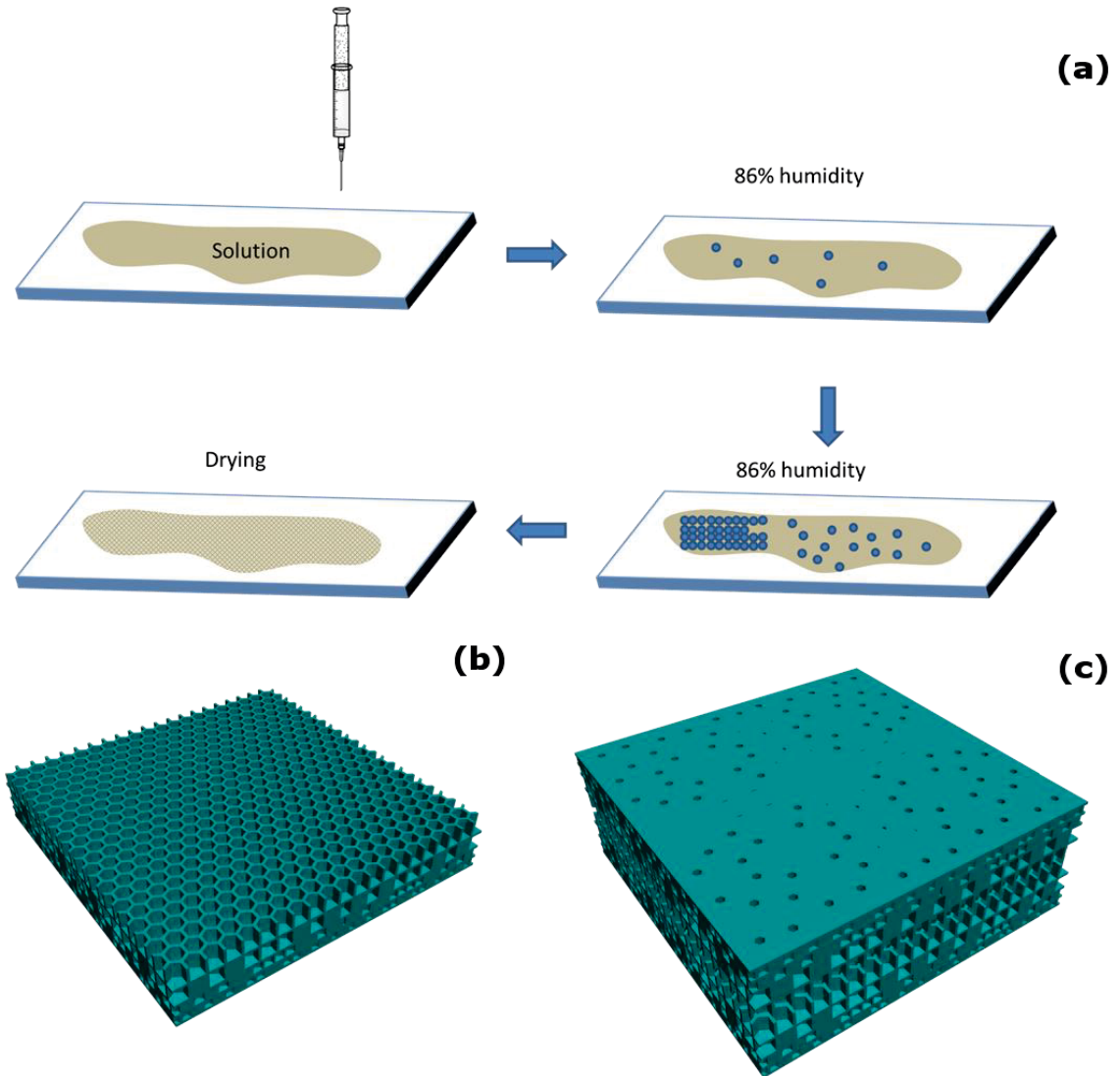


Figure 3-5 Schematic illustration: (a) The preparation process of the PVDF-HFP porous polymer membrane. (b) The 3D architecture of PVDF-HFP polymer membrane. And (c) the porous gel polymer electrolyte with the combination of two membranes as one integrated separator (two back sides are exposed to the outside).

In order to make better usage of the unique multi-porous architecture, we combined two membranes to make one separator. The honeycomb-like front side was put inside together with the back side exposed to the outside (as shown in Figure 3-5(c)). The thickness of the double-layered membrane is similar to the separators. The large, highly ordered pores inside the membranes are responsible for the absorption of electrolyte, while the flat back side exposed to the outside could help obstruct the transportation of electrode particles and the growth of lithium dendrite during cell operation. All the pores are interconnected and provide pathways for fast lithium ion transport. This unique double-layered membrane is expected to deliver good electrochemical performance when applied in lithium ion batteries.

3.3.3 Physical Characterization

Figure 3-6 shows the FTIR spectrum of the PVDF-HFP membrane. The characteristic peaks of PVDF-HFP copolymer are clearly presented in the spectrum. The peaks at 3028 and 2977 cm^{-1} originate from the stretching of $-\text{CH}_2-$ group and the peak at 1651 cm^{-1} is assigned to the $-\text{CH}=\text{CF}-$ skeletal bending. The $-\text{C}-\text{F}$ stretching peak is shown at 1401 cm^{-1} . The broad peaks near 1187 cm^{-1} are from the stretching of $-\text{CF}_2-$. The other peaks at 1065 (C-C skeletal vibration), 877 (vinylidene group), 841 ($-\text{CH}_2-$ rocking), 757 ($-\text{CF}_3$ stretching), 669 ($-\text{CH}_2-$ bending), 601 ($-\text{CF}_2-$ bending) and 489 cm^{-1} ($-\text{CF}_2-$ wagging) are all characteristic peaks of PVDF-HFP copolymer.

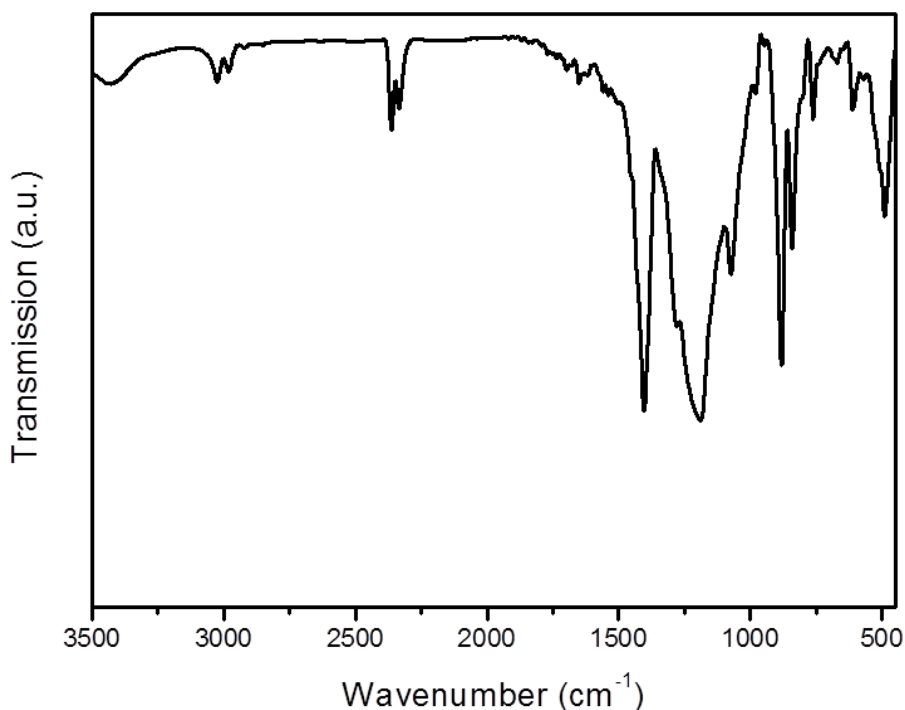


Figure 3-6 FTIR spectrum of the PVDF-HFP membrane

The stability of polymer electrolyte at high temperature is very crucial for Li-ion battery application. Figure 3-7 shows the thermogravimetry (TG) and differential scanning calorimetry (DSC) curves of the PVDF-HFP membrane. As shown in Figure 3-7, the membrane is thermally stable up to 140 °C and only shows a slight decrease in weight up to 350 °C, which is consistent with the DSC curve shown in Figure 3-5. There is an endothermic peak at 140 °C, which probably is related to the melting point of the PVDF-HFP. When the temperature increases above 150 °C, the membrane does not show endothermic peaks in air atmosphere. This indicates that the PVDF-HFP membrane is stable in the air at high temperature. The conventional separators usually shrink when the temperature reaches or exceeds the melting point, which causes an internal short circuit. In order to further investigate the dimensional stability of PVDF-HFP membranes in high

temperature, the membrane was stored at 150 °C for 30 min. Figure 3-8(a) and (b) show the digital photos of the membrane before and after heating. The PVDF-HFP membrane maintained the dimensional stability. This unique thermal property can effectively prevent the potential short circuit in lithium ion batteries. Conventional separators easily catch fire, and cause an explosion. Since PVDF-HFP is fire-resistant, PVDF-HFP polymer membranes should be fire-proof. Figure 3-8(c) and (d) show the digital photos of the membrane before and after being set on fire. Obviously, PVDF-HFP membranes can resist fire. The high thermal stability of the PVDF-HFP polymer membrane is desirable for lithium power batteries.

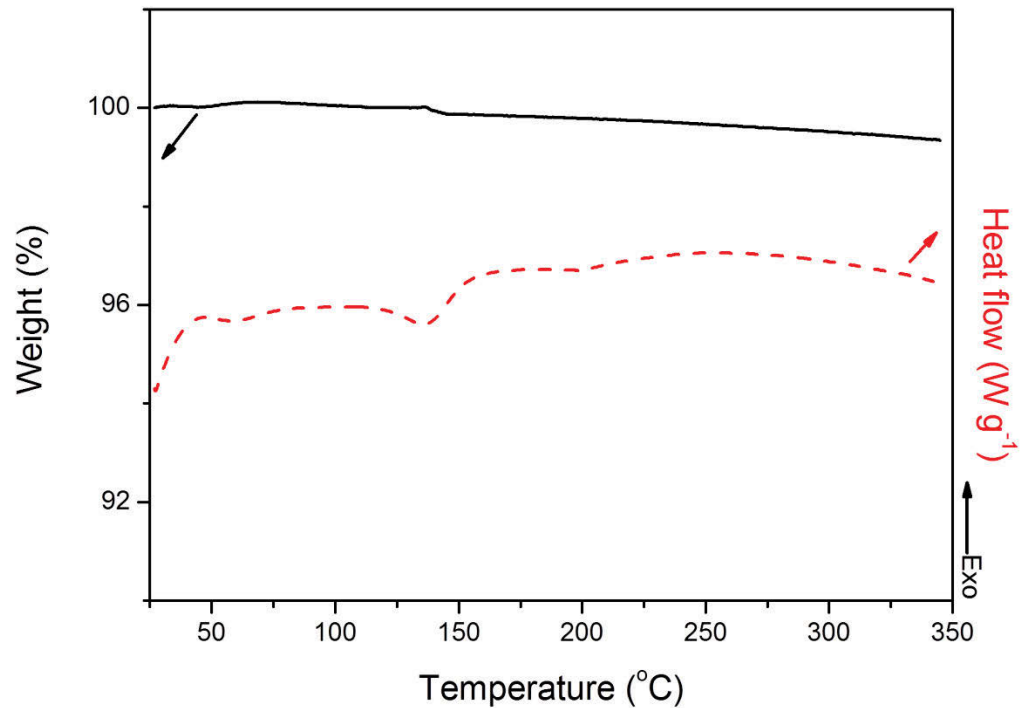


Figure 3-7 Thermogravimetry (TG, solid line) and differential scanning calorimetry (DSC, dot line) curves of PVDF-HFP porous polymer membrane in air. The temperature rising rate is 10 °C min⁻¹.

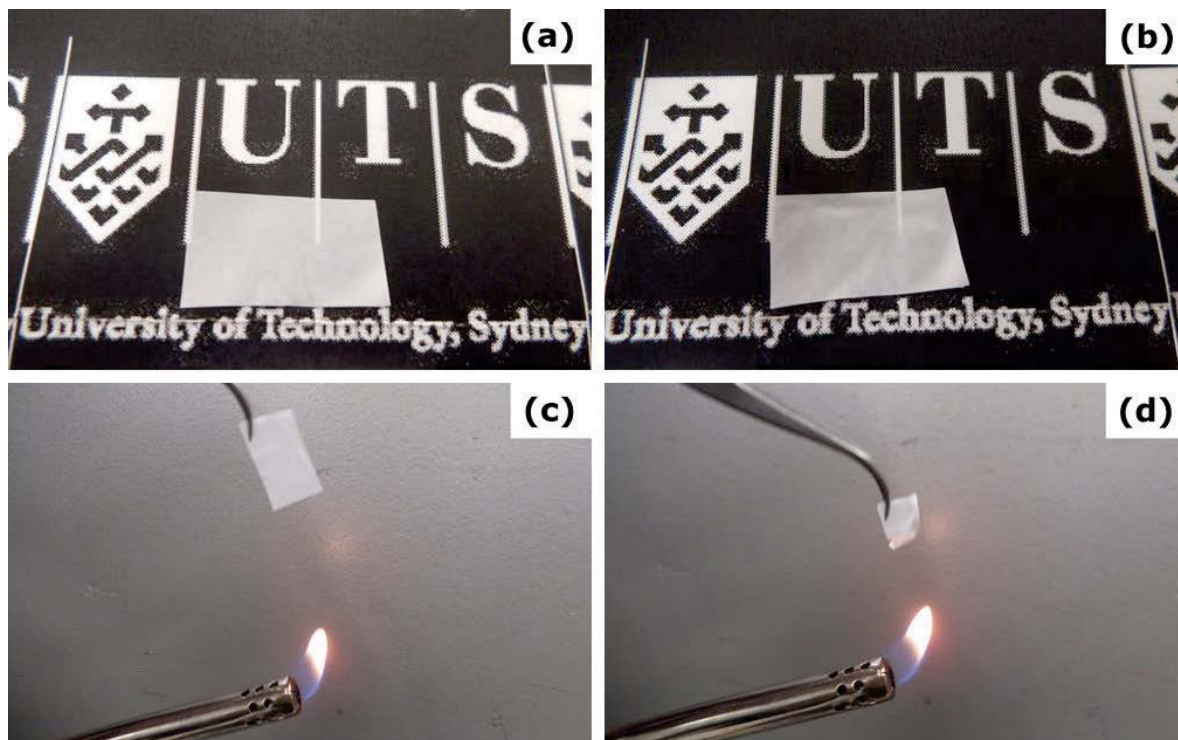


Figure 3-8 The thermal shrinking test of the PVDF-HFP porous membrane (a) before and (b) after heating to 150 °C for 30 min, and the combustion test of the membrane (c) before and (d) after set on fire.

The electrolyte retention capability of the PVDF-HFP polymer membrane was evaluated by TG and DSC analyses. Figure 3-9 shows the TG and DSC curves of the polymer membrane saturated with organic liquid electrolyte. The weight of the polymer membrane gradually decreases before 60 °C, which is probably related to the evaporation of electrolyte on the surface of the membrane. When the temperature increases to 150 °C, the polymer membrane with organic liquid electrolyte shows 40% weight loss, which is from the evaporation of the liquid electrolyte. However, compared with 86.2% electrolyte uptake calculated by measuring the mass before and after absorption, the content of retained electrolyte in the porous polymer membrane is still very high and sufficient for

electrochemical characterization when heating to 150 °C. Such good electrolyte retention capability can ensure the lithium ion battery operation at elevated temperatures.

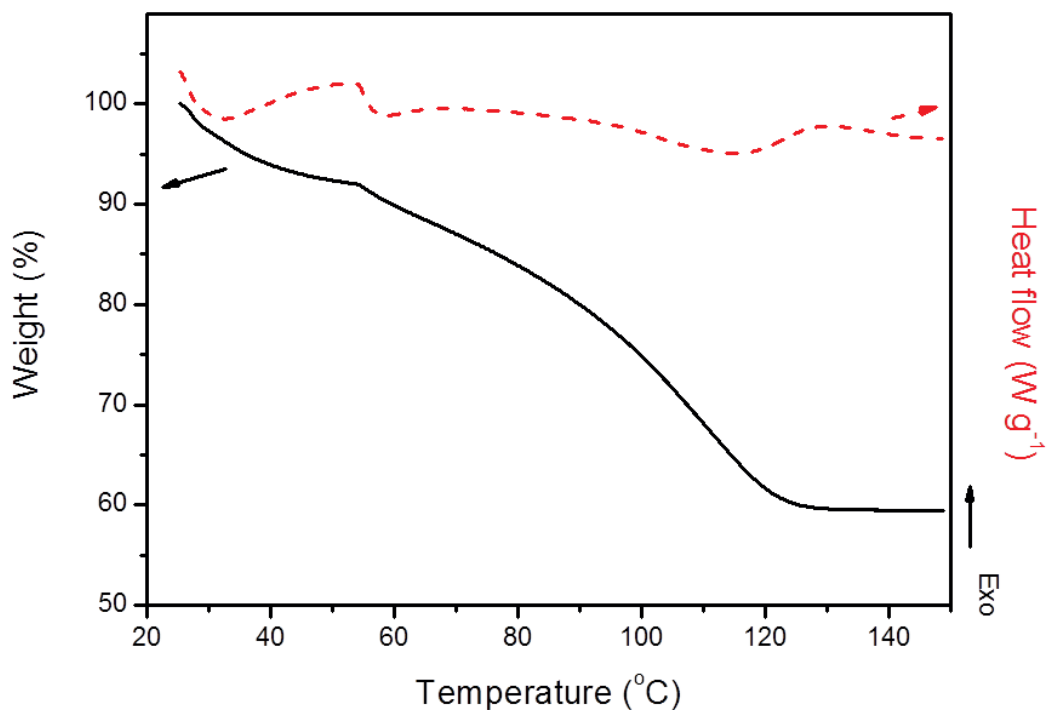


Figure 3-9 Thermogravimetry (TG) and differential scanning calorimetry (DSC) curves of the PVDF-HFP polymer electrolyte membrane in N₂. The temperature rising rate is 2 °C min⁻¹

3.3.4 Electrochemical characterizations

Ionic conductivity of the polymer electrolyte is the most critical factor in achieving good electrochemical performance of lithium ion batteries. Figure 3-10 shows the ionic conductivity dependence on temperatures of the PVDF-HFP polymer membrane and Celgard 2400 separator in the range of 25 °C to 65 °C. The ionic conductivities were calculated from the a.c. impedance plots shown in the inset in Figure 3-10. The resistance of the bulk electrolyte was obtained from the intercept of the straight line on the real axis.

The ionic conductivity of the PVDF-HFP polymer electrolyte membrane is 1.03 mS cm^{-1} at room temperature which is higher than the Celgard 2400 separator saturated with electrolyte (0.60 mS cm^{-1}), and increases with a rising temperature.^[132, 284] Such high ionic conductivity should be ascribed to the high porosity of the polymer membrane. There are three phases in the PVDF-HFP polymer electrolyte membrane, including solid polymer matrix, swollen polymer and absorbed liquid electrolyte solution. It is well known that polymer matrix is the mechanical support of the polymer electrolyte, while the absorbed liquid electrolyte solution is responsible for ionic conductivity. The PVDF-HFP polymer membrane has a porosity as high as 78%, which leads to high percentage electrolyte uptake (86.2 wt%). The pores in the membrane are also interconnected with each other, which is a further benefit for delivering high ionic conductivity.

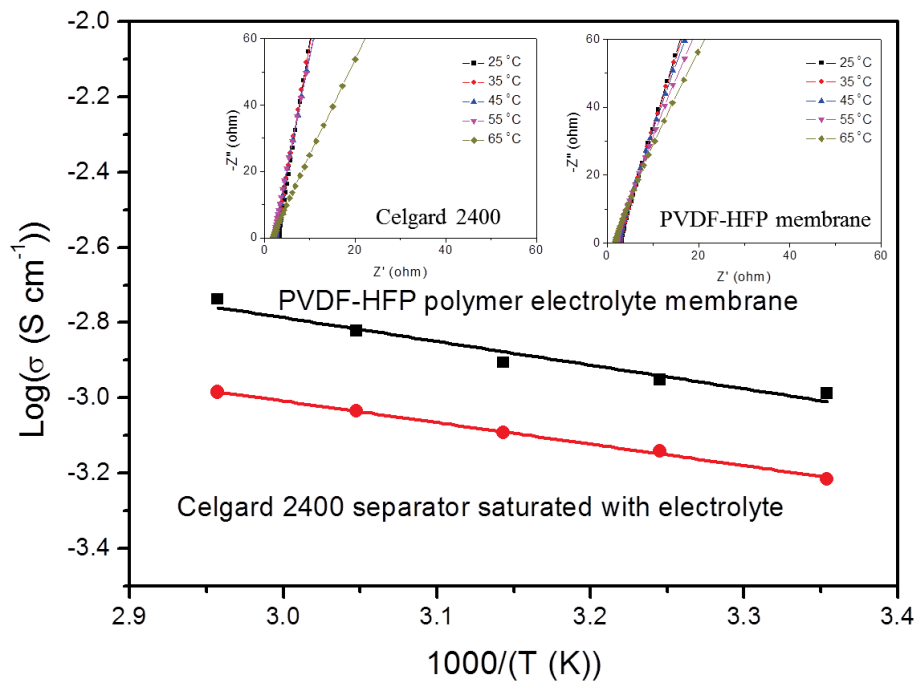


Figure 3-10 The Arrhenius plots of the ionic conductivity vs. temperature. The inset is the a.c. impedance spectra

The dependence of the ionic conductivity on temperature can be evaluated by the Arrhenius Equation,

$$\sigma = A \exp(-E_a / RT) \quad \text{(Equation 3-4)}$$

where A is the pre-exponential factor and E_a is activation energy. The calculated E_a value is 12.05 kJ mol⁻¹. This value is very similar to the activation energy of liquid electrolyte in Celgard 2400 separator (11.12 kJ mol⁻¹). This further explains the high ionic conductivity.

The electrochemical stability of the PVDF-HFP polymer electrolyte membrane was assessed by assembling Li-ion typed cells with the polymer electrolyte membrane sandwiched between a lithium metal electrode and stainless steel electrode. As shown in Figure 3-11, there is no obvious reaction peak up to 5 V, which indicates that the polymer electrolyte is stable up to 5 V. Normally, a stability window of up to 4.5 V is sufficient for the operation of lithium ion batteries.^[285]

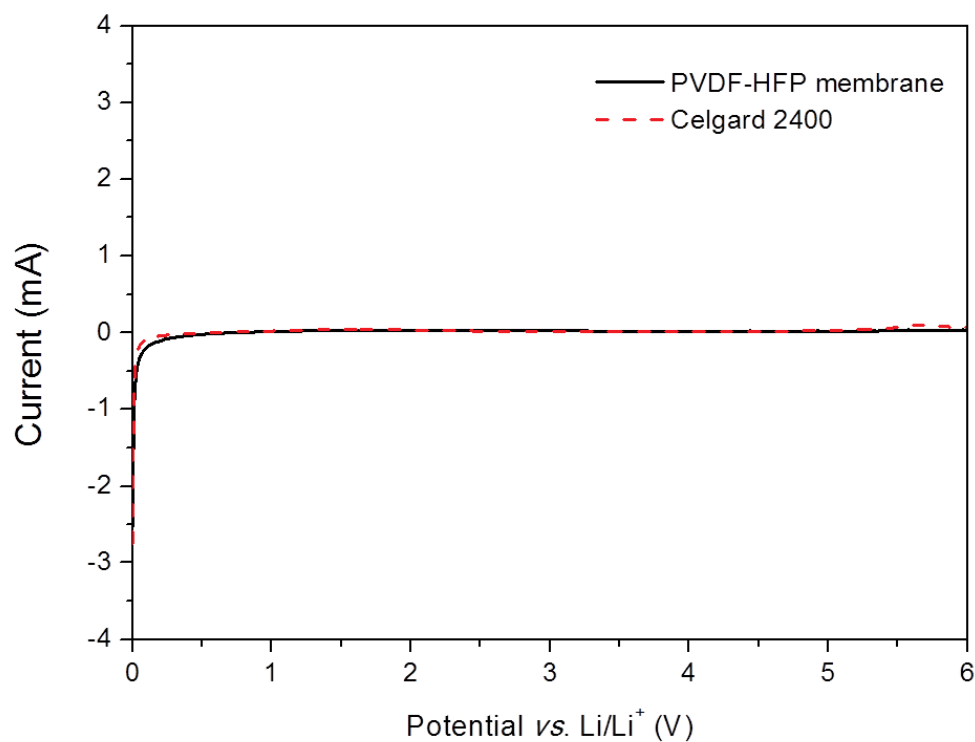


Figure 3-11 The linear sweep voltammogram of the PVDF-HFP polymer electrolyte membrane and Celgard 2400 separator. The scanning rate is 0.1 mV s^{-1} .

The electrochemical performances of the lithium ion battery with PVDF-HFP polymer electrolyte were further tested in coin type cells. Figure 3-12 shows the cyclic voltammetry curve of the assembled lithium ion cells. The redox potentials are 3.2 V and 3.6 V respectively, corresponding to the intercalation and de-intercalation of Li^+ in LiFePO_4 electrodes.^[286]

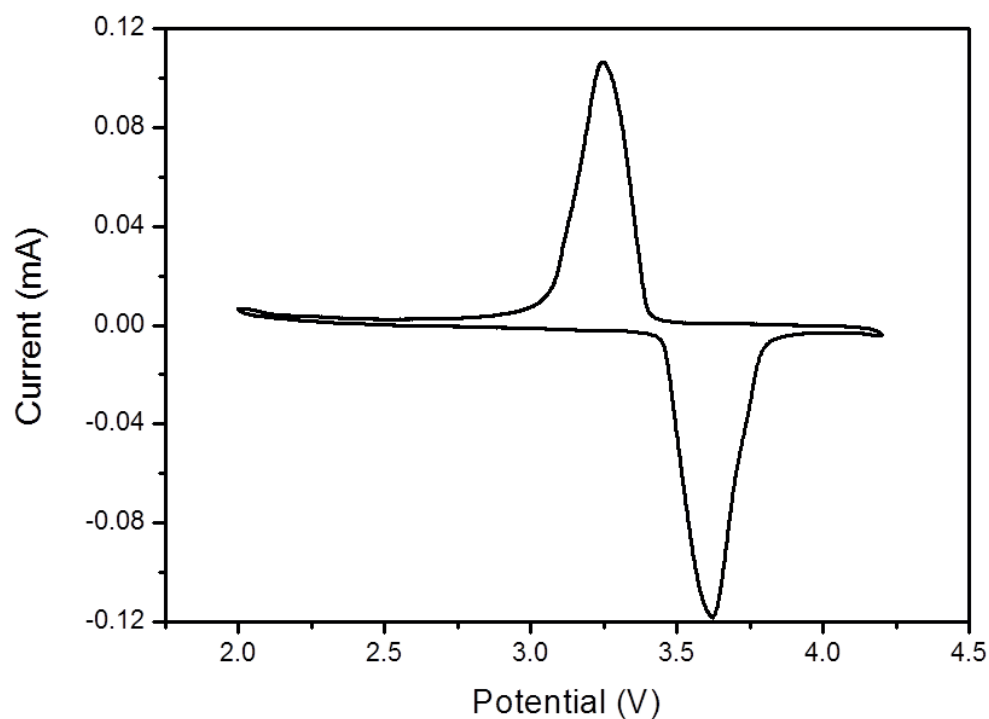


Figure 3-12 The cyclic voltammetry curve of lithium ion cells with the PVDF-HFP polymer electrolyte membranes. The scanning rate is 0.1 mV s^{-1} . The potential range is set between 2.0 to 4.2 V.

3.3.5 Battery performances

Figure 3-13 shows the electrochemical performances of lithium ion cells with LiFePO_4 as cathode materials, using PVDF-HFP polymer electrolyte membrane and Celgard 2400 as separators. The cut-off voltage was set at 2 V for discharge and 4.2 V for charge. Figure 3-13(a) shows the typical charge-discharge curves of the assembled lithium ion cells with PVDF-HFP polymer electrolyte membranes at the current density of 0.2 C ($1 \text{ C} = 170 \text{ mA g}^{-1}$). The charge and discharge plateaus are both around 3.4 V and the voltage difference between charge and discharge curves is smaller than 0.1 V, which is very similar to the direct use of liquid electrolyte with commercial separator (as shown in Figure 3-13(b)).^{[287-}

^{290]} The small over-potential maintains after 50 cycles, which suggests the capability of PVDF-HFP polymer electrolyte membranes to support superior battery performances. Figure 3-13(c) shows the cycling performances of lithium ion batteries with PVDF-HFP polymer electrolyte and liquid electrolyte. The lithium ion battery with PVDF-HFP polymer electrolyte could operate at least 50 cycles with no obvious capacity degradation. The reversible capacity of the lithium ion battery with PVDF-HFP polymer electrolyte was about 145 mAh g⁻¹ at 0.2 C, which is higher than that with a Celgard 2400 separator (130 mAh g⁻¹). The discharge performance of the lithium ion battery with PVDF-HFP polymer electrolyte at 1 C also showed good cycling stability up to 100 cycles (Figure 3-14).

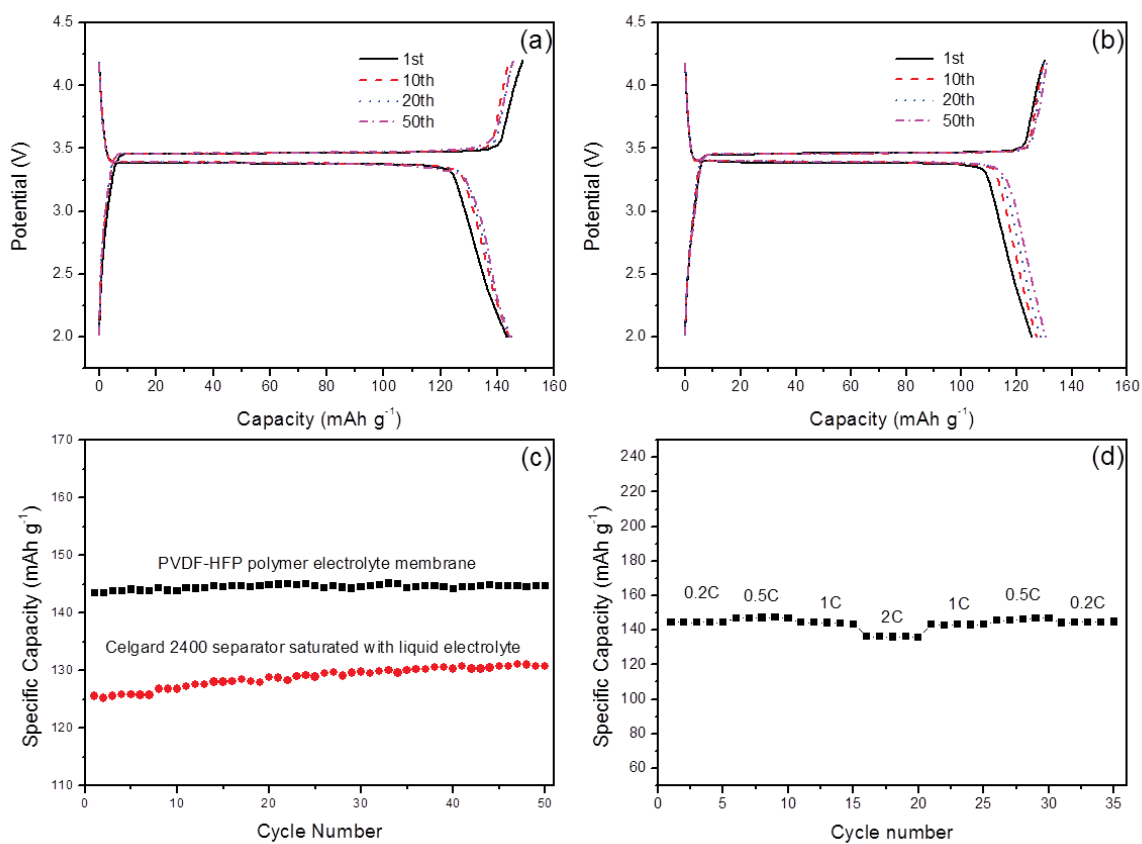


Figure 3-13 Electrochemical performances of lithium ion cells with LiFePO_4 as cathode materials: (a) Charge-discharge curves using PVDF-HFP polymer electrolyte membranes, (b) Charge-discharge curves using Celgard 2400 separators saturated with liquid electrolyte, (c) Cycling performances. The cut-off voltages are 2 V and 4.2 V. The current density is 0.2 C. (d) Rate behaviour. The current densities of discharge and charge are 0.2 C, 0.5 C, 1 C, and 2 C respectively.

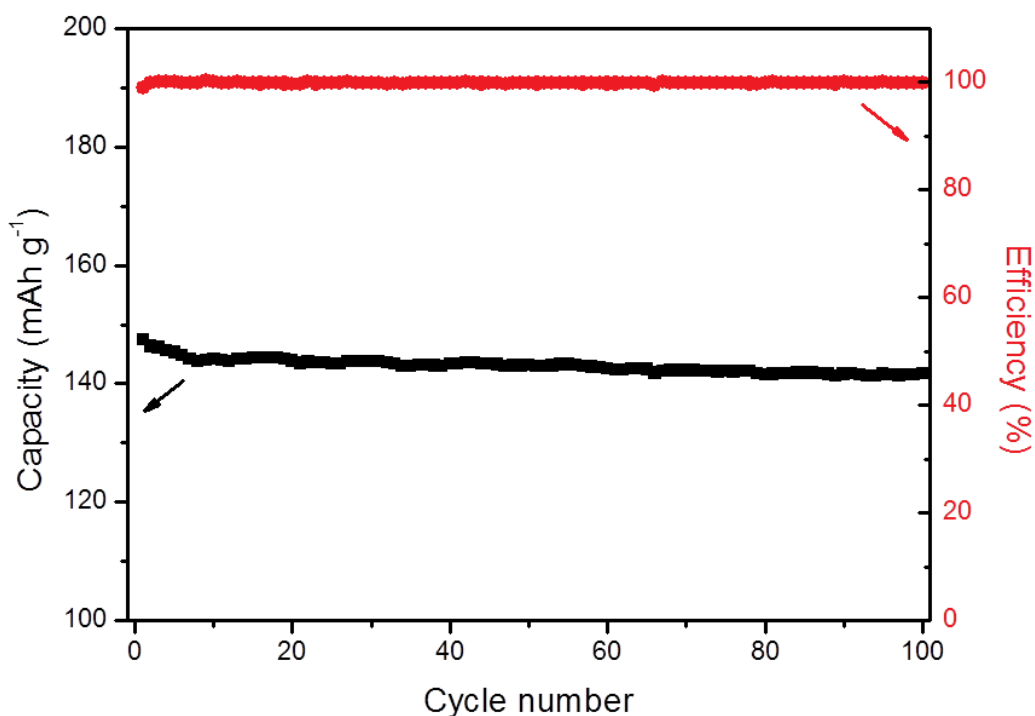


Figure 3-14 The cycling performance of the lithium ion cells with the PVDF-HFP polymer electrolyte membrane. The current density is 1 C.

When the cells were operated under different current densities, the capacity slightly decreased with the increase of the current density from 0.5 C to 2 C (as shown in Figure 3-13(d)). When the current density decreased back to 0.2 C, the reversible capacity recovered to its original value. The discharge and charge curves, shown in Figure 3-15, indicate the over-potential did not significantly increase when the current density escalated. These results further illustrate the PVDF-HFP polymer electrolyte membranes can support outstanding rate performances. Such high performances of lithium ion battery with PVDF-HFP polymer electrolyte are related to the multi-sized porous architecture of the PVDF-HFP polymer membrane. The large and interconnected pores inside the membrane provide high ionic conductivity, and the outside flat surface prevents lithium dendrite growth and

short circuiting, which eliminates the safety concerns and ensures a long and sufficient cycle life of lithium ion batteries.

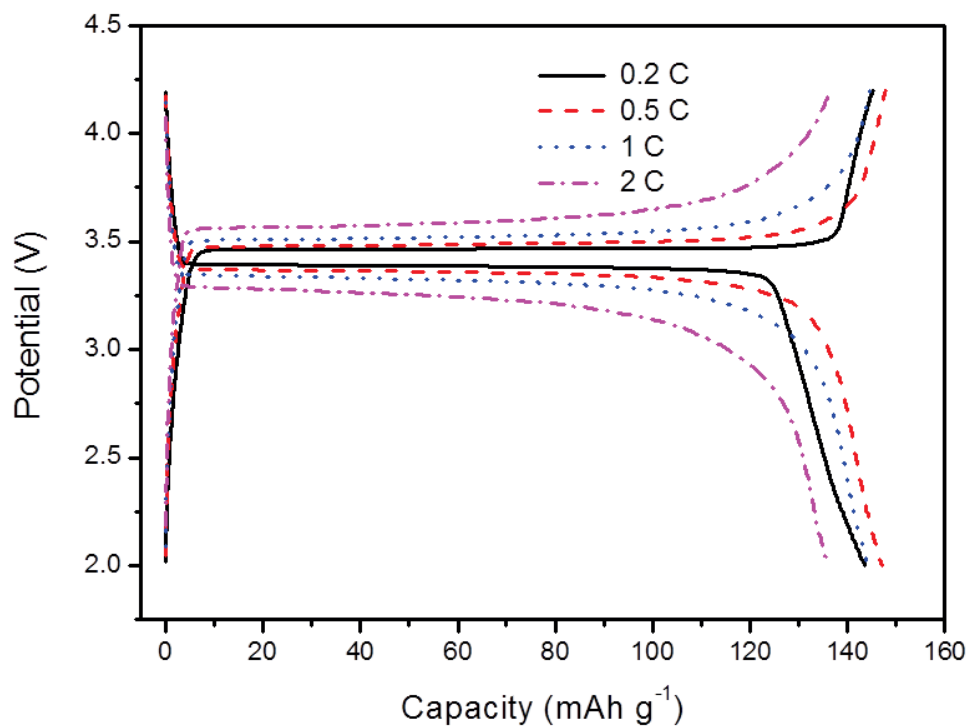


Figure 3-15 The charge-discharge curves of the lithium ion cells with the PVDF-HFP polymer electrolyte membranes at different current densities.

3.4 Summary

We report the development of poly(vinylidene difluoride-co-hexafluoropropylene) polymer membranes with multi-sized honeycomb-like porous architectures. The as-prepared polymer electrolyte membranes contain porosity as high as 78%, which leads to the high electrolyte uptake of 86.2 wt%. The PVDF-HFP gel polymer electrolyte membranes exhibited a high ionic conductivity of 1.03 mS cm⁻¹ at room temperature, which is much higher than that of commercial polymer membranes. Moreover, the as-obtained gel

polymer membranes are also thermally stable up to 350 °C and non-combustible in fire (fire-proof). When applied in lithium ion batteries with LiFePO_4 as cathode materials, the gel polymer electrolyte demonstrated excellent electrochemical performances. This investigation indicates that PVDF-HFP gel polymer membranes could be potentially applicable for high power lithium ion batteries with the features of high safety, low cost and good performance.

Chapter 4 Porous poly(vinylidene fluoride-co-hexafluoropylene) polymer membrane with sandwich-like architecture for highly safe lithium ion batteries

4.1 Introduction

Lithium ion batteries have been intensively investigated in the past few decades. Their high energy density and efficiency makes them promising candidates as the power sources for portable electronics, hybrid electronic vehicles, and electric vehicles.^[2, 291] Lithium ion batteries can also be used for electrical energy storage from renewable energy sources generated by solar or wind. Nevertheless, lithium ion batteries are still associated with severe safety risks such as fire and explosion hazards owing to the use of flammable separators and liquid organic electrolytes.^[292]

The concept of solid electrolytes was proposed in order to solve these safety issues. By eliminating flammable organic liquids, the risk of causing fires can be greatly reduced.^[116, 272-274] However, solid electrolytes usually contain inorganic Li^+ conductors as the main skeleton, which cannot provide sufficient ionic conductivity for fast ion transport during battery operation. Solid polymer electrolytes also suffer the same disadvantages. Gel polymer electrolytes, prepared by adding organic liquid electrolytes to a polymer system, can achieve high ionic conductivity and good safety.^[293, 294] By replacing the physical combination of separator and liquid electrolyte, gel polymer electrolytes, which are often made to be free-standing, can serve both roles. Porous gel polymer electrolytes showed distinguished characteristics such as high ionic conductivity, good processability, wide electrochemical operating windows, and thermal stabilities, as well as excellent capability

to prevent electrolyte leakage.^[135, 271, 295, 296] Compared to inorganic separators, porous gel polymer electrolytes provide more interactions between the liquid electrolytes and porous polymers by gelling with each other. Gelled skeleton and retained liquid electrolytes inside the porous polymer electrolyte membranes can both contribute to the ionic conductivity and mechanical property.^[297] Therefore, the electrochemical performance of porous polymer electrolytes is closely related to the porous structure of the polymer membrane matrix.^[138, 298] However, membranes with too large pore sizes can induce internal short circuits due to the mass transportation of electrode particles, leading to failure of the batteries. Several approaches such as embedding inorganic nanoparticles and the coating of other polymer species have been investigated to reduce the pore size of the polymer membranes.^[150, 152] Usually a glass substrate is used when there is an evaporation process involved during preparation of the membrane. Solution is poured on the glass substrate which acts as a support. It is interesting that the substrate has some influence on the surface morphology. Pu *et al.* investigated the effect of using substrate on morphologies on both surface sides.^[277]

The choices for polymer matrices are versatile. For example, poly(ethylene oxide) (PEO), polyacrylonitrile (PAN), poly(methyl methacrylate) (PMMA), poly(vinylidene fluoride) (PVDF), and poly(vinylidene fluoride-co-hexafluoropylene) (PVDF-HFP) have been intensively studied.^[299-301] PMMA demonstrated the best affinity with liquid electrolytes, resulting in high electrolyte uptake and high ionic conductivity. However, PMMA membranes are usually fragile and difficult to process. After absorption of liquid electrolytes, the integrity of membranes can be easily destroyed. The flammability of PMMA also limits its application as single polymer matrix in gel polymer electrolytes.

PVDF-HFP is able to provide sufficient mechanical properties and a relatively high ionic conductivity. The semi-crystal structure of crystal VDF and amorphous HFP makes it suitable to be used in porous gel polymer electrolytes.^[302] Several reports have already investigated the blend of PMMA and PVDF-HFP polymer electrolytes.^[118] Zhang *et al.* prepared a novel sandwich-like membrane by coating PVDF layers onto both sides of PMMA membrane, which exhibited enhanced electrochemical performances.^[303] Inspired by those outcomes, we prepared a sandwich-like polymer membrane with multi-size porous structure by coating PMMA onto PVDF-HFP porous membrane. The as-prepared polymer membrane showed an outstanding stability towards high temperature and fire. When gelling with a liquid electrolyte, the polymer membrane exhibited high electrolyte uptake and an excellent electrochemical performance in lithium ion batteries. This as-developed porous gel polymer electrolyte could be applied in lithium ion batteries with enhanced performance and safety.

4.2 Experimental details

4.2.1 Preparation of PVDF-HFP porous polymer membranes

PVDF-HFP porous polymer membranes were prepared by a breath-figure method. Firstly, a homogeneous 10 wt% PVDF-HFP/acetone solution was obtained by dissolving PVDF-HFP into acetone solvent. The solution was then cast onto a flat glass substrate and allowed to dry under a room humidity of 45%. After fully drying, the obtained membrane was carefully peeled off from the flat glass substrate, vacuumed, and stored inside a glovebox.

The as-prepared PVDF-HFP porous polymer membrane has two sides. For convenience, the side that was in direct contact with room humidity was called front side, and the other side in contact with the flat glass substrate was called back side.

4.2.2 Preparation of PMMA/PVDF-HFP porous polymer membranes

Two pieces of the as-prepared PVDF-HFP porous polymer membranes were used as one by putting them together with both front sides facing inside. The connected membranes were immersed in 2.5 wt% PMMA/CHCl₃ solution for 1 h. The membranes were then taken out and cleaned with a tissue to eliminate the surface solution residue. During the drying process, the membranes gradually self-adhered and became one piece of membrane after fully drying. The obtained PMMA/PVDF-HFP porous membrane was then stored in an argon-filled glovebox.

4.2.3 Preparation of gel polymer electrolyte membranes

The polymer electrolyte membranes were prepared by immersing the as-prepared porous membranes in liquid electrolyte solution (1 M LiPF₆ in 1:1 ethylene carbonate (EC): dimethyl carbonate (DMC)) overnight. The excess liquid residue on the membrane surface was carefully wiped off with a tissue.

4.2.4 Characterizations of the as-prepared porous polymer membranes

A field emission scanning electron microscope (FESEM, Zeiss Supra 55 VP) was used to observe the morphology of the as-prepared porous polymer membranes. Thermal stabilities of the polymer membranes were measured by Thermogravimetric analysis using a Mettler Toledo TGA/DSC instrument. Infrared spectroscopy was conducted on a Cary 630

FTIR-ATR spectrometer (Agilent Technologies). All spectra were obtained by using 8 cm^{-1} resolution and 32 scans at room temperature.

The amount of liquid electrolyte uptake is calculated using Equation 4-1.

$$\eta = \frac{W_t - W_o}{W_o} \times 100\% \quad (\text{Equation 4-1})$$

Where η is the uptake of liquid electrolyte, and W_o and W_t are the weight of the membranes before and after absorption of the liquid electrolyte, respectively.

4.2.5 Electrochemical characterization of polymer electrolyte membranes

To equate the thickness and morphology, two pieces of PVDF-HFP polymer electrolyte membrane were used as one where front side was put inside together with the back side exposed to the outside. The PMMA/PVDF-HFP polymer electrolyte membrane and Celgard 2400 separator were used a single piece, respectively, as electrolyte membrane.

Linear sweep voltammetry measurements were conducted to determine the stability of the polymer electrolyte membranes. The polymer membranes were sandwiched between a lithium anode and stainless steel (SS) electrode. The electrochemical impedances at different temperatures were measured by sandwiching polymer electrolyte membranes between two stainless steel electrodes. The ionic conductivity was calculated using Equation 4-2.

$$\sigma = d / (R_b \times S) \quad (\text{Equation 4-2})$$

Where σ is the ionic conductivity, d is the thickness of the membrane, R_b is the bulk resistance, and S is the area of the electrode. All electrochemical characterizations were conducted using a CH Instrument 660D electrochemical workstation.

The electrochemical performances of lithium ion batteries with polymer electrolyte membranes were conducted by assembling CR2032 coin cells with lithium metal as the counter and reference electrode. LiFePO_4 prepared by conventional solid state reaction was used as the working electrode active material. The working electrode was prepared by mixing PVDF (10%), carbon black (10%), and LiFePO_4 (80%) in 1-Methyl-2-pyrrolidinone (NMP). The mixture was then coated onto aluminium foil, dried at 80 °C for 12 h in a vacuum, and punched into disks. All cells were assembled in an argon-filled glovebox with water and oxygen content lower than 0.1 ppm.

4.3 Results and discussions

4.3.1 Morphology

Figure 4-1 shows the FESEM images of the PVDF-HFP and PMMA/PVDF-HFP porous polymer membranes. Figure 4-1(a) exhibits the morphology of the front side surface of PVDF-HFP porous polymer membrane. A porous morphology with very large pores can be seen from the image. The diameters of the pores are within the range of 4 – 6 μm . Inside the large micron pores on the surface, pores with smaller diameters can be identified, which are interconnected. Figure 4-1(b) shows the morphology of the back side of PVDF-HFP porous polymer membrane. Different from the front side, most of the pores on the back side are very small with diameters less than 1 μm , and the porosity is significantly lower than that of the front side. The cross-section image in Figure 4-1(c) also confirms the

morphologies of both sides. It is remarkable to note that the pores in the membrane spread in layers, and the entire membrane consists of many porous layers. The porosity of each layer decreases with the increase of depth from front to back side. The porosity of the entire structure is very high according to the cross-section image. However, the thickness of the membrane is around 9 to 10 μm , which is significantly thinner than most commercial separators.

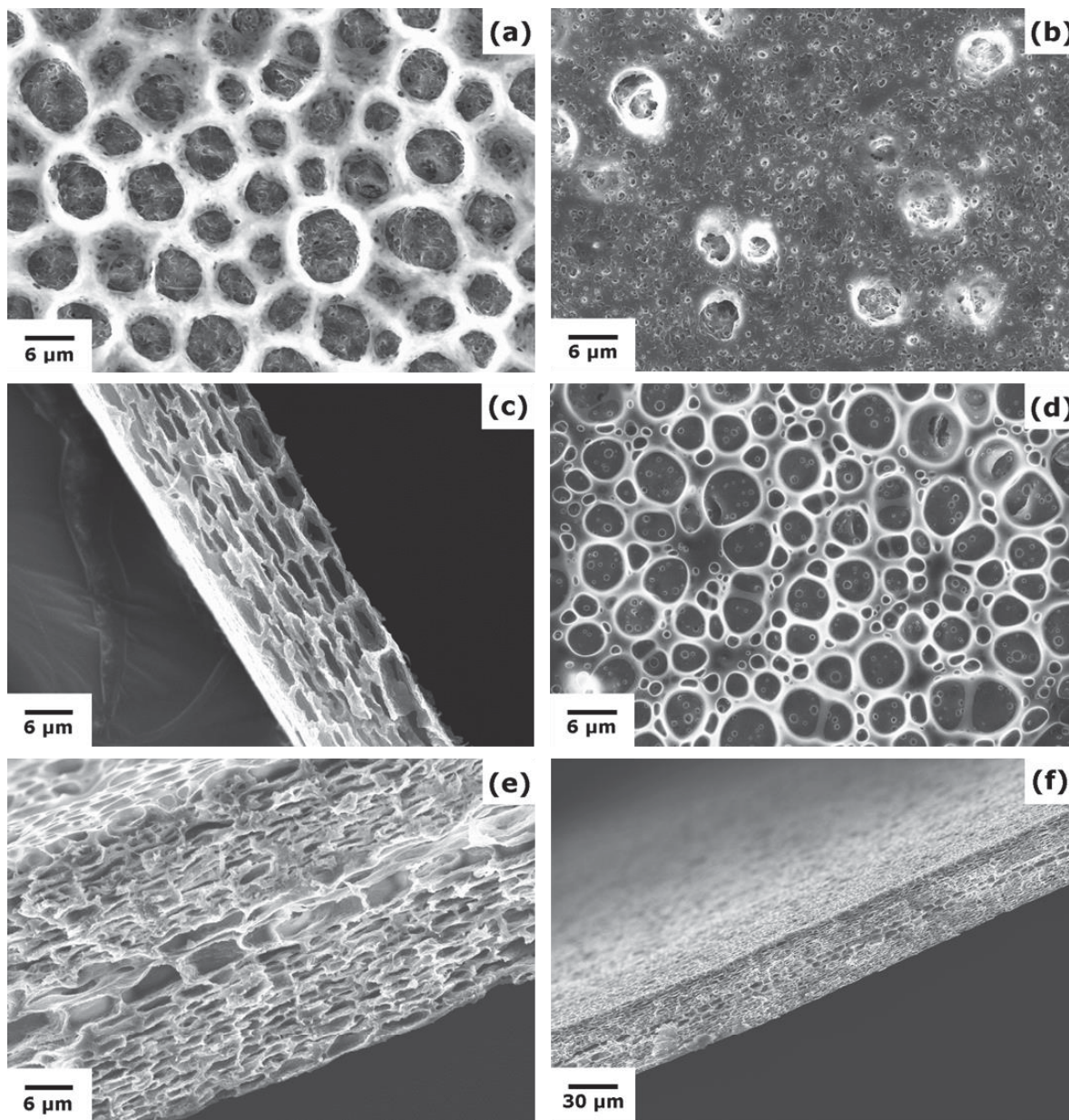


Figure 4-1 FESEM images of (a) the front side, (b) the back side, and (c) the cross-section of the PVDF-HFP porous polymer membrane, and (d) the outside surface, (e, f) the cross-section of the PMMA/PVDF-HFP porous polymer membrane.

The formation of this multi-sized porous structure is due to the use of a breath-figure method. By casting the PVDF-HFP acetone solution onto a flat glass substrate, an interface

between the ambient atmosphere and the polymer solution is created. During the evaporation process, the local temperature on the interface can be significantly reduced owing to the endothermic nature of the evaporating process. Water droplets can be formed at these low-temperature positions, and polymer chains will assemble and cover the water droplets, forming a polymer-rich shell. These droplets will be re-assembled and packed together due to the capillary force. After completely drying, a highly porous structure can be formed. As the evaporation process occurs mainly on the interface, it induces the layered porous structure. However, due to the decrease of humidity, increase of acetone vapour content and blocking of the geometry, the size and porosity of each layer decreases with the increase of depth. On the bottom of the membrane, which is referred to as the back side, the morphology can be greatly influenced by the flat glass substrate, resulting in a flat surface with small pores and low porosity. Due to the pore-forming mechanism, most of the pores are interconnected.

After the immersion processing of the PVDF-HFP membranes into PMMA/CHCl₃ solution, the morphology changed significantly. Since the preparation of the PMMA/PVDF-HFP porous polymer membrane was achieved by using two PVDF-HFP membranes together with front sides put inside and back sides exposed outside, the morphologies of both sides of the as-prepared PMMA/PVDF-HFP porous polymer are identical. The morphology is shown in Figure 4-1(d). A very thin layer of PMMA with large-size pores can be observed on the surface. The typical morphology of the PVDF-HFP membrane with small pores can still be recognised underneath this thin layer of PMMA. This result indicates that there is only a small amount of PMMA residue on the surface of the PVDF-HFP porous membrane. The cross-section morphology of the as-prepared

PMMA/PVDF-HFP porous polymer membrane is shown in Figure 4-1(e). The SEM image clearly indicates that the PMMA/PVDF-HFP porous polymer membrane consists of stacking porous layers. However, compared with pristine PVDF-HFP porous polymer membrane, the pore sizes have been significantly decreased, except for the one or two layers in the middle of the membrane. The shrink of pore size is contributed to the addition of PMMA. During the immersion of PVDF-HFP porous membrane into the PMMA/CHCl₃ solution, a large amount of PMMA solution flooded into the pores of PVDF-HFP membrane. After drying, PMMA was then coated on the inside surface of the membrane, resulting in smaller and more compressed pore structures. However, because the pores in the surface porous layer of PVDF-HFP porous membrane are too large to retain PMMA solution, the solution was then flooded between the two pieces of membranes and PMMA remained after evaporation. The interaction between PVDF-HFP surface large pore layers and PMMA resulted in one or two porous layers with very large pores, and the polymer nature of PMMA helped integrate two porous PVDF-HFP membranes into one. The morphology of this structure is unique and therefore could improve the electrochemical performances. Small pores in the outer layers can eliminate the risk of lithium dendrite growth and the exchange of electrode materials, while large pores are responsible for uptaking and retaining large amounts of electrolyte. The low magnification SEM image is shown in Figure 4-1(f), which illustrates that this unique structure is homogeneous through the entire polymer membrane.

4.3.2 Physical characterizations

Figure 4-2 shows the FTIR spectra of the as-prepared PVDF-HFP and PMMA/PVDF-HFP polymer membranes. The characteristic peaks of PVDF-HFP copolymer are clearly

presented in both spectra. The peaks at 3025 and 2973 cm^{-1} are assigned to the stretching of the $-\text{CH}_2-$ group. The $-\text{C}-\text{F}$ stretching peak is shown at 1393 cm^{-1} . The broad peaks near 1177 cm^{-1} are from the stretching of $-\text{CF}_2-$. The other peaks at 1065 cm^{-1} (C-C skeletal vibration), 871 cm^{-1} (vinylidene group), 834 cm^{-1} ($-\text{CH}_2-$ rocking), 760 cm^{-1} ($-\text{CF}_3$ stretching), and 678 cm^{-1} ($-\text{CH}_2-$ bending) are all characteristic peaks of PVDF-HFP copolymer. The only difference between the spectra of two polymer membranes is the peak at 1721 cm^{-1} , which is the characteristic band for the $\text{O}-\text{C}=\text{O}$ stretch. This peak is attributed to the ester group in the PMMA molecular structure. This result confirms that PMMA has been successfully coated inside the PVDF-HFP membrane.

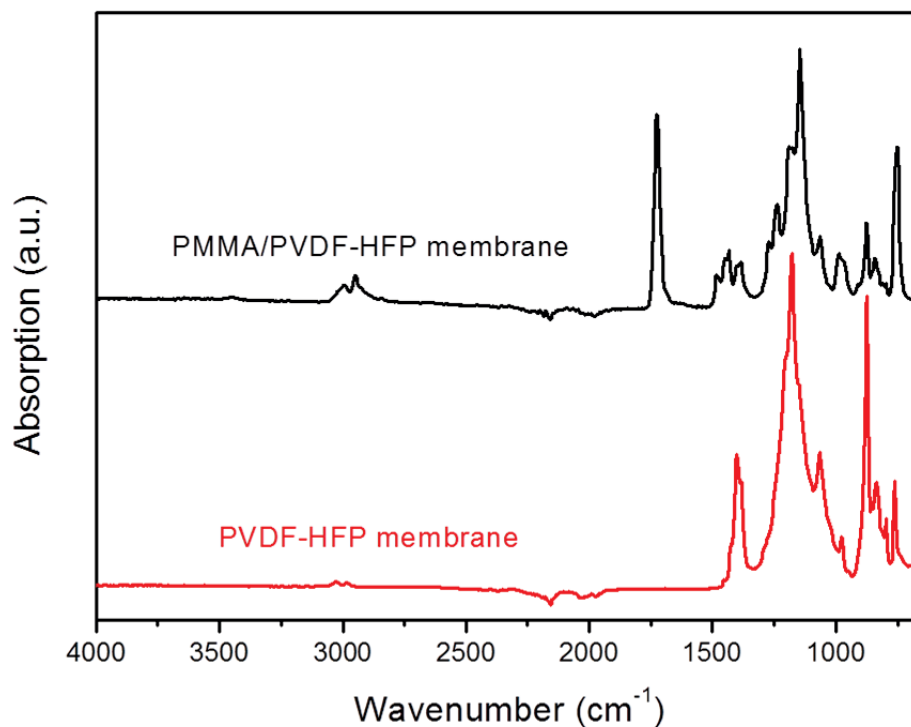


Figure 4-2 FTIR spectra of the PVDF-HFP and PMMA/PVDF-HFP membranes

It is crucial for a polymer matrix to have an acceptable stability, especially towards high temperatures. During cycling, there is a possibility that the battery reaction will generate

heat, which may cause decomposition and degradation of the separator, resulting in potentially serious safety problems. Figure 4-3 shows the thermogravimetry (TG) and differential scanning calorimetry (DSC) curves of both porous polymer matrices at a temperature range of room temperature to 350 °C. The TG results clearly demonstrate that both polymer matrices are stable up to 150 °C. They only show a slight decrease in weight at 300 °C. The DSC curves also confirm these results. However, compared with PVDF-HFP polymer membranes, the PMMA/PVDF-HFP polymer membrane has a significant endothermic effect. This is most likely attributed to the PMMA coating, which has been recognized to melt more easily. The polymer electrolyte can automatically shut down if the temperature approaches the critical flaming point of the liquid electrolyte. The stability of the PMMA/PVDF-HFP polymer porous membrane is outstanding towards high temperature and is sufficient to be used in lithium ion batteries.

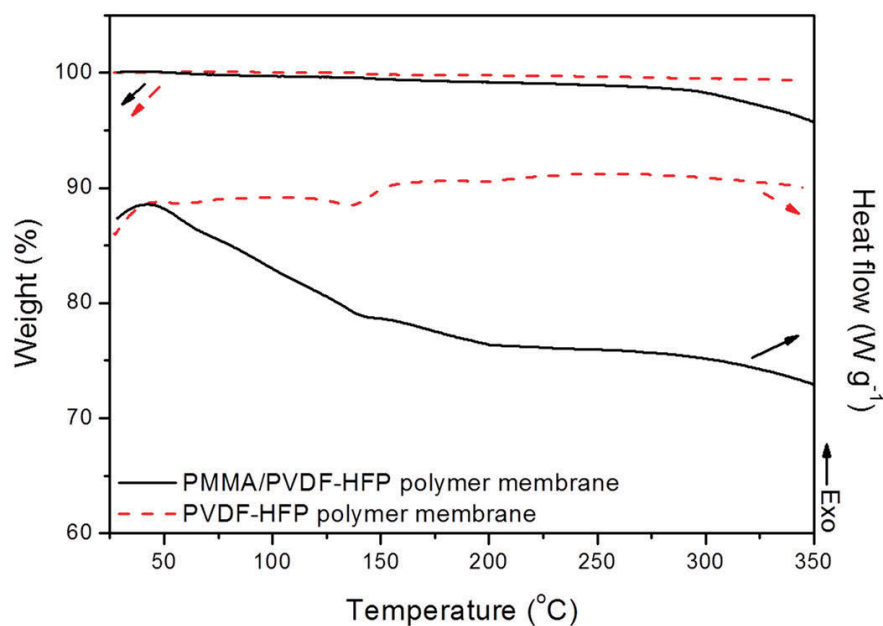


Figure 4-3 Thermogravimetry (TG) and differential scanning calorimetry (DSC) curves of the PVDF-HFP and PMMA/PVDF-HFP porous polymer membranes in air. The temperature rising rate is $10\text{ }^{\circ}\text{C min}^{-1}$

The general safety concern of lithium ion batteries is the potential fire risk caused by the direct use of flammable liquid organic electrolytes and conventional separators. Fire is caused by a self-induced internal short circuit originating from the shrinking of the conventional separator when the temperature reaches and exceeds the melting point. Our strategy is to introduce a non-shrinking membrane to replace the conventional separator. Figure 4-4(a) and (b) show the digital photos of the thermal shrinking test of PVDF-HFP and PMMA/PVDF-HFP porous polymer membranes in comparison with a commercial Celgard 2400 separator. After heating to $150\text{ }^{\circ}\text{C}$ for 30 min, the Celgard 2400 separator shrank, while the other two polymer membranes retained their dimensional stability. Such high thermal tolerance can significantly eliminate the potential risk of internal short

circuiting during battery operation. The digital photos of the combustion testing of the polymer membranes in comparison with the Celgard 2400 separator are shown in Figure 4-4(c) and (d). The conventional Celgard 2400 separator almost immediately shrank and burst into flames when brought in contact with fire, while the PVDF-HFP polymer membrane only shrank without burning. This is related to the non-flammable nature of PVDF-HFP. The PMMA/PVDF-HFP membrane, when first exposed to fire, only shrank, which is very similar to the PVDF-HFP membrane without the coating of PMMA. This is very unusual because PMMA is well known to be very flammable. The membrane finally caught on fire only during long-term exposure to the open flame. The possible reason for this interesting phenomenon is that although a large amount of PMMA was added to the PVDF-HFP porous membrane, the majority amount of PMMA was loaded inside the porous structure of the PVDF-HFP membrane. Only a very small amount of PMMA remained on the outside surface of the porous membrane. The morphology of the membrane surface in Figure 4-1(d) clearly confirms this structure. Therefore the PVDF-HFP first melted and shrank, protecting the PMMA from direct contact to the flame. However, after exposing to the fire for a longer period, the protecting effect of PVDF-HFP was overwhelmed by the flammable nature of PMMA. Even though, the combustion property of the PMMA/PVDF-HFP porous polymer membrane is still significantly higher than the conventional Celgard 2400 separator

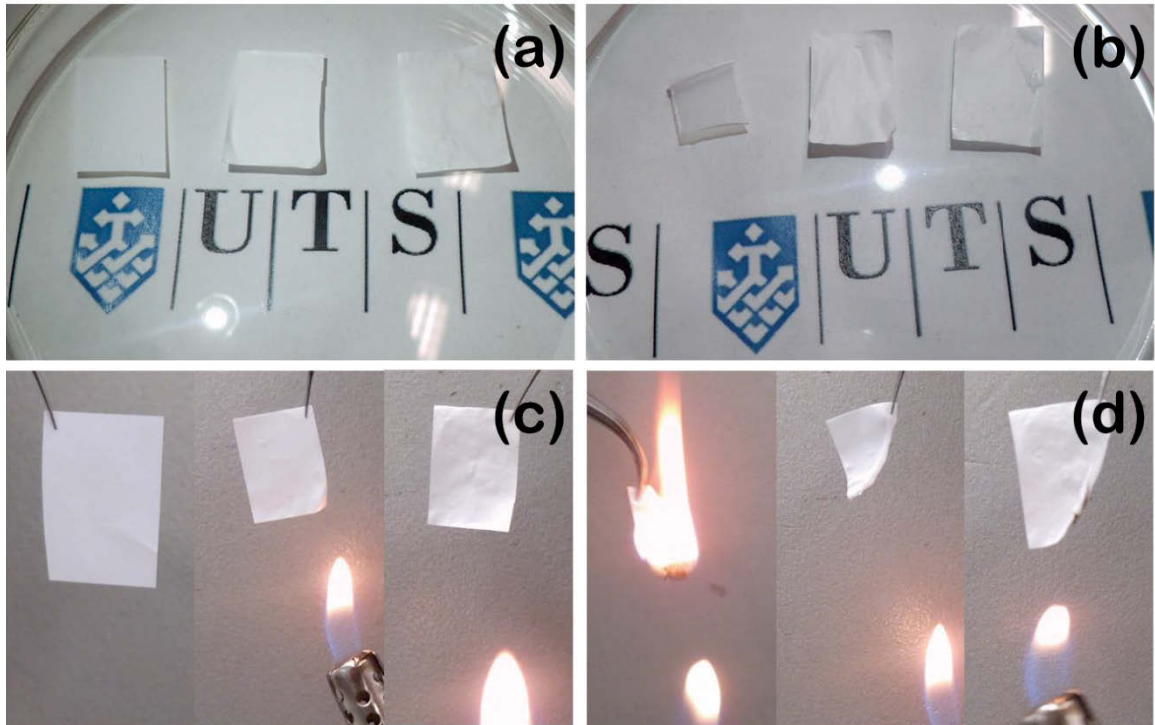


Figure 4-4 The thermal shrinking test of (left) the Celgard 2400 separator, (middle) the PVDF-HFP porous polymer membrane, and (right) the PMMA/PVDF-HFP porous polymer membrane (a) before and (b) after heating to 150 °C for 30 min, and the combustion test of (left) the Celgard 2400 separator, (middle) the PVDF-HFP porous polymer membrane, and (right) the PMMA/PVDF-HFP porous polymer membrane (c) before and (d) after set on fire

The polymer electrolyte membranes were obtained by soaking the porous polymer membranes in the liquid electrolyte overnight. Celgard 2400 separator was also used for comparison. It is a very interesting discovery that the electrolyte uptake of the PMMA/PVDF-HFP porous polymer membrane is as high as 342%, and that of PVDF-HFP membrane is 85%. The commercial Celgard 2400 separator only achieved 69% electrolyte uptake, which is far less than the prepared porous polymer membranes. This phenomenon

is owing to the large porosity of the porous polymer membranes and the gelling nature of the polymer matrices. However, the extremely large electrolyte uptake of PMMA/PVDF-HFP porous polymer membrane is mainly ascribed to the sandwich-like structure and the better affinity towards the electrolyte when the PMMA coating was used. As shown in Figure 4-1(e) and 1(f), several layers of large pores are sandwiched between other layers of smaller pores. This structure is very suitable for absorption and retention of a large quantity of liquid electrolyte. The PMMA coating inside the porous structures can further increase the absorption capability. PMMA has a better affinity towards liquid organic electrolytes than most other polymer matrices. However, since the mechanical strength can be easily destroyed after absorption of liquid electrolytes, PMMA is often used as blending polymer to enhance properties. The PMMA/PVDF-HFP porous polymer membrane has the advantage to enforce the mechanical property of PVDF-HFP while PMMA can provide extra affinity. These combining effects result in the large electrolyte uptake of the PMMA/PVDF-HFP porous polymer membrane.

Thermogravimetry (TG) and differential scanning calorimetry (DSC) curves of both polymer electrolyte membranes to determine the electrolyte retention are shown in Figure 4-5. The temperature range was set from room temperature to 150 °C. The weight of both membranes decreases slowly below 60 °C, which is associated with the evaporation of liquid electrolyte from surface layer pores. It should be note that the weight loss rate of the PMMA/PVDF-HFP electrolyte membrane is lower than the PVDF-HFP electrolyte membrane. This phenomenon should be related to the structures of both porous membranes. The PVDF-HFP porous membrane has large layered pores on the surface (shown in Figure 4-1(c)). Liquid electrolyte inside these pores can evaporate naturally with a slight increase

of temperature. The interconnected pores may be responsible for the continuous loss of electrolyte. Although a large amount of electrolyte was absorbed, the large open pore layer on the surface is not suitable for electrolyte retention. Compared with the PVDF-HFP membrane, PMMA/PVDF-HFP porous polymer membrane has much more compacted pore layers and relatively smaller size pores on the surface, based on the SEM observation (Figure 4-1(e) and 1(f)). This structure can efficiently suppress the evaporation of liquid electrolyte when the temperature slightly increases. The majority of liquid electrolyte is stored inside the large pores. Therefore it is difficult for the liquid electrolyte to pass through the compacted layers and evaporate. Furthermore, the good affinity of PMMA towards liquid electrolytes can also enhance the capability to lock electrolyte inside. PMMA/PVDF-HFP membrane exhibits a good retention of liquid electrolyte at low temperatures. The final weight loss is 40% for the PVDF-HFP polymer electrolyte membrane and 55% for the PMMA/PVDF-HFP polymer electrolyte membrane, respectively. Considering the large electrolyte uptake of 342% for PMMA/PVDF-HFP membrane, there is still sufficient electrolyte left to deliver superior electrochemical performance, even after heating to 150 °C.

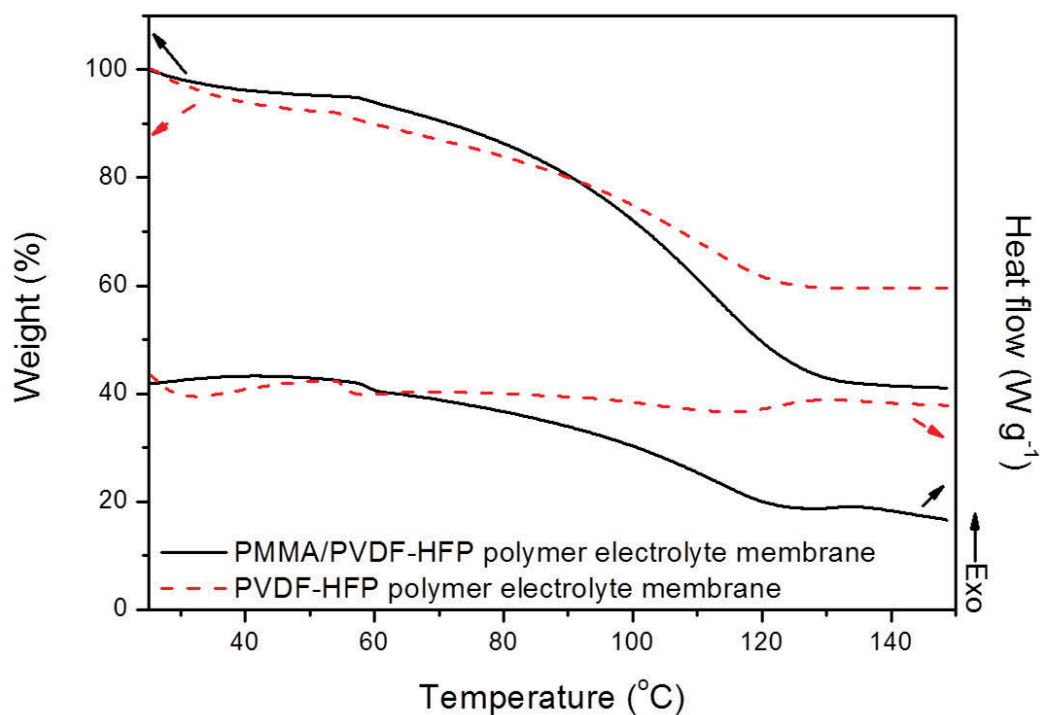


Figure 4-5 Thermogravimetry (TG) and differential scanning calorimetry (DSC) curves of the PVDF-HFP and PMMA/PVDF-HFP polymer electrolyte membrane in N₂. The temperature rising rate is 2 °C min⁻¹.

4.3.3 Electrochemical characterizations

The ionic conductivity is the most important factor that directly affects the electrochemical performances of an electrolyte. Figure 4-6 shows the ionic conductivity dependence on temperature of the polymer electrolyte membranes. A Celgard 2400 separator saturated with liquid electrolyte was also tested for comparison. The temperature range was set from 25 °C to 65 °C, which is the temperature range for most battery operations. The values of the ionic conductivity were calculated from the a.c. impedance plots shown in the inset of the Figure 4-6 by evaluating the intercept of the straight line on the real axis. The ionic conductivity of the obtained PMMA/PVDF-HFP electrolyte

membrane is calculated to be 1.31 mS cm^{-1} , while the ionic conductivity of the obtained PVDF-HFP electrolyte membrane is 1.03 mS cm^{-1} . It is obvious that both polymer electrolyte membranes have high ionic conductivity, which is higher than the conventional Celgard 2400 separator saturated with electrolyte (0.60 mS cm^{-1}). The large electrolyte uptake can contribute to the increase of the liquid and gelling phases in the membranes, which facilitates ionic transportation. The coating of PMMA in the pores of PVDF-HFP porous membrane further improves this advantage, since PMMA has very good affinity towards organic electrolytes. PVDF-HFP electrolyte membranes have lower ionic conductivity, possibly owing to the lower electrolyte uptake and the lack of PMMA coating. But the achieved ionic conductivity is still superior to the conventional Celgard 2400 separator because of the PVDF-HFP porous structure.

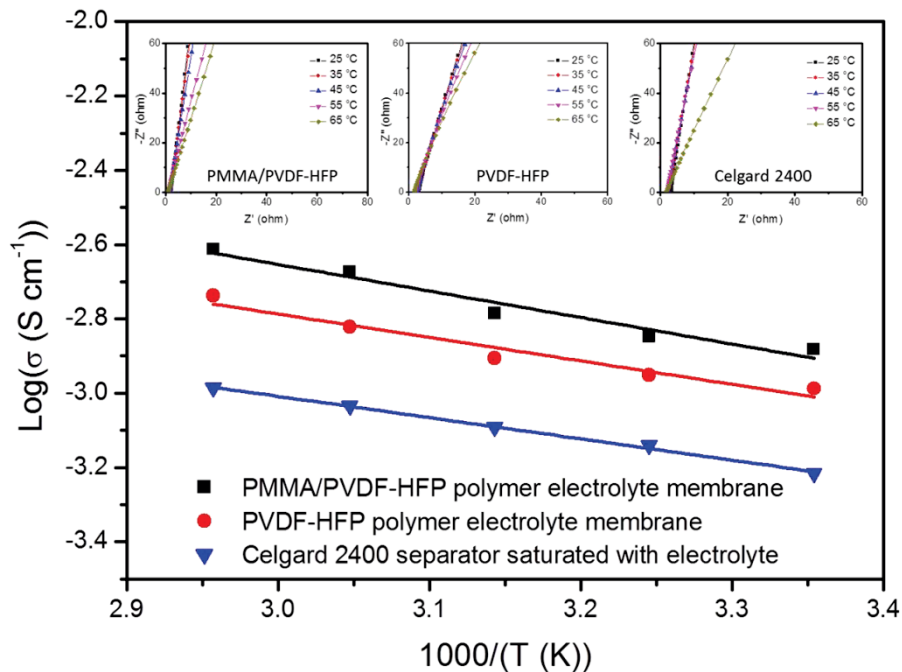


Figure 4-6 The Arrhenius plots of the ionic conductivity vs. temperature. The inset is the a.c. impedance spectra

With the elevation of temperature, the ionic conductivity of all electrolyte membranes gradually increases. The dependence of the ionic conductivity on temperature can be evaluated by the Arrhenius Equation,

$$\sigma = A \exp(-E_a/RT) \quad (\text{Equation 4-3})$$

Where A is the pre-exponential factor and E_a is the activation energy. The calculated E_a values are 13.01 kJ mol⁻¹ (PMMA/PVDF-HFP electrolyte membrane), 12.05 kJ mol⁻¹ (PVDF-HFP electrolyte membrane), and 11.21 kJ mol⁻¹ (Celgard 2400 separator saturated with liquid electrolyte), respectively. The values of all electrolyte membranes are similar.

Figure 4-7 shows the voltage stability of all electrolyte membranes. The tests were performed by assembling coin cells with electrolyte membranes sandwiched between a lithium metal electrode and a stainless steel electrode. There is no obvious peak observed for all three electrolyte membranes from open circuit voltage to 5 V, which is considered sufficient for lithium ion battery operations.^[280] When the potential exceeds 5 V, a small peak can be found around 5.7 V. This peak attributes to the decomposition of lithium salt in the liquid electrolyte. The results shown in Figure 4-7 clearly indicate the similar electrolyte stability behaviour of both polymer electrolyte membranes and the Celgard 2400 separator saturated with liquid electrolyte, and the suitability of the polymer electrolytes for lithium-ion batteries.

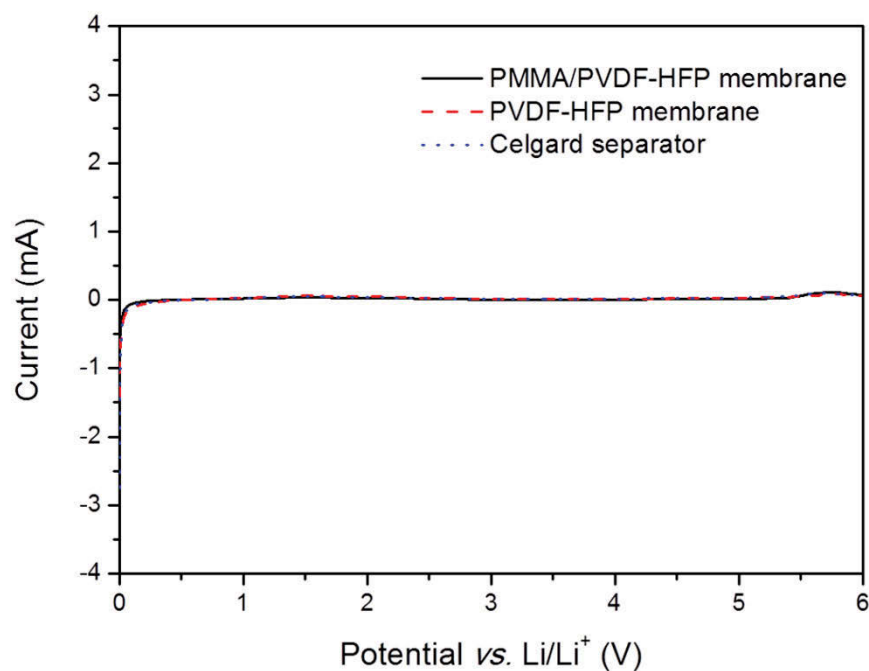


Figure 4-7 The linear sweep voltammogram of the electrolyte membranes and Celgard 2400 separator. The scanning rate is 0.1 V mV s^{-1} .

4.3.4 Battery performances

The electrochemical performances of all electrolyte membranes in lithium ion cells were tested in coin cells. A lithium metal was used as reference and counter electrode while LiFePO_4 was used as cathode. The cut-off voltage was set as 2 - 4.2 V. The current density was 0.2 C (1 C = 170 mA g^{-1}). Figure 4-8(a) shows the cycling results. The cells achieved the initial discharge capacity of 143 mAh g^{-1} , 137 mAh g^{-1} and 125 mAh g^{-1} for PMMA/PVDF-HFP electrolyte membrane, PVDF-HFP electrolyte membrane, Celgard 2400 separator, respectively. The discharge capacity of a lithium ion battery is mainly determined by the cathode materials. However, the electrolyte uptake and ionic conductivities of electrolytes can also influence the capacity of the cell. Large liquid electrolyte uptake can wet electrode materials more sufficiently, and achieve high ionic

conductivity for electrochemical reactions. Furthermore, the unique structure of the PMMA/PVDF-HFP porous membrane can help seal electrolyte and facilitate the ion transportation, resulting in less capacity loss during the discharge and charge process. With the increase of the cycle number, the cycling performance remained, over 100 cycles, with a slight increase of the capacity, probably due to the activation of electrode materials. The rate performances of all electrolyte membranes are shown in Figure 4-8(b). The performances were conducted under different current densities of 0.5 to 2 C. The capacities of the cell with a PMMA/PVDF-HFP electrolyte membrane is higher than the other two cells, while Celgard 2400 separator electrolyte membrane shows the lowest capacities. When the current densities decreased to 0.2 C, the capacities recovered to their original values. Such outstanding rate performances make porous polymer electrolyte membranes promising for the use in lithium ion batteries with fast and enhanced performances.

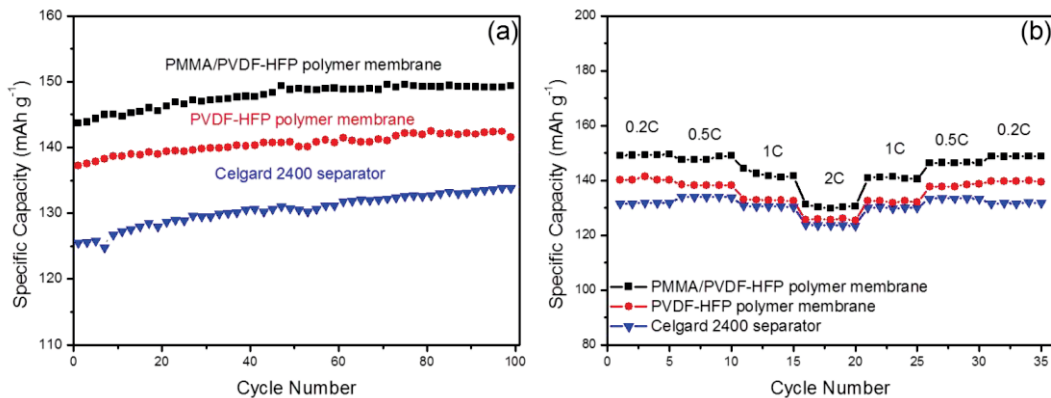


Figure 4-8 Electrochemical performances of lithium ion cells with LiFePO_4 as cathode material. (a) The cycling performances of the polymer electrolyte membranes and Celgard 2400 separator. The cut-off voltages are 2 V and 4.2 V. The current density is 0.2 C. (b) The rate behaviour. The current densities of discharge and charge are 0.2 C, 0.5 C, 1 C, and 2 C, respectively

PVDF-HFP membranes have been studied for centuries because of their semi-crystallinity. The addition of a PMMA coating can further increase the electrochemical properties by generating a unique porous structure and improved affinity towards electrolytes. Such a unique multi-porous-layered membrane structure provides an idea for further development of a high performance polymer electrolyte. Through this investigation, we demonstrated the development of a PMMA/PVDF-HFP porous polymer membrane for lithium ion batteries with improved electrochemical performance and enhanced safety.

4.4 Summary

A PMMA/PVDF-HFP porous polymer membrane has been successfully prepared by coating PMMA on PVDF-HFP porous polymer membranes. The as-prepared porous membrane has a sandwich-like architecture with multi-sized porous layers. The PMMA/PVDF-HFP porous polymer membrane exhibited good thermal stability, resistance to fire, high percentage uptake of liquid electrolyte, and outstanding electrolyte retention even at high temperature. Electrochemical characterization shows that the obtained PMMA/PVDF-HFP electrolyte membranes have a high ionic conductivity of 1.31 mS cm^{-1} at room temperature and low activation energy. When applied as separator and electrolyte in lithium ion batteries, the obtained PMMA/PVDF-HFP electrolyte membrane using LiFePO_4 as cathode active material showed high discharge capacity, good cycling performance, and outstanding rate capability, which outperforms the commercial Celgard 2400 separator. The PMMA/PVDF-HFP porous polymer membrane could be applied for lithium ion batteries with improved performance and enhanced safety.

Chapter 5 A Bi-functional Organic Redox Catalyst for Rechargeable Lithium-Oxygen Batteries with Enhanced Performances

5.1 Introduction

The lithium-oxygen (Li-O₂) battery has attracted considerable interest owing to its high energy density.^[6, 164, 200, 208, 304] Some critical drawbacks of Li-O₂ batteries have, however, limited its practical application to date. For instance, the formation of superoxide radical species (O₂⁻) causes serious problems.^[175, 198] Due to its highly reactive nature, O₂⁻ can attack the electrolyte and electrode materials when Li₂O₂ (the ideal oxygen reduction product) is formed resulting in large amounts of unwanted by-products. In efforts to address this, the use of ionic liquids as electrolytes and porous gold electrodes has been investigated.^[305, 306] These materials achieve long and stable cycle lives. However, these materials are usually very expensive and difficult to prepare. Additionally, large over-potentials during charge and discharge processes, resulting from the sluggish kinetics of the battery reaction, lead to poor round-trip efficiency and cycle life.^[307] Therefore, catalysts have been utilized to reduce the over-potentials and to increase the cycle life. Potential catalysts such as metals, metal oxides, perovskite, carbon nanotubes, graphene, and organic compounds have been investigated.^[307-321] Ruthenium metal has recently demonstrated superior capability to reduce charge over-potential during the oxygen evolution reaction (OER) over other catalysts.^[322] Furthermore, redox mediators such as tetrathiafulvalene (TTF), 2,2,6,6-tetramethyl-1-piperidinyloxy (TEMPO), lithium iodide, iron phthalocyanine, and methyl-10H-phenothiazine have shown the capability to enhance the round-trip efficiency and suppress side-reactions by reducing the charge potential to below 4.0 V.^{[174,}

221-223, 323-325] From an overall perspective, and because the oxygen reduction reaction (ORR) also plays an important role, it is desirable to develop catalysts with bi-functionality for both discharge and charge processes. For example, by mixing highly efficient OER catalysts with gold, which has good catalytic activity towards the ORR, the gap between discharge and charge voltage can be significantly reduced.^[326] Noble metal catalysts are not ideal owing to their high cost, and therefore, it is crucial to discover low cost catalysts with high catalytic activity. Recently, Zhu et al. reported the use of a combination of two organic redox mediators, in which one catalyzes the ORR and the other catalyzes the OER.^[327]

Herein, we report the remarkable properties of poly(2,2,6,6-tetramethylpiperidinyloxy-4-yl methacrylate) (PTMA) as an organic catalyst in Li-O₂ batteries. During the discharge process, PTMA in its n-doping state catalyzes O₂ reduction and formation of Li₂O₂, while during the charge process, PTMA converts to its p-doping form and facilitates Li₂O₂ decomposition. Furthermore, PTMA forms a protective layer to suppress side-reactions between the carbon electrode and the electrolyte.

5.2 Experimental details

5.2.1 Synthesis of PTMA

PTMA was synthesized according to the previously reported method. In a typical synthesis process, 2.25g 2,2,6,6-tetramethyl-4-piperidyl methacrylate (MTMP, TCI) monomer and 0.04g 2,2'-azobisisobutyronitrile (AIBN, Sigma-Aldrich) were mixed and stirred in 6 mL acetic acid at 70 °C for 12 h under Ar atmosphere. The mixture was then added into 50 mL ethyl ether (Chem-Supply). The pale white product (PMTMP) (1.7g, 75% yield) was obtained by filtration.

The product PMTMP (1.0 g) was then dissolved into 20 mL methanol (Chem-Supply), mixed with 0.3 g $\text{Na}_2\text{WO}_4 \cdot 2\text{H}_2\text{O}$ (Sigma-Aldrich), 0.2 g ethylenediaminetetraacetic acid (EDTA, Sigma-Aldrich), 2 mL 30% H_2O_2 (TCI), and 10 mL H_2O . The mixture was then stirred at 60 °C for 40 h. The product was filtrated and washed with de-ionised water and ethyl ether (Chem-Supply) to obtain PTMA (a pale red solid (1.0 g, 95% yield)).

The illustration of the process is shown in Figure 5-1.

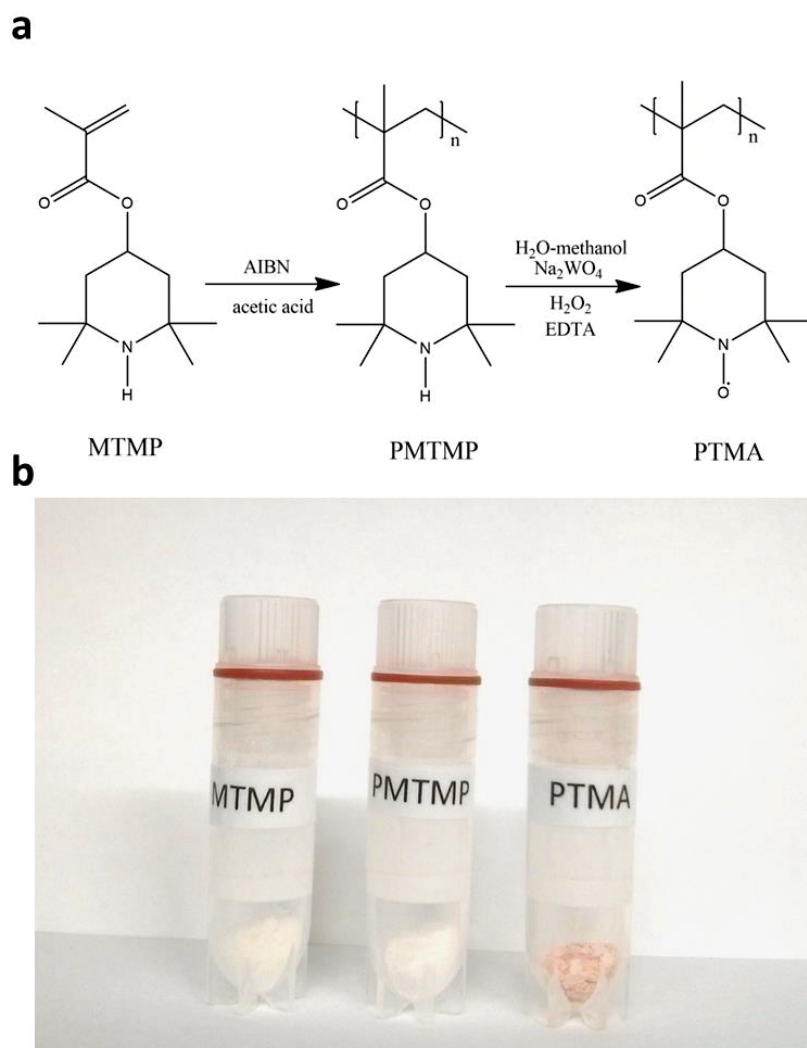


Figure 5-1 (a) The illustration of the PTMA synthesis process and (b) digital photo of the as-prepared PTMA, reactant MTMP, and intermediate PMTMP.

5.2.2 Characterization

Field emission scanning electron microscope (FESEM, Zeiss Supra 55 VP) was employed to observe the morphologies. Infrared spectroscopies of MTMP and the as-prepared PTMA were conducted on a Nicolet Magna 6700 FT-IR spectrometer. All spectra were obtained using 4 cm^{-1} resolution and 64 scans at room temperature. X-ray diffraction (XRD) measurement was conducted on a Siemens D5000 X-ray diffractionmeter. During the XRD analysis process, the cathodes were protected from exposure to the ambient atmosphere.

5.2.3 Electrochemical characterization

The cathodes were prepared by firstly mixing carbon black, PTMA, and polyvinylidene difluoride (PVDF) together in methylpyrrolidone (NMP, Sigma-Aldrich) with the weight ratio of 60:30:10. The mixture was then coated on a stainless steel mesh substrate and cut into discs with a diameter of 14 mm. The electrodes were dried at $80\text{ }^{\circ}\text{C}$ in a vacuum oven for 24 h. The loading of the cathode materials was about 1 mg cm^{-2} . The carbon black electrodes were prepared by the same process without the addition of PTMA. The Li_2O_2 electrodes were prepared with the addition of commercial Li_2O_2 (weight ratio 1:4 to the active materials).

All the electrochemical characterizations were conducted on a CH Instrument 660D electrochemical workstation and discharge/charge performances were evaluated by a Neware Battery Testing System. The cyclic voltammetry measurements were carried on within the range from 2 V to 4.5 V, with a scanning rate of 0.1 mV s^{-1} . Linear sweep voltammetry measurements were performed to measure the catalytic property of materials

towards the decomposition of Li_2O_2 . The scanning rate was 0.1 mV s^{-1} and the range was set from open circuit voltage to 4.4 V.

The discharge-charge performances were evaluated by assembling Li-O₂ batteries. A two-electrode system Swagelok-type cell with an air hole (0.785 cm^2) on the cathode side was used to test the electrochemical performances. The cell was assembled in an argon filled glove box with water and oxygen level less than 0.1 ppm. A lithium foil was used as anode. The electrolyte was prepared by dissolving bis(trifluoromethane) sulfonimide lithium salt (LiTFSI, Sigma-Aldrich, 99.95%) in diethylene glycol dimethyl ether (DEGDME, Sigma-Aldrich, 99%). The concentration was 0.5 M. The assembled cell was gas tight except for the cathode side window, which is exposed to the oxygen atmosphere. All measurements were conducted in 1 atm dry oxygen atmosphere.

The standard oxygen evolution reaction (OER) and oxygen reduction reaction (ORR) were performed in O₂-saturated 1 M KOH aqueous solution using a three electrode system on an electrochemical workstation (CHI 660E). The platinum wire and Ag/AgCl (1 M KCl) work as the counter and reference electrodes ($E_{\text{RHE}} = E_{\text{Ag/AgCl}} + 0.059 \times \text{pH} + 0.2224$), respectively. The working electrode was prepared by loading a catalyst layer on the glass carbon substrate of rotating disk electrode (RDE, Pine) with a diameter of 5 mm. 4 mg of catalyst and 80 μl of Nafion (5 wt %) were mixed in 1 ml solvent (1:1 v/v water/isopropanol) by sonication for more than 30 min to obtain a homogeneous ink. Then, the catalyst ink (10 μl) was loaded onto RDE and followed by drying at room temperature. The disk electrode was scanned at a rate of 5 mV s^{-1} for OER and ORR. During OER measurement, the working electrode was rotated at 1600 rpm to remove the generated

oxygen bubbles. And during the ORR measurement, the working electrode was scanned with varying rotating speed from 400 rpm to 2000 rpm.

5.3 Results and discussions

5.3.1 Physical characterizations

PTMA was synthesized using the previously reported method (Figure 5-1a) and has a distinctive red color (Figure 5-1b).^[328, 329] The FTIR spectra confirmed that PTMA had been successfully synthesized (Figure 5-2). The characteristic peaks at 1635 cm^{-1} (C=C group), 1707 cm^{-1} (C=O group) are known to be assigned to the MTMP monomer. The broad peaks near 3400 cm^{-1} are from the group of N-H. From the spectra of PTMA, it is evident that the peaks originated from C=C and N-H has disappeared or partially disappeared. Instead a clear new peak at 1370 cm^{-1} appeared, corresponding to the formation of the nitroxyl radical of PTMA.

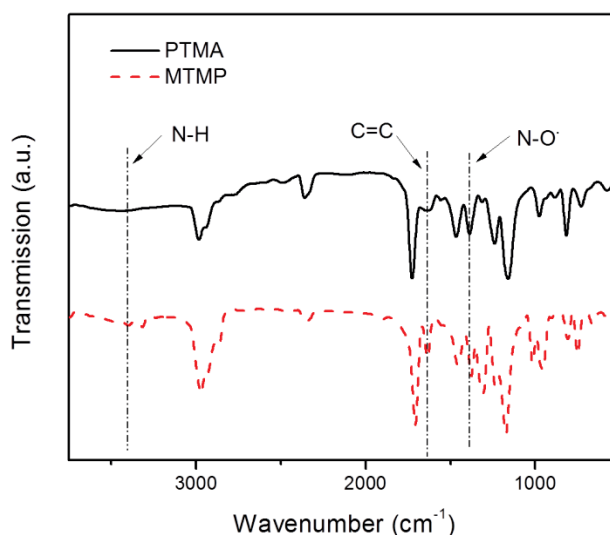


Figure 5-2 FT-IR spectra of the as-prepared MTMP and PTMA

PTMA electrodes were prepared by mechanically grinding PTMA and carbon black (CB) with the binder polyvinylidene difluoride (PVDF). The mixture was dispersed in NMP and then cast to form electrodes. The PTMA was found to uniformly distribute and coat onto the surface of carbon black due to its good solubility in NMP (Figure 5-3).

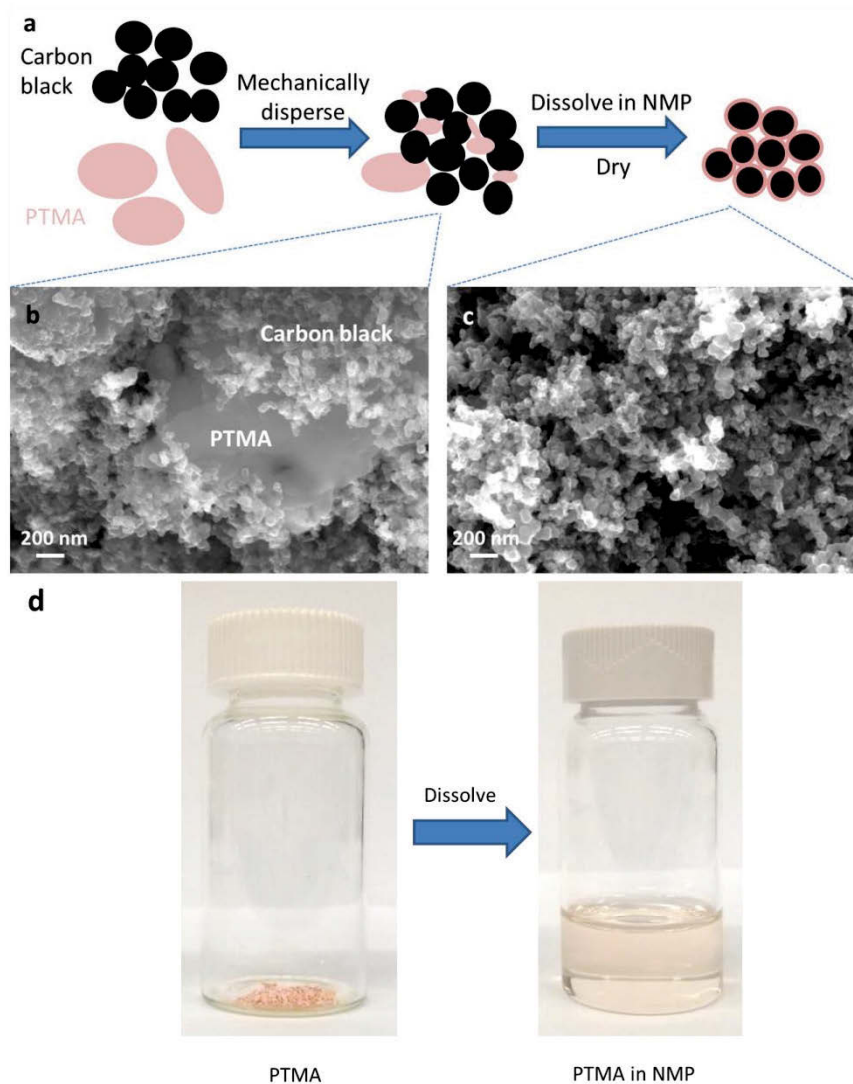


Figure 5-3 (a) Illustration of the processes to form the PTMA / carbon black electrode material. Insets show SEM images of the materials (b) before and (c) after dissolving in NMP. (d) The digital photos of PTMA dissolving into NMP.

SEM mapping images of the electrode (Figure 5-4) confirm an even coating of PTMA on the surface of CB.

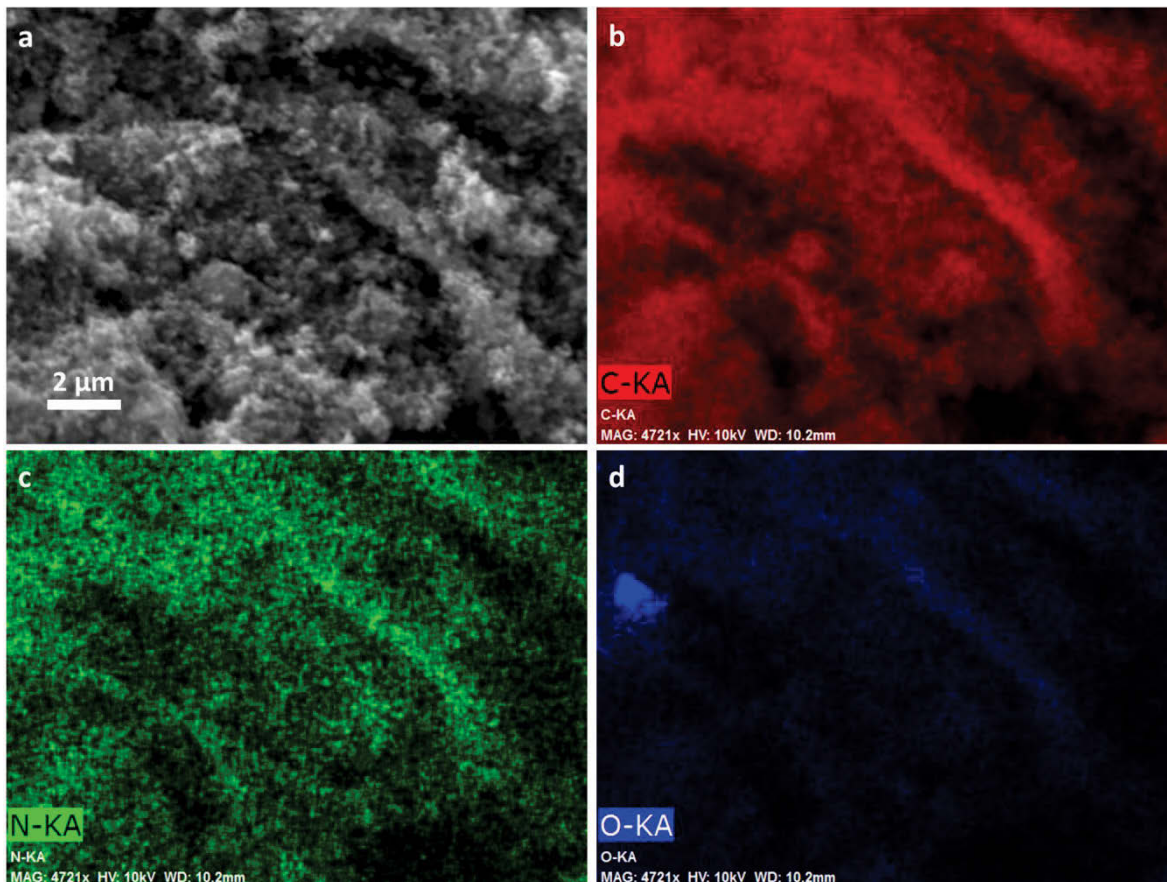


Figure 5-4 EDX mapping of the PTMA electrode

Figure 5-5a demonstrated that PTMA is not soluble in diethylene glycol dimethyl ether (DEGDME), which is consistent with the previous report.^[330] Furthermore, we measured the FTIR spectra of DEGMDE solvent and DEGDME soaked with PTMA for two hours. As shown in Figure 5-5b, there is no additional peak appeared in the FTIR spectra of DEGDME solvent after soaked with PTMA. This result clearly verified the insolubility of PTMA in the DEGDME solvent.

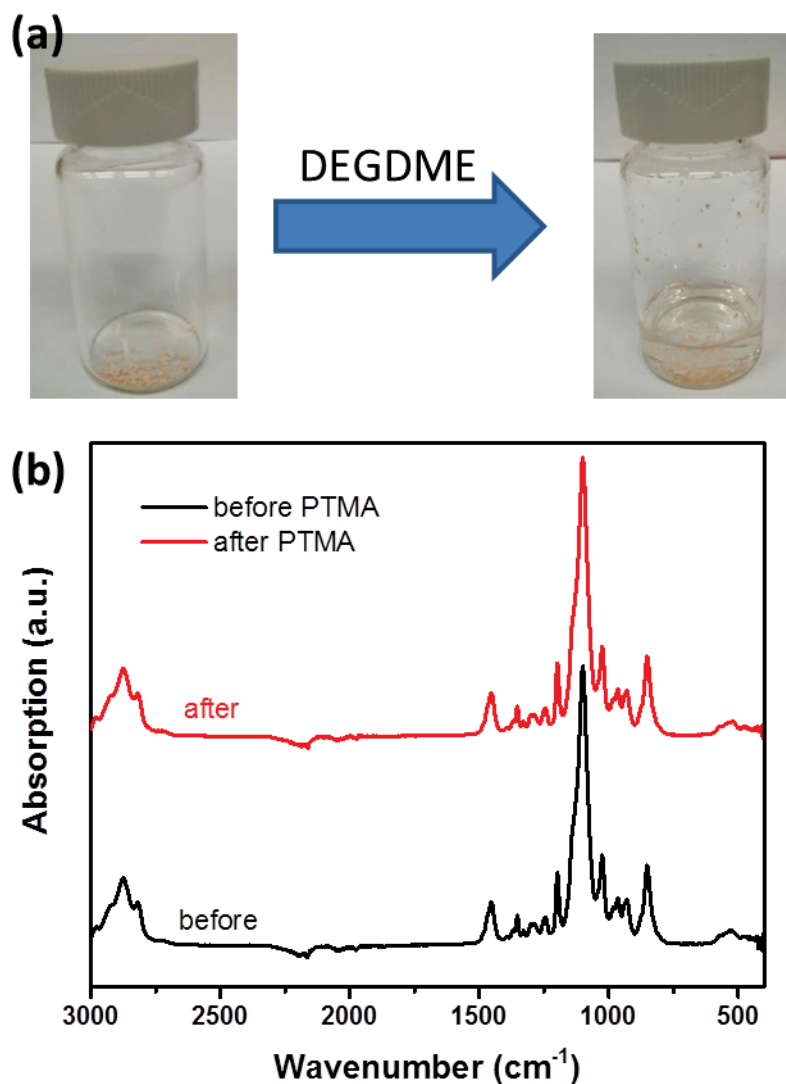


Figure 5-5 (a) Digital photos of PTMA before and after soaked in DEGDMC solvent. (b) FTIR spectra of the DEGDMC solvent before and after PTMA soaked for two hours.

5.3.2 Electrochemical characterizations

Li-O₂ cells were constructed using the new PTMA electrodes as cathode and lithium metal as the counter electrode and reference electrode. Cells prepared with bare CB electrodes were also tested for comparison. Figure 5-6a shows the cyclic voltammograms measured from 2 to 4.5 V with a scanning rate of 0.1 mV s⁻¹. No significant redox

processes were observed for the bare CB electrode. In contrast, a process at ~ 3.8 V is evident in the cell containing the PTMA electrode, which is related to the p-doping of PTMA. Importantly, the potential of this process meets the essential requirement of decomposing Li_2O_2 . An additional redox process was identified at 2.96 V, which is the theoretical potential of the formation of Li_2O_2 . We assign this process to n-doping of PTMA.^[331] Cell discharge usually occurs at ~ 2.7 V and it is important that the catalyst has a slightly more positive redox potential to allow the optimum battery discharge behavior. These data show that PTMA can catalyze the decomposition of Li_2O_2 (upon charging) and also facilitate the formation of Li_2O_2 (upon discharging). The CV curve of Li-O₂ battery with PTMA electrode in O₂ atmosphere is shown in Figure 5-6b, which also confirms the catalytic activity of PTMA towards ORR and OER.

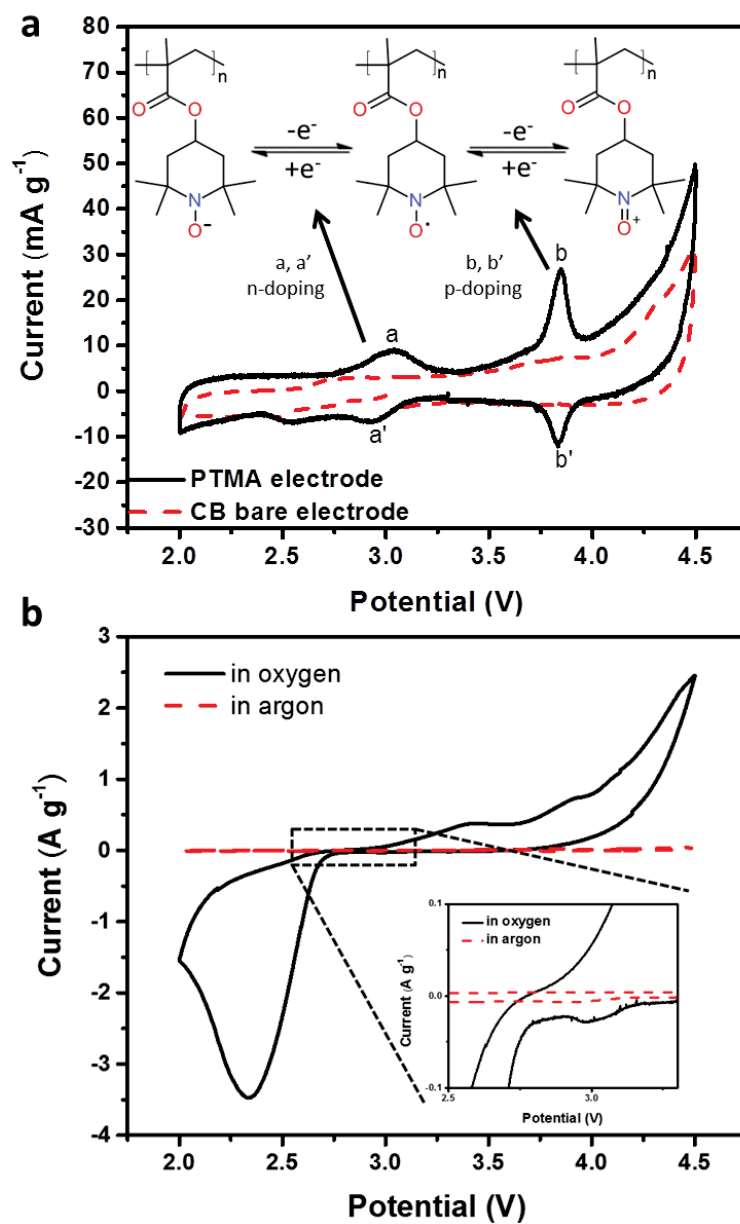


Figure 5-6 (a) The cyclic voltammetry curves of the sealed cells in an argon atmosphere with PTMA and bare CB electrodes. Scanning rate is 0.1 mV s⁻¹ and potential range is 2.0 to 4.5 V. The inset is the redox reactions of PTMA during p-doping and n-doping. (b) The CV curves of PTMA electrodes both in argon and oxygen atmosphere. Scanning rate is 0.1 mV s⁻¹ and potential range is 2.0 to 4.5 V. The inset is the enlarged curves from 2.5 V to 3.3 V.

5.3.3 Battery performances

Galvanostatic charge/discharge testing was conducted to evaluate the electrochemical performance of the Li-O₂ batteries under a restricted capacity of 1000 mAh g⁻¹. The results are shown in Figure 5-7a. The charge plateau of the Li-O₂ battery with a PTMA electrode presents a voltage of about 3.73 V, which is significantly lower than that of the bare CB electrode (4.15 V). This result indicates that PTMA can reduce the charge over-potentials during OER. The difference between the discharge plateaus of the PTMA and CB electrodes is about 0.06V, which reveals the superior catalytic activity of PTMA towards ORR over CB.

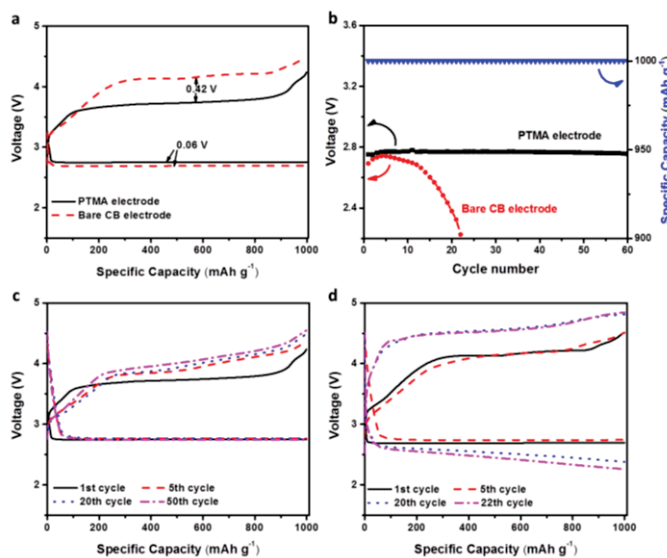


Figure 5-7 (a) Discharge/charge profiles of Li-O₂ batteries with PTMA electrode and bare CB electrode at a discharge depth of 1000 mAh g⁻¹ and a current density of 200 mA g⁻¹. (b) Cycling profile of both Li-O₂ batteries. And discharge/charge profile during cycling of Li-O₂ batteries with (c) PTMA electrode, and (d) bare CB electrode. The cut-off voltage was set to be 2.3 V/4.8 V. The current density and capacities were calculated by the weight of the active materials in the electrodes (PTMA+CB and CB).

The fully discharge/charge profiles were obtained with a cut-off voltage at 2.3 V/4.5 V (shown in Figure 5-8a). The results clearly indicate that PTMA can not only reduce the over-potentials during discharge and charge processes, but also increase discharge capacity, comparing with bare CB electrode. The discharge/charge profile of cell with PTMA electrode in argon atmosphere (Figure 5-8b) also confirms that the discharge capacity originates from the catalyzed ORR rather than PTMA itself.

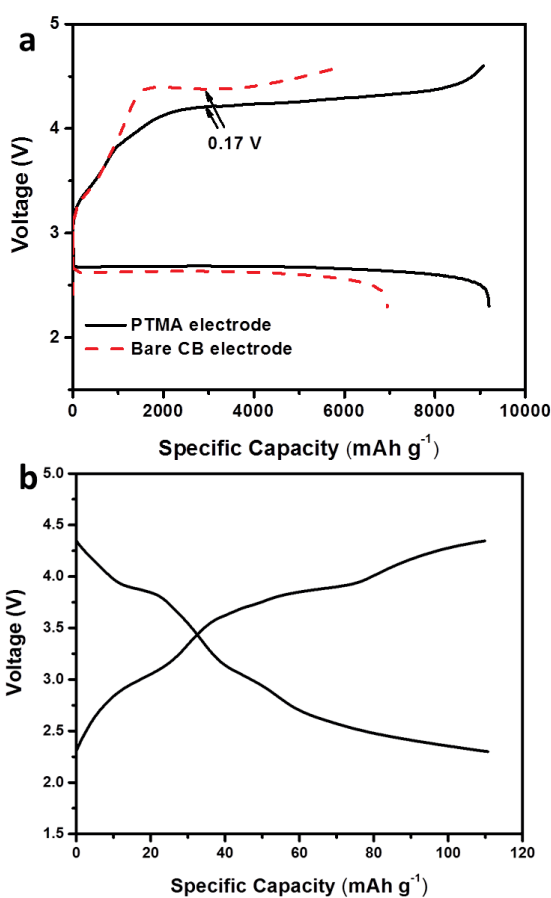


Figure 5-8 (a) Fully discharge/charge profile of Li-O₂ batteries with PTMA and bare CB electrodes. The current density is 200 mA h g⁻¹. The cut-off voltage is set at 2.3 V/4.5 V. (b) The full discharge/charge profile of the cell with PTMA electrode in Argon atmosphere. The current density is 200 mA h g⁻¹. The cut-off voltage is set as 2.3 V-4.5V.

Cycling performances of PTMA electrode in Li-O₂ batteries were evaluated by constant current discharge/charge cycling (shown in Figure 5-7b). The discharge and charge capacities were fixed to 1000 mAh g⁻¹, and the current density was 200 mA g⁻¹. The current density and capacities were calculated based on the weight of active materials in the electrodes (PTMA+CB and CB). Without PTMA in the electrode, the over-potentials of Li-O₂ battery continuously increased with cycling until terminating at the 23rd cycle (cut-off voltage was 2.3 V). However, with the addition of PTMA, the Li-O₂ battery lasted at least 60 cycles without any degradation. The discharge curves exhibited a constant flat plateau at around 2.75 V, whereas the plateaus of charge slightly increased with cycling, but remained lower than 4 V even at the 50th cycle. In general, the termination of Li-O₂ batteries is usually caused by the decomposition of the electrolyte or binder and the formation of side-products at voltages higher than 4 V.^[250] As shown in Figure 5-7a, the PTMA catalyst can efficiently reduce the over-potential during the charge process, which can suppress the side-reactions and therefore, improve cycling performance.

Li-O₂ batteries with PTMA electrodes were assembled and cycled at different current densities (Figure 5-9a). The current densities do not have a significant impact on the discharge-charge performance under a restricted capacity of 1000 mAh g⁻¹. The voltages of the charge plateaus only slightly increased when the current densities increased from 50 mAh g⁻¹ to 1000 mAh g⁻¹. When using bare CB electrode, the over-potentials in both discharge and charge processes increased dramatically (as shown in Figure 5-9b).

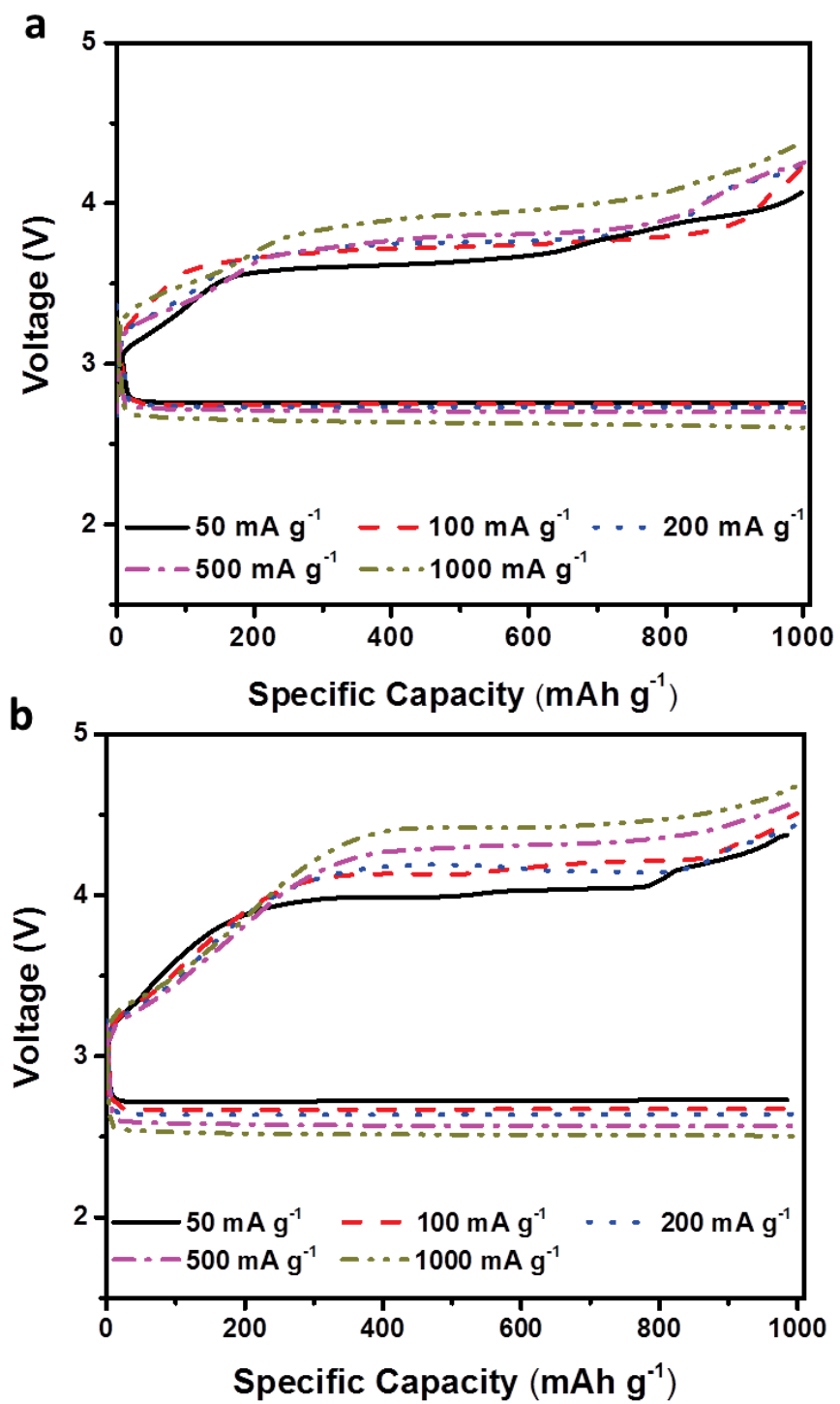


Figure 5-9 Rate capabilities of Li-O₂ batteries with PTMA (a), and bare CB (b) with current density from 50 to 1000 mA g⁻¹.

The fully discharge and charge profiles in Figure 5-10 also confirm good rate capability of the catalysts. We ascribe the significantly enhanced performances of the PTMA electrodes to the fast kinetics of the PTMA redox reactions. Thus, the PTMA electrode has a demonstrated high rate capability.

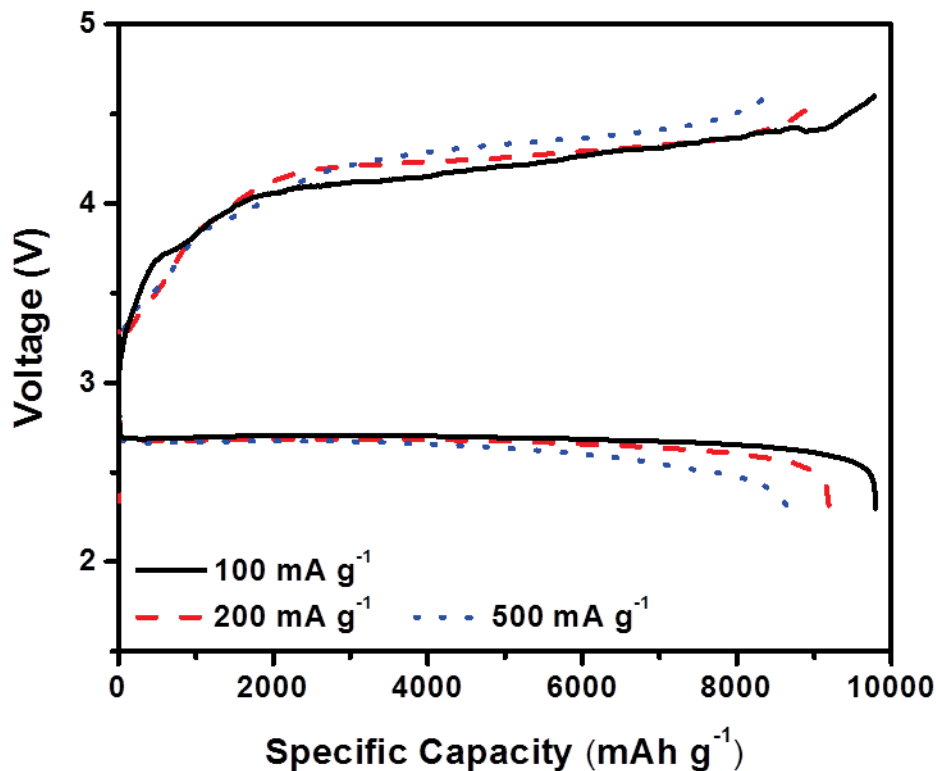


Figure 5-10 The rate capability of Li-O₂ batteries with PTMA electrodes with current densities from 100 to 500 mA g⁻¹. The cut-off voltage is set at 2.3 V/4.5 V.

SEM and XRD were used to characterize PTMA electrodes after discharge and charge cycles. SEM images (Figure 5-11) show the formation of nano-sized Li₂O₂ after discharge and large amounts of Li₂O₂ can be detected on the surface of the cathode. High magnification images (Figure 5-11b-inset) show Li₂O₂ plates with a toroidal shape, which

is consistent with previous reports.^[332] The XRD results (Figure 5-11) confirm that the products were dominated by Li_2O_2 .

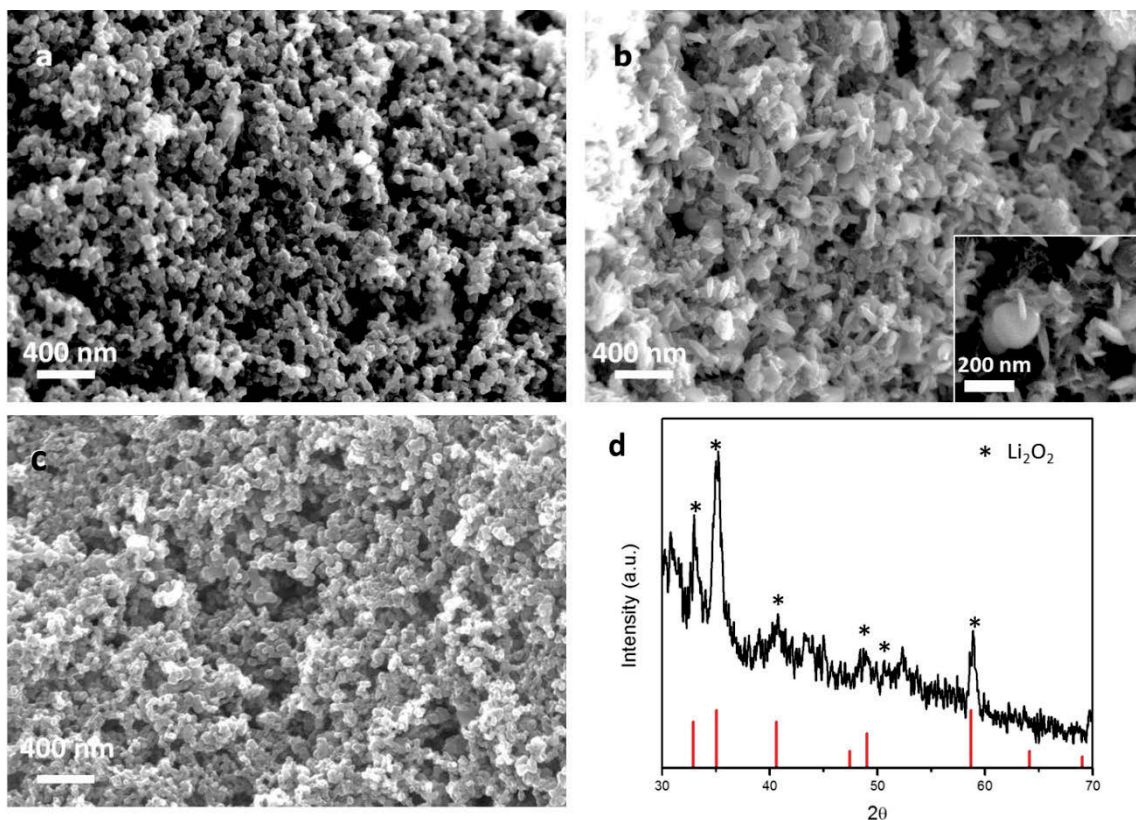


Figure 5-11 The SEM images of PTMA electrode (a) before discharge, (b) after first discharge, and (c) after first charge. (d) XRD pattern of the electrode after discharge.

The FTIR spectrum in Figure 5-12 further verified this conclusion. After charging, the toroidal-shaped Li_2O_2 disappeared (Figure 5-11c), indicating the reversibility of Li_2O_2 formation and decomposition.

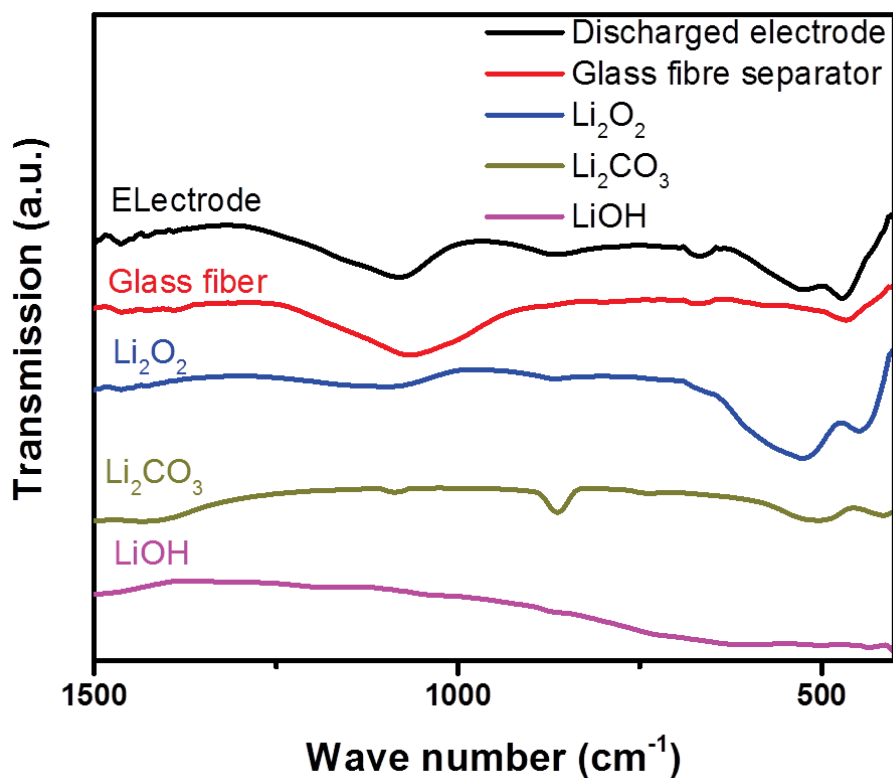


Figure 5-12 The FTIR spectrum of the PTMA electrode after discharge.

5.3.4 Mechanisms

We propose that PTMA functions as a bi-functional organic redox catalyst in Li-O₂ batteries. The nature of n-/p-doping of PTMA during discharge and charge processes contributes to the significant decrease of over-potentials. According to previous reports, PTMA or materials containing the TEMPO moieties can work as a catalyst for oxidation and reduction reactions by directly interacting with the reactants, in addition to acting as a redox electron mediator.^[333, 334] The result of standard catalytic activities towards ORR and OER (Figure 5-13) also indicates that PTMA has a rapid and efficient catalytic capability. To evaluate the electro-catalytic activity of PTMA, rotating disk electrode (RDE) measurements were conducted in O₂-saturated 1 M KOH aqueous solution. Comparative

study was performed on CB. PTMA exhibited a pronounced electro-catalytic ORR activity associated with lower onset potential and larger current density compared to that of CB at different rotation rates in aqueous media (Figure 5-13a, b). As displayed in Figure 5-13c, at a potential of -0.6 (vs. Ag/AgCl), PTMA achieved a current density of 2.95 mA cm⁻² at a rotation rate of 1600 rpm, whereas much smaller current density of 1.90 mA cm⁻² for CB. PTMA have further shown to be efficient in catalysing the oxidation of water to oxygen. According to the polarization curves (Figure 5-13d), it is evident that PTMA displays better OER performance than that of CB, showing an over-potential of 339 mV to achieve 5 mA cm⁻² (380 mV for CB).

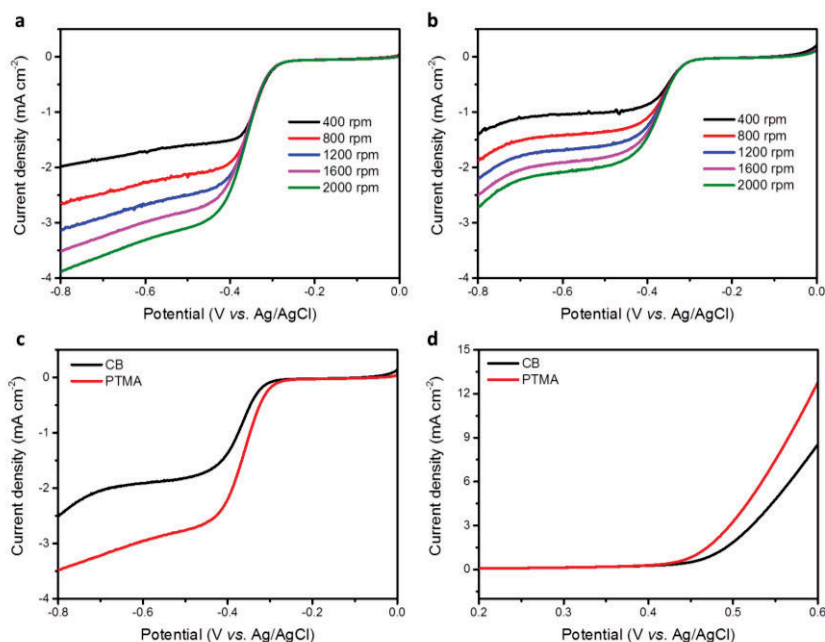


Figure 5-13 Aqueous ORR and OER with PTMA electrocatalyst. Operating in an O₂-saturated 1 M KOH aqueous solution, the results are electrochemically measured LSVs of (a) PTMA and (b) CB towards ORR at different rotation rates indicated; (c) ORR and (d) OER catalytic activity of PTMA and CB at a rotation rate of 1600 rpm.

Figure 5-14 illustrates the proposed mechanisms of the PTMA-catalyzed formation and decomposition of Li_2O_2 in the Li- O_2 battery. For clarity, the structure of PTMA is replaced by the main functional group, the nitride oxide radical. Figure 4a shows the discharge process whereby the nitride oxide radical moiety is firstly reduced to the n-doped form, and a Li^+ is drawn from electrolyte to balance the charge. Due to the attraction between Li^+ and oxygen, the oxygen molecules were absorbed to the surface of the PTMA electrode. By interacting with the reduced nitride oxide moiety through Li^+ , oxygen is then reduced to Li_2O_2 while the n-doped nitride oxide moiety reverts to its radical state. This catalytic cycle proceeds to produce more Li_2O_2 product. The catalytic effect of PTMA plays an important role in facilitating the formation of Li_2O_2 as well as suppressing the formation of side-products. Moreover, the similar radical nature of PTMA could make it much easier to attract and reduce the superoxide radicals (O_2^-) formed during the discharge process, which also reduces the risk of electrolyte decomposition.^[335]

A similar mechanism is proposed for the charge process (Figure 5-14b). The oxidized nitride oxide moiety interacts with Li_2O_2 and releases one Li^+ . The other Li^+ was attracted by the oxygen atom from the oxidized nitride oxide moiety. By rearranging the electrons in the intermediate structure, the oxygen was then released. Meanwhile, the other Li^+ remains attached to the PTMA surface. With the flow of electrons from the electrode, PTMA reverts back into its original radical form. This process reduces the reaction energy barrier for Li_2O_2 decomposition, which results in the decrease of charge over-potential. In addition, a lower charge voltage may suppress the decomposition of carbon and electrolyte. Moreover, the PTMA coating can prevent direct contact between Li_2O_2 and the carbon surface, reducing side-reactions between them.

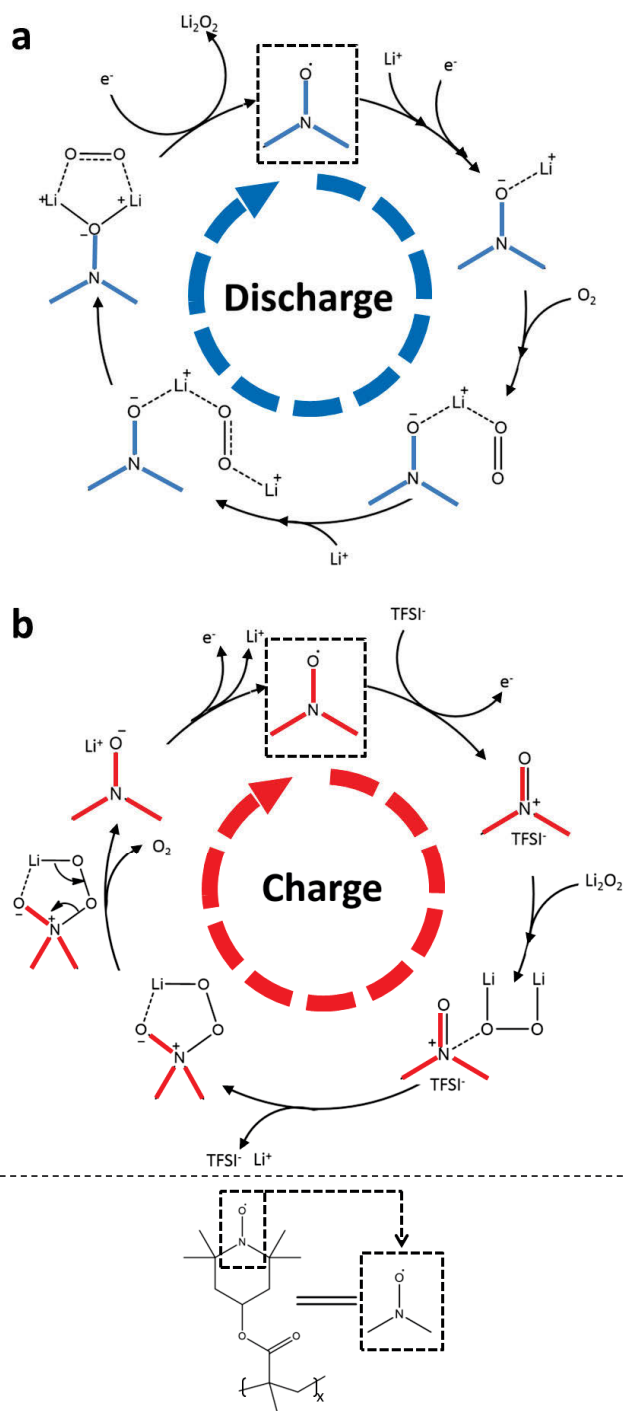


Figure 5-14 Schematic illustration of mechanism of PTMA during discharge and charge processes. To simplify the illustration, the structure of PTMA is replaced by its nitride oxide moiety as it is the main functional group.

5.3.5 Catalytic behavior

The use of catalysts in Li-O₂ batteries has been intensively debated recently with suggestions that catalysts could catalyze the decomposition of the electrolyte instead of Li₂O₂. It is therefore important to clarify whether PTMA has a superior catalytic activity towards Li₂O₂ oxidation than the electrolyte. The catalytic activities of PTMA towards the decomposition of Li₂O₂ were confirmed by linear sweep voltammetry, scanning from open circuit voltage to 4.4 V with a scanning rate of 0.1 mV s⁻¹ (Figure 5-15). Electrodes were prepared with or without the addition of commercial Li₂O₂. For the CB-Li₂O₂ electrode, the oxidation peak starting from 4.0 V originates evidently from the decomposition of Li₂O₂. For bare CB electrode there is no visible peak at the same potential range. A small peak can be identified above 4.3 V, which could be ascribed to the side-reactions such as electrolyte decomposition. The bare PTMA electrode without the commercial Li₂O₂ shows a small additional peak at around 3.8 V, which is associated with the p-doping of PTMA. There is no other oxidation peak observed for the bare PTMA electrode, indicating that negligible electrolyte decomposition at lower voltage range of 4.2 V. The PTMA-Li₂O₂ electrode exhibits a broad peak starting from 3.6 V, which can be assigned to the decomposition of Li₂O₂ under the catalysis of PTMA. The decomposition voltage is very close to the voltage of p-doping of PTMA. This confirmed that PTMA has a strong catalytic activity towards the decomposition of Li₂O₂.

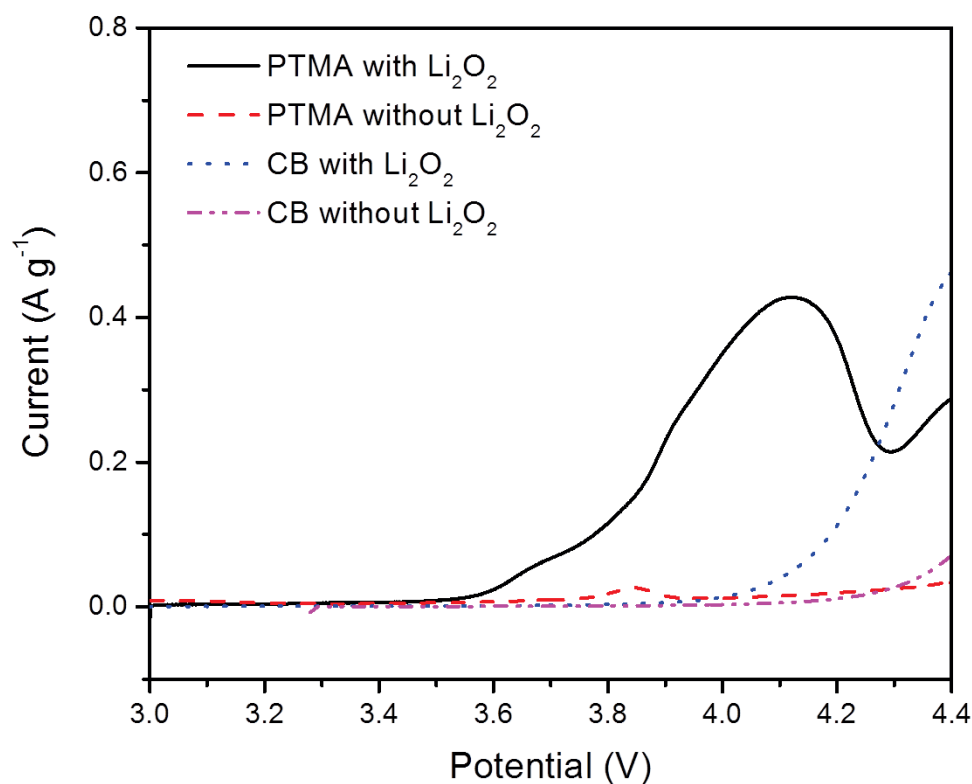


Figure 5-15 Liner sweep voltammety of electrode with and without commercial Li_2O_2 . The scanning rate is 0.1 mV s^{-1} . The range is set from open circuit voltage to 4.4 V.

5.4 Summary

In summary, a reversible Li-O₂ battery with high efficiency was demonstrated using a bi-functional organic catalyst, PTMA. This material can lower the over-potentials both in discharge and in charge processes due to its redox doping nature and catalytic properties. The coating of this efficient catalyst onto the carbon surface also reduced side-reactions between carbon and electrolyte, leading to a prolonged cycle life.

Chapter 6 A Multi-Functional Gel Co-Polymer Bridging Liquid Electrolyte and Solid Cathode Nanoparticles: An Efficient Route to Li-O₂ Batteries with Improved Performance

6.1 Introduction

Rechargeable batteries have become crucial in modern society where devices such as mobile phones, laptop computers and electric vehicles all depend on battery-based energy storage. Owing to its high theoretical energy density, the lithium oxygen (Li-O₂) battery has attracted intensive research.^[164, 304, 336, 337] Based on the reactions between lithium and oxygen, the Li-O₂ batteries have demonstrated their potential to replace the existing Li-ion batteries, however, several important issues remain to be resolved.^[314, 338]

One challenge is that in the open system of Li-O₂ batteries, unwanted loss of volatile electrolyte solvent can occur.^[312] The electrolyte in Li-O₂ batteries provides a medium for ion transport while separating the lithium anode from the cathode thus avoiding short-circuits. Loss of electrolyte solvent can significantly reduce cycle life. Commonly used electrolyte solvents include dimethyl sulphoxide (DMSO) and glymes such as diethylene glycol dimethyl ether (DEGDME), which have good solubility for lithium salts as well as reasonably low volatility. To date, some non-volatile electrolytes such as solid-state ceramic electrolytes, gel polymer electrolytes and ionic liquids have been explored.^[306, 339] However, these candidates usually exhibit poor ionic conductivity, which may significantly affect performance.

Furthermore, intermediate products such as superoxide radicals formed during the oxygen reduction reaction (ORR) are highly reactive and can attack battery components.^{[175,}

^{198, 340]} Stable materials can be employed to partially solve this problem. For instance, gel polymer electrolytes and ionic liquids can be used while gold nanoparticle electrodes can be employed to replace carbon electrodes. Recently, the addition of a 2,5-di-tert-butyl-1,4-benzoquinone (DBBQ) has been reported, which can efficiently promote the solution phase discharge in Li-O₂ batteries.^[269] By avoiding the formation of the highly reactive intermediate lithium superoxide (LiO₂), the performances of the Li-O₂ batteries can be significantly improved.

During discharge, solid products are usually formed on the surface of the cathode. The insulating nature of the discharge products results in sluggish kinetics of the oxygen evolution reaction (OER) and large over-potentials during charge. Additionally, large over-potentials can result in large quantities of unwanted by-products.^[341-343] Therefore, various catalysts are investigated to overcome these issues.^[208, 305, 307, 311, 316, 319, 322, 344, 345] Solution-based redox mediators have been developed in order to lower the reaction barrier of the OER. Different from the solid-state catalysts, redox mediators mainly function as electron shuttles, which deliver electrons between conductive matrix and discharge products. Functioning as interfacial media between electrolyte and cathode, they have demonstrated to reduce the charge plateau below 4 V, which could efficiently suppress the formation of side-products. Based on this principle, many candidates have been reported.^[174, 221-223, 323, 324, 346-349] However, the direct contact of redox mediators with lithium anodes could potentially cause additional unwanted side-reactions, degrading the battery performance.^[324] Methods such as using protection layers have been investigated to suppress the side-reactions.^[194]

Herein, we report a novel multi-functional gel co-polymer for Li-O₂ batteries, which bridges the liquid electrolyte and solid cathode nanoparticles. First functioning as a binder,

the co-polymer P(TMA-MMA) shows the capability to bind the conductive carbon nanoparticles. After the absorption of the liquid electrolyte, it forms a gel polymer membrane between the interface of the electrolyte and conductive carbon nanoparticles, which significantly improves the ionic transport and stability of the cathode. The combination of the catalytic TMA moiety and gelable MMA moiety enables the gel polymer membrane to function as an effective medium between electrolyte and cathode to promote lithium peroxide (Li_2O_2) formation during discharge (Li^+ shuttle) and to reduce over-potentials during charge (restricted redox mediator), while eliminates the contact between lithium anode and the medium to suppress side-reactions.

6.2 Experimental

6.2.1 Synthesis of P(TMA-MMA) co-polymers

P(TMA-MMA) co-polymers were synthesized through a co-polymerization process similar to previous reports.^[328, 329, 350] In a typical synthesis process, a mixture of 2,2,6,6-tetramethyl-4-piperidyl methacrylate (MTMP, TCI) and methyl methacrylate (MMA, Sigma-Aldrich) was added to acetic acid (6 mL) together with 2,2'-azobisisobutyronitrile (0.04 g, Sigma-Aldrich) and stirred at 70 °C for 12 h under an argon atmosphere. The total amount of the monomer mixture was 10 mmol. The mixture was then transferred into a flask containing ethyl ether (50 mL, Chem-Supply). The resultant white precipitate was collected by filtration. A portion of the white product (1.6 g) was dissolved in methanol (20 mL, Chem-Supply) and mixed with $\text{Na}_2\text{WO}_4 \cdot 2\text{H}_2\text{O}$ (0.3 g, Sigma-Aldrich), aqueous hydrogen peroxide (2 mL, 30 %, TCI), and water (10 mL). The mixture was then stirred at 60 °C for 40 h. The resultant solution was heated at 80 °C until the methanol was completely evaporated and a precipitate formed. The product was collected by filtration and

washed with de-ionised water, acetone, and then ethyl ether to obtain P(TMA-MMA) co-polymer. The acetone wash is important ensure the product is free from residual PMMA. An illustration of the synthetic process is shown in Figure 6-1.

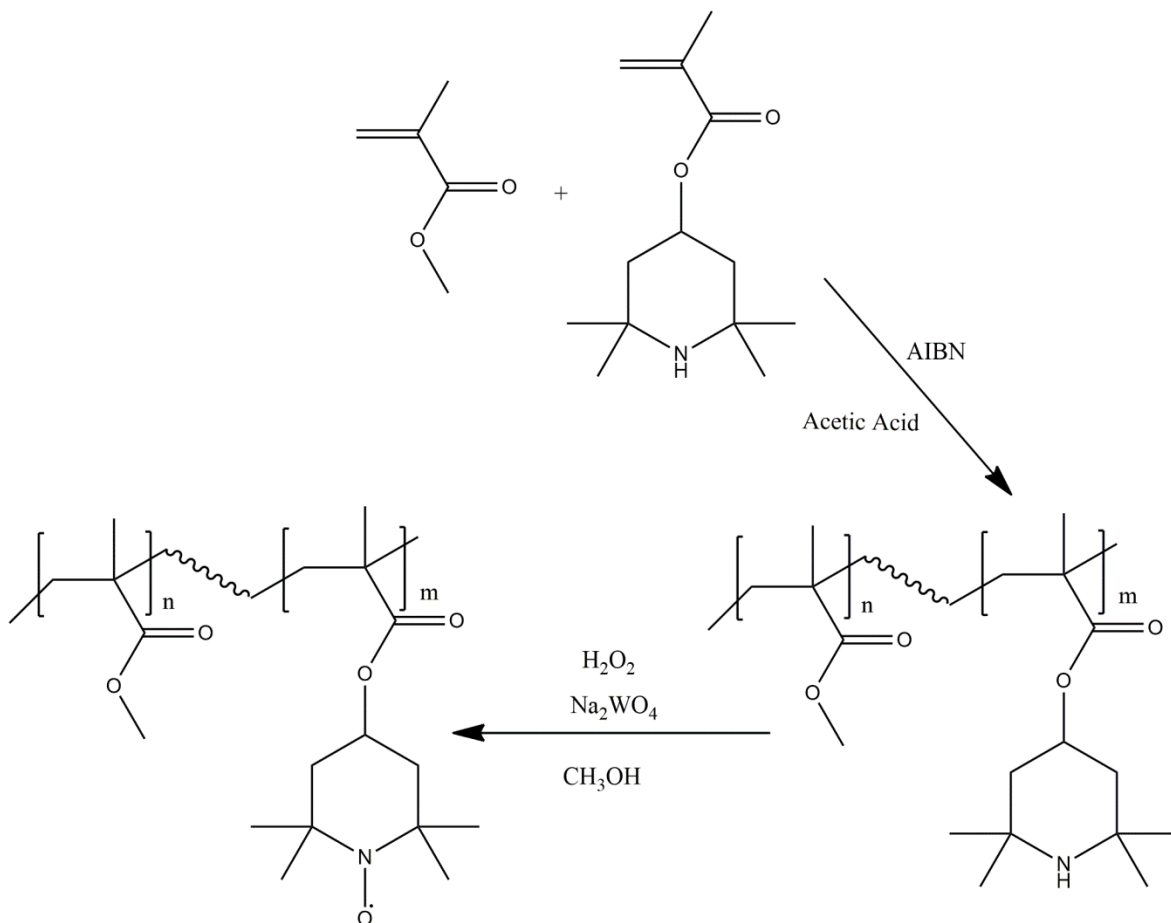


Figure 6-1 Schematic synthesis process of the co-polymers

Different co-polymers were synthesized through the same route with different molar ratios of MTMP (or TMA) and MMA monomers of 1:1, 1:2, 1:3, and 1:4, respectively. For convenience, the obtained co-polymers are named P(TMA₁-MMA₁) (P₁₁), P(TMA₁-MMA₂) (P₁₂), P(TMA₁-MMA₃) (P₁₃), and P(TMA₁-MMA₄) (P₁₄). The pure PTMA and PMMA were also prepared through the same process.

6.2.2 Characterization

A field emission scanning electron microscope (FESEM, Zeiss Supra 55 VP) was employed to observe the electrode morphologies and Zeiss EVO MA 15 SEM for EDX mapping. The infrared spectroscopy measurements of the as-prepared co-polymers were conducted on a Nicolet Magna 6700 FT-IR spectrometer. All spectra were obtained using 4 cm^{-1} resolution and 64 scans at room temperature. The spectra of ATR-FTIR were obtained using 4 cm^{-1} resolution and 16 scans at room temperature. Raman spectra were recorded on an inVia Renishaw Raman spectrometer system (HR Micro Raman spectrometer, Horiba JOBIN YVON US/HR800 UV) equipped with a 632.8 nm wavelength laser. X-ray diffraction (XRD) measurement was performed on a Bruker D8 X-ray diffractometer using $\text{Cu K}\alpha$ radiation. For the XRD analysis, the electrodes (discharge depth is 2000 mAh g^{-1}) from the disassembled cells were washed and dried first, and then sealed with “Parafilm”™ to exclude moisture and carbon dioxide from the discharge products, which are very sensitive to normal atmospheric air components. The ^1H NMR spectra were recorded on an Agilent 500 Spectrometer at 25 °C in D_2O (TSP standard).

6.2.3 Electrochemical characterization

Cathodes were prepared by firstly mixing carbon black and the co-polymers (without any other binder) in methanol with the weight ratio of 90:10. The mixture was then coated onto a glass fibre substrate and cut into discs. For convenience when described in ATR-FTIR spectra, the electrode materials coated side refers as front side while the other back side. The electrodes were dried at 80 °C in a vacuum oven for 24 h. The loading of the whole cathode materials was $\sim 1 \text{ mg cm}^{-2}$. The PTFE electrodes were prepared by the same process with the same amount of PTFE instead of co-polymer.

All the electrochemical characterizations were conducted on a CH Instrument 660D electrochemical workstation and discharge/charge performances were evaluated by a Neware Battery Testing System. The impedance spectra were measured in a frequency range of 0.01 to 10^6 Hz.

The discharge-charge performances were evaluated by assembling Li-O₂ batteries. A two-electrode Swagelok-type cell with an air hole (0.785 cm²) on the cathode side was used to test the electrochemical performances. The cells were assembled in an argon filled glove box with water and oxygen level less than 0.1 ppm. Lithium foil was used as the anode. The electrolyte was prepared by dissolving lithium bis(trifluoromethane)sulfonimide (LiTFSI, Sigma-Aldrich, 99.95 %) in diethylene glycol dimethyl ether (DEGDME, Sigma-Aldrich, 99 %, anhydrous) to give a 0.5 M solution. The solvent was pre-dried over molecular sieves (4A, Sigma-Aldrich) for at least one week before use. The water content was measured by the Karl-Fischer titration method (Karl-Fischer titrator, Mettler Toledo C20). The water content was determined to be about 35 ppm. The assembled cell was gas tight except for the cathode side window, which is exposed to the oxygen atmosphere. All measurements were conducted in 1 atm dry oxygen atmosphere. The capacities of the batteries were calculated based on the total mass of cathodes.

6.3 Results and discussions

6.3.1 Physical characterizations

P(TMA-MMA) with different TMA and MMA monomer ratios (ratio 1:1, 1:2, 1:3, and 1:4 referred to as P₁₁, P₁₂, P₁₃, and P₁₄, respectively) were synthesized *via* a two-step method (Figure 6-1). The co-polymers with different ratios show distinguishable colours,

from red to white (digital photo in Figure 6-2). The change of colours may be related to the content of the TMA moiety. The structures of these co-polymers were confirmed by FTIR and Raman (Figure 6-2b-c). FTIR spectra indicate that all the co-polymers possess the structure of TMA moiety while the Raman spectra confirm the MMA moiety. The digital photos displayed that P₁₁ co-polymer shows a distinguished red colour. However, with the increased content of the monomer MMA, the colour shifts to the lighter red and ends at pale white for the co-polymer P₁₄, which is very similar to the colour of PMMA.

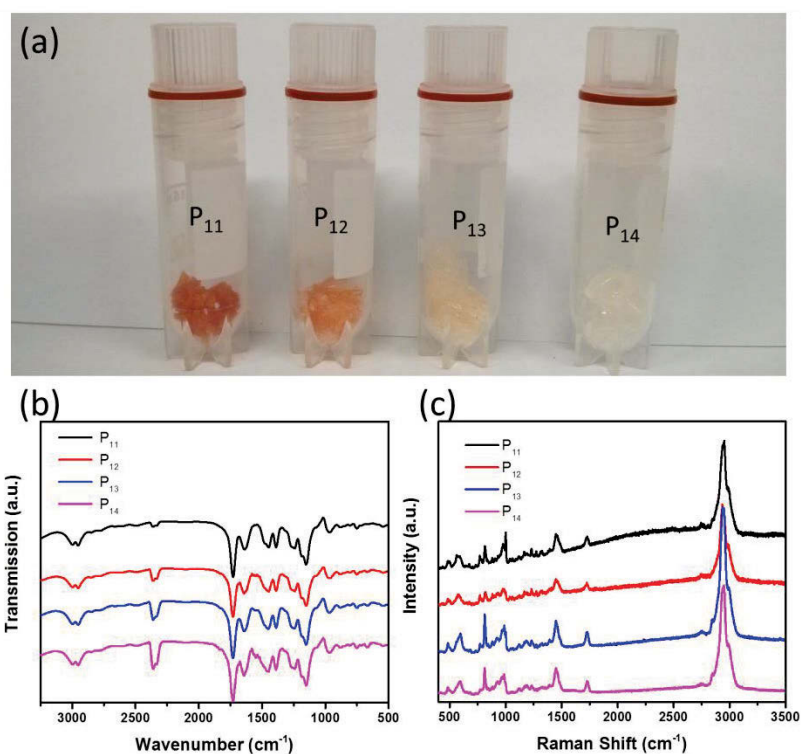


Figure 6-2 (a) Digital photos, (b) FTIR spectra, and (c) Raman spectra of the as-prepared P₁₁, P₁₂, P₁₃, and P₁₄ co-polymers.

The electrodes for Li-O₂ batteries were fabricated by casting the mixture of co-polymers and carbon black together in the presence of methanol on glass fibre substrates

(Figure 6-3). Upon drying, the co-polymers were homogeneously distributed in the electrodes, demonstrated by EDX mapping results in Figure 6-4. The SEM images shown in Figure 6-3b-e confirm that the increase of the MMA proportion in the co-polymers results in less and smaller cracking of the electrode. The P₁₁ and P₁₂ electrodes display large cracks which indicate that P₁₁ and P₁₂ may not be suitable as binders to hold the electrode nanoparticles together. This phenomenon demonstrates that the MMA moiety provides the binding capability for the overall co-polymer binders and a higher content of MMA is desirable for electrode fabrication.

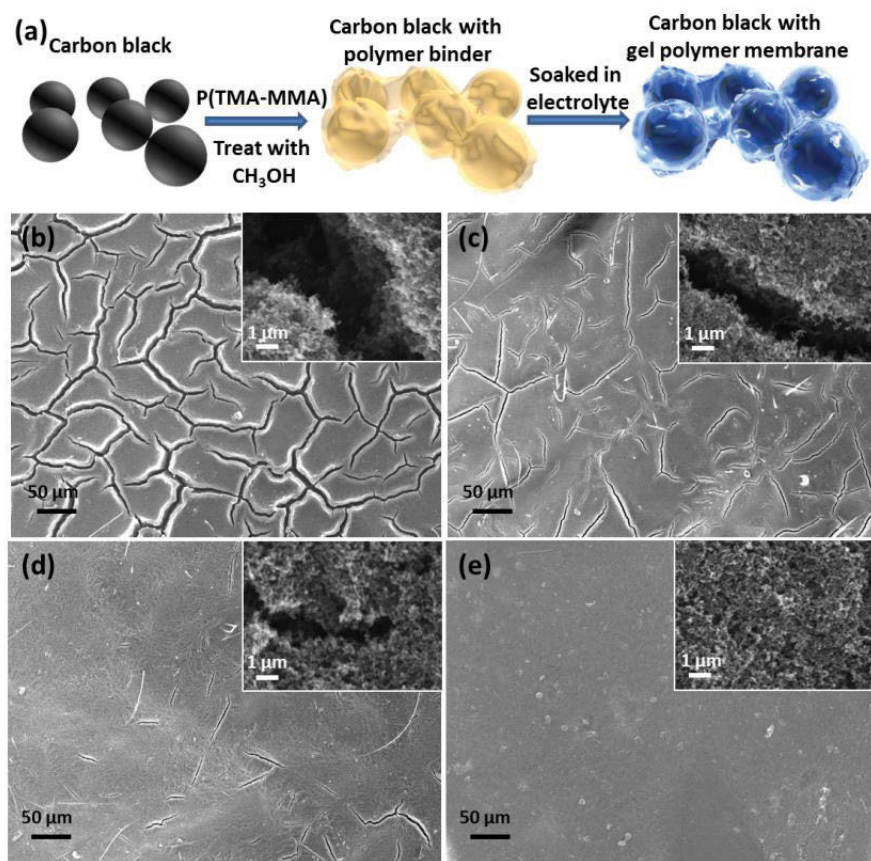


Figure 6-3 (a) Schematic illustration of the electrode fabrication process, and SEM images of the electrodes with (b) P₁₁, (c) P₁₂, (d) P₁₃, and (e) P₁₄ co-polymer binders. The insets are higher magnification SEM images of the electrodes.

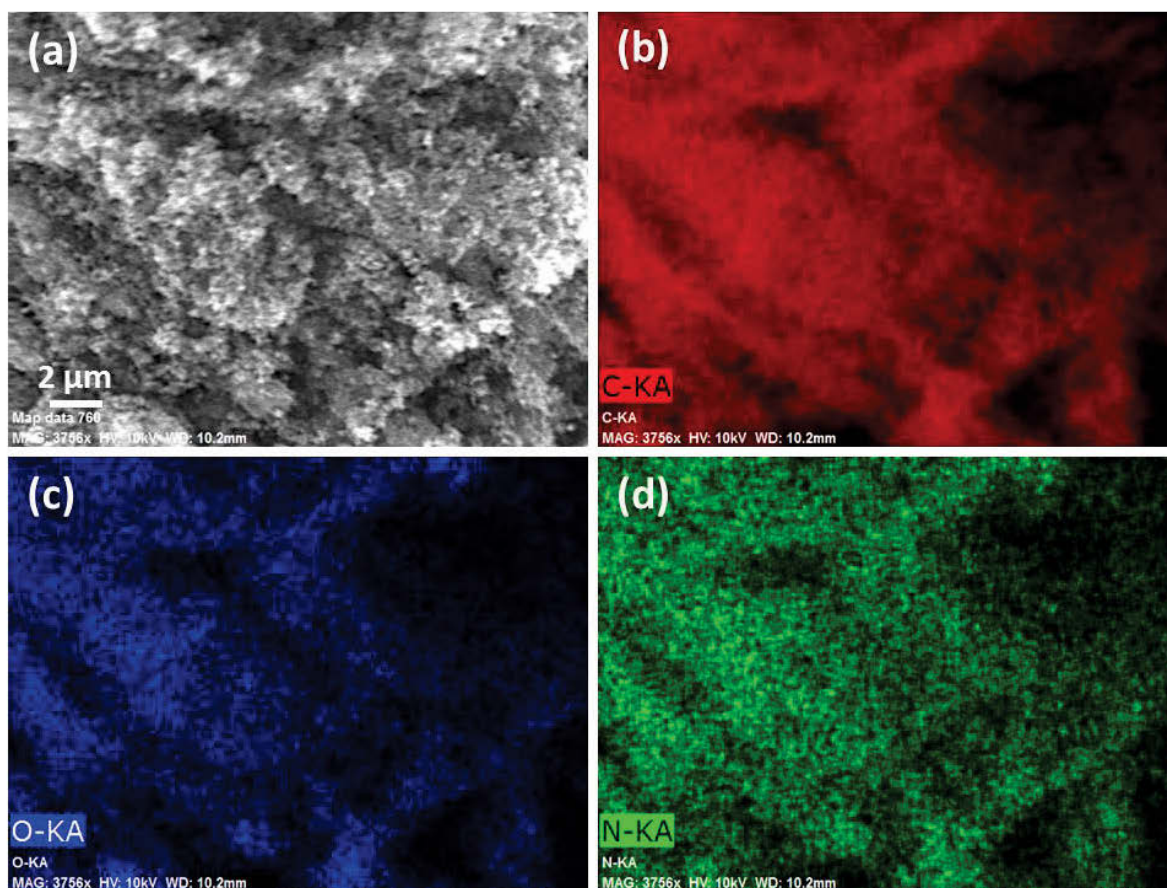


Figure 6-4 EDX mapping results of the electrode. A P₁₃ co-polymer electrode was chosen to represent the co-polymers.

6.3.2 Electrochemical performances

Figure 6-5 shows the Nyquist plots of the a.c. impedance spectra when the electrodes were used in Li-O₂ batteries. The co-polymer electrodes have significantly smaller charge transfer resistances than the PTFE counterpart, based on the diameters of the semicircles. This phenomenon probably relates to the tendency of forming gel polymer membranes (illustrated in Figure 6-3a, demonstrated by Figure 6-6), resulting in the increase of the ionic conductivity. As shown in Figure 6-5a, the charge transfer resistance of the PMMA electrode is smaller than that of the PTFE electrode, attributed to the formation of a gel

polymer electrolyte. However, the resistance of the PMMA electrode is higher than those of the co-polymer electrodes. This may be because the catalytic TMA moiety is also important for the charge transfer. The content of the catalytic TMA moiety decreases with the increase of MMA content, leading to a higher charge transfer resistance.

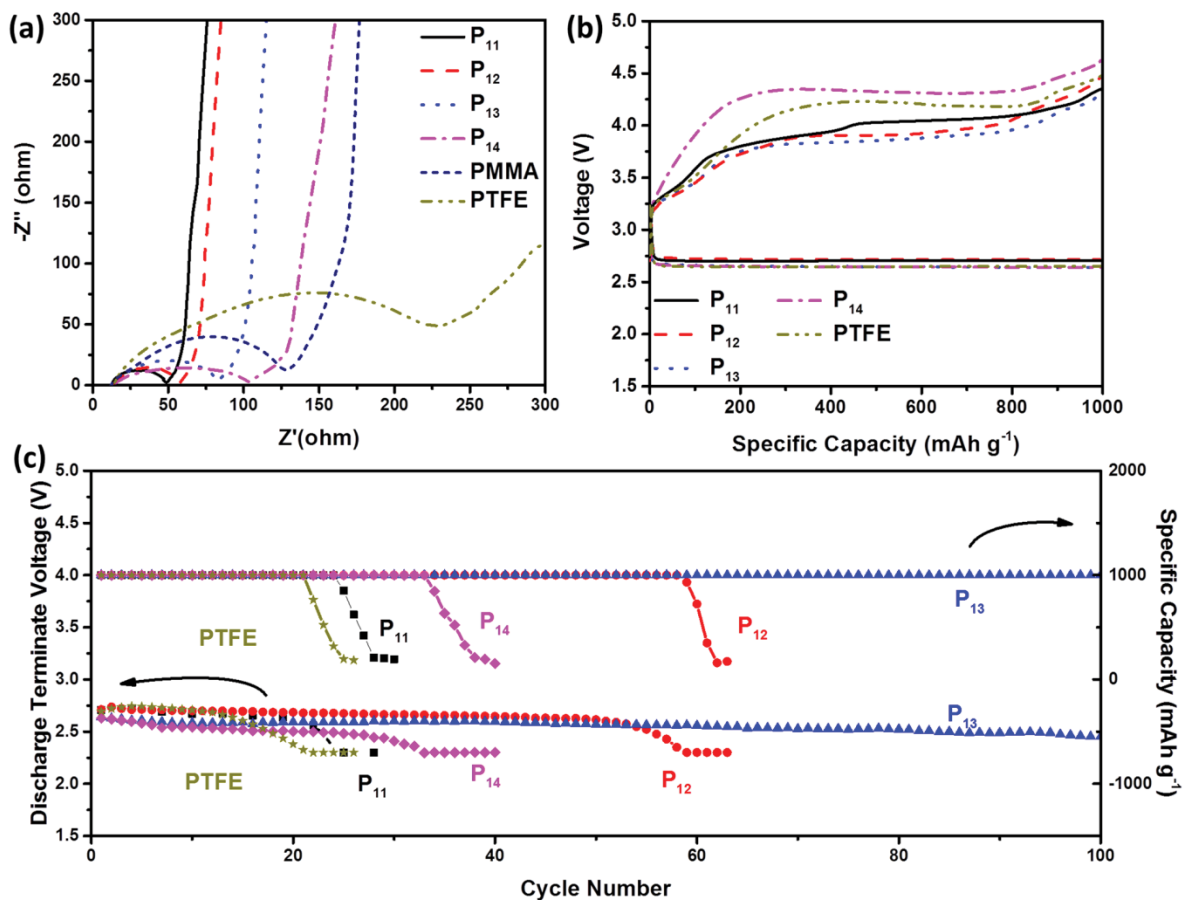


Figure 6-5 (a) Impedance spectra of test batteries with different binders in Argon atmosphere. (b) The discharge-charge profiles and (c) cyclabilities of the Li-O₂ batteries with P₁₁, P₁₂, P₁₃, P₁₄ co-polymers, and PTFE binder. The current density was 200 mA g⁻¹. The cut-off voltages were 2.3 V /4.6 V.

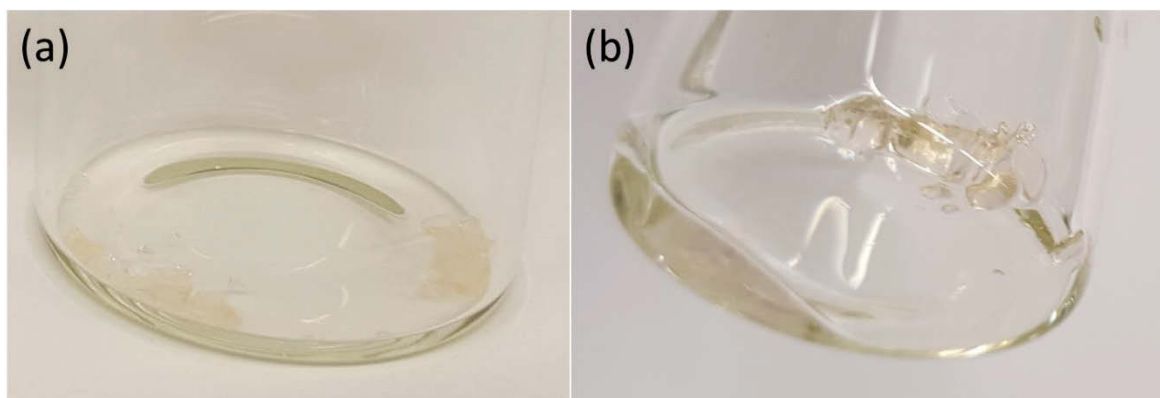


Figure 6-6 The digital image of P₁₃ co-polymer (a) before and (b) after soaking with electrolyte for one day. P₁₃ co-polymer has been used as a representative for the P(TMA-MMA) co-polymers. It is evident that the powder-like P₁₃ co-polymer changed to a transparent gel-like morphology after soaking in liquid electrolyte, confirming its capability to form a gel polymer membrane.

6.3.3 ¹HNMR tests

A further investigation by ¹HNMR (Figure 6-7) performed on the soaked electrodes demonstrated that the co-polymers could retain electrolyte solvent after vacuuming, which proves the assertion of forming gel polymer electrolyte membranes when the co-polymers are used. A P₁₃ co-polymer electrode was used to represent the co-polymer binders and a PTFE electrode was used as reference. The electrodes were first soaked in the liquid electrolyte solvent DEGDME for 24 h. After that, the electrodes were dried under vacuum for 5 h. The electrode materials were then carefully scratched off from the dried electrode and soaked into D₂O solvents. ¹HNMR was used to identify the species washed off the electrode materials. The spectra were regulated by the intensity of the H-O-D peak. It is evident that the solvent peaks between 3 and 4 ppm can be detected on the P₁₃ electrode while there's negligible peaks found for the PTFE electrode. It demonstrates that the co-

polymer could offer strong capability to retain electrolyte in the electrode through forming a gel polymer membrane.

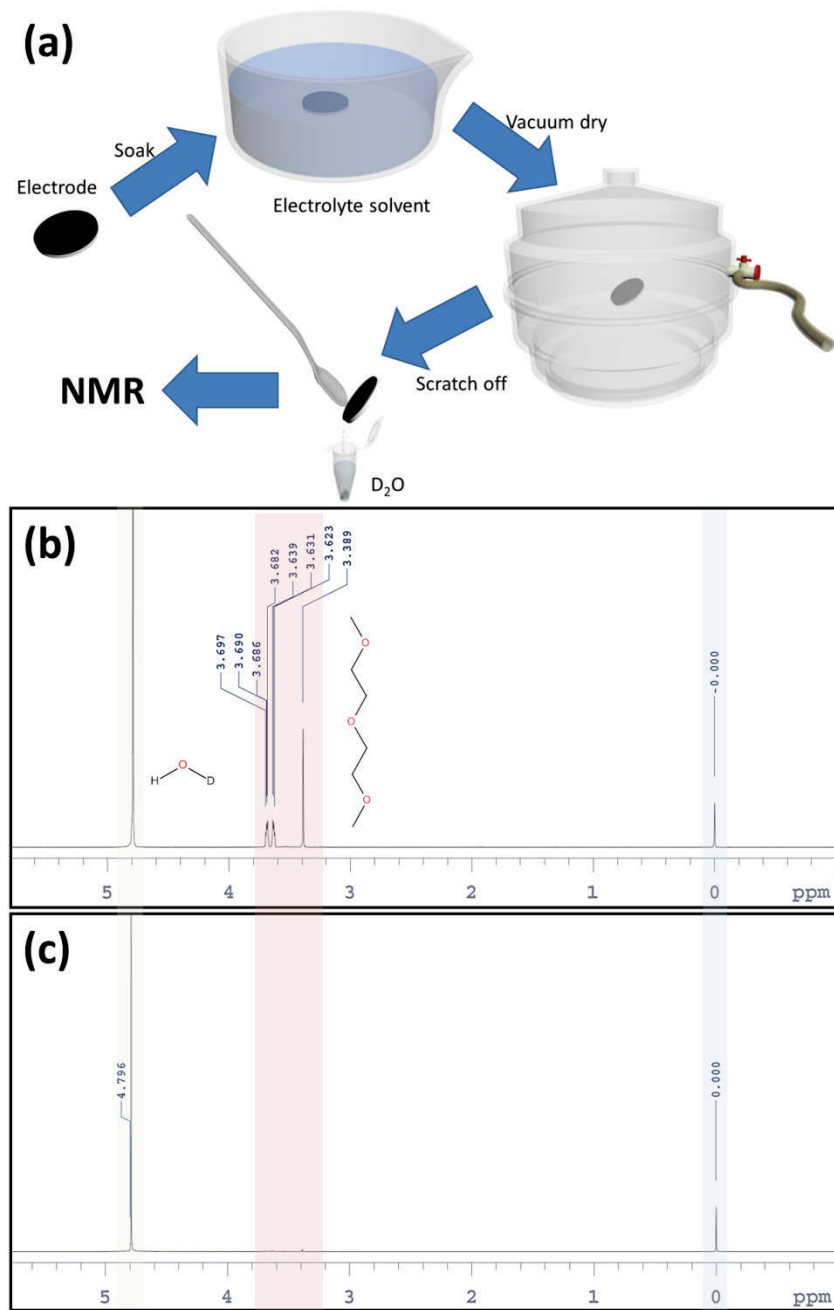


Figure 6-7 (a) Schematic illustration of the preparation for NMR testing. The ¹H NMR results of the solution extracted from (b) the P₁₃ electrode, and (c) the PTFE electrode.

6.3.4 Battery performances

Galvanostatic charge/discharge testing was conducted to evaluate the electrochemical performances of Li-O₂ batteries under a fixed capacity of 1000 mAh g⁻¹ (Figure 6-5). The Li-O₂ batteries with P₁₁, P₁₂ and P₁₃ co-polymers have charging plateaus below 4 V, while the cell with PTFE binder shows a plateau as high as 4.25 V. Similar results are found when the current densities increase to 500 mA g⁻¹ (Figure 6-8). The charging behaviours of the co-polymer cells are very much similar to the one with PTMA catalyst reported previously, indicating the catalytic activity of the TMA moiety in the co-polymer chain.^[351] Meanwhile, the discharge plateaus of Li-O₂ batteries with co-polymer binders show slightly decreased discharge over-potentials than those with PTFE binder, which reveals the bi-functional catalytic behaviour of TMA. The abnormal charging behaviour of the P₁₁ and P₁₂ cell with slightly higher over-potentials than that of P₁₃ is probably caused by the low content of MMA moiety in P₁₁ and P₁₂. Both of them do not work properly as binders, and the TMA moiety may not function well in the cracked electrodes without sufficient contact with the conducting carbon black (SEM images shown in Figure 6-3b, c). Additionally, the over-potentials of the Li-O₂ cell with P₁₄ are much higher than that with PTFE binder, probably due to the thick gel polymer layer generated by P₁₄, hindering the decomposition of Li₂O₂. These results reveal that monomer moieties play important roles in affecting the electrochemical performances of Li-O₂ batteries.

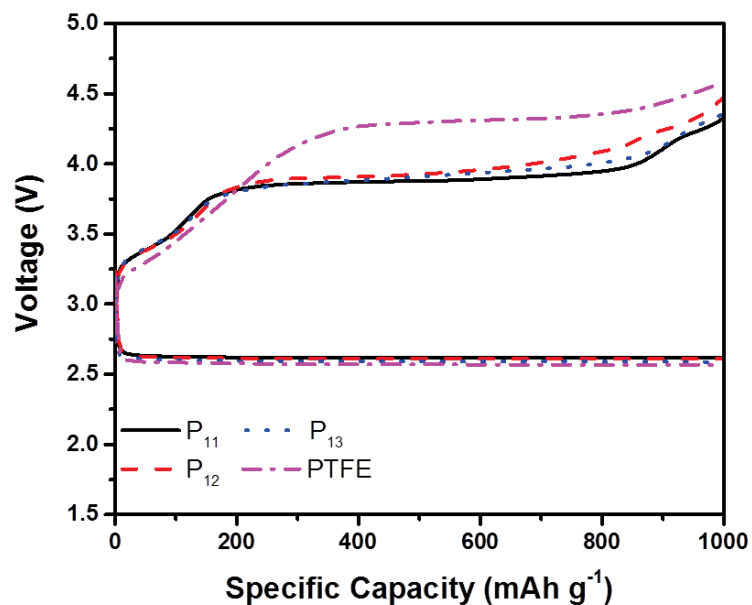


Figure 6-8 Discharge-charge profiles of the Li-O₂ batteries with P₁₁, P₁₂, P₁₃ co-polymers and PTFE binder. The current density was 500 mA g⁻¹.

Figure 6-5c shows the cycling profiles of the Li-O₂ batteries under a fixed capacity of 1000 mAh g⁻¹. The cell with P₁₃ co-polymer has the best cyclability, which maintains an end discharge voltage higher than 2.3 V even after 100 cycles, while the cell with PTFE binder only survives 22 cycles. The cyclability improves with increased content of the MMA moiety from P₁₁ to P₁₃, except for the cell with P₁₄. It indicates that the higher content of MMA moiety could contribute to better stability by forming gel polymer membranes in the cathode. However, with the content of the MMA moiety higher than P₁₃, the benefits seem to be neutralized by the drawback of the lower ionic conductivity. It is worth noting that the increase of the MMA moiety leads to a decrease of the corresponding content of the catalytic moiety TMA, which results in a decrease of the catalytic capability. Overall, the content ratio of P₁₃ is considered the optimum for Li-O₂ batteries.

Post-discharge/charge characterizations of the P₁₃ electrode were conducted by SEM and XRD. As shown in Figure 6-9b, toroidal-shaped Li₂O₂ (confirmed by XRD result in Figure 6-9d) with a diameter of 200 nm was formed after discharge. The morphology of the Li₂O₂ disappeared after charge, indicating the reversibility of Li₂O₂ formation and decomposition when P₁₃ was used.

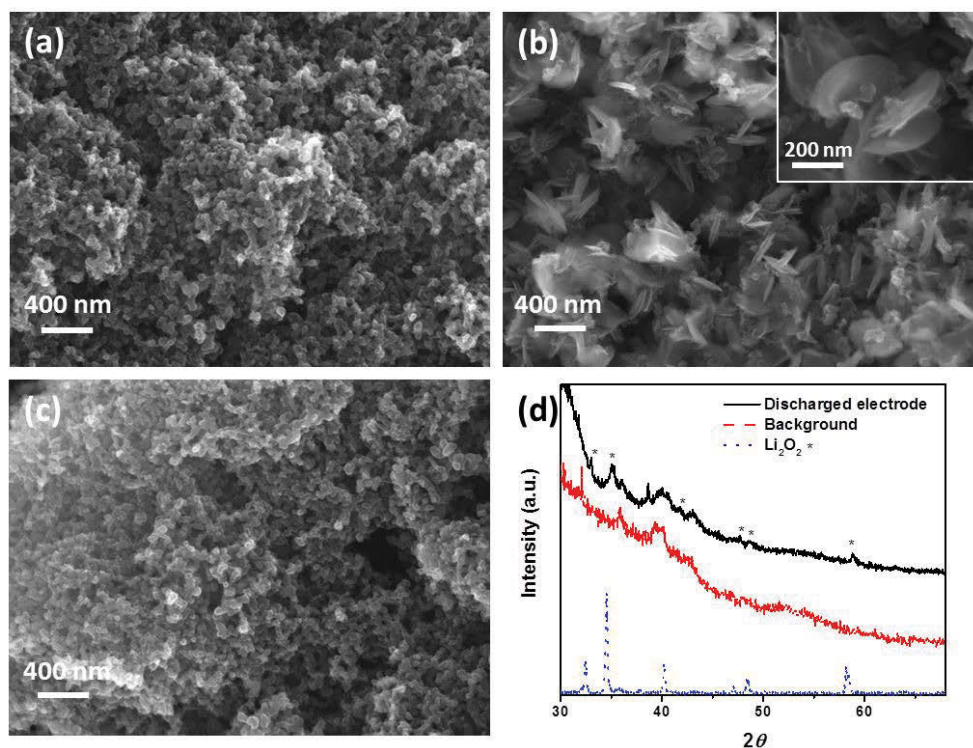


Figure 6-9 SEM images of (a) the pristine electrode, (b) the electrode after discharge, and (c) the electrode after charge. A P₁₃ co-polymer was used as a representative, and the current density was 200 mA g⁻¹. (d) XRD patterns of the electrode after discharge. Compared with the pristine electrode (a), toroidal-shaped structures were observed after discharge (b) and vanished after charge (c). The discharge products have been confirmed to be Li₂O₂ by XRD measurement (d). These results further indicate the stability and compatibility of P₁₃ in Li-O₂ batteries.

The FTIR spectra of the electrodes with P₁₃ after 5 cycles shown in Figure 6-10 indicate the exceptional stability of P₁₃ against the main discharge product Li₂O₂.

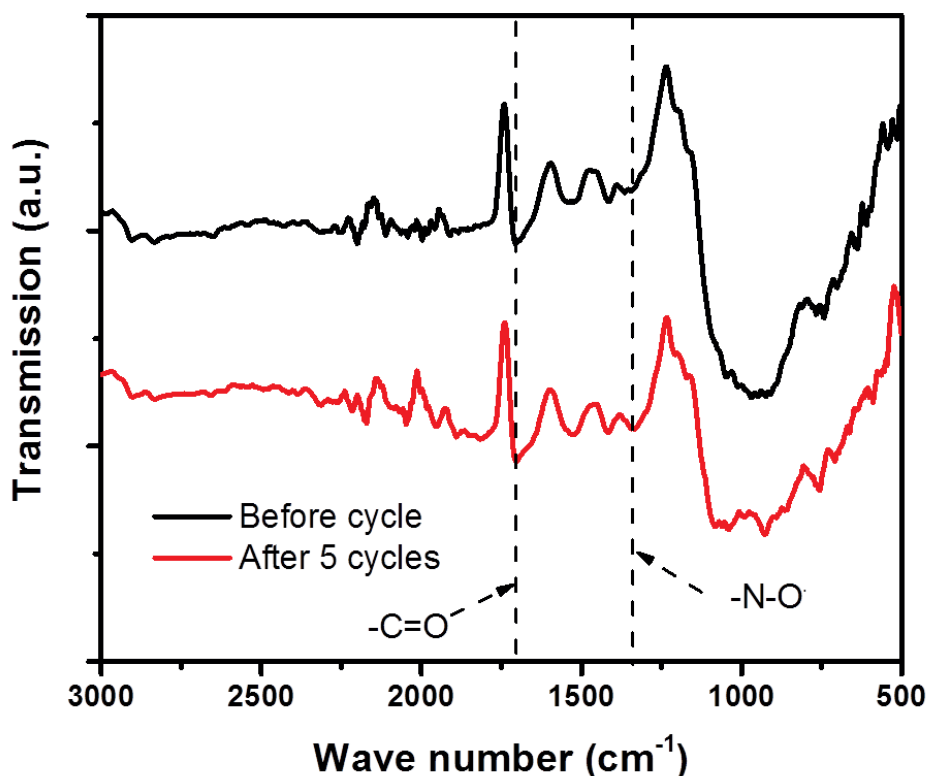


Figure 6-10 FTIR spectra of the cathode with P₁₃ before cycle and after 5 cycles. The characteristic peaks of the co-polymer remain unchanged after 5 cycles, indicating the exceptional stability of the co-polymer in the attack of Li₂O₂.

6.3.5 Mechanisms

The co-polymer P(TMA-MMA) is proposed to act as a multi-functional medium in Li-O₂ batteries, which significantly enhances the interface of the liquid electrolyte and the solid cathode. The mechanism is illustrated in Figure 6-11. In particular, the inclusion of TMA in the P(MMA-TMA) copolymer plays an important role in enhancing the overall performances. PMMA has previously been demonstrated to be a useful binder of carbon

black electrode nanoparticles and the P(TMA-MMA) polymer is shown here to also provide effective binding properties. An important property of the polymer is that it can be permeated by the ether-based electrolyte to form a gel polymer layer that is stable and ionically conductive. The results clearly demonstrate that this layer provides sufficient ionic conductivity for efficient battery reactions.

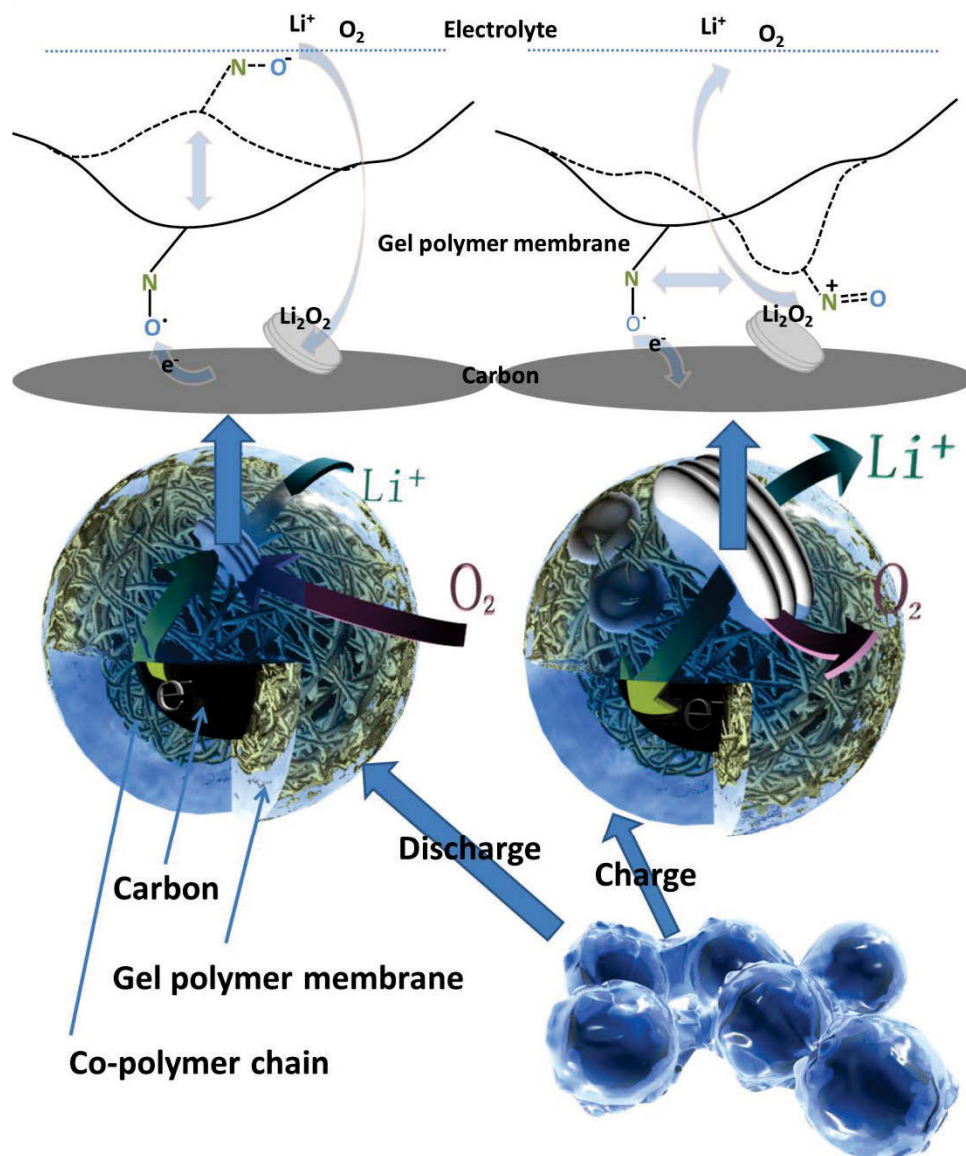


Figure 6-11 Schematic mechanisms of the co-polymers facilitating Li-O₂ battery reactions during discharge and charge

In addition, the -NO^\bullet group associated with the TMA moiety functions as a catalyst for the ORR and OER. Previous work has demonstrated that the stable -NO^\bullet radical is effective at catalysing the formation and decomposition of Li_2O_2 in Li-O₂ battery. In the work presented here, the permeability of the P(TMA-MMA) to the electrolyte allows the

gel significantly more flexibility than solid state catalytic systems and thus the $-\text{NO}$ group can adopt various orientations to more effectively facilitate the ORR and OER, which is demonstrated by LSV measurement shown in Figure 6-12. The $\text{CB}+\text{Li}_2\text{O}_2$ electrodes were prepared by mixing carbon black, binder (P_{13} or PTFE) and Li_2O_2 (ratio 9:1:4) in NMP, which was casted on glass fiber substrate. The dramatic increase of the cathodic current density when P_{13} was used indicates the capability of P_{13} to facilitate the formation of Li_2O_2 . The capability of decomposing Li_2O_2 was evaluated by adding Li_2O_2 when making electrodes. The peak associated with the decomposition of Li_2O_2 shifts from over 4.4 V to 3.8 V, which should originate from the catalytic activity of P_{13} . This is important because during discharge, the $-\text{NO}$ groups on the TMA moiety are reduced at the carbon black surface and Li^+ is absorbed. The flexibility of the gel polymer structure allows for enhanced transportation of Li^+ from the liquid electrolyte and electrons from the carbon nanoparticles surface and thus enabling continuous growth of Li_2O_2 within the stable gel polymer layer. This is manifested in an improved discharge performance. During charging, the $-\text{NO}$ groups from the TMA moiety are oxidized releasing electrons to the carbon electrode. Thus, the nitride oxides function as bound redox mediators that facilitate the shuttle of electrons. This process facilitates Li_2O_2 decomposition releasing Li^+ at the liquid electrolyte interface. As a result, the new gel polymer material enhances both discharge and charge characteristics.

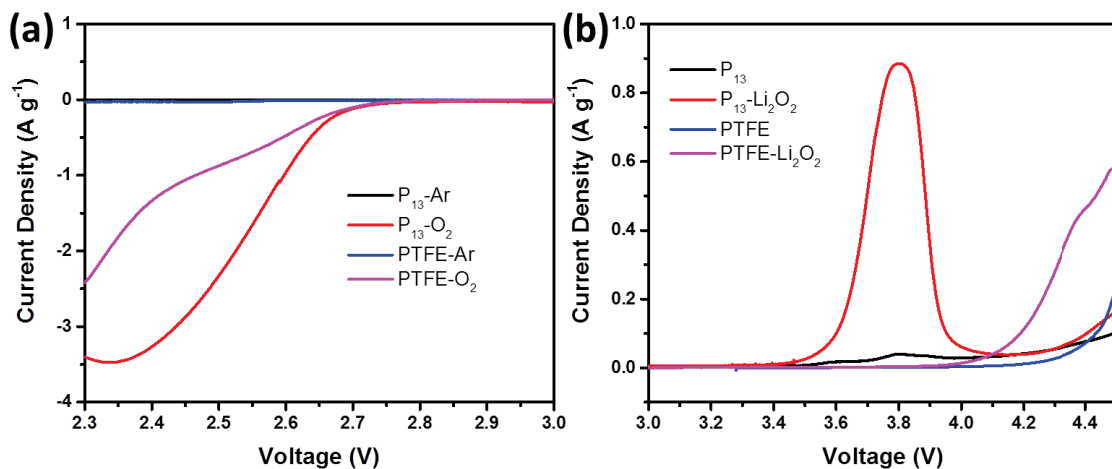


Figure 6-12 The LSV curves of the Li-O₂ batteries with (a) CB electrodes and (b) CB+Li₂O₂ electrodes. The scan rate is 0.1 mV s⁻¹.

To confirm the superior performance of the P(MMA-TMA) copolymer, a comparison (PTMA+PMMA) electrode was prepared by mixing carbon black, PTMA, and PMMA in the same ratio as the P₁₃ electrode and then employed in a Li-O₂ battery. As shown in Figure 6-13a, the PTMA+PMMA cell exhibits somewhat different charging behaviour compared to that of the P₁₃ cell. We attribute this to an improved catalytic process in the P₁₃ electrode. In Li-O₂ batteries, Li₂O₂ has been shown to grow on the top of the stationary catalytic layer upon discharge. Since the catalytic capability relies on direct contact with the conducting carbon surface, when all of the catalytic surfaces are occupied, discharge will become difficult. In the PTMA+PMMA mixture, there are limited catalytic sites (PTMA particles) near the carbon surface. In contrast, the P₁₃ gel electrode contains catalytic sites throughout the membrane layer and thus can provide more active sites for Li₂O₂ formation (Figure 6-13c).

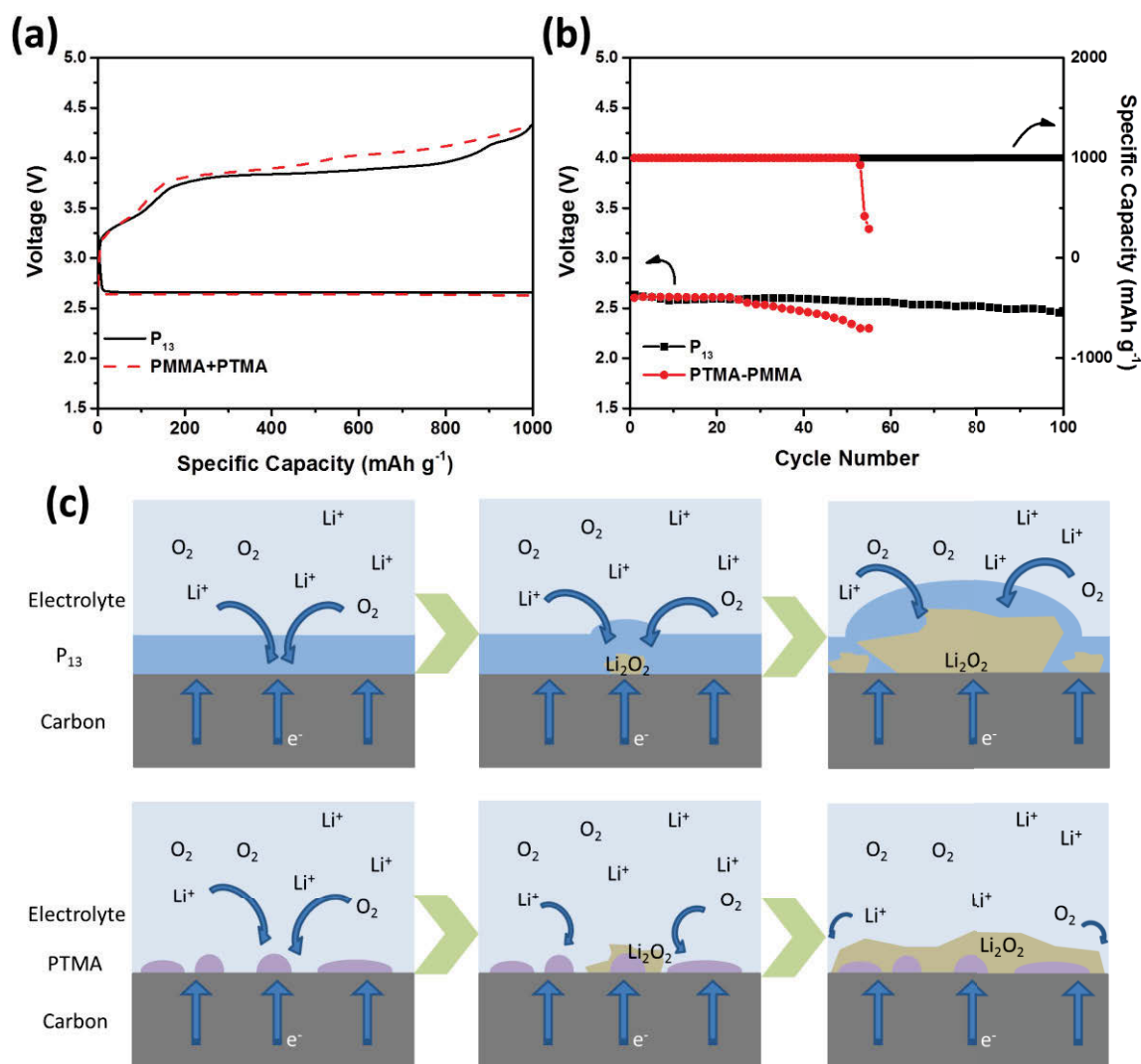


Figure 6-13 (a) The discharge-charge profiles and (b) cyclabilities of Li-O₂ batteries with P₁₃ and PTMA-PMMA. The current density was 200 mA g⁻¹, and the cut-off voltages were 2.3 V/4.6 V. (c) Graphical illustration of the Li₂O₂ formation mechanism on P₁₃ and PTMA+PMMA electrodes during discharge.

ATR-FTIR experiments provide evidence for this mechanism where peaks associated with the N-O stretch at 1332 cm⁻¹ are observed in the discharged P₁₃ electrode but are absent in the discharged PTMA+PMMA electrode (Figure 6-14). Electrodes with P₁₃,

PTMA-PMMA, or PTFE were first assembled into Li-O₂ batteries and discharged to 3000 mAh g⁻¹. The electrodes were taken removed and washed with DEGDME solvents, followed by drying under vacuum. For ATR-FTIR experiments, the carbon surfaces (front) were placed against the ATR crystal and 16 scans were recorded. A band assigned to the N-O group of the TMA unit in P₁₃ is apparent at 1332 cm⁻¹ but absent in the other samples. The presence of is band in conjunction with an IR penetration depth of ~ 1 μm in this technique indicates that the P₁₃ material is present throughout the Li₂O₂ deposit while the PTMA-PMMA layer is covered by Li₂O₂ after the discharge process (and thus not detectable by the IR at the penetration depth). This indicates that the catalytic N-O groups are present throughout the region of Li₂O₂ deposition (which is significantly thicker than the depth of IR penetration) in the P₁₃ electrode but not in the mixed PTMA+PMMA electrode.

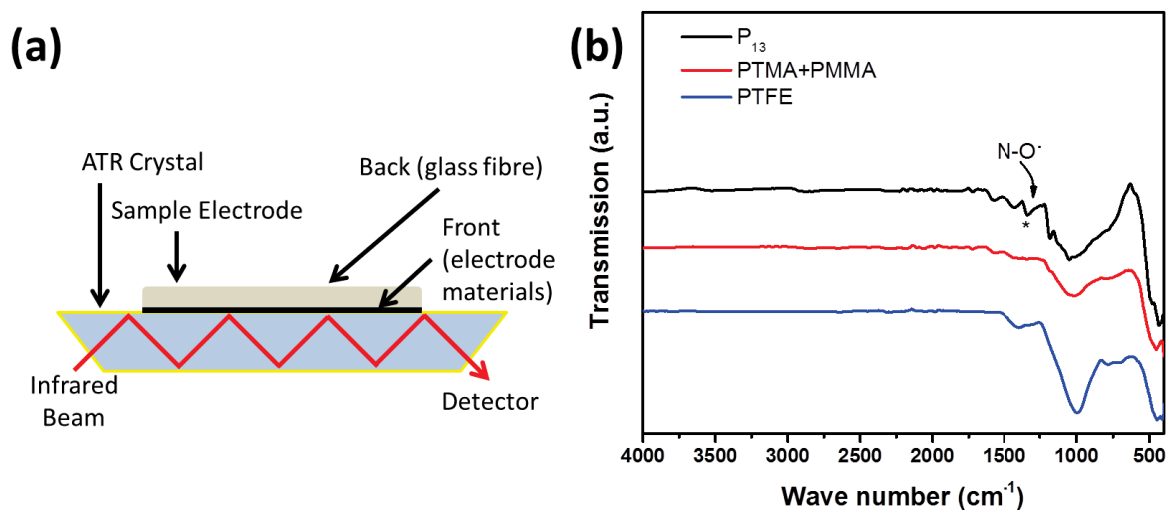


Figure 6-14 (a) Orientation of the sample during ATR-FTIR experiments. (b) ATR-FTIR spectra of the electrodes surfaces. A band assigned to the N-O group of the TMA unit in P₁₃ at 1332 cm⁻¹ is indicated by *.

Furthermore, upon discharging to 2.3 V in Figure 6-15, cells containing the P₁₃ electrode deliver significantly more capacity than those containing the PTMA+PMMA mixture, a reflection of the greater number of active sites within the P₁₃ electrodes.

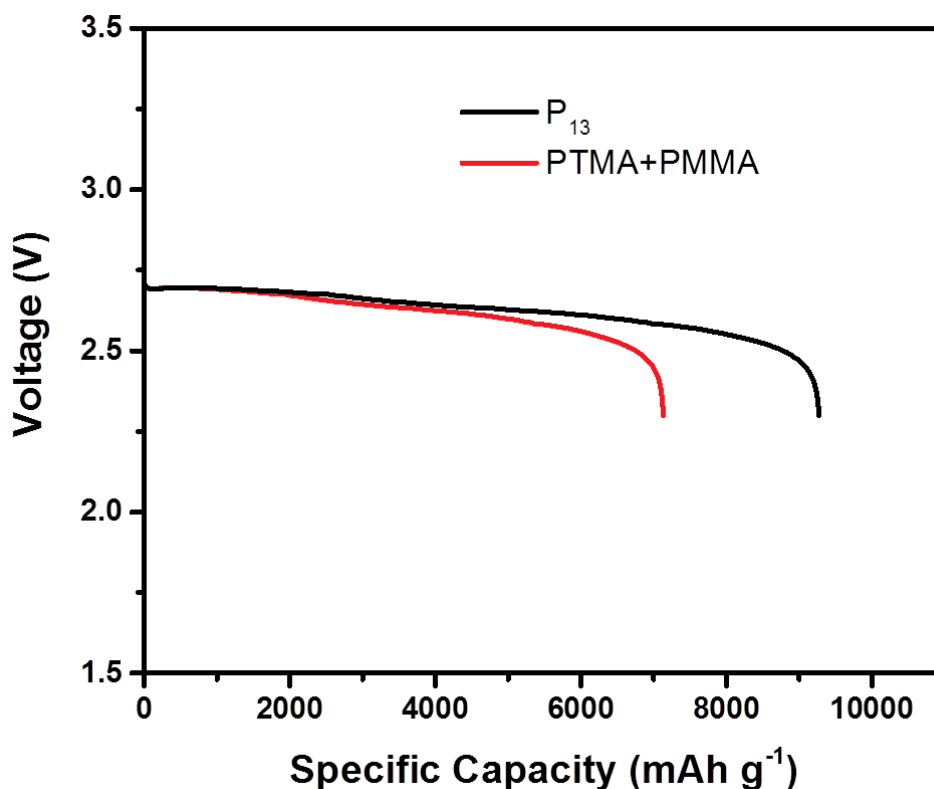


Figure 6-15 Discharge profiles of Li-O₂ batteries with P₁₃ and PTMA+PMMA electrodes. The current density was 200 mA g⁻¹, and the cut-off voltage was 2.3 V.

Importantly, the capacity does not originate from the self-discharge of the co-polymer. The discharge and charge profiles of both electrodes in an argon atmosphere are displayed in Figure 6-16. The capacities are insignificant compared with those for cells operating in an oxygen atmosphere. Furthermore, the dQ/dV vs voltage profiles indicate the broader voltage range of n-/p-doping of the TMA moiety. All of these observations are consistent with the P₁₃ gel polymer membrane acting as a flexible catalytic medium. As a result, P₁₃

allows efficient formation and decomposition of Li_2O_2 , leading to an improved cyclability (Figure 6-13b).

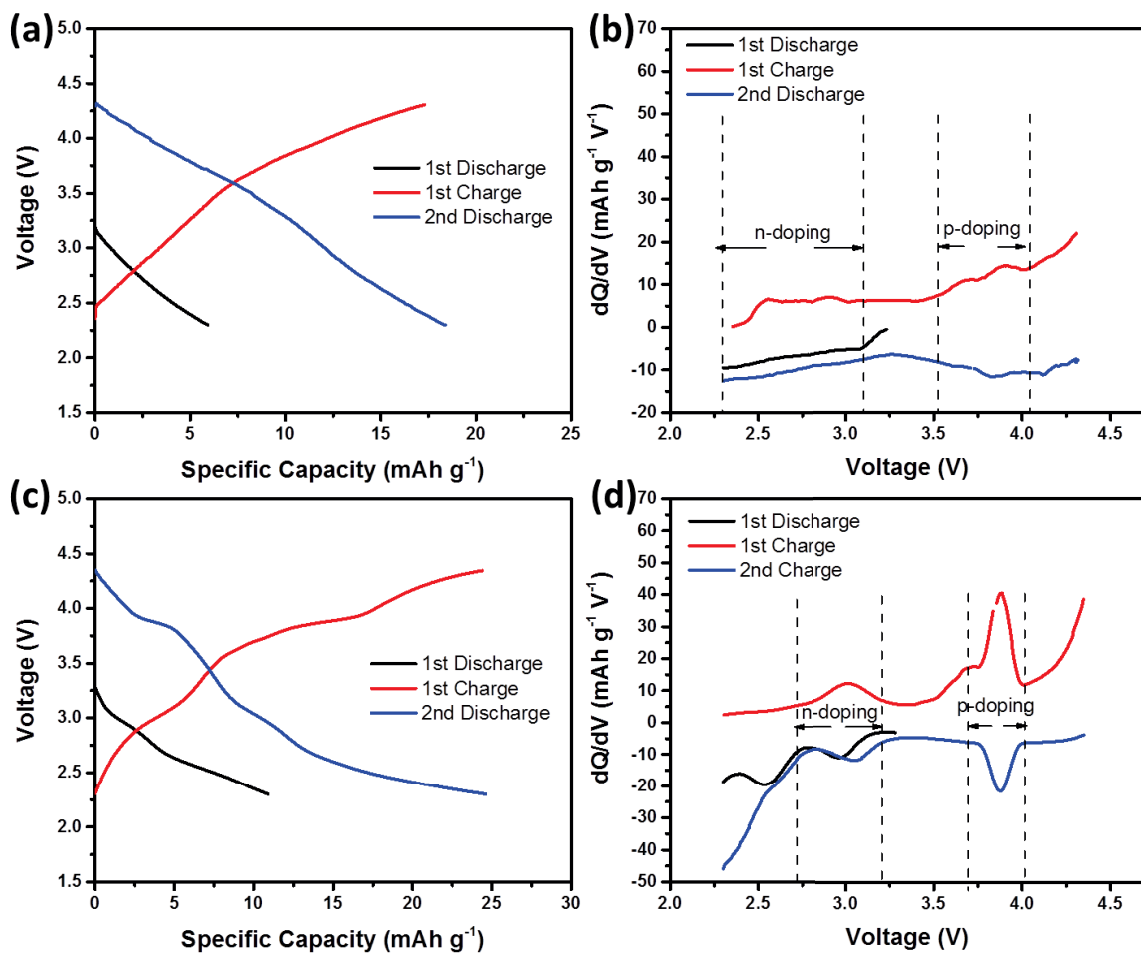


Figure 6-16 Discharge-charge profiles of Li-O₂ batteries with (a) P₁₃ and (c) PTMA+PMMA electrodes. The current density was 200 mA g⁻¹ and cut-off potentials were 2.3 V/4.3 V. The dQ/dV vs voltage profiles of (b) P₁₃ and (d) PTMA+PMMA electrodes based on (a, c) profiles.

The P₁₃ co-polymer also provides excellent rate performance for Li-O₂ batteries as shown in Figure 6-17.

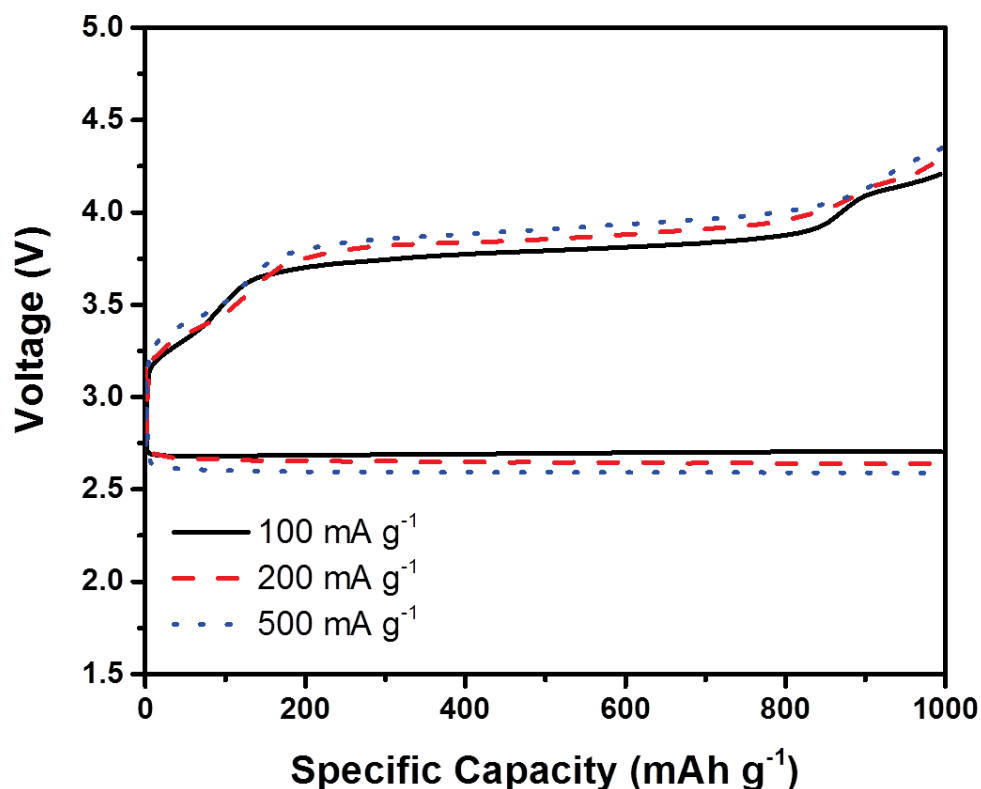


Figure 6-17 Rate performance of the Li-O₂ batteries with P₁₃ co-polymer as catalyst/binder. The discharge and charge current densities of each cell were kept the same.

Further rate capability analyses of Li-O₂ batteries with P₁₃ were conducted using different current densities (Figure 6-18, 6-19). After discharge at the same current density, the cells show no significant increase of over-potentials when charged at increased current densities (Figure 6-18a, b). Intriguing results are observed when different discharge current densities were used, with the charge current densities all held at 100 mA g⁻¹ (Figure 6-18c, d). The charge curve is flatter when higher discharge current densities are applied for both P₁₃- and PTFE-containing cells. However, cells with P₁₃ exhibit a lower potential of the charge plateau, compared to the cells with PTFE.

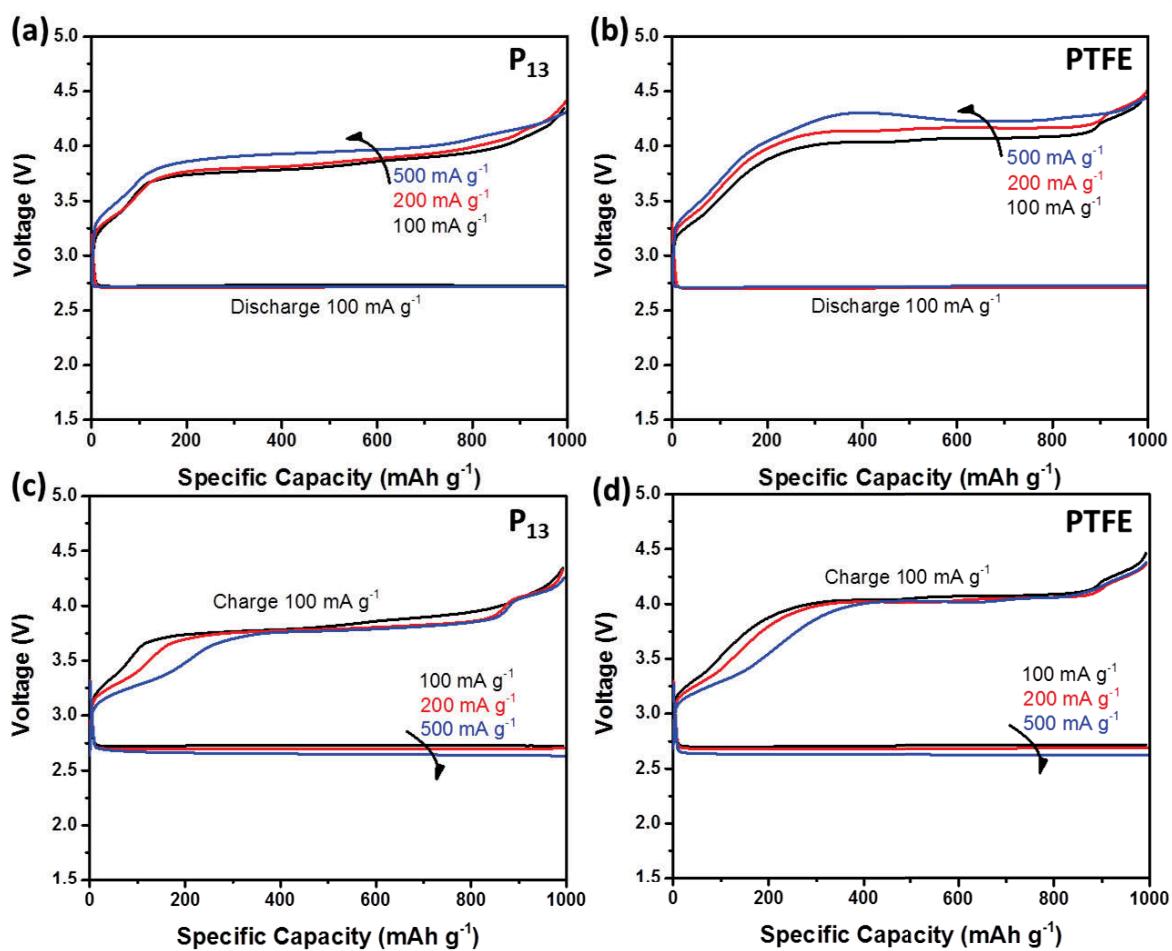


Figure 6-18 Discharge-charge profiles of Li-O₂ batteries with (a) P₁₃ and (b) PTFE all discharged at 100 mA g⁻¹, charged at 100, 200, and 500 mA g⁻¹, respectively. Discharge-charge profiles of Li-O₂ batteries with (c) P₁₃ and (d) PTFE discharged at 100, 200, and 500 mA g⁻¹, respectively, all charged at 100 mA g⁻¹.

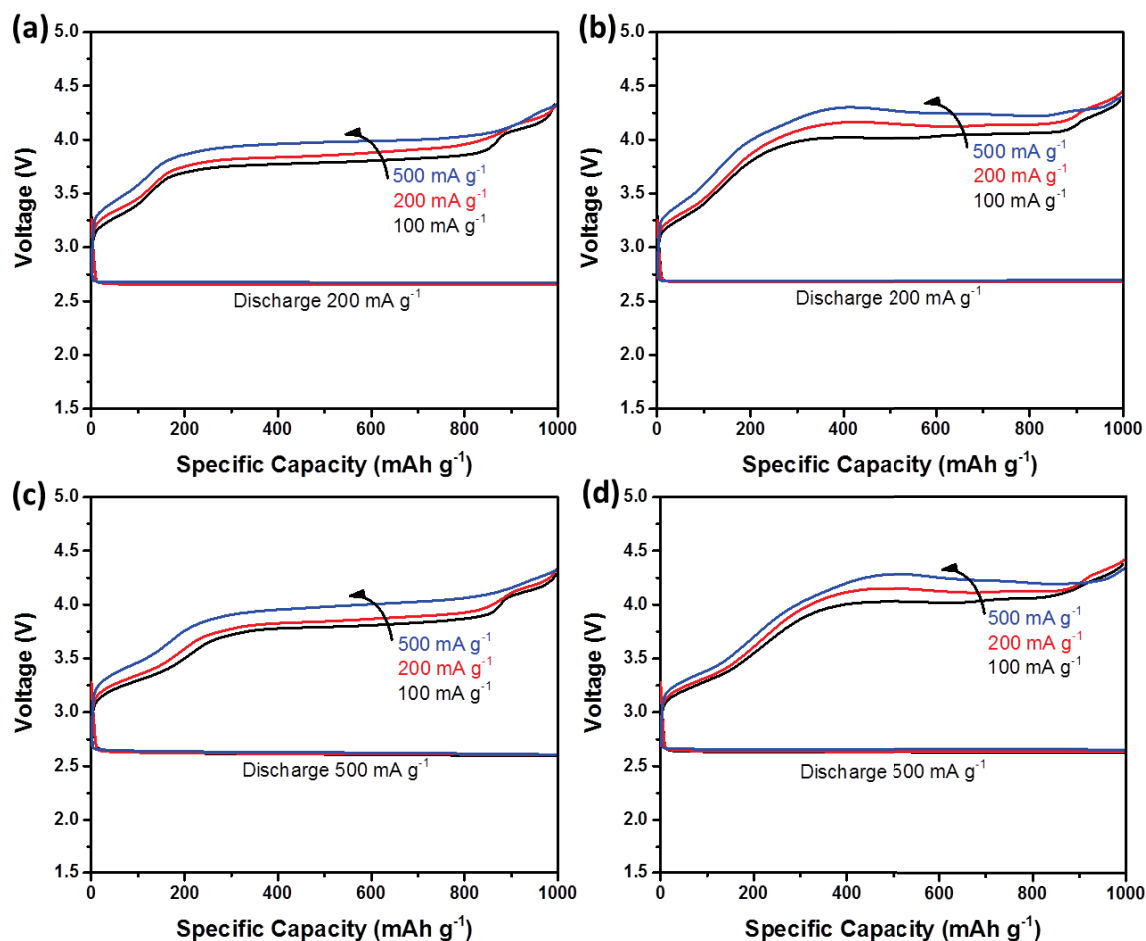


Figure 6-19 Discharge-charge profiles of Li-O₂ batteries with (a, c) P₁₃ and (b, d) PTFE all discharged at (a, b) 200 mA g⁻¹ or (c, d) 500 mA g⁻¹, charged at 100, 200, and 500 mA g⁻¹, respectively.

SEM images in Figure 6-20 indicate that the size of Li₂O₂ is reduced when large current densities were applied, accompanied by a change of morphology from a toroidal shape to a film-like structure. When the cell was discharged at a low current density of 100 mA g⁻¹, the product Li₂O₂ showed a regular large toroidal shape with a large diameter of around 600 nm. However, when the current density was increased to 200 mA g⁻¹, the size of the Li₂O₂ was significantly reduced to 200 nm and a Li₂O₂ film can be observed. When the

current density was further increased to 500 mA g^{-1} , the toroidal shapes of Li_2O_2 disappeared, and instead, the entire cathode was covered with a Li_2O_2 film.^[343] Therefore, the P_{13} co-polymer functions well with a small particle size of Li_2O_2 .

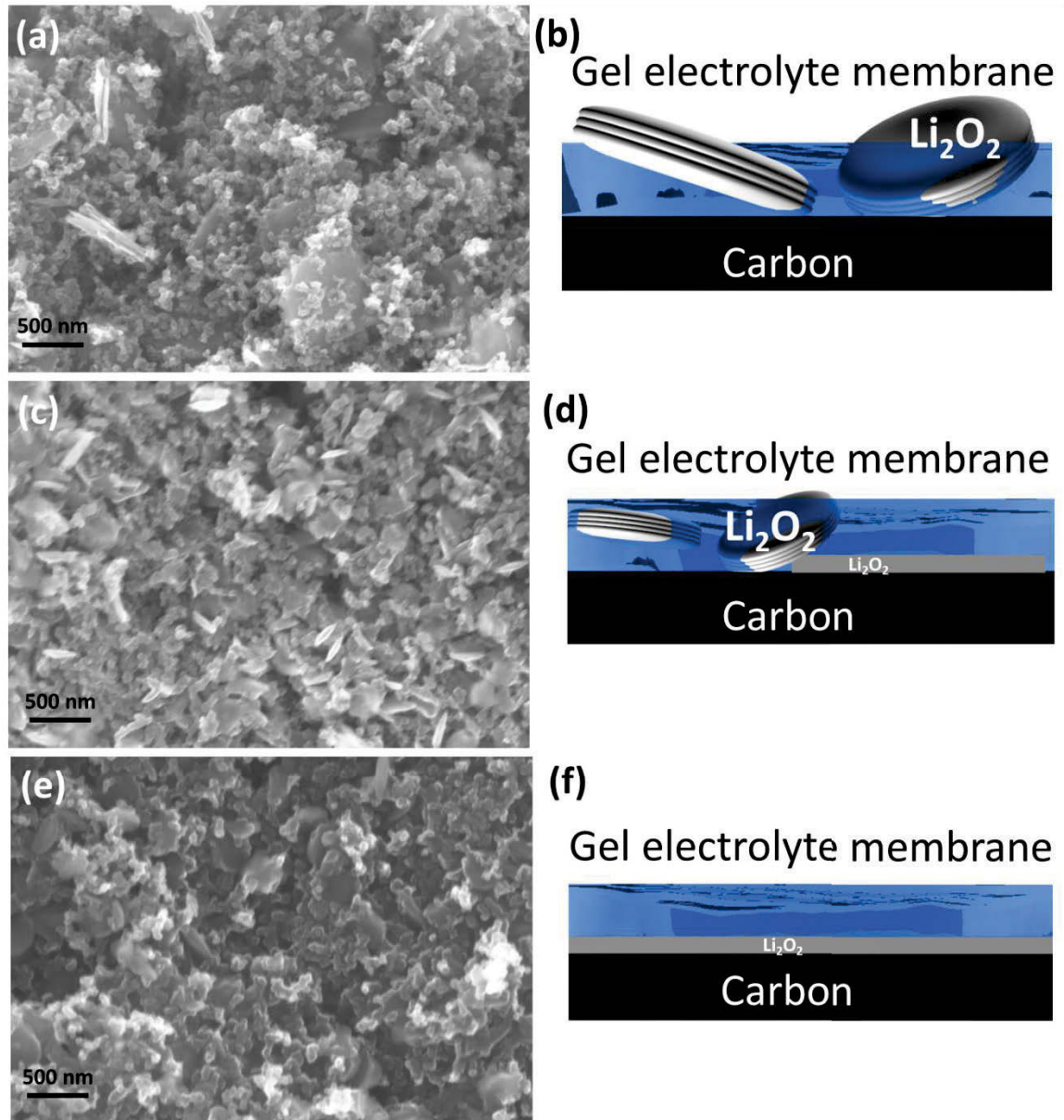


Figure 6-20 The SEM images of discharged electrodes at current densities of (a) 100 mA g^{-1} , (c) 200 mA g^{-1} , and (e) 500 mA g^{-1} . (b, d, f) Illustration of the proposed mechanism for forming different morphologies of Li_2O_2 .

This phenomenon is probably because the movement of the TMA moiety is restricted (confirmed by FTIR spectra before and after cycling in Figure 6-21). The result confirms no co-polymer detected in the electrolyte. It demonstrated that P₁₃ only moved restrictedly in the cathode, minimizing the risk of the side-reactions originated from the direct contact between the lithium anode and the catalyst, which can significantly enhance the cycling performance of Li-O₂ batteries. Large current densities led to a high contact area due to the decrease of Li₂O₂ size, resulting in a low charge over-potential.

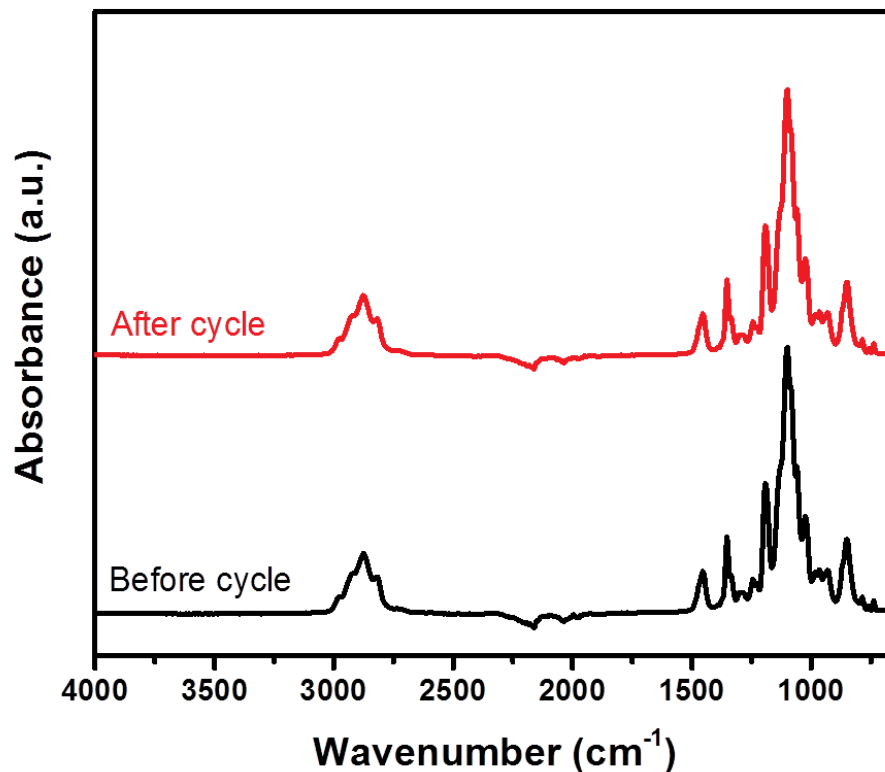


Figure 6-21 FTIR spectra of the electrolyte before and after 1 cycle when using P₁₃ co-polymer catalyst/binder.

However, adding more P₁₃ to form a thicker layer of polymer membrane in the electrode did not generate better performances (as shown in Figure 6-22). The Li-O₂ battery

with higher percentage of co-polymer catalyst/binder in the electrode shows slightly lower over-potentials, due to the thicker gel polymer membrane formed, providing better contact areas between discharge products and catalyst moiety. However, when the content increased to 30%, the performance of the battery was not as good as the one with 20 %. This phenomenon was probably related to the lower conductivity caused by adding too much binder, which may reduce the battery reaction kinetics and increase over-potentials. To conclude, binder content lower than 20% is favourable in the co-polymer catalyst/binder systems.

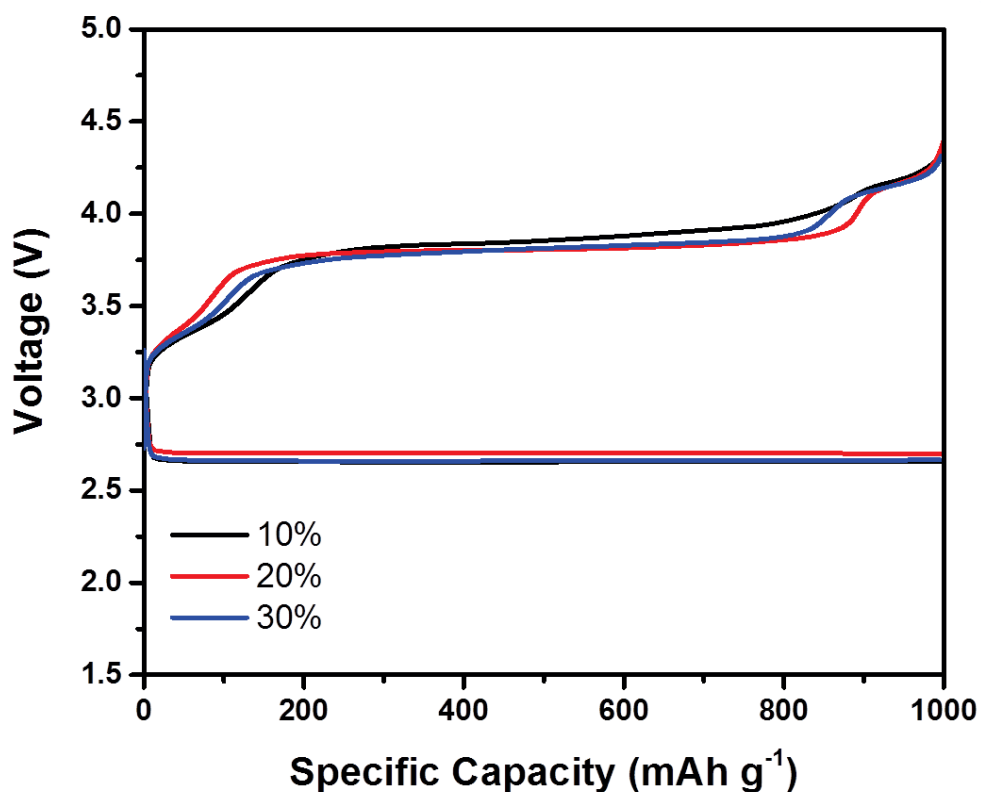


Figure 6-22 The discharge-charge profiles of Li-O₂ batteries with different percentages of P₁₃ co-polymer in the cathode. The current density was 200 mA g⁻¹.

6.4 Summary

In summary, a multi-functional co-polymer, P(TMA-MMA), has been synthesised with an optimized monomer ratio *via* a two-step method. The MMA moiety enables the fabrication of electrodes without further addition of polymeric binders and allows formation of a gel polymer membrane to retain volatile liquid electrolyte and enhance stability. The TMA moiety acts as a bi-functional unit to promote the ORR and OER in Li-O₂ batteries. In addition to the TMA-bound catalytic moieties throughout the polymer membrane, the co-polymer functions as an effective medium to transport Li⁺ ions (during discharge) and electrons (during charge). The multi-functionality of the co-polymer efficiently improves electrochemical performance and delivers a prolonged cycle life for the Li-O₂ batteries.

Chapter 7 Transform tetrathiafulvalene as an organic conductor for improving performances of Li-O₂ batteries

7.1 Introduction

Due to the ever increasing demand for high energy density, new battery systems have been systematically developed. Among all of them, lithium oxygen (Li-O₂) batteries have attracted extensive attentions.^[164, 215, 304, 337, 352] However, the insulating nature of the main discharge product Li₂O₂ generally requires extra energy for its decomposition, leading to large over-potentials and unwanted side-products. To overcome this drawback, solid-state catalysts have been widely studied, including precious metals, transition metals, and transition metal oxides.^[256, 308, 322, 353-358] However, the large particle size of Li₂O₂ often results in insufficient solid-solid contact when using these catalysts, leading to undesirable low catalytic efficiency.^[359] Redox mediators, on the other hand, can function as an electron shuttle while moving from the conductive cathode surface to Li₂O₂ at a certain voltage, owing to their solubility in the electrolyte.^[174] The resultant alternative pathways for electron transfer could efficiently enhance the capability to reversibly decompose Li₂O₂ during charging. So far, various redox mediators have been studied, such as tetrathiafulvalene (TTF), tetramethylpiperidinyloxy (TEMPO), iron phthalocyanine (FePc), heme, and lithium halides, among others.^[217-222, 323, 360-364] All of them show the capability to reduce over-potentials. Nevertheless, the usage of redox mediators could also cause additional issues. The free movement of redox mediators in the electrolyte enables the direct contact between the lithium anode and the oxidized state of the redox mediator, leading to unwanted side-reactions.^[52, 223, 365] Therefore, additional protection layers are required to resolve this issue and to enhance electrochemical performances.^[194, 224, 352]

Herein, we combine TTF and lithium chloride (LiCl) in the electrolyte for Li-O₂ batteries. The combination of LiCl and oxidized TTF⁺ results in the deposition of TTF⁺Cl_x⁻, an organic conductor, on the surface of the cathode.^[366-369] The resultant compound not only restricts TTF⁺ movement around the cathode, but also increases efficient electron transport pathways. Owing to its high electronic conductivity, the electrons can move through the direct contact between the conducting carbon and Li₂O₂, TTF⁺ electron shuttle, or the surface of Li₂O₂ covered by the TTF⁺Cl_x⁻ organic conductor. This unique structure significantly enhances the efficiency of the decomposition of Li₂O₂, leading to a prolonged cycle life.

7.2 Experimental details

7.2.1 Electrolyte preparation

Pure electrolyte was prepared by mixing 0.5 M bis(trifluoromethane)sulfonimide lithium salt (LiTFSI, Sigma-Aldrich) into diethylene glycol dimethyl ether (DEGDME, Sigma-Aldrich) solvent. TTF-containing electrodes were prepared by adding different concentration of tetrathiafulvalene (TTF, Sigma-Aldrich) and lithium chloride (LiCl, Sigma-Aldrich) in the pure electrolyte. The concentrations were 30 mM TTF, 30 mM TTF+15 mM LiCl, 30 mM TTF+30 mM LiCl, 30 mM TTF+45 mM LiCl. The high LiCl concentration electrolytes were prepared through the similar process with 0.1 M LiCl.

7.2.2 Carbon black electrode preparation

The cathodes were prepared by firstly mixing carbon black and poly(tetrafluoroethylene) (PTFE) together in isopropanol/water with the weight ratio of 90:10. The mixture was then coated on a glass fibre substrate and cut into discs with a diameter of 14 mm. The

electrodes were dried at 80 °C in a vacuum oven for 12 h. The loading of the cathode materials is about 1 mg cm⁻².

7.2.3 Porous graphene electrode preparation

Graphene oxide (GO) was synthesized using natural graphite flakes via the modified Hummers method. Then, an aqueous suspension of GO at a concentration of 2 mg mL⁻¹ was prepared by ultrasonication (~ 30 min). Porous graphene (PGE) was obtained by hydrothermal assembly of GO. Typically, graphene oxide (20 ml) was sealed in a Teflon-lined stainless steel autoclave and heated at 150 °C for 12 h. After cooling naturally, graphene hydrogel was obtained and dialyzed in water for 24 h. PGE was obtained by freeze-drying.

The PGE electrode was prepared through the same method as the carbon black electrode.

7.2.4 Characterizations

Field emission scanning electron microscopy (FESEM, Zeiss Supra 55 VP) was used to investigate the morphologies of the electrodes. Infrared spectroscopy of the electrodes was conducted on a Nicolet Magna 6700 FT-IR spectrometer. All spectra were obtained using 4 cm⁻¹ resolution and 64 scans at room temperature. X-ray diffraction (XRD) was conducted on a Siemens D5000 X-ray diffractometer. During the XRD analysis process, the cathodes were protected from exposure to the ambient atmosphere. Ultraviolet–visible (UV-vis) spectroscopy was conducted through an Agilent Cary 60 UV-Vis spectrophotometer, scanning from 800 nm to 200 nm. To prepare the samples for UV-vis, the separators

including electrolytes were first taken from the batteries and then soaked in the purified DEGDME solvent.

7.2.5 Electrochemical characterizations

All electrochemical characterizations of the electrolytes were conducted on a CH Instrument 660D electrochemical workstation and discharge/charge performances were evaluated by a Neware Battery Testing System. Linear sweep voltammetry measurements were used to measure the catalytic property of the materials towards Li_2O_2 decomposition. The scanning rate was 0.1 mV s^{-1} and the range was set from open circuit voltage to 4.4 V. The cyclic voltammetry measurements on two-electrode cells were carried out within the range from 2 V to 4.2 V, with a scanning rate of 0.5 mV s^{-1} . Two-electrode cells were prepared by assembling Swagelok cells with lithium metal as the counter and reference electrode.

The discharge-charge performance was evaluated by assembling Li-O₂ batteries. A Swagelok type cell with an air hole (0.785 cm^2) on the cathode side was used to test the electrochemical performance. The cell was assembled in an argon filled glove box with water and oxygen level less than 0.1 ppm. A lithium foil was used as anode. The electrolytes were added to the glass fibre separators during assembly. The amount of electrolyte used in the battery is 0.24 mL. The assembled cell was gas tight except for the cathode side window, which exposed the cathode film to the oxygen atmosphere. All measurements were conducted in 1 atm dry oxygen atmosphere to avoid any negative effects of humidity and CO₂.

7.3 Results and discussions

7.3.1 Electrochemical characterizations

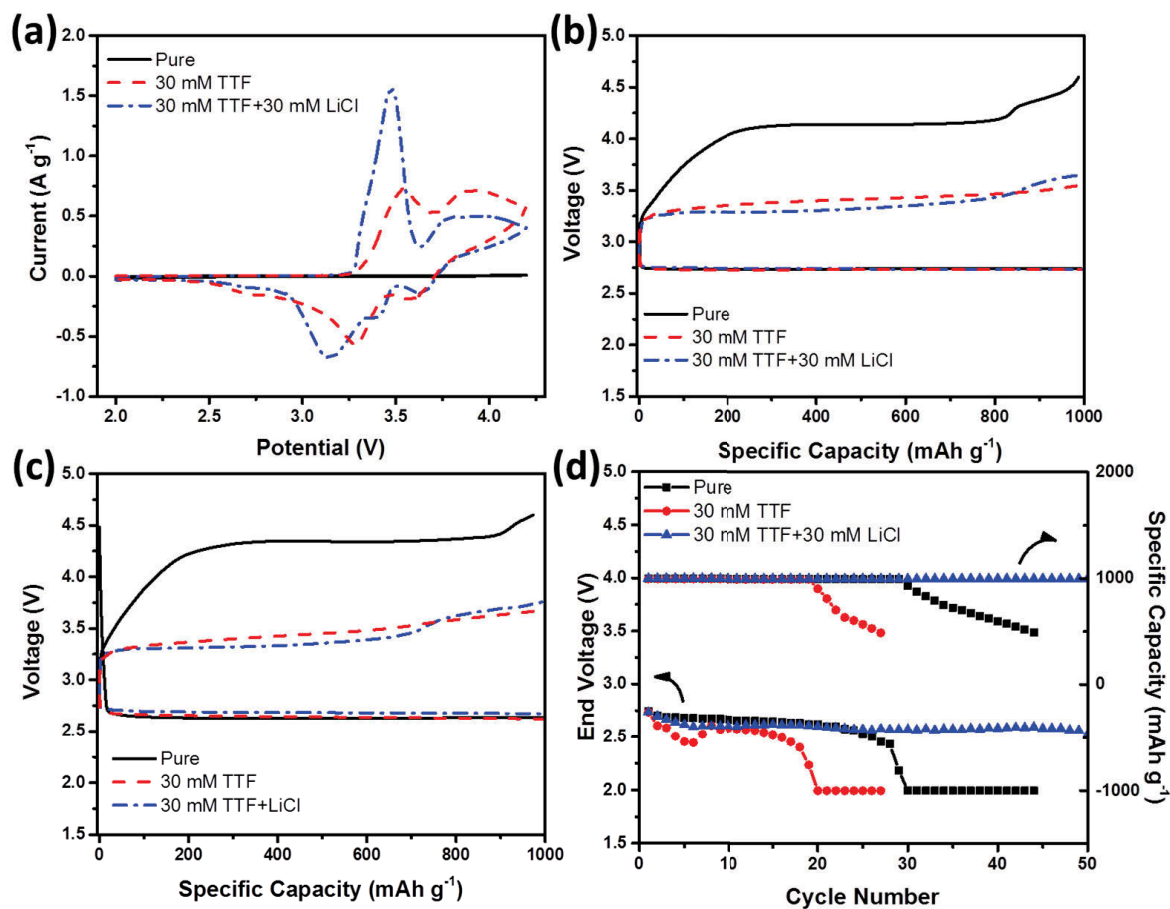


Figure 7-1 (a) CV curves of the cells with different electrolytes in argon atmosphere. The scan rate is 0.5 mV s^{-1} . The galvanostatic discharge and charge profiles with current densities of (b) 200 mA g^{-1} and (c) 500 mA g^{-1} , and (d) the cycling performances of Li-O₂ batteries in oxygen atmosphere. The current density is 200 mA g^{-1} , and the cut-off voltages are 2.0 V/4.6 V. The positive electrodes are prepared with carbon black.

The cyclic voltammetry (CV) curves of Li-O₂ cells with TTF electrolyte (30mM TTF, Figure 7-1) shows two distinguishable oxidation peaks at 3.5 V and 3.9 V, which

correspond to the redox couples of TTF^+/TTF and $\text{TTF}^{2+}/\text{TTF}^+$, respectively. The reduction peaks during the cathodic scan are also visible, indicating their high reversibility. These peaks are still present when LiCl is added. We found that the first anodic peak (3.5 V) associated with the TTF^+/TTF redox couple sharpens and its intensity increases accordingly. The peak shifts from 3.5 V to 3.4 V, suggesting that a lower reaction barrier has been achieved. Meanwhile, the second anodic peak fades, indicating that the reaction of TTF^+ to TTF^{2+} becomes difficult. This phenomenon implies that TTF^+ interacts with LiCl, which efficiently reduces the reaction barrier and stabilizes the as-formed $\text{TTF}^+\text{Cl}_x^-$. We attribute this to the precipitation of the organic conductor $\text{TTF}^+\text{Cl}_x^-$ on the surface of the electrode. It partially overcomes the issue that slow diffusion rates of solution-based TTF^+ generally lead to its accumulation in local areas, limiting further proceedings of the oxidation reaction of TTF. Because of the electronically conductive nature of the as-formed $\text{TTF}^+\text{Cl}_x^-$, the reaction rate would not be affected by continuous precipitation. The CV curves in oxygen atmosphere (Figure 7-2) show the capabilities of LiCl and TTF to facilitate the oxygen evolution reaction (OER).

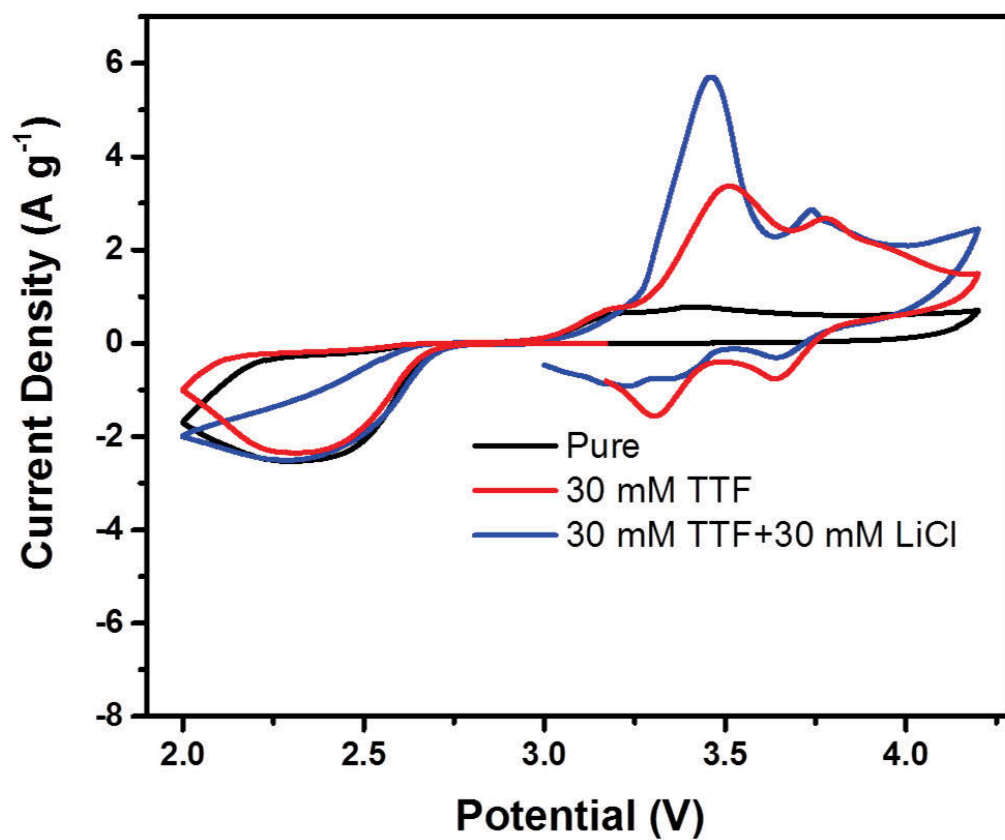


Figure 7-2 CV curves of the two-electrode (Li-O₂) cells with different electrolytes in oxygen atmosphere. The scan rate is 0.5 mV s⁻¹. The cell is constructed by assembling a swagelok-type cell using a lithium metal as the anode, and a carbon black electrode as the cathode.

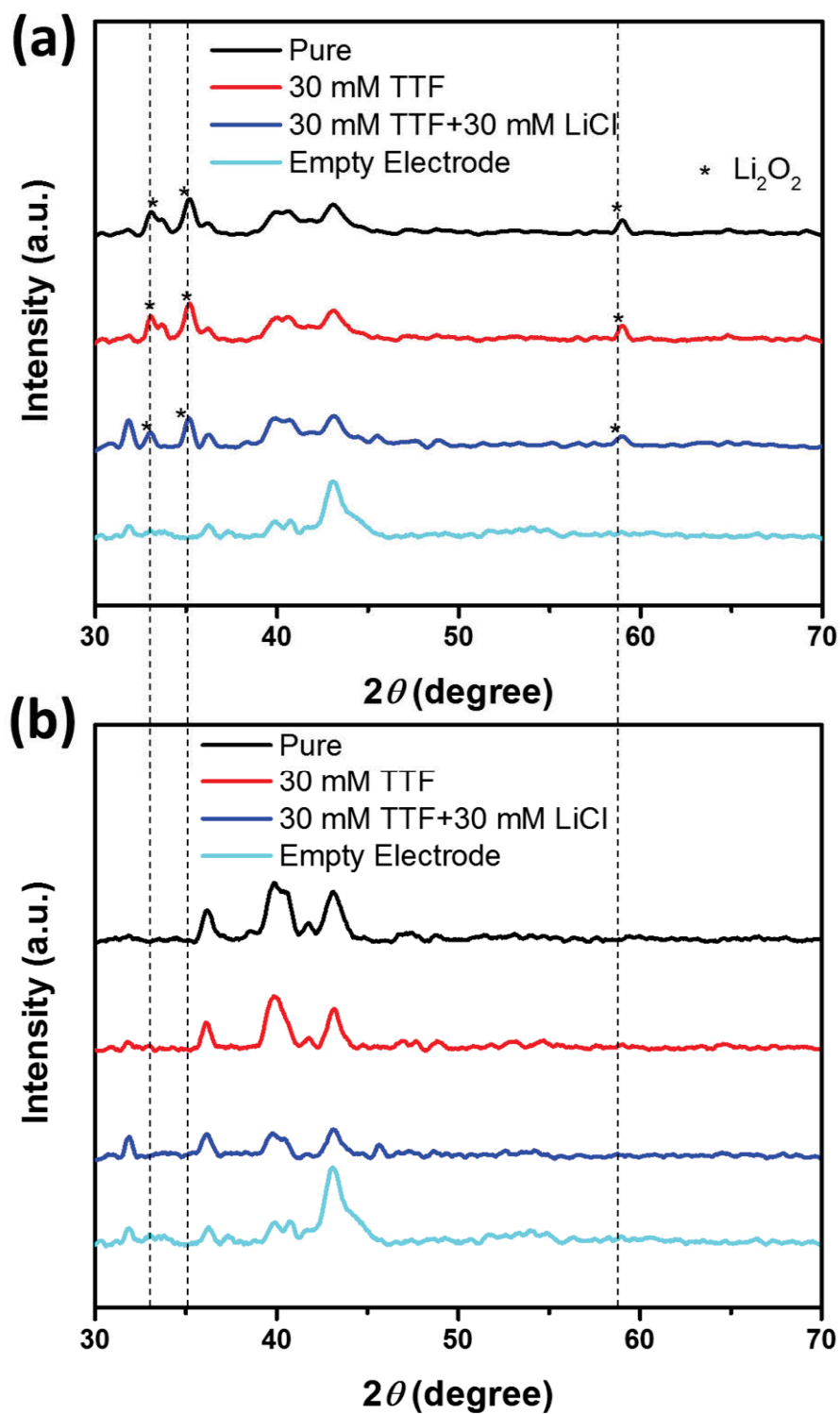


Figure 7-3 XRD patterns of the electrodes after (a) discharge and (b) charge

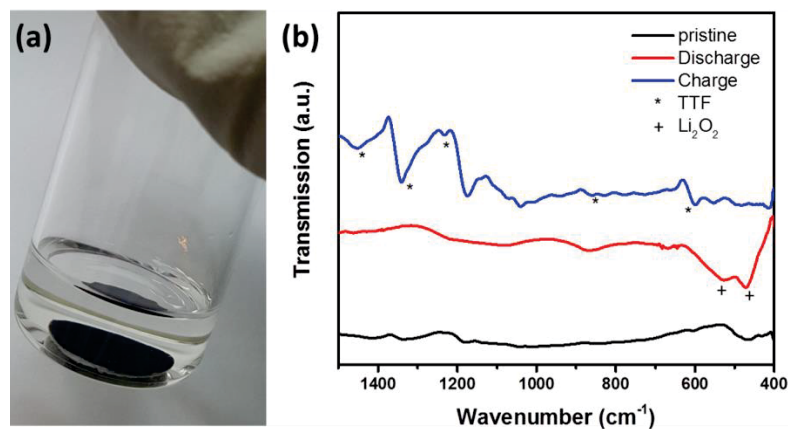


Figure 7-4 FTIR post-characterization of the electrode before and after first cycle. The electrolyte contains 30 mM TTF and 30 mM LiCl. (a) All the electrodes are carefully rinsed several times with electrolyte solvents DEGDME until there is no colour detected in the upper liquid. The electrodes are then dried in vacuum before test. (b) FTIR result of the electrodes.

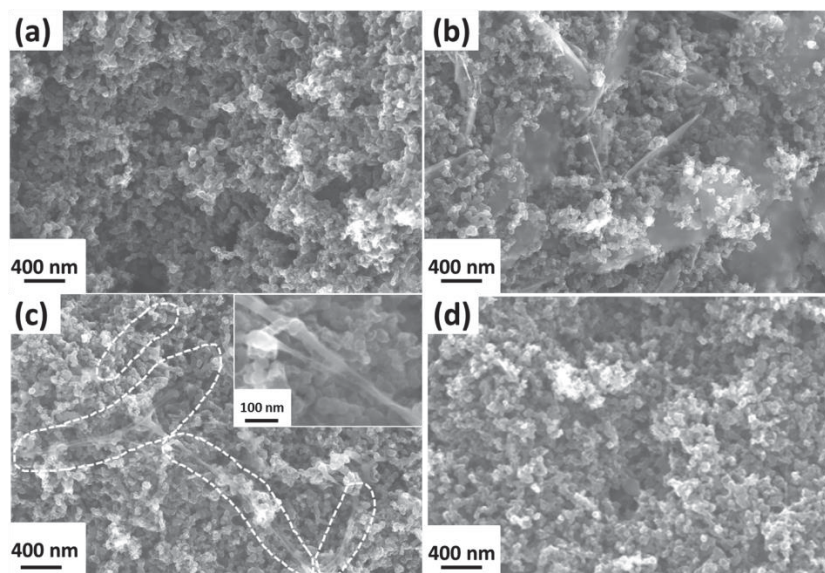


Figure 7-5 SEM images of carbon black electrodes (a) before cycling, (b) after discharge, (c) after charge, and (d) after second discharge to 3.0 V. The electrolyte is 30 mM TTF+30 mM LiCl. The highlighted thread-like structure is the deposited $\text{TTF}^+\text{Cl}_x^-$. The cycle depth is 1000 mAh g^{-1} based on the electrode mass.

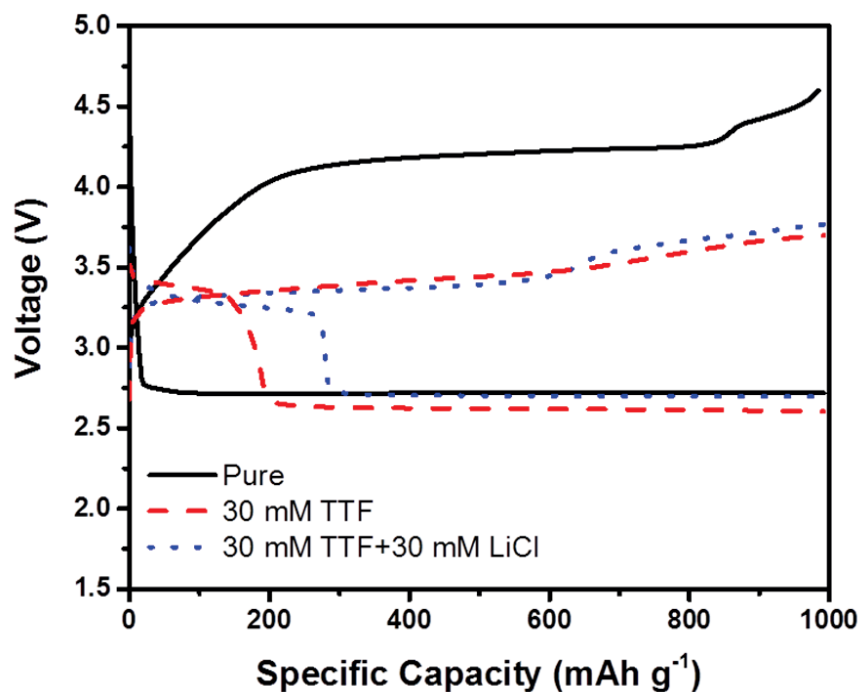


Figure 7-6 The second cycle discharge-charge profiles of the batteries with different electrolytes. The current density is 200 mA g^{-1} .

Figure 7-1b shows the discharge/charge curves of Li-O₂ batteries with different electrolytes. Regardless of the addition of TTF, almost identical discharge curves indicate that TTF has negligible impact on the discharge process. However, the charge curves differ significantly from each other when electrolytes with different additives are used. The cell with pure electrolyte shows the highest charge voltage of 4.25 V. The cell with TTF-containing electrolyte shows a much lower charge voltage of 3.4 V, revealing the exceptional catalytic capability of TTF. Furthermore, with the addition of LiCl, lower charge over-potential was achieved (3.25 V). The low over-potential is retained even at higher current density (Figure 7-1c). It should be noted that the decomposition of Li₂O₂ proceeds during the potential slope, which is confirmed by XRD, FTIR, and SEM results (Figure 7-3, 7-4, 7-5) of the electrodes. There are additional plateaus in the second

discharge curves with all TTF-containing electrolytes (Figure 7-6), and the capacity is almost unchanged when the reversible discharge-charge capacity increases to 2000 and 3000 mA h g⁻¹ (Figure 7-8). This could be attributed to the reduction of the TTF⁺ species. Intriguingly, the reduction capacity of TTF/TTF⁺ is lower than that of TTF/TTF⁺Cl_x⁻. This is due to the migration of TTF⁺ to the anode area, leading to an incomplete reduction.

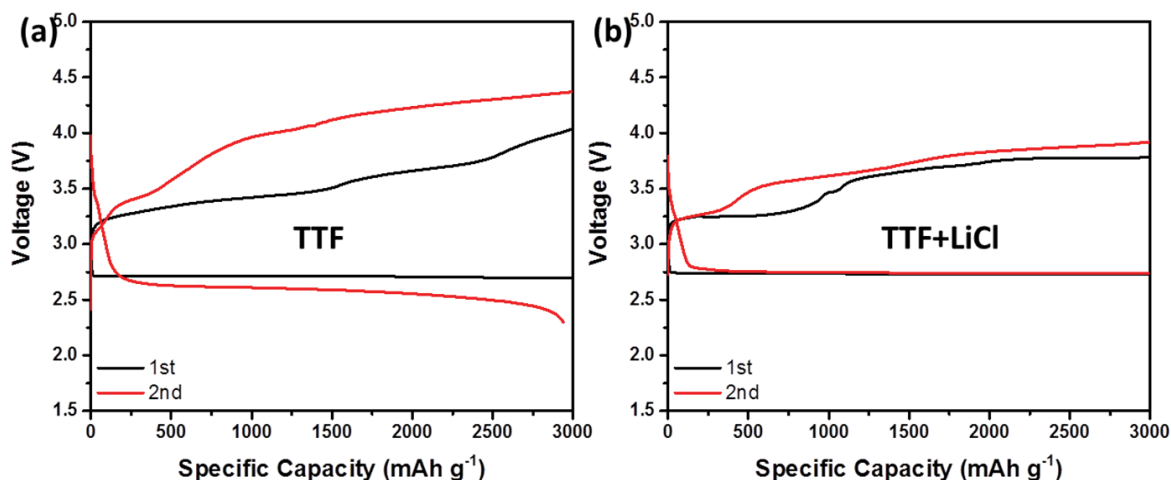


Figure 7-7 The discharge-charge profiles of the Li-O₂ batteries with different electrolyte cycling at larger fixed capacities of 3000 mAh g⁻¹. The electrolytes used are (a) 30 mM TTF and (b) 30 mM TTF+30 mM LiCl in DEGDME electrolyte. The current density is 200 mA g⁻¹. Compared to the large reversible capacities, the capacity of TTF redox is insignificant.

The cycling performances of Li-O₂ batteries are shown in Figure 1d. Evidently, the combination of TTF and LiCl in the electrolytes significantly enhances the cyclabilities. Figure 7-8 shows the digital photos of the separators taken from cells with different electrolytes after five cycles. The accumulation problem of TTF⁺ is severe when LiCl is absent in the electrolyte, which explains the limited cycling performance. However, solid

precipitation was observed on the separator of the TTF+LiCl electrolyte, which may be caused by the accumulation of $\text{TTF}^+\text{Cl}_x^-$ on the cathodes. It suggests that the cycle life of Li-O₂ batteries could be further enhanced by restricting the as-formed $\text{TTF}^+\text{Cl}_x^-$ inside of the electrode. Therefore, LiCl is desirable for improving the overall Li-O₂ battery performances when TTF is added.

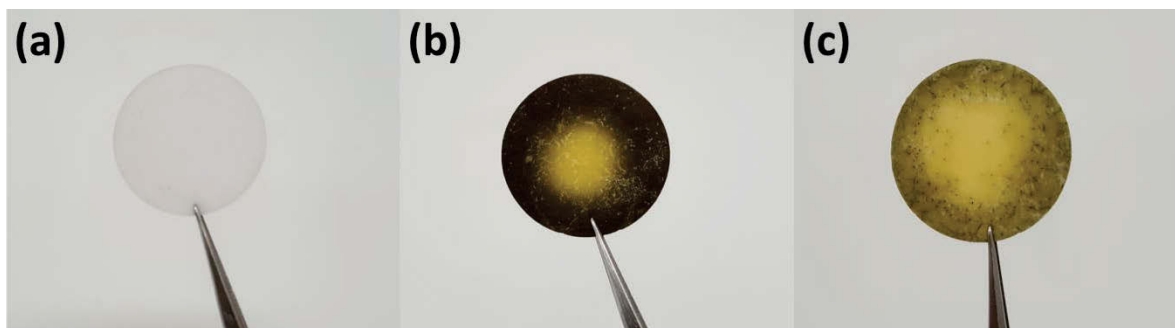


Figure 7-8 Digital photos of the separators after 5 cycles in the Li-O₂ batteries (discharge state). The electrolytes are (a) pure electrolyte, (b) 30 mM TTF, (c) 30 mM TTF+30 mM LiCl.

A possible mechanism for this phenomenon could be associated with the coordination of TTF and LiCl to form a $\text{TTF}^+\text{Cl}_x^-$ conductive precipitate instead of mobile TTF^+ in the electrolyte. The FTIR spectra (Figure 7-9) of the post-charged electrodes indicate that $\text{TTF}^+\text{Cl}_x^-$ has been evidently deposited on the electrodes when LiCl is added. This result is consistent with the EDX result shown in Figure 7-10.

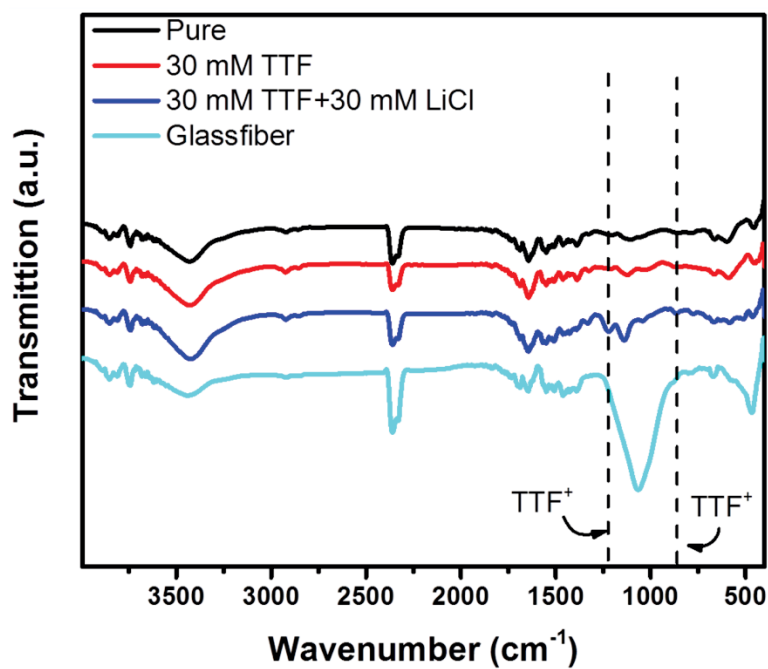


Figure 7-9 FTIR spectra of the electrodes after the first charge. The peaks referring to the formation of TTF are visible on the charged TTF+LiCl electrode indicating the deposit of TTF-species.

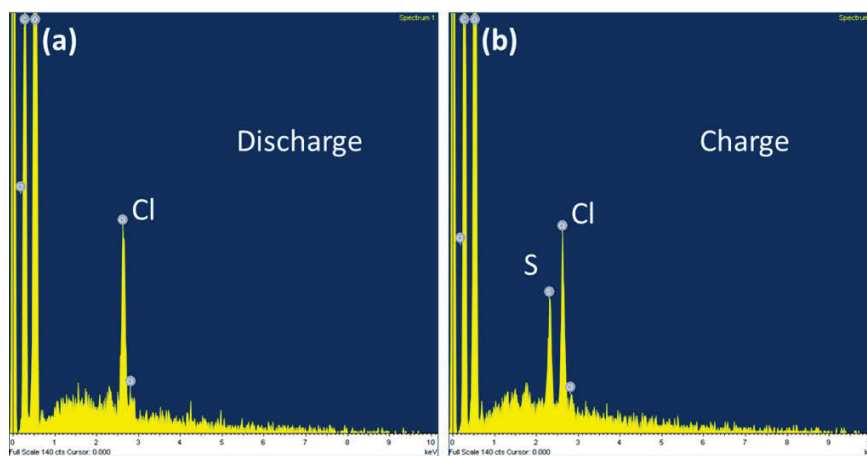


Figure 7-10 EDX results of the electrode after first cycle (a) discharge and (b) charge. The electrolyte is 30 mM TTF+30 mM LiCl+ 0.5 M LiTFSI in DEGDME

The UV spectra of the electrolytes after discharge and charge (Figure 7-11) also reveal that, for the electrolyte with the addition of LiCl, the intensity of the free TTF⁺ peak (450 nm) decreases.^[370] This means that the formation of the TTF⁺Cl_x precipitate decreased the concentration of TTF⁺ in the electrolyte. Direct evidence is found by assembling a two-electrode device where a linear sweep voltammetry (LSV) technique is used to control the external voltage. As shown in Figure 7-11c, the electrolyte near the cathode darkens when the voltage reaches 3.5 V, indicating the oxidation of TTF into free TTF⁺. With the further increase of the external potential, the darkened electrolyte accumulates and slowly diffuses into the lithium anode area, which may result in TTF⁺ reacting with the lithium anode. In contrast, the darkened electrolyte does not appear in the electrolyte with TTF and LiCl. Instead, a thread-like precipitate grows on the surface of the electrode. Since the amount of electrolyte far exceeds the common usage in a Li-O₂ cell, the large amount of precipitates is convenient for visual observations. With the continuous increase of the external voltage, the amount of precipitate gradually increases and no visible darkened electrolyte is detected. This process is important because it will prevent the diffusion of TTF⁺ to the anode area, leading to minimum side-reactions.

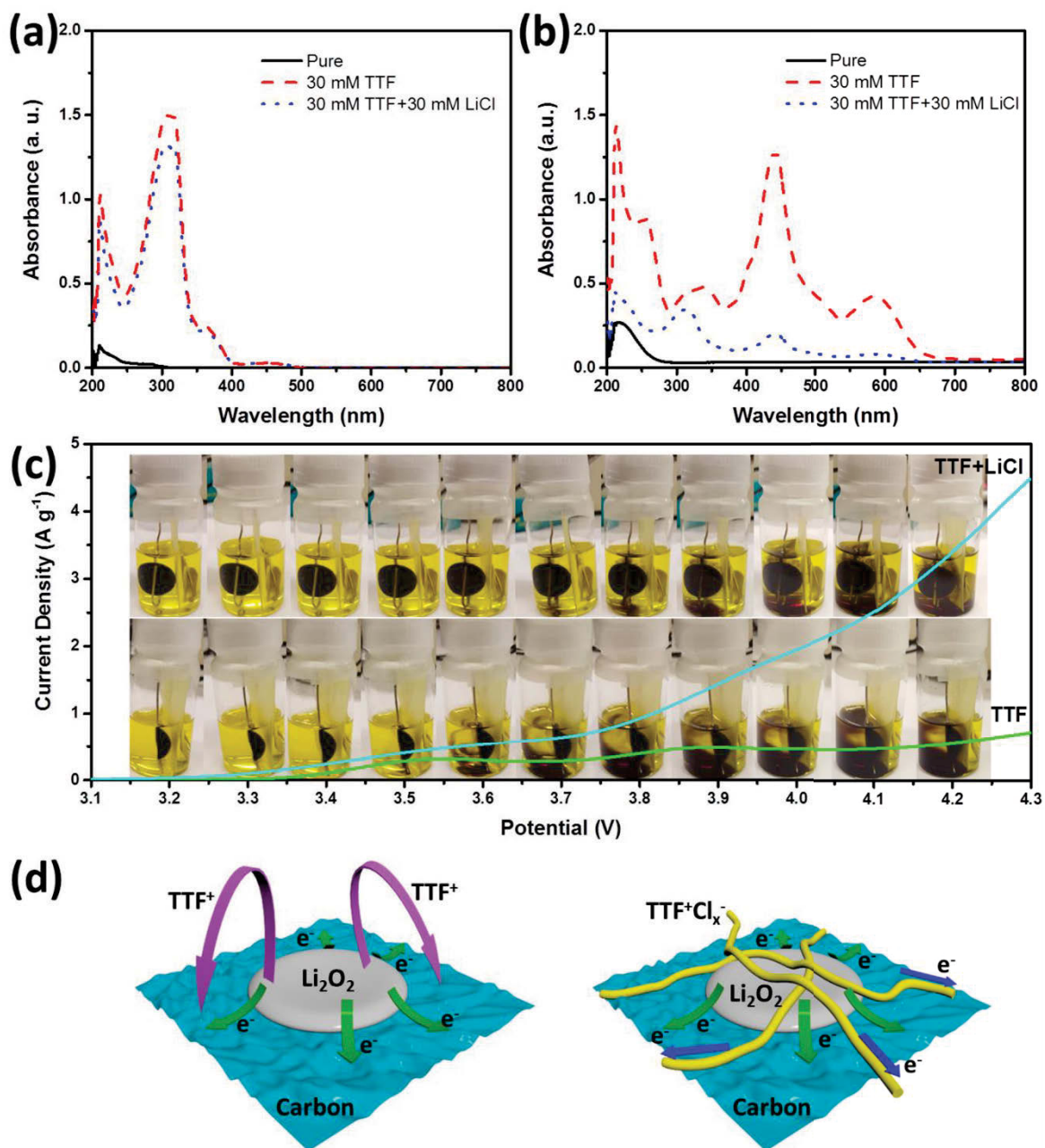


Figure 7-11 UV spectra of the electrolytes after the first (a) discharge and (b) charge. (c) The digital photos of a two-electrode device with TTF electrolyte and TTF+LiCl electrolyte. The scan rate is 1 mV s^{-1} . (d) Schematic illustration of the mechanism of $\text{TTF}^+\text{Cl}_x^-$ facilitating the decomposition of Li_2O_2 .

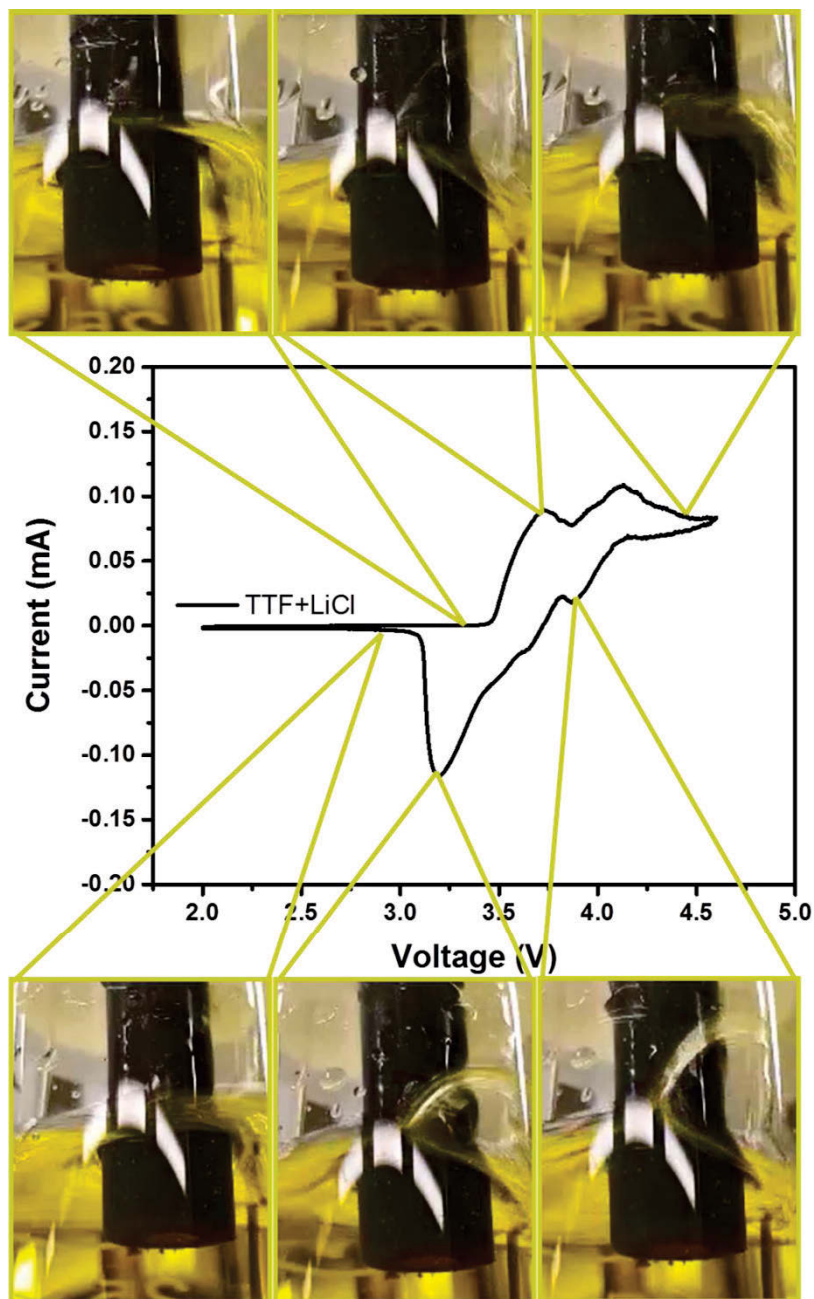


Figure 7-12 Visual experiment of $\text{TTF}^+\text{Cl}_x^-$ when a GC electrode is used. The scanning rate is 50 mV s^{-1} .

Additionally, the formation and decomposition of $\text{TTF}^+\text{Cl}_x^-$ is reversible, based on the supporting video (SV) and Figure 7-12 of this electrolyte system using glassy carbon (GC) as the working electrode. This observation clearly confirms that precipitates form during

the anodic scan and decompose during the cathodic scan. The SEM images of the electrode shown in Figure 7-13 also clearly demonstrate the existence of the thread-like $\text{TTF}^+\text{Cl}_x^-$ after charge.

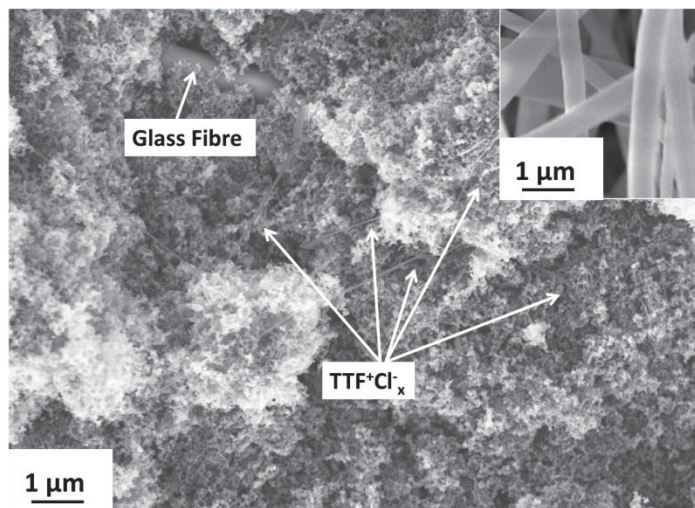


Figure 7-13 The SEM image of the electrode after charge. The thread-like structure is the as-deposit $\text{TTF}^+\text{Cl}_x^-$, which is different from the morphology of glass fibre (shown in the inset image).

The benefit of forming a $\text{TTF}^+\text{Cl}_x^-$ precipitate is that the as-formed compound is electronically conductive. Upon deposition on the electrode (covered by the discharge products) in the initial state of charge, the conductive $\text{TTF}^+\text{Cl}_x^-$ provides an additional path for electron transfer to the surface of Li_2O_2 , which efficiently electronically connects Li_2O_2 from both top ($\text{TTF}^+\text{Cl}_x^-$) and bottom (conductive carbon). This process overcomes the restricted electron transfer issue caused by the insulating nature of Li_2O_2 .^[371] Unlike sole TTF which functions as the electron shuttle in the electrolyte, the electronically conductive precipitates provide a faster solid-solid pathway for electron transfer. Furthermore, TTF^+ is restricted to the cathode, leading to a minimum contact with the lithium anode, and thus,

limited side-reactions. Further characterizations of the lithium anodes are conducted by disassembling the cells after five cycles. As shown in Figure 7-14, the lithium anode in TTF electrolyte is severely corrupted, originating from the direct contact reactions between mobile TTF^+ and the lithium anode. Contrarily, the lithium anode in TTF+LiCl electrolyte barely changes, indicating the restriction of mobile TTF^+ on the cathode can enhance the stability of the lithium anode.

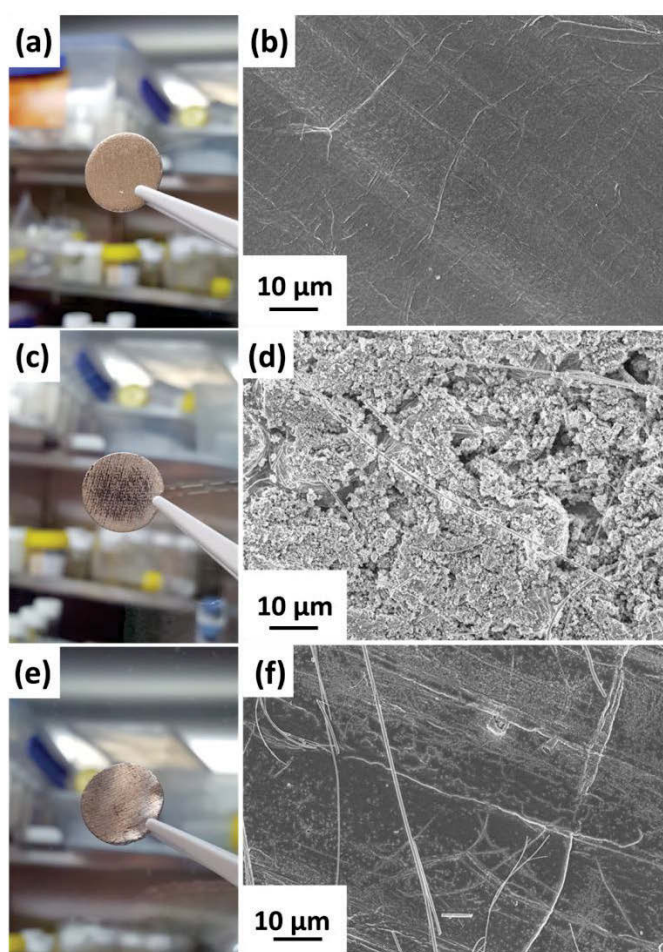


Figure 7-14 (c, e) Digital photos and (d, f) SEM images of the lithium anode after five cycles. (a, b) are the pristine lithium anode. (c, d) are the lithium anode in 30 mM TTF electrolyte, and (e, f) are the lithium anode in 30 mM TTF+30 mM LiCl electrolyte. The fibre-like structures in (b, d) originate from the glass fibre separators.

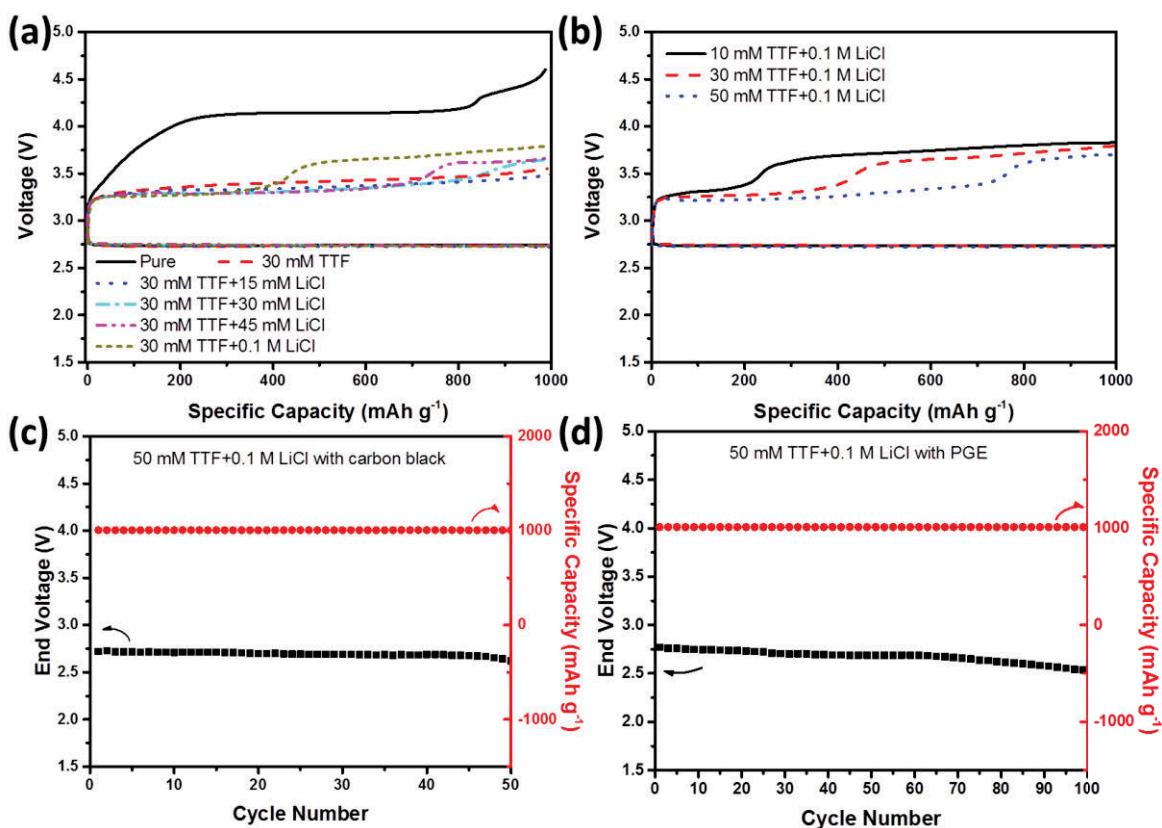


Figure 7-15 The discharge and charge profiles of Li-O₂ batteries containing electrolytes with different concentrations of (a) TTF and (b) LiCl in oxygen atmosphere. The cycling performance of a Li-O₂ battery with 50 mM TTF and 0.1 M LiCl in oxygen atmosphere with (c) a carbon black electrode and (d) a porous graphene electrode. The current densities are 200 mA g⁻¹. The cut-off voltages are 2.3 V/4.6 V.

Further investigations displayed in Figure 7-15 show that higher concentrations of both TTF and LiCl are desirable for optimal electrochemical performance. Additional experiments have been conducted to prove that the existence of LiCl in the electrolyte does not induce the release of Cl₂ (Figure 7-16, 7-17).^[372] Therefore the use of high concentration LiCl in the electrolyte is acceptable. The Li-O₂ battery with 50 mM TTF and

0.1 M LiCl (Figure 7-15c-d) demonstrates the exceptional capability to enhance cycling performances.

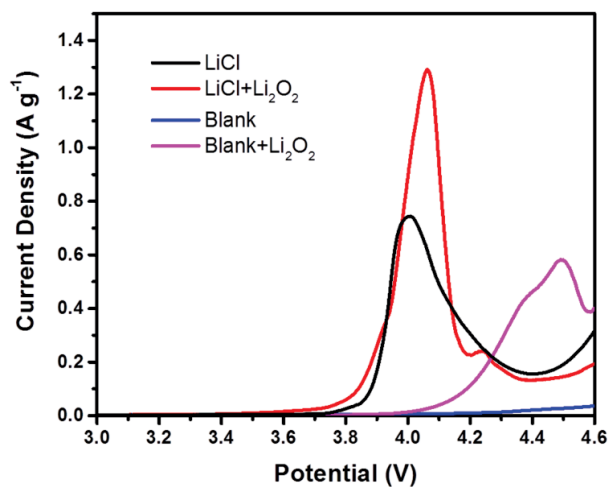


Figure 7-16 LSV result of the cells with different electrolytes and electrodes. The electrolytes are 30 mM LiCl in DEGDME (referring as LiCl) and pure DEGDME (referring as Blank), and the electrodes used are carbon black electrode and carbon black+Li₂O₂ electrode.

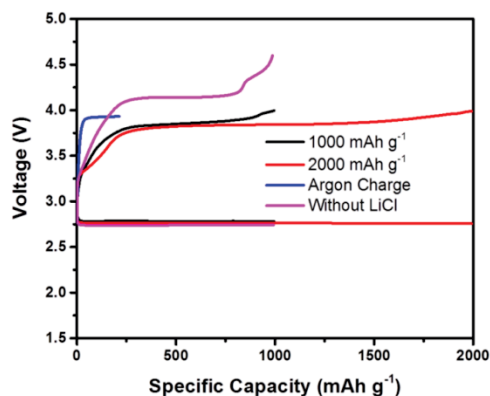


Figure 7-17 The discharge-charge profiles of the Li-O₂ batteries with 30 mM LiCl in DEGDME electrolyte at different fixed capacities in oxygen atmosphere. One cell is directly charged in argon atmosphere and another cell is used without the addition of LiCl, as comparisons. The current densities are 200 mA g⁻¹

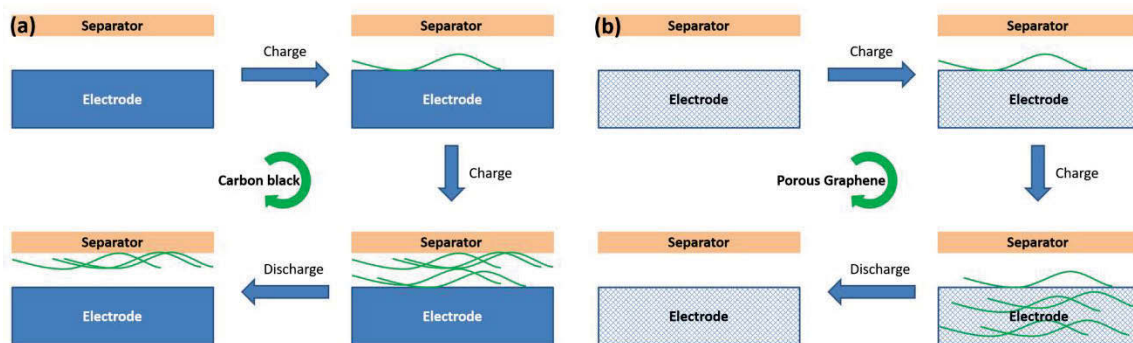


Figure 7-18 Schematic illustration of the material loss during discharge and charge processes with (a) carbon black electrode and (b) porous graphene electrode.

However, the charge over-potential gradually increases upon cycling, probably caused by the accumulative loss of TTF on the separator (Figure 7-18). Porous graphene (PGE) is further used to replace carbon black in the electrode to better accommodate the loose structure of the $\text{TTF}^+\text{Cl}_x^-$ conductor. The large pores and relatively high porosity of PGE (Figure 7-19) lead to minimum material loss, therefore no visible change of the charge curves upon cycling is found in Figure 7-15d and 7-20. The deposition of $\text{TTF}^+\text{Cl}_x^-$ in the large pores, rather than on the surface of the electrode, ensures negligible amounts of $\text{TTF}^+\text{Cl}_x^-$ are being irreversibly deposited on the separator, and the efficiencies of the overall reactions have been significantly enhanced.

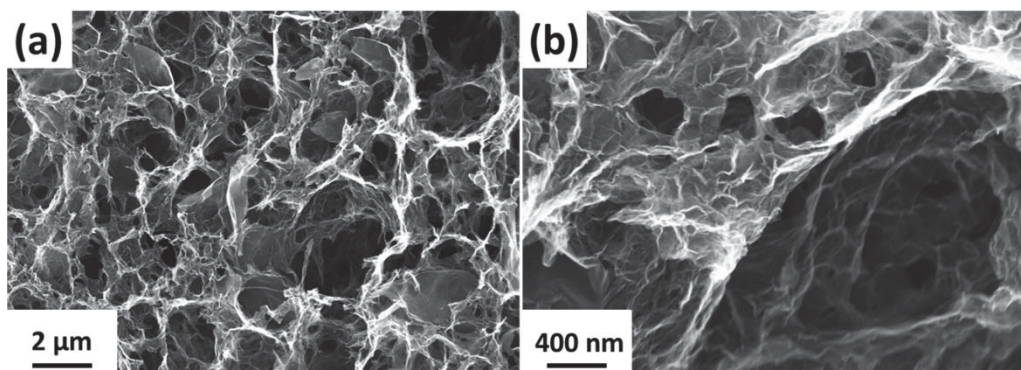


Figure 7-19 SEM images of PGE.

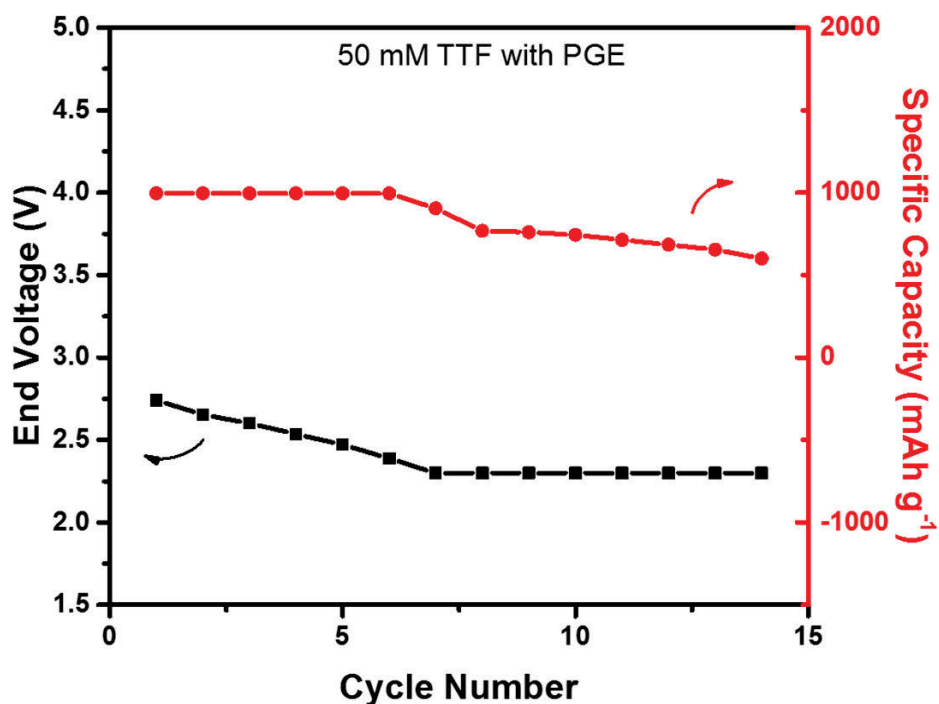


Figure 7-20 The cycling performance of the battery with 50 mM TTF electrolyte using a PGE electrode. The current density is 200 mA g⁻¹.

7.4 Summary

In summary, we have discovered that the combination of TTF and LiCl in the electrolyte can offer an alternative fast and efficient route for facilitating electrochemical reactions in Li-O₂ batteries. Instead of forming mobile solution-based TTF⁺ in the electrolyte as a redox mediator, a conductive TTF⁺Cl_x⁻ compound precipitates on the surface of the discharge product, which limits the side-reactions between TTF⁺ and the lithium anode. By further replacing carbon black with a PGE electrode, the cycle life of Li-O₂ batteries can be significantly enhanced.

Chapter 8 Conclusions

8.1 General conclusions

Organic materials are a group of unique materials which in theory have numerous potentials to fit almost all applications by tailoring the functional groups. The organic materials are significantly underrated in lithium batteries due to the fact that recent research on Li-ion and Li-O₂ batteries are mostly about inorganic materials. In this PhD project, we investigated some of the organic components in Li-ion and Li-O₂ batteries. Based on the breath-figure method, porous gel polymer membranes were prepared and enabled enhanced electrochemical performances in Li-ion batteries. The results are shown in Chapter 3 and 4. In Chapter 5 and 6, TEMPO-based organic polymers were synthesized and used as catalyst and binder, respectively, in Li-O₂ batteries. We also investigated the mechanism change of TTF with the addition of LiCl, which is discussed in Chapter 7.

Porous polymer membranes with highly ordered honeycomb-like structures based on PVDF-HFP were prepared using the breath-figure method. The as-prepared porous membrane showed a porosity as high as 78%, which led to a high percentage electrolyte uptake of 86.2 wt%. The ionic conductivity reached 1.03 mS cm⁻¹ at room temperature which is higher than that of a Celgard 2400 separator. Meanwhile, the membrane showed exceptional thermal and electrochemical stability. As a result, the discharge capacity was improved to 145 mAh g⁻¹ when LiFePO₄ was used as cathode material at 0.2 C.

PMMA-coated PVDF-HFP porous polymer membrane with a sandwich-like structure on the basis of honeycombs PVDF-HFP membranes. The better affinity of PMMA towards the liquid electrolyte and large porosity of the membrane result in extremely high liquid

electrolyte uptake of 342 wt%, leading to a high ionic conductivity of 1.31 mS cm^{-1} . These enhanced properties ensured an improved electrochemical performance of Li-ion battery with this membrane.

PTMA was synthesized using a two-step polymerization method. The as-synthesized PTMA showed unique n-doping and p-doping properties at 3.0 and 3.5 V vs. Li^+/Li , respectively. The redox reactions of PTMA would further improve the discharge and charge process, leading to low over-potentials both during discharge and charge processes. The as-assembled Li-O₂ batteries showed significantly improved discharge capacities, and prolonged cycle life. The post-characterization of the batteries indicated that the functional mechanism of PTMA relied closely on the reduction and oxidation of N-O radicals.

A co-polymer based on the co-polymerization of MMA and TMA monomers was synthesized and used in Li-O₂ batteries as binder. The combination of gellable MMA and catalytic TMA moieties made it possible to enhance the electrochemical performances of Li-O₂ batteries. Furthermore, by investigating the functional mechanism, it was discovered that the capability to form a gel polymer electrolyte enabled the catalytic moieties to move as a restricted redox mediator, which was better than a stationary catalyst in Li-O₂ batteries.

Lastly, the functional mechanism of TTF in Li-O₂ batteries was altered by adding LiCl in the electrolyte. The addition of LiCl enabled TTF to precipitate as an organic conductor on the surface of Li₂O₂ during the charge process instead of simply functioning as a solution-based redox mediator. As a result, the efficiency of TTF was significantly improved, and the side-reactions due to the migrating of oxidized TTF to lithium anode were eliminated. The coverage of organic conductor on Li₂O₂ created additional pathways

for electron flow, resulting in enhanced electrochemical performances. With the combination of a porous graphene electrode, the cycle life of the battery was prolonged.

8.2 Outlook

We have demonstrated that by using suitable organic materials with functional groups, the electrochemical performances can be significantly enhanced. It has been demonstrated that the porous structures of organic polymer membranes can be tailored to further enhance the electrochemical performances, by increasing the electrolyte uptake. Therefore, by carefully changing the morphologies, the porous membranes can be further enhanced and used in different areas in future works.

The N-O radical group has been demonstrated to be suitable as catalyst for Li-O₂ batteries. The unique redox reactions can significantly influence the electrochemical performances. In theory, by grafting N-O radical groups on different substrates, the as-obtained materials should process numerous potentials to be used in different applications. Therefore, functional organic materials based on N-O radical groups can be further investigated.

Meanwhile, organic redox mediators are still a heated topic in the scientific community. The migration of redox mediators in the electrolyte could potentially induce side-reactions, despite its capability of decomposing Li₂O₂ efficiently. Finding solutions to overcome this issue becomes the main research direction in this aspect. Our research indicated that the mechanism of functional redox mediators can be tailored by applying additives. Therefore, it can be used as further research topic in the future work.

In summary, the materials used in this PhD project have been demonstrated to be beneficial for lithium batteries. However, to be fully suitable for high-performance batteries, future work is still needed on developing novel organic materials.

References

- [1] Kotz, S.L., Electrode architectures for enhanced lithium ion battery performance, Northeastern University, 2016.
- [2] Scrosati, B., Hassoun, J., Sun, Y.-K., Lithium-ion batteries. A look into the future, *Energy & Environmental Science*, **2011**, *4*, 3287-3295.
- [3] Song, M.-K., Park, S., Alamgir, F.M., Cho, J., Liu, M., Nanostructured electrodes for lithium-ion and lithium-air batteries: the latest developments, challenges, and perspectives, *Materials Science and Engineering: R: Reports*, **2011**, *72*, 203-252.
- [4] Wagner, F.T., Lakshmanan, B., Mathias, M.F., Electrochemistry and the future of the automobile, *J. Phys. Chem. Lett*, **2010**, *1*, 2204-2219.
- [5] Armand, M., Tarascon, J.-M., Building better batteries, *Nature*, **2008**, *451*, 652-657.
- [6] Girishkumar, G., McCloskey, B., Luntz, A., Swanson, S., Wilcke, W., Lithium– air battery: promise and challenges, *The Journal of Physical Chemistry Letters*, **2010**, *1*, 2193-2203.
- [7] Gamble, F., Osiecki, J., Cais, M., Pisharody, R., DiSalvo, F., Geballe, T., Intercalation complexes of Lewis bases and layered sulfides: a large class of new superconductors, *Science*, **1971**, *174*, 493-497.
- [8] Whittingham, M.S., The hydrated intercalation complexes of the layered disulfides, *Materials Research Bulletin*, **1974**, *9*, 1681-1689.
- [9] Whittingham, M.S., Electrointercalation in transition-metal disulphides, *Journal of the Chemical Society, Chemical Communications*, **1974**, 328-329.
- [10] Whittingham, M.S., Electrical energy storage and intercalation chemistry, *Science*, **1976**, *192*, 1126-1127.

- [11] Thompson, A., Electron-Electron Scattering in TiS_2 , *Physical Review Letters*, **1975**, 35, 1786.
- [12] Whittingham, M.S., The role of ternary phases in cathode reactions, *Journal of The Electrochemical Society*, **1976**, 123, 315-320.
- [13] Whittingham, M.S., Lithium batteries and cathode materials, *Chemical reviews*, **2004**, 104, 4271-4302.
- [14] Walk, C.R., Gore, J.S., $\text{Li-V}_2\text{O}_5$ secondary cell, *J. Electrochem. Soc.*, **1975**, 122, C68-C68.
- [15] Delmas, C., Cognac-Auradou, H., Cocciantelli, J., Menetrier, M., Doumerc, J., The $\text{Li}_x\text{V}_2\text{O}_5$ system: An overview of the structure modifications induced by the lithium intercalation, *Solid State Ionics*, **1994**, 69, 257-264.
- [16] Dickens, P., French, S., Hight, A., Pye, M., Phase relationships in the ambient temperature $\text{Li}_x\text{V}_2\text{O}_5$ system ($0.1 < x < 1.0$), *Materials Research Bulletin*, **1979**, 14, 1295-1299.
- [17] Mizushima, K., Jones, P., Wiseman, P., Goodenough, J.B., Li_xCoO_2 ($0 < x < 1$): A new cathode material for batteries of high energy density, *Materials Research Bulletin*, **1980**, 15, 783-789.
- [18] Amatucci, G., Tarascon, J., Klein, L., CoO_2 , the end member of the Li_xCoO_2 solid solution, *Journal of The Electrochemical Society*, **1996**, 143, 1114-1123.
- [19] Yazami, R., Touzain, P., A reversible graphite-lithium negative electrode for electrochemical generators, *Journal of Power Sources*, **1983**, 9, 365-371.
- [20] Ozawa, K., Lithium-ion rechargeable batteries with LiCoO_2 and carbon electrodes: the LiCoO_2/C system, *Solid State Ionics*, **1994**, 69, 212-221.

- [21] Bruce, P.G., Energy storage beyond the horizon: Rechargeable lithium batteries, *Solid State Ionics*, **2008**, *179*, 752-760.
- [22] Nozu, R., Nakamura, M., Banno, K., Maruo, T., Sato, T., Studying a phenomenon during overcharge of a lithium-ion battery with methacrylate additives for the gel electrolyte, *Journal of The Electrochemical Society*, **2006**, *153*, A1031-A1037.
- [23] Winter, M., Brodd, R.J., in, ACS Publications, 2004.
- [24] Wadia, C., Albertus, P., Srinivasan, V., Resource constraints on the battery energy storage potential for grid and transportation applications, *Journal of Power Sources*, **2011**, *196*, 1593-1598.
- [25] Hayashi, K., Nemoto, Y., Tobishima, S.-i., Yamaki, J.-i., Mixed solvent electrolyte for high voltage lithium metal secondary cells, *Electrochimica Acta*, **1999**, *44*, 2337-2344.
- [26] Koch, V., Dominey, L., Nanjundiah, C., Ondrechen, M., The intrinsic anodic stability of several anions comprising solvent-free ionic liquids, *Journal of the Electrochemical Society*, **1996**, *143*, 798-803.
- [27] Garcia, B., Lavallée, S., Perron, G., Michot, C., Armand, M., Room temperature molten salts as lithium battery electrolyte, *Electrochimica Acta*, **2004**, *49*, 4583-4588.
- [28] Li, Y., Xu, B., Xu, H., Duan, H., Lü, X., Xin, S., Zhou, W., Xue, L., Fu, G., Manthiram, A., Hybrid Polymer/Garnet Electrolyte with a Small Interfacial Resistance for Lithium-Ion Batteries, *Angewandte Chemie*, **2017**, *129*, 771-774.

- [29] Markevich, E., Baranchugov, V., Aurbach, D., On the possibility of using ionic liquids as electrolyte solutions for rechargeable 5V Li ion batteries, *Electrochemistry communications*, **2006**, *8*, 1331-1334.
- [30] Wang, Y., Zaghbi, K., Guerfi, A., Bazito, F.F., Torresi, R.M., Dahn, J., Accelerating rate calorimetry studies of the reactions between ionic liquids and charged lithium ion battery electrode materials, *Electrochimica acta*, **2007**, *52*, 6346-6352.
- [31] Nykaza, J.R., Savage, A.M., Pan, Q., Wang, S., Beyer, F.L., Tang, M.H., Li, C.Y., Elabd, Y.A., Polymerized ionic liquid diblock copolymer as solid-state electrolyte and separator in lithium-ion battery, *Polymer*, **2016**, *101*, 311-318.
- [32] Stassen, I., Hambitzer, G., Metallic lithium batteries for high power applications, *Journal of power sources*, **2002**, *105*, 145-150.
- [33] Zinck, L., Borck, M., Ripp, C., Hambitzer, G., Purification process for an inorganic rechargeable lithium battery and new safety concepts, *Journal of applied electrochemistry*, **2006**, *36*, 1291-1295.
- [34] Nishimoto, A., Watanabe, M., Ikeda, Y., Kohjiya, S., High ionic conductivity of new polymer electrolytes based on high molecular weight polyether comb polymers, *Electrochimica acta*, **1998**, *43*, 1177-1184.
- [35] Pradel, A., Ribes, M., Lithium chalcogenide conductive glasses, *Materials chemistry and physics*, **1989**, *23*, 121-142.
- [36] Adachi, G.y., Imanaka, N., Aono, H., Fast Li⁺ conducting ceramic electrolytes, *Advanced Materials*, **1996**, *8*, 127-135.

- [37] Minami, T., Hayashi, A., Tatsumisago, M., Recent progress of glass and glass-ceramics as solid electrolytes for lithium secondary batteries, *Solid State Ionics*, **2006**, *177*, 2715-2720.
- [38] Kim, Y., Saienga, J., Martin, S.W., Anomalous ionic conductivity increase in $\text{Li}_2\text{S}+\text{GeS}_2+\text{GeO}_2$ glasses, *The Journal of Physical Chemistry B*, **2006**, *110*, 16318-16325.
- [39] Inda, Y., Katoh, T., Baba, M., Development of all-solid lithium-ion battery using Li-ion conducting glass-ceramics, *Journal of Power Sources*, **2007**, *174*, 741-744.
- [40] Shin, J.-H., Henderson, W.A., Passerini, S., Ionic liquids to the rescue? Overcoming the ionic conductivity limitations of polymer electrolytes, *Electrochemistry Communications*, **2003**, *5*, 1016-1020.
- [41] Ye, H., Huang, J., Xu, J.J., Khalfan, A., Greenbaum, S.G., Li ion conducting polymer gel electrolytes based on ionic liquid/PVDF-HFP blends, *Journal of the Electrochemical Society*, **2007**, *154*, A1048-A1057.
- [42] Fuller, J., Breda, A., Carlin, R., Ionic liquid-polymer gel electrolytes, *Journal of the Electrochemical Society*, **1997**, *144*, L67-L70.
- [43] Croce, F., Curini, R., Martinelli, A., Persi, L., Ronci, F., Scrosati, B., Caminiti, R., Physical and chemical properties of nanocomposite polymer electrolytes, *The Journal of Physical Chemistry B*, **1999**, *103*, 10632-10638.
- [44] Sirisopanaporn, C., Fericola, A., Scrosati, B., New, ionic liquid-based membranes for lithium battery application, *Journal of Power Sources*, **2009**, *186*, 490-495.
- [45] Hayashi, A., Kitade, T., Ikeda, Y., Kohjiya, S., Matsuda, A., Tatsumisago, M., Minami, T., Preparation and Characterization of Lithium Ion Conducting Glass-Polymer Composites, *Chemistry Letters*, **2001**, *30*, 814-815.

- [46] Cho, J., Liu, M., Preparation and electrochemical properties of glass-polymer composite electrolytes for lithium batteries, *Electrochimica acta*, **1997**, *42*, 1481-1488.
- [47] Feuillade, G., Perche, P., Ion-conductive macromolecular gels and membranes for solid lithium cells, *Journal of Applied Electrochemistry*, **1975**, *5*, 63-69.
- [48] Goodenough, J.B., Kim, Y., Challenges for rechargeable Li batteries, *Chemistry of materials*, **2009**, *22*, 587-603.
- [49] Xu, K., Nonaqueous liquid electrolytes for lithium-based rechargeable batteries, *Chemical reviews*, **2004**, *104*, 4303-4418.
- [50] Arora, P., Zhang, Z., Battery separators, *Chemical reviews*, **2004**, *104*, 4419-4462.
- [51] Tarascon, J.-M., Armand, M., Issues and challenges facing rechargeable lithium batteries, *Nature*, **2001**, *414*, 359-367.
- [52] Xu, K., Electrolytes and interphases in Li-ion batteries and beyond, *Chemical reviews*, **2014**, *114*, 11503-11618.
- [53] Ding, M.S., Conductivity and Viscosity of PC-DEC and PC-EC Solutions of LiBF₄, *Journal of The Electrochemical Society*, **2004**, *151*, A40-A47.
- [54] Ding, M.S., Jow, T.R., How Conductivities and Viscosities of PC-DEC and PC-EC Solutions of LiBF₄, LiPF₆, LiBOB, Et₄NBF₄, and Et₄NPF₆ Differ and Why, *Journal of The Electrochemical Society*, **2004**, *151*, A2007-A2015.
- [55] Aihara, Y., Bando, T., Nakagawa, H., Yoshida, H., Hayamizu, K., Akiba, E., Price, W.S., Ion transport properties of six lithium salts dissolved in γ -butyrolactone studied by self-diffusion and ionic conductivity measurements, *Journal of The Electrochemical Society*, **2004**, *151*, A119-A122.

- [56] Schweiger, H.-G., Multerer, M., Schweizer-Berberich, M., Gores, H., Finding conductivity optima of battery electrolytes by conductivity measurements guided by a simplex algorithm, *Journal of The Electrochemical Society*, **2005**, *152*, A577-A582.
- [57] Ding, M., Xu, K., Zhang, S., Amine, K., Henriksen, G., Jow, T., Change of conductivity with salt content, solvent composition, and temperature for electrolytes of LiPF₆ in ethylene carbonate-ethyl methyl carbonate, *Journal of the Electrochemical Society*, **2001**, *148*, A1196-A1204.
- [58] Zugmann, S., Fleischmann, M., Amereller, M., Gschwind, R.M., Wiemhöfer, H., Gores, H., Measurement of transference numbers for lithium ion electrolytes via four different methods, a comparative study, *Electrochimica Acta*, **2011**, *56*, 3926-3933.
- [59] Bockris, J.O.M., Reddy, A.K., Modern electrochemistry 2B: electrodictics in chemistry, engineering, biology and environmental science, Springer Science & Business Media, 2000.
- [60] Postupna, O., Kolesnik, Y., Kalugin, O., Prezhdo, O., Microscopic structure and dynamics of LiBF₄ solutions in cyclic and linear carbonates, *The Journal of Physical Chemistry B*, **2011**, *115*, 14563-14571.
- [61] Vetter, J., Buqa, H., Holzapfel, M., Novák, P., Impact of co-solvent chain branching on lithium-ion battery performance, *Journal of power sources*, **2005**, *146*, 355-359.
- [62] Chiba, K., Ueda, T., Yamaguchi, Y., Oki, Y., Saiki, F., Naoi, K., Electrolyte systems for high withstand voltage and Durability II. alkylated cyclic carbonates for

- electric double-layer capacitors, *Journal of The Electrochemical Society*, **2011**, *158*, A1320-A1327.
- [63] Xue, L., Ueno, K., Lee, S.-Y., Angell, C.A., Enhanced performance of sulfone-based electrolytes at lithium ion battery electrodes, including the $\text{LiNi}_{0.5}\text{Mn}_{1.5}\text{O}_4$ high voltage cathode, *Journal of Power Sources*, **2014**, *262*, 123-128.
- [64] Sun, X.-G., Angell, C.A., New sulfone electrolytes for rechargeable lithium batteries.: Part I. Oligoether-containing sulfones, *Electrochemistry communications*, **2005**, *7*, 261-266.
- [65] Sun, X.-G., Angell, C.A., New sulfone electrolytes: part II. Cyclo alkyl group containing sulfones, *Solid State Ionics*, **2004**, *175*, 257-260.
- [66] Sun, X., Angell, C.A., Doped sulfone electrolytes for high voltage Li-ion cell applications, *Electrochemistry Communications*, **2009**, *11*, 1418-1421.
- [67] Abouimrane, A., Belharouak, I., Amine, K., Sulfone-based electrolytes for high-voltage Li-ion batteries, *Electrochemistry Communications*, **2009**, *11*, 1073-1076.
- [68] Lee, S.-Y., Ueno, K., Angell, C.A., Lithium salt solutions in mixed sulfone and sulfone-carbonate solvents: a walden plot analysis of the maximally conductive compositions, *The Journal of Physical Chemistry C*, **2012**, *116*, 23915-23920.
- [69] Sirenko, V., Potapenko, A., Prisiazhnyi, V., Cost-effective and ecologically safe electrolyte for lithium batteries, *Journal of Power Sources*, **2008**, *175*, 581-585.
- [70] Yamada, Y., Takazawa, Y., Miyazaki, K., Abe, T., Electrochemical lithium intercalation into graphite in dimethyl sulfoxide-based electrolytes: effect of solvation structure of lithium ion, *The Journal of Physical Chemistry C*, **2010**, *114*, 11680-11685.

- [71] Nagahama, M., Hasegawa, N., Okada, S., High voltage performances of Li₂NiPO₄F cathode with dinitrile-based electrolytes, *Journal of The Electrochemical Society*, **2010**, *157*, A748-A752.
- [72] Duncan, H., Salem, N., Abu-Lebdeh, Y., Electrolyte formulations based on dinitrile solvents for high voltage Li-ion batteries, *Journal of The Electrochemical Society*, **2013**, *160*, A838-A848.
- [73] Abu-Lebdeh, Y., Davidson, I., High-voltage electrolytes based on adiponitrile for Li-ion batteries, *Journal of The Electrochemical Society*, **2009**, *156*, A60-A65.
- [74] Abu-Lebdeh, Y., Davidson, I., New electrolytes based on glutaronitrile for high energy/power Li-ion batteries, *Journal of Power Sources*, **2009**, *189*, 576-579.
- [75] Abouimrane, A., Davidson, I., Solid electrolyte based on succinonitrile and LiBOB interface stability and application in lithium batteries, *Journal of the Electrochemical Society*, **2007**, *154*, A1031-A1034.
- [76] Wang, Q., Zakeeruddin, S.M., Exnar, I., Grätzel, M., 3-Methoxypropionitrile-Based Novel Electrolytes for High-Power Li-Ion Batteries with Nanocrystalline Li₄Ti₅O₁₂ Anode, *Journal of The Electrochemical Society*, **2004**, *151*, A1598-A1603.
- [77] Guyomard, D., Tarascon, J., Rechargeable Li_{1+x}Mn₂O₄/Carbon Cells with a New Electrolyte Composition Potentiostatic Studies and Application to Practical Cells, *Journal of the electrochemical society*, **1993**, *140*, 3071-3081.
- [78] Arai, J., Nonflammable methyl nonafluorobutyl ether for electrolyte used in lithium secondary batteries, *Journal of the Electrochemical Society*, **2003**, *150*, A219-A228.
- [79] Naoi, K., Iwama, E., Ogihara, N., Nakamura, Y., Segawa, H., Ino, Y., Nonflammable hydrofluoroether for lithium-ion batteries: Enhanced rate capability,

- cyclability, and low-temperature performance, *Journal of the Electrochemical Society*, **2009**, *156*, A272-A276.
- [80] Naoi, K., Iwama, E., Honda, Y., Shimodate, F., Discharge behavior and rate performances of lithium-ion batteries in nonflammable hydrofluoroethers (II), *Journal of the Electrochemical Society*, **2010**, *157*, A190-A195.
- [81] Sazhin, S.V., Harrup, M.K., Gering, K.L., Characterization of low-flammability electrolytes for lithium-ion batteries, *Journal of Power Sources*, **2011**, *196*, 3433-3438.
- [82] Dalavi, S., Xu, M., Ravdel, B., Zhou, L., Lucht, B.L., Nonflammable electrolytes for lithium-ion batteries containing dimethyl methylphosphonate, *Journal of The Electrochemical Society*, **2010**, *157*, A1113-A1120.
- [83] Xu, M., Lu, D., Garsuch, A., Lucht, B.L., Improved performance of $\text{LiNi}_{0.5}\text{Mn}_{1.5}\text{O}_4$ cathodes with electrolytes containing dimethylmethylphosphonate (DMMP), *Journal of The Electrochemical Society*, **2012**, *159*, A2130-A2134.
- [84] Jin, Z., Wu, L., Song, Z., Yan, K., Zhan, H., Li, Z., A New Class of Phosphates as Co-Solvents for Nonflammable Lithium Ion Batteries Electrolytes, *ECS Electrochemistry Letters*, **2012**, *1*, A55-A58.
- [85] Zhang, Z., Sherlock, D., West, R., West, R., Amine, K., Lyons, L.J., Cross-linked network polymer electrolytes based on a polysiloxane backbone with oligo (oxyethylene) side chains: synthesis and conductivity, *Macromolecules*, **2003**, *36*, 9176-9180.

- [86] Zhang, Z., Lyons, L.J., Jin, J.J., Amine, K., West, R., Synthesis and ionic conductivity of cyclosiloxanes with ethyleneoxy-containing substituents, *Chemistry of materials*, **2005**, *17*, 5646-5650.
- [87] Amine, K., Wang, Q., Vissers, D.R., Zhang, Z., Rossi, N.A., West, R., Novel silane compounds as electrolyte solvents for Li-ion batteries, *Electrochemistry communications*, **2006**, *8*, 429-433.
- [88] Kusachi, Y., Zhang, Z., Dong, J., Amine, K., Electrode surface film formation in tris (ethylene glycol)-substituted trimethylsilane–lithium bis (oxalate) borate electrolyte, *The Journal of Physical Chemistry C*, **2011**, *115*, 24013-24020.
- [89] Gabriel, S., Weiner, J., Ueber einige abkömmlinge des propylamins, *European Journal of Inorganic Chemistry*, **1888**, *21*, 2669-2679.
- [90] Walden, P., Molecular weights and electrical conductivity of several fused salts, *Bull. Acad. Imper. Sci.(St. Petersburg)*, **1914**, *1800*.
- [91] Chum, H.L., Koch, V., Miller, L., Osteryoung, R., Electrochemical scrutiny of organometallic iron complexes and hexamethylbenzene in a room temperature molten salt, *Journal of the American Chemical Society*, **1975**, *97*, 3264-3265.
- [92] Wilkes, J.S., Levisky, J.A., Wilson, R.A., Hussey, C.L., Dialkylimidazolium chloroaluminate melts: a new class of room-temperature ionic liquids for electrochemistry, spectroscopy and synthesis, *Inorganic Chemistry*, **1982**, *21*, 1263-1264.
- [93] MacFarlane, D., Meakin, P., Sun, J., Amini, N., Forsyth, M., Pyrrolidinium imides: a new family of molten salts and conductive plastic crystal phases, *The Journal of Physical Chemistry B*, **1999**, *103*, 4164-4170.

- [94] MacFarlane, D.R., Huang, J., Forsyth, M., Lithium-doped plastic crystal electrolytes exhibiting fast ion conduction for secondary batteries, *Nature*, **1999**, *402*, 792-794.
- [95] Markevich, E., Baranchugov, V., Salitra, G., Aurbach, D., Schmidt, M.A., Behavior of graphite electrodes in solutions based on ionic liquids in in situ Raman studies, *Journal of The Electrochemical Society*, **2008**, *155*, A132-A137.
- [96] Salem, N., Nicodemou, L., Abu-Lebdeh, Y., Davidson, I.J., Room temperature ionic liquid electrolytes based on azepanium imide salts for lithium batteries, *Journal of The Electrochemical Society*, **2011**, *159*, A172-A176.
- [97] MacFarlane, D.R., Tachikawa, N., Forsyth, M., Pringle, J.M., Howlett, P.C., Elliott, G.D., Davis, J.H., Watanabe, M., Simon, P., Angell, C.A., Energy applications of ionic liquids, *Energy & Environmental Science*, **2014**, *7*, 232-250.
- [98] Ong, S.P., Andreussi, O., Wu, Y., Marzari, N., Ceder, G., Electrochemical windows of room-temperature ionic liquids from molecular dynamics and density functional theory calculations, *Chemistry of Materials*, **2011**, *23*, 2979-2986.
- [99] Best, A., Bhatt, A., Hollenkamp, A., Ionic liquids with the bis (fluorosulfonyl) imide anion: electrochemical properties and applications in battery technology, *Journal of The Electrochemical Society*, **2010**, *157*, A903-A911.
- [100] Garche, J., Dyer, C.K., Moseley, P.T., Ogumi, Z., Rand, D.A., Scrosati, B., Encyclopedia of electrochemical power sources, Newnes, 2013.
- [101] Xu, K., Deveney, B., Nechev, K., Lam, Y., Jow, T.R., Evaluating LiBOB/lactone electrolytes in large-format lithium-ion cells based on nickelate and iron phosphate, *Journal of The Electrochemical Society*, **2008**, *155*, A959-A964.

- [102] Zhang, Z., Lyons, L.J., Amine, K., West, R., Network-type ionic conductors based on oligoethyleneoxy-functionalized pentamethylcyclopentasiloxanes, *Macromolecules*, **2005**, *38*, 5714-5720.
- [103] Li, L., Zhou, S., Han, H., Li, H., Nie, J., Armand, M., Zhou, Z., Huang, X., Transport and electrochemical properties and spectral features of non-aqueous electrolytes containing LiFSI in linear carbonate solvents, *Journal of the Electrochemical Society*, **2011**, *158*, A74-A82.
- [104] Ratner, M.A., Shriver, D.F., Ion transport in solvent-free polymers, *Chemical Reviews*, **1988**, *88*, 109-124.
- [105] Armand, M., The history of polymer electrolytes, *Solid State Ionics*, **1994**, *69*, 309-319.
- [106] Dias, F.B., Plomp, L., Veldhuis, J.B., Trends in polymer electrolytes for secondary lithium batteries, *Journal of Power Sources*, **2000**, *88*, 169-191.
- [107] Song, J., Wang, Y., Wan, C.C., Review of gel-type polymer electrolytes for lithium-ion batteries, *Journal of Power Sources*, **1999**, *77*, 183-197.
- [108] Fenton, D., Parker, J., Wright, P., Complexes of alkali metal ions with poly (ethylene oxide), *polymer*, **1973**, *14*, 589.
- [109] Meyer, W.H., Polymer electrolytes for lithium-ion batteries, *Advanced materials*, **1998**, *10*, 439-448.
- [110] Müller-Plathe, F., van Gunsteren, W.F., Computer simulation of a polymer electrolyte: lithium iodide in amorphous poly (ethylene oxide), *The Journal of chemical physics*, **1995**, *103*, 4745-4756.

- [111] Cheung, I., Chin, K., Greene, E., Smart, M., Abbrent, S., Greenbaum, S., Prakash, G., Surampudi, S., Electrochemical and solid state NMR characterization of composite PEO-based polymer electrolytes, *Electrochimica acta*, **2003**, *48*, 2149-2156.
- [112] Krawiec, W., Scanlon, L., Fellner, J., Vaia, R., Vasudevan, S., Giannelis, E., Polymer nanocomposites: a new strategy for synthesizing solid electrolytes for rechargeable lithium batteries, *Journal of Power Sources*, **1995**, *54*, 310-315.
- [113] Appetecchi, G., Croce, F., Hassoun, J., Scrosati, B., Salomon, M., Cassel, F., Hot-pressed, dry, composite, PEO-based electrolyte membranes: I. Ionic conductivity characterization, *Journal of power sources*, **2003**, *114*, 105-112.
- [114] Inoue, K., Nishikawa, Y., Tanigaki, T., Ionic conductivity of polymer complexes formed by polystyrene derivatives with a pendant oligo (oxyethylene) cyclotriphosphazene and lithium perchlorate, *Macromolecules*, **1991**, *24*, 3464-3465.
- [115] Lauter, U., Meyer, W.H., Wegner, G., Molecular composites from rigid-rod poly (p-phenylene) s with oligo (oxyethylene) side chains as novel polymer electrolytes, *Macromolecules*, **1997**, *30*, 2092-2101.
- [116] Croce, F., Appetecchi, G., Persi, L., Scrosati, B., Nanocomposite polymer electrolytes for lithium batteries, *Nature*, **1998**, *394*, 456-458.
- [117] Bronstein, L.M., Karlinsey, R.L., Ritter, K., Joo, C.G., Stein, B., Zwanziger, J.W., Design of organic–inorganic solid polymer electrolytes: synthesis, structure, and properties, *Journal of Materials Chemistry*, **2004**, *14*, 1812-1820.
- [118] Stephan, A.M., Nahm, K., Review on composite polymer electrolytes for lithium batteries, *Polymer*, **2006**, *47*, 5952-5964.

- [119] Ito, Y., Kanehori, K., Miyauchi, K., Kudo, T., Ionic conductivity of electrolytes formed from PEO-LiCF₃SO₃ complex low molecular weight poly (ethylene glycol), *Journal of materials science*, **1987**, *22*, 1845-1849.
- [120] Kelly, I., Owen, J., Steele, B., Poly (ethylene oxide) electrolytes for operation at near room temperature, *Journal of Power Sources*, **1985**, *14*, 13-21.
- [121] Appetecchi, G., Dautzenberg, G., Scrosati, B., A New Class of Advanced Polymer Electrolytes and Their Relevance in Plastic-like, Rechargeable Lithium Batteries, *Journal of The Electrochemical Society*, **1996**, *143*, 6-12.
- [122] Iijima, T., Toyoguchi, Y., Eda, N., Quasi-solid organic electrolytes gelatinized with polymethyl-methacrylate and their applications for lithium batteries, *Denki Kagaku*, **1985**, *53*, 619-623.
- [123] Bohnke, O., Frand, G., Rezrazi, M., Rousselot, C., Truche, C., Fast ion transport in new lithium electrolytes gelled with PMMA. 1. Influence of polymer concentration, *Solid State Ionics*, **1993**, *66*, 97-104.
- [124] Appetecchi, G., Croce, F., Scrosati, B., Kinetics and stability of the lithium electrode in poly (methylmethacrylate)-based gel electrolytes, *Electrochimica Acta*, **1995**, *40*, 991-997.
- [125] Zhang, H., Zhang, P., Li, Z., Sun, M., Wu, Y., Wu, H., A novel sandwiched membrane as polymer electrolyte for lithium ion battery, *Electrochemistry communications*, **2007**, *9*, 1700-1703.
- [126] Stephan, A.M., Thirunakaran, R., Renganathan, N., Sundaram, V., Pitchumani, S., Muniyandi, N., Gangadharan, R., Ramamoorthy, P., A study on polymer blend

- electrolyte based on PVC/PMMA with lithium salt, *Journal of power sources*, **1999**, *81*, 752-758.
- [127] Sukeshini, A.M., Nishimoto, A., Watanabe, M., Transport and electrochemical characterization of plasticized poly (vinyl chloride) solid electrolytes, *Solid State Ionics*, **1996**, *86*, 385-393.
- [128] Alamgir, M., Abraham, K., Li ion conductive electrolytes based on poly (vinyl chloride), *Journal of the Electrochemical Society*, **1993**, *140*, L96-L97.
- [129] Choe, H., Giaccari, J., Alamgir, M., Abraham, K., Preparation and characterization of poly (vinyl sulfone)-and poly (vinylidene fluoride)-based electrolytes, *Electrochimica Acta*, **1995**, *40*, 2289-2293.
- [130] Li, G., Zhang, P., Zhang, H., Yang, L., Wu, Y., A porous polymer electrolyte based on P (VDF-HFP) prepared by a simple phase separation process, *Electrochemistry Communications*, **2008**, *10*, 1883-1885.
- [131] Xiao, W., Li, X., Wang, Z., Guo, H., Li, Y., Yang, B., Performance of PVDF-HFP-based gel polymer electrolytes with different pore forming agents, *Iranian Polymer Journal*, **2012**, *21*, 755-761.
- [132] Li, Z., Cheng, C., Zhan, X., Wu, Y., Zhou, X., A foaming process to prepare porous polymer membrane for lithium ion batteries, *Electrochimica Acta*, **2009**, *54*, 4403-4407.
- [133] Abraham, K., Jiang, Z., Carroll, B., Highly conductive PEO-like polymer electrolytes, *Chemistry of materials*, **1997**, *9*, 1978-1988.
- [134] Huang, X., Separator technologies for lithium-ion batteries, *Journal of Solid State Electrochemistry*, **2011**, *15*, 649-662.

- [135] Kim, M., Park, J.H., Multi-Scale Pore Generation from Controlled Phase Inversion: Application to Separators for Li-Ion Batteries, *Advanced Energy Materials*, **2013**, *3*, 1417-1420.
- [136] Li, Z., Su, G., Wang, X., Gao, D., Micro-porous P (VDF-HFP)-based polymer electrolyte filled with Al₂O₃ nanoparticles, *Solid State Ionics*, **2005**, *176*, 1903-1908.
- [137] Magistris, A., Quartarone, E., Mustarelli, P., Saito, Y., Kataoka, H., PVDF-based porous polymer electrolytes for lithium batteries, *Solid State Ionics*, **2002**, *152*, 347-354.
- [138] Shi, Q., Yu, M., Zhou, X., Yan, Y., Wan, C., Structure and performance of porous polymer electrolytes based on P (VDF-HFP) for lithium ion batteries, *Journal of power Sources*, **2002**, *103*, 286-292.
- [139] Song, J., Kang, H., Kim, S., Lee, W., Kim, H., Electrochemical characteristics of phase-separated polymer electrolyte based on poly (vinylidene fluoride-co-hexafluoropropane) and ethylene carbonate, *Electrochimica acta*, **2003**, *48*, 1339-1346.
- [140] Sundaram, N.K., Subramania, A., Microstructure of PVdF-co-HFP based electrolyte prepared by preferential polymer dissolution process, *Journal of membrane science*, **2007**, *289*, 1-6.
- [141] Zhang, S.S., A review on the separators of liquid electrolyte Li-ion batteries, *Journal of Power Sources*, **2007**, *164*, 351-364.
- [142] Gentili, V., Panero, S., Reale, P., Scrosati, B., Composite gel-type polymer electrolytes for advanced, rechargeable lithium batteries, *Journal of power sources*, **2007**, *170*, 185-190.

- [143] Li, Z., Zhang, H., Zhang, P., Li, G., Wu, Y., Zhou, X., Effects of the porous structure on conductivity of nanocomposite polymer electrolyte for lithium ion batteries, *Journal of Membrane Science*, **2008**, *322*, 416-422.
- [144] Miao, R., Liu, B., Zhu, Z., Liu, Y., Li, J., Wang, X., Li, Q., PVDF-HFP-based porous polymer electrolyte membranes for lithium-ion batteries, *Journal of Power Sources*, **2008**, *184*, 420-426.
- [145] Pu, W., He, X., Wang, L., Tian, Z., Jiang, C., Wan, C., Preparation of P (AN–MMA) microporous membrane for Li-ion batteries by phase inversion, *Journal of membrane science*, **2006**, *280*, 6-9.
- [146] Raghavan, P., Zhao, X., Manuel, J., Chauhan, G.S., Ahn, J.-H., Ryu, H.-S., Ahn, H.-J., Kim, K.-W., Nah, C., Electrochemical performance of electrospun poly (vinylidene fluoride-co-hexafluoropropylene)-based nanocomposite polymer electrolytes incorporating ceramic fillers and room temperature ionic liquid, *Electrochimica Acta*, **2010**, *55*, 1347-1354.
- [147] Zhao, Y.-H., Xu, Y.-Y., Zhu, B.-K., Effect of amphiphilic hyperbranched-star polymer on the structure and properties of PVDF based porous polymer electrolytes, *Solid State Ionics*, **2009**, *180*, 1517-1524.
- [148] Augustin, S., Hennige, V., Hörpel, G., Hying, C., Ceramic but flexible: new ceramic membrane foils for fuel cells and batteries, *Desalination*, **2002**, *146*, 23-28.
- [149] Jeong, H.-S., Choi, E.-S., Kim, J.H., Lee, S.-Y., Potential application of microporous structured poly (vinylidene fluoride-hexafluoropropylene)/poly (ethylene terephthalate) composite nonwoven separators to high-voltage and high-power lithium-ion batteries, *Electrochimica Acta*, **2011**, *56*, 5201-5204.

- [150] Jeong, H.-S., Kim, J.H., Lee, S.-Y., A novel poly (vinylidene fluoride-hexafluoropropylene)/poly (ethylene terephthalate) composite nonwoven separator with phase inversion-controlled microporous structure for a lithium-ion battery, *Journal of Materials Chemistry*, **2010**, *20*, 9180-9186.
- [151] Jung, S., Kim, D.-W., Lee, S.-D., Cheong, M.C., Nguyen, D.Q., Cho, B.-W., Kim, H.-S., Fillers for solid-state polymer electrolytes: highlight, *Bulletin of the Korean Chemical Society*, **2009**, *30*, 2355-2361.
- [152] Kim, M., Sohn, J.Y., Nho, Y.C., Park, J.H., Effects of E-beam irradiation on physical and electrochemical properties of inorganic nanoparticle separators with different particle sizes, *Journal of The Electrochemical Society*, **2011**, *158*, A511-A515.
- [153] Wang, Y.-J., Kim, D., Crystallinity, morphology, mechanical properties and conductivity study of in situ formed PVdF/LiClO₄/TiO₂ nanocomposite polymer electrolytes, *Electrochimica acta*, **2007**, *52*, 3181-3189.
- [154] Saito, Y., Kataoka, H., Quartarone, E., Mustarelli, P., Carrier migration mechanism of physically cross-linked polymer gel electrolytes based on PVDF membranes, *The Journal of Physical Chemistry B*, **2002**, *106*, 7200-7204.
- [155] Vincent, C.A., Polymer electrolytes, *Progress in solid state chemistry*, **1987**, *17*, 145-261.
- [156] Saunier, J., Gorecki, W., Alloin, F., Sanchez, J.-Y., NMR study of cation, anion, and solvent mobilities in macroporous poly (vinylidene fluoride), *The Journal of Physical Chemistry B*, **2005**, *109*, 2487-2492.

- [157] Saunier, J., Alloin, F., Sanchez, J., Maniguet, L., Plasticized microporous poly (vinylidene fluoride) separators for lithium-ion batteries. III. Gel properties and irreversible modifications of poly (vinylidene fluoride) membranes under swelling in liquid electrolytes, *Journal of Polymer Science Part B: Polymer Physics*, **2004**, *42*, 2308-2317.
- [158] Abbrent, S., Plestil, J., Hlavata, D., Lindgren, J., Tegenfeldt, J., Wendsjö, Å., Crystallinity and morphology of PVdF–HFP-based gel electrolytes, *Polymer*, **2001**, *42*, 1407-1416.
- [159] Tarascon, J.-M., Gozdz, A., Schmutz, C., Shokoohi, F., Warren, P., Performance of Bellcore's plastic rechargeable Li-ion batteries, *Solid State Ionics*, **1996**, *86*, 49-54.
- [160] Xi, J., Qiu, X., Li, J., Tang, X., Zhu, W., Chen, L., PVDF–PEO blends based microporous polymer electrolyte: Effect of PEO on pore configurations and ionic conductivity, *Journal of power sources*, **2006**, *157*, 501-506.
- [161] Liu, X., Kusawake, H., Kuwajima, S., Preparation of a PVdF-HFP/polyethylene composite gel electrolyte with shutdown function for lithium-ion secondary battery, *Journal of power sources*, **2001**, *97*, 661-663.
- [162] Kim, D.-W., Sun, Y.-K., Electrochemical characterization of gel polymer electrolytes prepared with porous membranes, *Journal of power sources*, **2001**, *102*, 41-45.
- [163] Capsoni, D., Bini, M., Ferrari, S., Quartarone, E., Mustarelli, P., Recent advances in the development of Li–air batteries, *Journal of Power Sources*, **2012**, *220*, 253-263.
- [164] Bruce, P.G., Freunberger, S.A., Hardwick, L.J., Tarascon, J.-M., Li-O₂ and Li-S batteries with high energy storage, *Nature materials*, **2012**, *11*, 19-29.

- [165] Kraysberg, A., Ein-Eli, Y., Review on Li-air batteries—Opportunities, limitations and perspective, *Journal of Power Sources*, **2011**, *196*, 886-893.
- [166] Padbury, R., Zhang, X., Lithium-oxygen batteries—Limiting factors that affect performance, *Journal of Power Sources*, **2011**, *196*, 4436-4444.
- [167] Guo, X., Sun, B., Su, D., Liu, X., Liu, H., Wang, Y., Wang, G., Recent developments of aprotic lithium-oxygen batteries: functional materials determine the electrochemical performance, *Science Bulletin*, **2017**.
- [168] Tan, P., Wei, Z., Shyy, W., Zhao, T., Zhu, X., A nano-structured RuO₂/NiO cathode enables the operation of non-aqueous lithium-air batteries in ambient air, *Energy & Environmental Science*, **2016**, *9*, 1783-1793.
- [169] Shui, J.-L., Okasinski, J.S., Kenesei, P., Dobbs, H.A., Zhao, D., Almer, J.D., Liu, D.-J., Reversibility of anodic lithium in rechargeable lithium-oxygen batteries, *Nature communications*, **2013**, *4*, 2255.
- [170] Cheng, X.B., Zhang, R., Zhao, C.Z., Wei, F., Zhang, J.G., Zhang, Q., A review of solid electrolyte interphases on lithium metal anode, *Advanced Science*, **2016**, *3*.
- [171] Choi, N.S., Chen, Z., Freunberger, S.A., Ji, X., Sun, Y.K., Amine, K., Yushin, G., Nazar, L.F., Cho, J., Bruce, P.G., Challenges facing lithium batteries and electrical double-layer capacitors, *Angewandte Chemie International Edition*, **2012**, *51*, 9994-10024.
- [172] Scrosati, B., Garche, J., Lithium batteries: Status, prospects and future, *Journal of Power Sources*, **2010**, *195*, 2419-2430.

- [173] Chen, Y., Freunberger, S.A., Peng, Z., Bardé, F., Bruce, P.G., Li–O₂ battery with a dimethylformamide electrolyte, *Journal of the American Chemical Society*, **2012**, *134*, 7952-7957.
- [174] Chen, Y., Freunberger, S.A., Peng, Z., Fontaine, O., Bruce, P.G., Charging a Li–O₂ battery using a redox mediator, *Nature chemistry*, **2013**, *5*, 489-494.
- [175] McCloskey, B., Bethune, D., Shelby, R., Mori, T., Scheffler, R., Speidel, A., Sherwood, M., Luntz, A., Limitations in rechargeability of Li-O₂ batteries and possible origins, *The journal of physical chemistry letters*, **2012**, *3*, 3043-3047.
- [176] ZHANG, Y.-T., LIU, Z.-J., WANG, J.-W., WANG, L., PENG, Z.-Q., Recent Advances in Li Anode for Aprotic Li-O₂ Batteries, *Acta Physico-Chimica Sinica*, **2017**, *33*, 486-499.
- [177] Chun, J., Kim, H., Jo, C., Lim, E., Lee, J., Kim, Y., Reversibility of Lithium-Ion–Air Batteries Using Lithium Intercalation Compounds as Anodes, *ChemPlusChem*, **2015**, *80*, 349-353.
- [178] Hassoun, J., Jung, H.-G., Lee, D.-J., Park, J.-B., Amine, K., Sun, Y.-K., Scrosati, B., A metal-free, lithium-ion oxygen battery: A step forward to safety in lithium-air batteries, *Nano letters*, **2012**, *12*, 5775-5779.
- [179] Elia, G.A., Bresser, D., Reiter, J., Oberhumer, P., Sun, Y.-K., Scrosati, B., Passerini, S., Hassoun, J., Interphase Evolution of a Lithium-Ion/Oxygen Battery, *ACS applied materials & interfaces*, **2015**, *7*, 22638-22643.
- [180] Aurbach, D., Pollak, E., Elazari, R., Salitra, G., Kelley, C.S., Affinito, J., On the surface chemical aspects of very high energy density, rechargeable Li–sulfur batteries, *Journal of The Electrochemical Society*, **2009**, *156*, A694-A702.

- [181] Liang, X., Wen, Z., Liu, Y., Wu, M., Jin, J., Zhang, H., Wu, X., Improved cycling performances of lithium sulfur batteries with LiNO₃-modified electrolyte, *Journal of Power Sources*, **2011**, *196*, 9839-9843.
- [182] Zhang, S.S., A new finding on the role of LiNO₃ in lithium-sulfur battery, *Journal of Power Sources*, **2016**, *322*, 99-105.
- [183] Walker, W., Giordani, V., Uddin, J., Bryantsev, V.S., Chase, G.V., Addison, D., A rechargeable Li–O₂ battery using a lithium nitrate/N, N-dimethylacetamide electrolyte, *Journal of the American Chemical Society*, **2013**, *135*, 2076-2079.
- [184] Giordani, V., Walker, W., Bryantsev, V.S., Uddin, J., Chase, G.V., Addison, D., Synergistic Effect of Oxygen and LiNO₃ on the Interfacial Stability of Lithium Metal in a Li/O₂ Battery, *Journal of The Electrochemical Society*, **2013**, *160*, A1544-A1550.
- [185] Sun, B., Huang, X., Chen, S., Zhang, J., Wang, G., An optimized LiNO₃/DMSO electrolyte for high-performance rechargeable Li–O₂ batteries, *Rsc Advances*, **2014**, *4*, 11115-11120.
- [186] Roberts, M., Younesi, R., Richardson, W., Liu, J., Gustafsson, T., Zhu, J., Edström, K., Increased Cycling Efficiency of Lithium Anodes in Dimethyl Sulfoxide Electrolytes For Use in Li-O₂ Batteries, *ECS Electrochemistry Letters*, **2014**, *3*, A62-A65.
- [187] Bryantsev, V.S., Giordani, V., Walker, W., Uddin, J., Lee, I., van Duin, A.C., Chase, G.V., Addison, D., Investigation of Fluorinated Amides for Solid–Electrolyte Interphase Stabilization in Li–O₂ Batteries Using Amide-Based Electrolytes, *The Journal of Physical Chemistry C*, **2013**, *117*, 11977-11988.

- [188] Liu, Q.C., Xu, J.J., Yuan, S., Chang, Z.W., Xu, D., Yin, Y.B., Li, L., Zhong, H.X., Jiang, Y.S., Yan, J.M., Artificial Protection Film on Lithium Metal Anode toward Long-Cycle-Life Lithium–Oxygen Batteries, *Advanced Materials*, **2015**, *27*, 5241-5247.
- [189] Wang, Y., Zhou, H., A lithium-air battery with a potential to continuously reduce O₂ from air for delivering energy, *Journal of Power Sources*, **2010**, *195*, 358-361.
- [190] Wang, Y., He, P., Zhou, H., A lithium–air capacitor–battery based on a hybrid electrolyte, *Energy & Environmental Science*, **2011**, *4*, 4994-4999.
- [191] Elia, G.A., Hassoun, J., A gel polymer membrane for lithium-ion oxygen battery, *Solid State Ionics*, **2016**, *287*, 22-27.
- [192] Lee, D.J., Lee, H., Song, J., Ryou, M.-H., Lee, Y.M., Kim, H.-T., Park, J.-K., Composite protective layer for Li metal anode in high-performance lithium–oxygen batteries, *Electrochemistry Communications*, **2014**, *40*, 45-48.
- [193] Wang, Y., Xia, Y., Li-O₂ batteries: an agent for change, *Nature chemistry*, **2013**, *5*, 445-447.
- [194] Lee, D.J., Lee, H., Kim, Y.J., Park, J.K., Kim, H.T., Sustainable Redox Mediation for Lithium–Oxygen Batteries by a Composite Protective Layer on the Lithium-Metal Anode, *Advanced Materials*, **2016**, *28*, 857-863.
- [195] Kim, B.G., Kim, J.S., Min, J., Lee, Y.H., Choi, J.H., Jang, M.C., Freunberger, S.A., Choi, J.W., A Moisture-and Oxygen-Impermeable Separator for Aprotic Li-O₂ Batteries, *Advanced Functional Materials*, **2016**, *26*, 1747-1756.
- [196] Flamme, B., Garcia, G.R., Weil, M., Haddad, M., Phansavath, P., Ratovelomanana-Vidal, V., Chagnes, A., Guidelines to design organic electrolytes for lithium-ion

- batteries: environmental impact, physicochemical and electrochemical properties, *Green Chemistry*, **2017**, *19*, 1828-1849.
- [197] Freunberger, S.A., Chen, Y., Peng, Z., Griffin, J.M., Hardwick, L.J., Bardé, F., Novák, P., Bruce, P.G., Reactions in the rechargeable lithium–O₂ battery with alkyl carbonate electrolytes, *Journal of the American Chemical Society*, **2011**, *133*, 8040-8047.
- [198] McCloskey, B.D., Bethune, D., Shelby, R., Girishkumar, G., Luntz, A., Solvents' critical role in nonaqueous lithium–oxygen battery electrochemistry, *The Journal of Physical Chemistry Letters*, **2011**, *2*, 1161-1166.
- [199] Xiao, J., Mei, D., Li, X., Xu, W., Wang, D., Graff, G.L., Bennett, W.D., Nie, Z., Saraf, L.V., Aksay, I.A., Hierarchically porous graphene as a lithium–air battery electrode, *Nano letters*, **2011**, *11*, 5071-5078.
- [200] Jung, H.-G., Hassoun, J., Park, J.-B., Sun, Y.-K., Scrosati, B., An improved high-performance lithium–air battery, *Nature chemistry*, **2012**, *4*, 579-585.
- [201] Xu, W., Hu, J., Engelhard, M.H., Towne, S.A., Hardy, J.S., Xiao, J., Feng, J., Hu, M.Y., Zhang, J., Ding, F., The stability of organic solvents and carbon electrode in nonaqueous Li–O₂ batteries, *Journal of Power Sources*, **2012**, *215*, 240-247.
- [202] Laoire, C., Mukerjee, S., Plichta, E.J., Hendrickson, M.A., Abraham, K., Rechargeable lithium/TEGDME–LiPF₆/O₂ battery, *Journal of The Electrochemical Society*, **2011**, *158*, A302-A308.
- [203] Lim, H.-D., Park, K.-Y., Gwon, H., Hong, J., Kim, H., Kang, K., The potential for long-term operation of a lithium–oxygen battery using a non-carbonate-based electrolyte, *Chemical Communications*, **2012**, *48*, 8374-8376.

- [204] Freunberger, S.A., Chen, Y., Drewett, N.E., Hardwick, L.J., Bardé, F., Bruce, P.G., The lithium–oxygen battery with ether-based electrolytes, *Angewandte Chemie International Edition*, **2011**, *50*, 8609-8613.
- [205] Ryan, K.R., Trahey, L., Ingram, B.J., Burrell, A.K., Limited stability of ether-based solvents in lithium–oxygen batteries, *The Journal of Physical Chemistry C*, **2012**, *116*, 19724-19728.
- [206] Xu, D., Wang, Z.-l., Xu, J.-j., Zhang, L.-l., Zhang, X.-b., Novel DMSO-based electrolyte for high performance rechargeable Li–O₂ batteries, *Chemical Communications*, **2012**, *48*, 6948-6950.
- [207] Trahan, M.J., Mukerjee, S., Plichta, E.J., Hendrickson, M.A., Abraham, K., Studies of Li-air cells utilizing dimethyl sulfoxide-based electrolyte, *Journal of The Electrochemical Society*, **2013**, *160*, A259-A267.
- [208] Peng, Z., Freunberger, S.A., Chen, Y., Bruce, P.G., A reversible and higher-rate Li–O₂ battery, *Science*, **2012**, *337*, 563-566.
- [209] Bryantsev, V.S., Giordani, V., Walker, W., Blanco, M., Zecevic, S., Sasaki, K., Uddin, J., Addison, D., Chase, G.V., Predicting solvent stability in aprotic electrolyte Li–air batteries: nucleophilic substitution by the superoxide anion radical (O₂^{•-}), *The Journal of Physical Chemistry A*, **2011**, *115*, 12399-12409.
- [210] Bryantsev, V.S., Uddin, J., Giordani, V., Walker, W., Addison, D., Chase, G.V., The identification of stable solvents for nonaqueous rechargeable Li-air batteries, *Journal of the Electrochemical Society*, **2013**, *160*, A160-A171.

- [211] Takechi, K., Higashi, S., Mizuno, F., Nishikoori, H., Iba, H., Shiga, T., Stability of solvents against superoxide radical species for the electrolyte of lithium-air battery, *ECS Electrochemistry Letters*, **2012**, *1*, A27-A29.
- [212] De Giorgio, F., Soavi, F., Mastragostino, M., Effect of lithium ions on oxygen reduction in ionic liquid-based electrolytes, *Electrochemistry Communications*, **2011**, *13*, 1090-1093.
- [213] Hayyan, M., Mjalli, F.S., Hashim, M.A., AlNashef, I.M., Al-Zahrani, S.M., Chooi, K.L., Long term stability of superoxide ion in piperidinium, pyrrolidinium and phosphonium cations-based ionic liquids and its utilization in the destruction of chlorobenzenes, *Journal of Electroanalytical Chemistry*, **2012**, *664*, 26-32.
- [214] Kim, B.G., Lee, J.N., Lee, D.J., Park, J.K., Choi, J.W., Robust cycling of Li–O₂ batteries through the synergistic effect of blended electrolytes, *ChemSusChem*, **2013**, *6*, 443-448.
- [215] Lu, J., Li, L., Park, J.-B., Sun, Y.-K., Wu, F., Amine, K., Aprotic and aqueous Li–O₂ batteries, *Chemical reviews*, **2014**, *114*, 5611-5640.
- [216] Veith, G.M., Nanda, J., Delmau, L.H., Dudney, N.J., Influence of lithium salts on the discharge chemistry of Li–air cells, *The journal of physical chemistry letters*, **2012**, *3*, 1242-1247.
- [217] Lim, H.-D., Lee, B., Zheng, Y., Hong, J., Kim, J., Gwon, H., Ko, Y., Lee, M., Cho, K., Kang, K., Rational design of redox mediators for advanced Li–O₂ batteries, *Nature Energy*, **2016**, *1*, 16066.

- [218] Schaltin, S., Vanhoutte, G., Wu, M., Bardé, F., Fransaer, J., A QCM study of ORR-OER and an in situ study of a redox mediator in DMSO for Li-O₂ batteries, *Physical Chemistry Chemical Physics*, **2015**, *17*, 12575-12586.
- [219] Torres, W.R., Herrera, S.E., Tesio, A.Y., del Pozo, M., Calvo, E.J., Soluble TTF catalyst for the oxidation of cathode products in Li-Oxygen battery: A chemical scavenger, *Electrochimica Acta*, **2015**, *182*, 1118-1123.
- [220] Yang, H., Wang, Q., Zhang, R., Trimm, B., Whittingham, M., The electrochemical behaviour of TTF in Li-O₂ batteries using a TEGDME-based electrolyte, *Chemical Communications*, **2016**, *52*, 7580-7583.
- [221] Lim, H.D., Song, H., Kim, J., Gwon, H., Bae, Y., Park, K.Y., Hong, J., Kim, H., Kim, T., Kim, Y.H., Superior rechargeability and efficiency of lithium-oxygen batteries: hierarchical air electrode architecture combined with a soluble catalyst, *Angewandte Chemie International Edition*, **2014**, *53*, 3926-3931.
- [222] Sun, D., Shen, Y., Zhang, W., Yu, L., Yi, Z., Yin, W., Wang, D., Huang, Y., Wang, J., Wang, D., A solution-phase bifunctional catalyst for lithium-oxygen batteries, *Journal of the American Chemical Society*, **2014**, *136*, 8941-8946.
- [223] Feng, N., He, P., Zhou, H., Enabling catalytic oxidation of Li₂O₂ at the liquid-solid interface: the evolution of an aprotic Li-O₂ battery, *ChemSusChem*, **2015**, *8*, 600-602.
- [224] Zhang, T., Liao, K., He, P., Zhou, H., A self-defense redox mediator for efficient lithium-O₂ batteries, *Energy & Environmental Science*, **2016**, *9*, 1024-1030.
- [225] Abraham, K., Jiang, Z., A polymer electrolyte-based rechargeable lithium/oxygen battery, *J. Electrochem. Soc.*, **1996**, *143*, 1-5.

- [226] Mohamed, S., Johari, N., Ali, A., Harun, M., Yahya, M., Electrochemical studies on epoxidised natural rubber-based gel polymer electrolytes for lithium–air cells, *Journal of Power Sources*, **2008**, *183*, 351-354.
- [227] Zhang, D., Li, R., Huang, T., Yu, A., Novel composite polymer electrolyte for lithium air batteries, *Journal of Power Sources*, **2010**, *195*, 1202-1206.
- [228] Kumar, B., Kumar, J., Leese, R., Fellner, J.P., Rodrigues, S.J., Abraham, K., A solid-state, rechargeable, long cycle life lithium–air battery, *Journal of The Electrochemical Society*, **2010**, *157*, A50-A54.
- [229] Li, F., Kitaura, H., Zhou, H., The pursuit of rechargeable solid-state Li–air batteries, *Energy & environmental science*, **2013**, *6*, 2302-2311.
- [230] Hassoun, J., Croce, F., Armand, M., Scrosati, B., Investigation of the O₂ Electrochemistry in a Polymer Electrolyte Solid-State Cell, *Angewandte Chemie International Edition*, **2011**, *50*, 2999-3002.
- [231] Tran, C., Yang, X.-Q., Qu, D., Investigation of the gas-diffusion-electrode used as lithium/air cathode in non-aqueous electrolyte and the importance of carbon material porosity, *Journal of Power Sources*, **2010**, *195*, 2057-2063.
- [232] Mirzaeian, M., Hall, P.J., Preparation of controlled porosity carbon aerogels for energy storage in rechargeable lithium oxygen batteries, *Electrochimica Acta*, **2009**, *54*, 7444-7451.
- [233] Yang, X.-h., He, P., Xia, Y.-y., Preparation of mesocellular carbon foam and its application for lithium/oxygen battery, *Electrochemistry Communications*, **2009**, *11*, 1127-1130.

- [234] Hayashi, M., Minowa, H., Takahashi, M., Shodai, T., Surface properties and electrochemical performance of carbon materials for air electrodes of lithium-air batteries, *Electrochemistry*, **2010**, *78*, 325-328.
- [235] Lin, X., Zhou, L., Huang, T., Yu, A., Hierarchically porous honeycomb-like carbon as a lithium–oxygen electrode, *Journal of Materials Chemistry A*, **2013**, *1*, 1239-1245.
- [236] Kichambare, P., Kumar, J., Rodrigues, S., Kumar, B., Electrochemical performance of highly mesoporous nitrogen doped carbon cathode in lithium–oxygen batteries, *Journal of Power Sources*, **2011**, *196*, 3310-3316.
- [237] Lu, Y., Wen, Z., Jin, J., Cui, Y., Wu, M., Sun, S., Mesoporous carbon nitride loaded with Pt nanoparticles as a bifunctional air electrode for rechargeable lithium-air battery, *Journal of Solid State Electrochemistry*, **2012**, *16*, 1863-1868.
- [238] Zhang, G., Zheng, J., Liang, R., Zhang, C., Wang, B., Hendrickson, M., Plichta, E., Lithium–air batteries using SWNT/CNF buckypapers as air electrodes, *Journal of The Electrochemical Society*, **2010**, *157*, A953-A956.
- [239] Zhang, T., Zhou, H., From Li–O₂ to Li–air batteries: carbon nanotubes/ionic liquid gels with a tricontinuous passage of electrons, ions, and oxygen, *Angewandte Chemie*, **2012**, *124*, 11224-11229.
- [240] Nakanishi, S., Mizuno, F., Nobuhara, K., Abe, T., Iba, H., Influence of the carbon surface on cathode deposits in non-aqueous Li–O₂ batteries, *Carbon*, **2012**, *50*, 4794-4803.

- [241] Mitchell, R.R., Gallant, B.M., Thompson, C.V., Shao-Horn, Y., All-carbon-nanofiber electrodes for high-energy rechargeable Li–O₂ batteries, *Energy & Environmental Science*, **2011**, *4*, 2952-2958.
- [242] Li, Y., Wang, J., Li, X., Liu, J., Geng, D., Yang, J., Li, R., Sun, X., Nitrogen-doped carbon nanotubes as cathode for lithium–air batteries, *Electrochemistry Communications*, **2011**, *13*, 668-672.
- [243] McCloskey, B., Speidel, A., Scheffler, R., Miller, D., Viswanathan, V., Hummelshøj, J., Nørskov, J., Luntz, A., Twin problems of interfacial carbonate formation in nonaqueous Li–O₂ batteries, *The journal of physical chemistry letters*, **2012**, *3*, 997-1001.
- [244] Ottakam Thotiyl, M.M., Freunberger, S.A., Peng, Z., Bruce, P.G., The carbon electrode in nonaqueous Li–O₂ cells, *Journal of the American Chemical Society*, **2012**, *135*, 494-500.
- [245] Cui, Y., Wen, Z., Liu, Y., A free-standing-type design for cathodes of rechargeable Li–O₂ batteries, *Energy & Environmental Science*, **2011**, *4*, 4727-4734.
- [246] Cui, Y., Wen, Z., Liang, X., Lu, Y., Jin, J., Wu, M., Wu, X., A tubular polypyrrole based air electrode with improved O₂ diffusivity for Li–O₂ batteries, *Energy & Environmental Science*, **2012**, *5*, 7893-7897.
- [247] Tran, C., Kafle, J., Yang, X.-Q., Qu, D., Increased discharge capacity of a Li-air activated carbon cathode produced by preventing carbon surface passivation, *Carbon*, **2011**, *49*, 1266-1271.
- [248] Cui, Y., Wen, Z., Lu, Y., Wu, M., Liang, X., Jin, J., Functional binder for high-performance Li–O₂ batteries, *Journal of Power Sources*, **2013**, *244*, 614-619.

- [249] Papp, J.K., Forster, J.D., Burke, C.M., Kim, H.W., Luntz, A.C., Shelby, R.M., Urban, J.J., McCloskey, B.D., Poly (vinylidene fluoride)(PVDF) Binder Degradation in Li-O₂ Batteries: A Consideration for the Characterization of Lithium Superoxide, *The Journal of Physical Chemistry Letters*, **2017**, *8*, 1169-1174.
- [250] Black, R., Oh, S.H., Lee, J.-H., Yim, T., Adams, B., Nazar, L.F., Screening for superoxide reactivity in Li-O₂ batteries: effect on Li₂O₂/LiOH crystallization, *Journal of the American Chemical Society*, **2012**, *134*, 2902-2905.
- [251] Vankova, S., Francia, C., Amici, J., Zeng, J., Bodoardo, S., Penazzi, N., Collins, G., Geaney, H., O'Dwyer, C., Influence of Binders and Solvents on Stability of Ru/RuO_x Nanoparticles on ITO Nanocrystals as Li-O₂ Battery Cathodes, *ChemSusChem*, **2017**, *10*, 575-586.
- [252] Li, Y., Wang, J., Li, X., Geng, D., Li, R., Sun, X., Superior energy capacity of graphene nanosheets for a nonaqueous lithium-oxygen battery, *Chemical Communications*, **2011**, *47*, 9438-9440.
- [253] Yoo, E., Zhou, H., Li- air rechargeable battery based on metal-free graphene nanosheet catalysts, *ACS nano*, **2011**, *5*, 3020-3026.
- [254] Luo, W.B., Gao, X.W., Shi, D.Q., Chou, S.L., Wang, J.Z., Liu, H.K., Binder-Free and Carbon-Free 3D Porous Air Electrode for Li-O₂ Batteries with High Efficiency, High Capacity, and Long Life, *Small*, **2016**, *12*, 3031-3038.
- [255] Liu, H., Zheng, Y., Wang, G., Qiao, S.Z., A Three-Component Nanocomposite with Synergistic Reactivity for Oxygen Reduction Reaction in Alkaline Solution, *Advanced Energy Materials*, **2015**, *5*.

- [256] Lu, Y.-C., Gasteiger, H.A., Shao-Horn, Y., Catalytic activity trends of oxygen reduction reaction for nonaqueous Li-air batteries, *Journal of the American Chemical Society*, **2011**, *133*, 19048-19051.
- [257] Su, D., Dou, S., Wang, G., Hierarchical Ru nanospheres as highly effective cathode catalysts for Li-O₂ batteries, *Journal of Materials Chemistry A*, **2015**, *3*, 18384-18388.
- [258] Liao, K., Zhang, T., Wang, Y., Li, F., Jian, Z., Yu, H., Zhou, H., Nanoporous Ru as a Carbon-and Binder-Free Cathode for Li-O₂ Batteries, *ChemSusChem*, **2015**, *8*, 1429-1434.
- [259] Li, F., Tang, D.M., Zhang, T., Liao, K., He, P., Golberg, D., Yamada, A., Zhou, H., Superior Performance of a Li-O₂ Battery with Metallic RuO₂ Hollow Spheres as the Carbon-Free Cathode, *Advanced Energy Materials*, **2015**, *5*.
- [260] Guo, X., Liu, P., Han, J., Ito, Y., Hirata, A., Fujita, T., Chen, M., 3D Nanoporous Nitrogen-Doped Graphene with Encapsulated RuO₂ Nanoparticles for Li-O₂ Batteries, *Advanced Materials*, **2015**, *27*, 6137-6143.
- [261] Su, D., Seo, D.H., Ju, Y., Han, Z., Ostrikov, K., Dou, S., Ahn, H.-J., Peng, Z., Wang, G., Ruthenium nanocrystal decorated vertical graphene nanosheets@ Ni foam as highly efficient cathode catalysts for lithium-oxygen batteries, *NPG Asia Materials*, **2016**, *8*, e286.
- [262] Li, F., Chen, Y., Tang, D.-M., Jian, Z., Liu, C., Golberg, D., Yamada, A., Zhou, H., Performance-improved Li-O₂ battery with Ru nanoparticles supported on binder-free multi-walled carbon nanotube paper as cathode, *Energy & Environmental Science*, **2014**, *7*, 1648-1652.

- [263] Sun, B., Munroe, P., Wang, G., Ruthenium nanocrystals as cathode catalysts for lithium-oxygen batteries with a superior performance, *Scientific reports*, **2013**, *3*.
- [264] Débart, A., Paterson, A.J., Bao, J., Bruce, P.G., α -MnO₂ Nanowires: A Catalyst for the O₂ Electrode in Rechargeable Lithium Batteries, *Angewandte Chemie*, **2008**, *120*, 4597-4600.
- [265] Tong, S., Zheng, M., Lu, Y., Lin, Z., Li, J., Zhang, X., Shi, Y., He, P., Zhou, H., Mesoporous NiO with a single-crystalline structure utilized as a noble metal-free catalyst for non-aqueous Li–O₂ batteries, *Journal of Materials Chemistry A*, **2015**, *3*, 16177-16182.
- [266] Yin, J., Carlin, J.M., Kim, J., Li, Z., Park, J.H., Patel, B., Chakrapani, S., Lee, S., Joo, Y.L., Synergy Between Metal Oxide Nanofibers and Graphene Nanoribbons for Rechargeable Lithium-Oxygen Battery Cathodes, *Advanced Energy Materials*, **2015**, *5*.
- [267] Zhang, J., Li, P., Wang, Z., Qiao, J., Rooney, D., Sun, W., Sun, K., Three-dimensional graphene–Co₃O₄ cathodes for rechargeable Li–O₂ batteries, *Journal of Materials Chemistry A*, **2015**, *3*, 1504-1510.
- [268] Mohamed, S.G., Tsai, Y.-Q., Chen, C.-J., Tsai, Y.-T., Hung, T.-F., Chang, W.-S., Liu, R.-S., Ternary Spinel MCo₂O₄ (M= Mn, Fe, Ni, and Zn) Porous Nanorods as Bifunctional Cathode Materials for Lithium–O₂ Batteries, *ACS applied materials & interfaces*, **2015**, *7*, 12038-12046.
- [269] Gao, X., Chen, Y., Johnson, L., Bruce, P.G., Promoting solution phase discharge in Li–O₂ batteries containing weakly solvating electrolyte solutions, *Nature materials*, **2016**, *15*, 882-888.

- [270] Zhu, Y., Gao, X., Wang, X., Hou, Y., Liu, L., Wu, Y., A single-ion polymer electrolyte based on boronate for lithium ion batteries, *Electrochemistry Communications*, **2012**, *22*, 29-32.
- [271] Zhu, Y., Wang, F., Liu, L., Xiao, S., Chang, Z., Wu, Y., Composite of a nonwoven fabric with poly (vinylidene fluoride) as a gel membrane of high safety for lithium ion battery, *Energy & Environmental Science*, **2013**, *6*, 618-624.
- [272] Christie, A.M., Lilley, S.J., Staunton, E., Andreev, Y.G., Bruce, P.G., Increasing the conductivity of crystalline polymer electrolytes, *Nature*, **2005**, *433*, 50-53.
- [273] MacGlashan, G.S., Andreev, Y.G., Bruce, P.G., Structure of the polymer electrolyte poly (ethylene oxide)₆: LiAsF₆, *Nature*, **1999**, *398*, 792-794.
- [274] Varshney, P.K., Gupta, S., Natural polymer-based electrolytes for electrochemical devices: a review, *Ionics*, **2011**, *17*, 479-483.
- [275] Li, Y.-H., Wu, X.-L., Kim, J.-H., Xin, S., Su, J., Yan, Y., Lee, J.-S., Guo, Y.-G., A novel polymer electrolyte with improved high-temperature-tolerance up to 170 C for high-temperature lithium-ion batteries, *Journal of Power Sources*, **2013**, *244*, 234-239.
- [276] Wu, X.-L., Li, Y.-H., Wu, N., Xin, S., Kim, J.-H., Yan, Y., Lee, J.-S., Guo, Y.-G., Enhanced working temperature of PEO-based polymer electrolyte via porous PTFE film as an efficient heat resister, *Solid State Ionics*, **2013**, *245*, 1-7.
- [277] Pu, W., He, X., Wang, L., Jiang, C., Wan, C., Preparation of PVDF-HFP microporous membrane for Li-ion batteries by phase inversion, *Journal of Membrane Science*, **2006**, *272*, 11-14.

- [278] Heng, L., Wang, B., Li, M., Zhang, Y., Jiang, L., Advances in fabrication materials of honeycomb structure films by the breath-figure method, *Materials*, **2013**, *6*, 460-482.
- [279] Widawski, G., Rawiso, M., François, B., Self-organized honeycomb morphology of star-polymer polystyrene films, *Nature*, **1994**, *369*, 387-389.
- [280] Srinivasarao, M., Collings, D., Philips, A., Patel, S., Three-dimensionally ordered array of air bubbles in a polymer film, *Science*, **2001**, *292*, 79-83.
- [281] Bolognesi, A., Mercogliano, C., Yunus, S., Civardi, M., Comoretto, D., Turturro, A., Self-organization of polystyrenes into ordered microstructured films and their replication by soft lithography, *Langmuir*, **2005**, *21*, 3480-3485.
- [282] Li, M., Xu, S., Kumacheva, E., Convection in polymeric fluids subjected to vertical temperature gradients, *Macromolecules*, **2000**, *33*, 4972-4978.
- [283] Peng, J., Han, Y., Fu, J., Yang, Y., Li, B., Formation of regular hole pattern in polymer films, *Macromolecular Chemistry and Physics*, **2003**, *204*, 125-130.
- [284] Zhang, P., Yang, L., Li, L., Ding, M., Wu, Y., Holze, R., Enhanced electrochemical and mechanical properties of P (VDF-HFP)-based composite polymer electrolytes with SiO₂ nanowires, *Journal of membrane science*, **2011**, *379*, 80-85.
- [285] Xu, J.J., Ye, H., Polymer gel electrolytes based on oligomeric polyether/cross-linked PMMA blends prepared via in situ polymerization, *Electrochemistry communications*, **2005**, *7*, 829-835.
- [286] Denis, Y., Fietzek, C., Weydanz, W., Donoue, K., Inoue, T., Kurokawa, H., Fujitani, S., Study of LiFePO₄ by cyclic voltammetry, *Journal of The Electrochemical Society*, **2007**, *154*, A253-A257.

- [287] Yamada, A., Koizumi, H., Nishimura, S.-i., Sonoyama, N., Kanno, R., Yonemura, M., Nakamura, T., Kobayashi, Y., Room-temperature miscibility gap in Li_xFePO_4 , *Nature materials*, **2006**, *5*, 357-360.
- [288] Liu, H., Cao, Q., Fu, L.J., Li, C., Wu, Y., Wu, H., Doping effects of zinc on LiFePO_4 cathode material for lithium ion batteries, *Electrochemistry Communications*, **2006**, *8*, 1553-1557.
- [289] Liu, J., Conry, T.E., Song, X., Doeff, M.M., Richardson, T.J., Nanoporous spherical LiFePO_4 for high performance cathodes, *Energy & Environmental Science*, **2011**, *4*, 885-888.
- [290] Sun, C., Rajasekhara, S., Goodenough, J.B., Zhou, F., Monodisperse porous LiFePO_4 microspheres for a high power Li-ion battery cathode, *Journal of the American Chemical Society*, **2011**, *133*, 2132-2135.
- [291] Stephan, A.M., Review on gel polymer electrolytes for lithium batteries, *European polymer journal*, **2006**, *42*, 21-42.
- [292] Kim, H.-S., Periasamy, P., Moon, S.-I., Electrochemical properties of the Li-ion polymer batteries with P (VdF-co-HFP)-based gel polymer electrolyte, *Journal of power sources*, **2005**, *141*, 293-297.
- [293] Lu, L., Han, X., Li, J., Hua, J., Ouyang, M., A review on the key issues for lithium-ion battery management in electric vehicles, *Journal of power sources*, **2013**, *226*, 272-288.
- [294] Wang, Q., Ping, P., Zhao, X., Chu, G., Sun, J., Chen, C., Thermal runaway caused fire and explosion of lithium ion battery, *Journal of power sources*, **2012**, *208*, 210-224.

- [295] Idris, N.H., Rahman, M.M., Wang, J.-Z., Liu, H.-K., Microporous gel polymer electrolytes for lithium rechargeable battery application, *Journal of Power Sources*, **2012**, *201*, 294-300.
- [296] Li, H., Lin, C.-E., Shi, J.-L., Ma, X.-T., Zhu, B.-K., Zhu, L.-P., Preparation and characterization of safety PVDF/P (MMA-co-PEGMA) active separators by studying the liquid electrolyte distribution in this kind of membrane, *Electrochimica Acta*, **2014**, *115*, 317-325.
- [297] Saito, Y., Kataoka, H., Capiglia, C., Yamamoto, H., Ionic conduction properties of PVDF– HFP type gel polymer electrolytes with lithium imide salts, *The Journal of Physical Chemistry B*, **2000**, *104*, 2189-2192.
- [298] Costa, C.M., Silva, M.M., Lanceros-Mendez, S., Battery separators based on vinylidene fluoride (VDF) polymers and copolymers for lithium ion battery applications, *Rsc Advances*, **2013**, *3*, 11404-11417.
- [299] Gopalan, A.I., Santhosh, P., Manesh, K.M., Nho, J.H., Kim, S.H., Hwang, C.-G., Lee, K.-P., Development of electrospun PVdF–PAN membrane-based polymer electrolytes for lithium batteries, *Journal of membrane science*, **2008**, *325*, 683-690.
- [300] [300] Wang, X.-L., Mei, A., Li, X.-L., Lin, Y.-H., Nan, C.-W., Novel polymer electrolytes based on triblock poly (ethylene oxide)-poly (propylene oxide)-poly (ethylene oxide) with ionically active SiO₂, *Journal of Power Sources*, **2007**, *171*, 913-916.
- [301] Rao, M., Geng, X., Liao, Y., Hu, S., Li, W., Preparation and performance of gel polymer electrolyte based on electrospun polymer membrane and ionic liquid for lithium ion battery, *Journal of membrane science*, **2012**, *399*, 37-42.

- [302] Zhu, Y., Wang, F., Liu, L., Xiao, S., Yang, Y., Wu, Y., Cheap glass fiber mats as a matrix of gel polymer electrolytes for lithium ion batteries, *Scientific reports*, **2013**, 3.
- [303] Ma, T., Cui, Z., Wu, Y., Qin, S., Wang, H., Yan, F., Han, N., Li, J., Preparation of PVDF based blend microporous membranes for lithium ion batteries by thermally induced phase separation: I. Effect of PMMA on the membrane formation process and the properties, *Journal of membrane science*, **2013**, 444, 213-222.
- [304] Abraham, K., Jiang, Z., A polymer electrolyte-based rechargeable lithium/oxygen battery, *Journal of The Electrochemical Society*, **1996**, 143, 1-5.
- [305] Rogers, E.I., Huang, X.-J., Dickinson, E.J., Hardacre, C., Compton, R.G., Investigating the mechanism and electrode kinetics of the oxygen| superoxide ($O_2|O_2^{\cdot-}$) couple in various room-temperature ionic liquids at gold and platinum electrodes in the temperature range 298– 318 K, *The Journal of Physical Chemistry C*, **2009**, 113, 17811-17823.
- [306] Allen, C.J., Mukerjee, S., Plichta, E.J., Hendrickson, M.A., Abraham, K., Oxygen electrode rechargeability in an ionic liquid for the Li–air battery, *The Journal of Physical Chemistry Letters*, **2011**, 2, 2420-2424.
- [307] Thotiyl, M.M.O., Freunberger, S.A., Peng, Z., Chen, Y., Liu, Z., Bruce, P.G., A stable cathode for the aprotic Li-O₂ battery, *Nature materials*, **2013**, 12, 1050-1056.
- [308] Lu, J., Lei, Y., Lau, K.C., Luo, X., Du, P., Wen, J., Assary, R.S., Das, U., Miller, D.J., Elam, J.W., A nanostructured cathode architecture for low charge overpotential in lithium-oxygen batteries, *Nature communications*, **2013**, 4, 2383.

- [309] Lim, H.D., Park, K.Y., Song, H., Jang, E.Y., Gwon, H., Kim, J., Kim, Y.H., Lima, M.D., Robles, R.O., Lepró, X., Enhanced Power and Rechargeability of a Li-O₂ Battery Based on a Hierarchical-Fibril CNT Electrode, *Advanced Materials*, **2013**, 25, 1348-1352.
- [310] Wang, H., Liang, Y., Gong, M., Li, Y., Chang, W., Mefford, T., Zhou, J., Wang, J., Regier, T., Wei, F., An ultrafast nickel-iron battery from strongly coupled inorganic nanoparticle/nanocarbon hybrid materials, *Nature communications*, **2012**, 3, 917.
- [311] Xu, J.-J., Wang, Z.-L., Xu, D., Zhang, L.-L., Zhang, X.-B., Tailoring deposition and morphology of discharge products towards high-rate and long-life lithium-oxygen batteries, *Nature communications*, **2013**, 4, 2438.
- [312] Zhang, T., Zhou, H., A reversible long-life lithium-air battery in ambient air, *Nature communications*, **2013**, 4, 1817.
- [313] Oh, S.H., Black, R., Pomerantseva, E., Lee, J.-H., Nazar, L.F., Synthesis of a metallic mesoporous pyrochlore as a catalyst for lithium-O₂ batteries, *Nature chemistry*, **2012**, 4, 1004-1010.
- [314] Lu, Y.-C., Shao-Horn, Y., Probing the reaction kinetics of the charge reactions of nonaqueous Li-O₂ batteries, *The journal of physical chemistry letters*, **2012**, 4, 93-99.
- [315] Li, Q., Xu, P., Gao, W., Ma, S., Zhang, G., Cao, R., Cho, J., Wang, H.L., Wu, G., Graphene/Graphene-Tube Nanocomposites Templated from Cage-Containing Metal-Organic Frameworks for Oxygen Reduction in Li-O₂ Batteries, *Advanced materials*, **2014**, 26, 1378-1386.

- [316] Cheng, F., Zhang, T., Zhang, Y., Du, J., Han, X., Chen, J., Enhancing electrocatalytic oxygen reduction on MnO₂ with vacancies, *Angewandte Chemie International Edition*, **2013**, *52*, 2474-2477.
- [317] Sun, B., Wang, B., Su, D., Xiao, L., Ahn, H., Wang, G., Graphene nanosheets as cathode catalysts for lithium-air batteries with an enhanced electrochemical performance, *Carbon*, **2012**, *50*, 727-733.
- [318] Xu, J.-J., Wang, Z.-L., Xu, D., Meng, F.-Z., Zhang, X.-B., 3D ordered macroporous LaFeO₃ as efficient electrocatalyst for Li–O₂ batteries with enhanced rate capability and cyclic performance, *Energy & environmental science*, **2014**, *7*, 2213-2219.
- [319] Guo, Z., Zhou, D., Dong, X., Qiu, Z., Wang, Y., Xia, Y., Ordered Hierarchical Mesoporous/Macroporous Carbon: A High-Performance Catalyst for Rechargeable Li–O₂ Batteries, *Advanced Materials*, **2013**, *25*, 5668-5672.
- [320] Han, S., Wu, D., Li, S., Zhang, F., Feng, X., Porous graphene materials for advanced electrochemical energy storage and conversion devices, *Advanced Materials*, **2014**, *26*, 849-864.
- [321] Liu, Q., Jiang, Y., Xu, J., Xu, D., Chang, Z., Yin, Y., Liu, W., Zhang, X., Hierarchical CO₃O₄ porous nanowires as an efficient bifunctional cathode catalyst for long life Li-O₂ batteries, *Nano Research*, **2015**, *8*, 576.
- [322] Sun, B., Huang, X., Chen, S., Munroe, P., Wang, G., Porous graphene nanoarchitectures: an efficient catalyst for low charge-overpotential, long life, and high capacity lithium–oxygen batteries, *Nano letters*, **2014**, *14*, 3145-3152.

- [323] Bergner, B.J., Schürmann, A., Peppler, K., Garsuch, A., Janek, J.r., TEMPO: a mobile catalyst for rechargeable Li-O₂ batteries, *Journal of the American Chemical Society*, **2014**, *136*, 15054-15064.
- [324] Kwak, W.-J., Hirshberg, D., Sharon, D., Shin, H.-J., Afri, M., Park, J.-B., Garsuch, A., Chesneau, F.F., Frimer, A.A., Aurbach, D., Understanding the behavior of Li-oxygen cells containing LiI, *Journal of Materials Chemistry A*, **2015**, *3*, 8855-8864.
- [325] Zhang, J., Sun, B., Ahn, H.-J., Wang, C., Wang, G., Conducting polymer-doped polyprrole as an effective cathode catalyst for Li-O₂ batteries, *Materials Research Bulletin*, **2013**, *48*, 4979-4983.
- [326] Lu, Y.-C., Gasteiger, H.A., Parent, M.C., Chiloyan, V., Shao-Horn, Y., The influence of catalysts on discharge and charge voltages of rechargeable Li-oxygen batteries, *Electrochemical and Solid-State Letters*, **2010**, *13*, A69-A72.
- [327] Zhu, Y.G., Jia, C., Yang, J., Pan, F., Huang, Q., Wang, Q., Dual redox catalysts for oxygen reduction and evolution reactions: towards a redox flow Li-O₂ battery, *Chemical Communications*, **2015**, *51*, 9451-9454.
- [328] Guo, W., Yin, Y.-X., Xin, S., Guo, Y.-G., Wan, L.-J., Superior radical polymer cathode material with a two-electron process redox reaction promoted by graphene, *Energy & Environmental Science*, **2012**, *5*, 5221-5225.
- [329] Kim, J.-K., Ahn, J.-H., Cheruvally, G., Chauhan, G.S., Choi, J.-W., Kim, D.-S., Ahn, H.-J., Lee, S.H., Song, C.E., Electrochemical properties of rechargeable organic radical battery with PTMA cathode, *Metals and Materials International*, **2009**, *15*, 77-82.

- [330] Nishide, H., Iwasa, S., Pu, Y.-J., Suga, T., Nakahara, K., Satoh, M., Organic radical battery: nitroxide polymers as a cathode-active material, *Electrochimica acta*, **2004**, *50*, 827-831.
- [331] Guo, W., Su, J., Li, Y.-H., Wan, L.-J., Guo, Y.-G., Nitroxide radical polymer/graphene nanocomposite as an improved cathode material for rechargeable lithium batteries, *Electrochimica Acta*, **2012**, *72*, 81-86.
- [332] Aetukuri, N.B., McCloskey, B.D., Garcia, J.M., Krupp, L.E., Viswanathan, V., Luntz, A.C., Solvating additives drive solution-mediated electrochemistry and enhance toroid growth in non-aqueous Li-O₂ batteries, *Nature chemistry*, **2015**, *7*, 50-56.
- [333] Geißlmeir, D., Jary, W.G., Falk, H., The TEMPO/copper catalyzed oxidation of primary alcohols to aldehydes using oxygen as stoichiometric oxidant, *Monatshefte für Chemie/Chemical Monthly*, **2005**, *136*, 1591-1599.
- [334] Sheldon, R.A., Arends, I.W., Organocatalytic oxidations mediated by nitroxyl radicals, *Advanced Synthesis & Catalysis*, **2004**, *346*, 1051-1071.
- [335] Hodgson, J.L., Namazian, M., Bottle, S.E., Coote, M.L., One-electron oxidation and reduction potentials of nitroxide antioxidants: A theoretical study, *The Journal of Physical Chemistry A*, **2007**, *111*, 13595-13605.
- [336] Wang, J., Li, Y., Sun, X., Challenges and opportunities of nanostructured materials for aprotic rechargeable lithium-air batteries, *Nano Energy*, **2013**, *2*, 443-467.
- [337] Luntz, A.C., McCloskey, B.D., Nonaqueous Li-air batteries: a status report, *Chemical reviews*, **2014**, *114*, 11721-11750.

- [338] Amanchukwu, C.V., Harding, J.R., Shao-Horn, Y., Hammond, P.T., Understanding the chemical stability of polymers for lithium–air batteries, *Chemistry of Materials*, **2015**, *27*, 550-561.
- [339] Zhang, J., Sun, B., Xie, X., Kretschmer, K., Wang, G., Enhancement of stability for lithium oxygen batteries by employing electrolytes gelled by poly (vinylidene fluoride-co-hexafluoropropylene) and tetraethylene glycol dimethyl ether, *Electrochimica Acta*, **2015**, *183*, 56-62.
- [340] Black, R., Adams, B., Nazar, L., Non-Aqueous and Hybrid Li-O₂ Batteries, *Advanced Energy Materials*, **2012**, *2*, 801-815.
- [341] Gallagher, K.G., Goebel, S., Greszler, T., Mathias, M., Oelerich, W., Eroglu, D., Srinivasan, V., Quantifying the promise of lithium–air batteries for electric vehicles, *Energy & Environmental Science*, **2014**, *7*, 1555-1563.
- [342] Choi, R., Jung, J., Kim, G., Song, K., Kim, Y.-I., Jung, S.C., Han, Y.-K., Song, H., Kang, Y.-M., Ultra-low overpotential and high rate capability in Li-O₂ batteries through surface atom arrangement of PdCu nanocatalysts, *Energy & Environmental Science*, **2014**, *7*, 1362-1368.
- [343] Adams, B.D., Radtke, C., Black, R., Trudeau, M.L., Zaghbi, K., Nazar, L.F., Current density dependence of peroxide formation in the Li-O₂ battery and its effect on charge, *Energy & Environmental Science*, **2013**, *6*, 1772-1778.
- [344] Shao, Y., Ding, F., Xiao, J., Zhang, J., Xu, W., Park, S., Zhang, J.G., Wang, Y., Liu, J., Making Li-air batteries rechargeable: Material challenges, *Advanced Functional Materials*, **2013**, *23*, 987-1004.

- [345] Ammundsen, B., Paulsen, J., Novel Lithium-Ion Cathode Materials Based on Layered Manganese Oxides, *Advanced Materials*, **2001**, *13*, 943-956.
- [346] Liu, Q.C., Liu, T., Liu, D.P., Li, Z.J., Zhang, X.B., Zhang, Y., A flexible and wearable lithium–oxygen battery with record energy density achieved by the interlaced architecture inspired by bamboo slips, *Advanced Materials*, **2016**, *28*, 8413-8418.
- [347] Liu, T., Liu, Q.C., Xu, J.J., Zhang, X.B., Cable-Type Water-Survivable Flexible Li-O₂ Battery, *Small*, **2016**, *12*, 3101-3105.
- [348] Yin, Y.B., Xu, J.J., Liu, Q.C., Zhang, X.B., Macroporous Interconnected Hollow Carbon Nanofibers Inspired by Golden-Toad Eggs toward a Binder-Free, High-Rate, and Flexible Electrode, *Advanced Materials*, **2016**, *28*, 7494-7500.
- [349] Kundu, D., Black, R., Adams, B., Nazar, L.F., A highly active low voltage redox mediator for enhanced rechargeability of lithium–oxygen batteries, *ACS central science*, **2015**, *1*, 510-515.
- [350] Liang, Y., Tao, Z., Chen, J., Organic electrode materials for rechargeable lithium batteries, *Advanced Energy Materials*, **2012**, *2*, 742-769.
- [351] Zhang, J., Sun, B., Xie, X., Zhao, Y., Wang, G., A Bifunctional Organic Redox Catalyst for Rechargeable Lithium–Oxygen Batteries with Enhanced Performances, *Advanced Science*, **2016**, *3*.
- [352] Aurbach, D., McCloskey, B.D., Nazar, L.F., Bruce, P.G., Advances in understanding mechanisms underpinning lithium–air batteries, *Nature Energy*, **2016**, *1*, 16128.

- [353] Park, H.W., Lee, D.U., Nazar, L.F., Chen, Z., Oxygen reduction reaction using MnO₂ nanotubes/nitrogen-doped exfoliated graphene hybrid catalyst for Li-O₂ battery applications, *Journal of The Electrochemical Society*, **2013**, *160*, A344-A350.
- [354] McCloskey, B.D., Scheffler, R., Speidel, A., Bethune, D.S., Shelby, R.M., Luntz, A., On the efficacy of electrocatalysis in nonaqueous Li-O₂ batteries, *Journal of the American Chemical Society*, **2011**, *133*, 18038-18041.
- [355] Wang, J., Yang, J., Xie, J., Xu, N., A novel conductive polymer–sulfur composite cathode material for rechargeable lithium batteries, *Advanced Materials*, **2002**, *14*, 963-965.
- [356] Aricò, A.S., Bruce, P., Scrosati, B., Tarascon, J.-M., Van Schalkwijk, W., Nanostructured materials for advanced energy conversion and storage devices, *Nature materials*, **2005**, *4*, 366-377.
- [357] Chang, Y., Dong, S., Ju, Y., Xiao, D., Zhou, X., Zhang, L., Chen, X., Shang, C., Gu, L., Peng, Z., A Carbon-and Binder-Free Nanostructured Cathode for High-Performance Nonaqueous Li-O₂ Battery, *Advanced Science*, **2015**, *2*.
- [358] Xu, J.J., Xu, D., Wang, Z.L., Wang, H.G., Zhang, L.L., Zhang, X.B., Synthesis of perovskite-based porous La_{0.75}Sr_{0.25}MnO₃ nanotubes as a highly efficient electrocatalyst for rechargeable lithium–oxygen batteries, *Angewandte Chemie International Edition*, **2013**, *52*, 3887-3890.
- [359] McCloskey, B.D., Scheffler, R., Speidel, A., Girishkumar, G., Luntz, A.C., On the mechanism of nonaqueous Li-O₂ electrochemistry on C and its kinetic

- overpotentials: some implications for Li-air batteries, *The Journal of Physical Chemistry C*, **2012**, *116*, 23897-23905.
- [360] Ryu, W.-H., Gittleson, F.S., Thomsen, J.M., Li, J., Schwab, M.J., Brudvig, G.W., Taylor, A.D., Heme biomolecule as redox mediator and oxygen shuttle for efficient charging of lithium-oxygen batteries, *Nature communications*, **2016**, *7*, 12925.
- [361] Guo, X., Han, J., Liu, P., Chen, L., Ito, Y., Jian, Z., Jin, T., Hirata, A., Li, F., Fujita, T., Hierarchical nanoporosity enhanced reversible capacity of bicontinuous nanoporous metal based Li-O₂ battery, *Scientific reports*, **2016**, *6*.
- [362] Kwak, W.-J., Hirshberg, D., Sharon, D., Afri, M., Frimer, A.A., Jung, H.-G., Aurbach, D., Sun, Y.-K., Li-O₂ cells with LiBr as an electrolyte and a redox mediator, *Energy & Environmental Science*, **2016**, *9*, 2334-2345.
- [363] Liang, Z., Lu, Y.-C., Critical Role of Redox Mediator in Suppressing Charging Instabilities of Lithium-Oxygen Batteries, *Journal of the American Chemical Society*, **2016**, *138*, 7574-7583.
- [364] Haregewoin, A.M., Wotango, A.S., Hwang, B.-J., Electrolyte additives for lithium ion battery electrodes: progress and perspectives, *Energy & Environmental Science*, **2016**, *9*, 1955-1988.
- [365] Ates, M.N., Allen, C.J., Mukerjee, S., Abraham, K., Electronic effects of substituents on redox shuttles for overcharge protection of Li-ion batteries, *Journal of The Electrochemical Society*, **2012**, *159*, A1057-A1064.
- [366] Wudl, F., Wobschall, D., Hufnagel, E.J., Electrical conductivity by the bis (1, 3-dithiole)-bis (1, 3-dithiolium) system, *Journal of the American Chemical Society*, **1972**, *94*, 670-672.

- [367] Williams, R., Lowe Ma, C., Samson, S., Khanna, S., Somoano, R., Structural phase transition and disorder in tetrathiafulvalenium chloride [(TTF) Cl_x], *The Journal of Chemical Physics*, **1980**, *72*, 3781-3788.
- [368] Martín, N., Tetrathiafulvalene: the advent of organic metals, *Chemical Communications*, **2013**, *49*, 7025-7027.
- [369] Bergkamp, J.J., Decurtins, S., Liu, S.-X., Current advances in fused tetrathiafulvalene donor–acceptor systems, *Chemical Society Reviews*, **2015**, *44*, 863-874.
- [370] Qiao, Y., Ye, S., Spectroscopic Investigation for Oxygen Reduction and Evolution Reactions with Tetrathiafulvalene as a Redox Mediator in Li-O₂ Battery, *The Journal of Physical Chemistry C*, **2016**, *120*, 15830-15845.
- [371] McCloskey, B.D., Burke, C.M., Nichols, J.E., Renfrew, S.E., Mechanistic insights for the development of Li-O₂ battery materials: addressing Li₂O₂ conductivity limitations and electrolyte and cathode instabilities, *Chemical Communications*, **2015**, *51*, 12701-12715.
- [372] Matsuda, S., Kubo, Y., Uosaki, K., Hashimoto, K., Nakanishi, S., Improved energy capacity of aprotic Li-O₂ batteries by forming Cl-incorporated Li₂O₂ as the discharge product, *The Journal of Physical Chemistry C*, **2016**, *120*, 13360-13365.